SOME EXPERIMENTAL AND THEORETICAL STUDIES IN CRYSTAL OPTICS

by

Mark Julian Gunning

Submitted in partial fulfilment of
the requirements for the degree of
Doctor of Philosophy in the
School of Chemical and Physical Sciences,
University of Natal

Pietermaritzburg
March 1999

ABSTRACT

The contents of this thesis are divided into two separate parts, both of which are concerned with optical phenomena for light propagation through source-free nonmagnetic media. Considered in the first part are various theoretical investigations pertaining to nonmagnetic crystals, while the second part focuses specifically on the experimental investigation of the quadratic electro-optic effect in some crystals of the KDP family.

The opening theoretical chapters of this thesis are based almost entirely on four publications which are the result of work completed in this PhD study. These papers, in the order that they appear in the following chapters, are: *Systematic Eigenvalue Approach to Crystal Optics: An Analytic Alternative to the Geometric Ellipsoid Model* (Gunning and Raab 1998a); *Algebraic Determination of the Principal Refractive Indices and Axes in the Electrooptic Effect* (Gunning and Raab 1998b); *Physical Implications of the Use of Primitive and Traceless Electric Quadrupole Moments* (Gunning and Raab 1997a); and *Electric-Field-Induced Optical Activity in Nonmagnetic Crystals* (Gunning and Raab 1997b). In later chapters two separate experimental projects on the quadratic electro-optic effect in KDP-type crystals are described. Some of the results of these investigations have yet to be published, while others, for both the interferometric and polarimetric experiments, appear in the papers: *The Quadratic Electrooptic Coefficient* g_{xxxx} - g_{yyxx} *of DKDP Crystals* (Gunning *et al.* 1998a); *The Quadratic Electrooptic Effect and Estimation of Antipolarization in ADP* (Gunning *et al.* 1998b); and *Studies of the Quadratic Electrooptic Effect in KDP-type Crystals* (Gunning *et al.* 1999).

The first chapter introduces a multipole eigenvalue theory of light propagation through a nonmagnetic anisotropic dielectric. This theory, in the appropriate multipole order, explains a range of optical phenomena, including circular birefringence and the linear birefringences of Jones and Lorentz, not otherwise fully explained by the widely-used Fresnel ellipsoid or related indicatrix ellipsoid. By means of this model the birefringences, optic axes, and eigenpolarizations of light propagating through a transparent medium are fully accounted for. The theory presented here concentrates on the electric-dipole description, which is the formal basis of the ellipsoid models, and the description of the birefringences, optic axes, and eigenpolarizations is algebraic,

rather than geometric, and in terms of measurable crystal property tensors.

Chapter 2 follows the multipole approach of Chapter 1 with a systematic algebraic means to derive expressions for the principal refractive indices and dielectric axes of a source-free nonmagnetic crystal in a uniform electric field. This is seen as a preferred alternative to the more common iterative numerical approaches to the problem. Results obtained in this chapter, to the chosen order in the field, are again expressed algebraically in terms of crystal property tensors. A number of illustrations of the approach are given for the linear electro-optic effect in crystals of the symmetry point groups $\bar{4}3m$, $3m$, $\bar{4}2m$, and 1. Also, to demonstrate the inadequacies of the numeric method, the quadratic effect in $\bar{4}2m$ is investigated. Throughout these examples, comparisons are drawn with published numerical results.

Chapters 3 and 4 start to allow for higher-order multipole moments, in contrast to the opening two chapters which are limited to the electric-dipole description. Specifically, electromagnetic effects to the order of electric quadrupole and magnetic dipole are considered. Since these effects, such as chiral phenomena in fluids and crystals and gyrotropic birefringence in anti-ferromagnetic crystals, require for their full description the inclusion of electric quadrupoles, the nature of the electric-quadrupole moment is considered in Chapter 3. In many theories this moment is defined to be traceless, but this chapter shows that when this definition is used in the derivation of a wave equation to describe light propagation through an optically active uniaxial medium, this equation as well as properties derived from it, in particular the refractive index of the eigenpolarizations, are in general dependent on the origin used to define the moment. This is physically unacceptable for the theoretical expression of an observed effect. It is shown that if the primitive definition of the quadrupole moment is used in this theory instead, this difficulty does not arise.

Also to the order of electric quadrupole and magnetic dipole, Chapter 4 presents a macroscopic theory of electric-field-induced optical activity in source-free nonmagnetic crystals. In this approach a wave equation, to this multipole order and including distortions linear in an applied electric field, is derived which allows for the description of the linear electric-field-induced circular birefringence. It also identifies other coexisting birefringences, both natural and field-induced which are described in this multipole order. All these birefringences are expressed in terms of measurable crystal property tensors. In this chapter, nonmagnetic crystal classes are

identified which exhibit this field-induced optical activity for particular light-propagation and applied-field configurations for light waves with purely transverse fields. These crystals, symmetry considerations, and other coexisting natural and field-induced birefringence are presented in Table 4.1.

The first chapter of Part 2 of this thesis introduces the quadratic electro-optic effect in KDP-type crystals and provides motivation for the present experimental inquiry of the effect. Tabulated are previous experimental results for components of the quadratic electro-optic coefficients of crystals of KDP, ADP, and DKDP investigated in this work. Also introduced is the electrostrictive effect in these crystals, since it plays a part in the experimental determination of quadratic electro-optic coefficients of these crystals, and values for coefficients of this effect are listed. A multipole theory, based on that in Chapters 1 and 2 to the order of electric dipole and allowing for perturbations quadratic in a low-frequency applied electric field, is presented which describes fully the observed quadratic electro-optic effect in these crystals for the light-propagation and applied-field geometries of interest. The analytic results derived for the observed induced refractive index changes for the polarization eigenvectors for a particular propagation path through the medium are expressed in terms of the quadratic electro-optic coefficients g_{xxxx}, g_{yyxx}, and g_{zzxx}.

One of the two methods proposed in this work for the measurement of coefficients of the quadratic electro-optic effect in specimens of KDP-type crystals is the interferometric technique. Chapter 6 serves to introduce this approach and to provide the theoretical basis for it, within the context of determining small induced phase changes. After a number of experimental factors are highlighted the method proposed for this work is explained. Specifically, this approach utilizes a Michelson arrangement, invoking active stabilization against low-frequency noise influences, and the coefficients are measured by phase-compensation means. This apparatus and its various components is then fully described in Chapter 7, including the method for its operation. The results of this interferometric research appear in Chapter 8 for the various light-propagation and applied-field geometries used, and values are presented for the individual coefficients g_{xxxx}, g_{yyxx}, and g_{zzxx} in KDP and ADP, and also the electrostrictive coefficients γ_{xxyy} and γ_{xxzz} in the same crystals.

An explanation of the second approach to measure quadratic electro-optic coefficients in this

work, the dynamic polarimetric technique, is given in Chapter 9. Two proposed means to investigate the KDP-type crystals by this approach are described and explained theoretically, and the layout of the apparatus and its various components is highlighted. Results of this polarimetric investigation for two light-propagation directions are given in Chapter 10 for investigations on KDP, ADP, and DKDP single crystals. These give values for the difference in quadratic electro-optic coefficients $|g_{xxxx} - g_{yyxx}|$ and $|n_o^3 g_{xxxx} - n_e^3 g_{zzxx}|$.

Finally, in concluding this thesis a summary of the quadratic electro-optic and electrostrictive results determined by the interferometric and polarimetric techniques is given and comparison of these results is drawn with those published previously. Considered briefly are some further conclusions that may be derived from these values for the nature of the electro-optic effect in KDP, ADP, and DKDP.

DECLARATION

I declare that this work is a result of my own research, except where specifically indicated to the contrary, and has not been submitted for any other degree or examination to any other university.

Signed Mark Gunning

Date 16 March 1999

ACKNOWLEDGEMENTS

There are a number of people and organizations to whom I wish to express my most sincere thanks and appreciation for their support and assistance over the past four years that this PhD project has lasted. In no particular order these are:

- Prof. R. E. Raab, for his exceptionally committed supervision of this research, and for generous financial assistance throughout;

- Prof. W. Kucharczyk, for his co-supervision of this project, particularly with regard to the experimental work; I am further indebted for the loan of the KDP-type crystals which formed the subject of the experimental projects, and also for kindly arranging the invitation to study with his research group at the Technical University of Łódź in Łódź, Poland;

- Dr. P. Górski, K. Bondarczuk, and R. Ledzion, for their friendship, and assistance with the research undertaken, whilst visiting the Technical University of Łódź;

- Prof. C. Graham, for his aid and insights when problems were encountered with the interferometric project;

- Mr. J. Wilsenach of the Physics Department Workshop, for always being willing to help with making parts for the experimental apparatus;

- Mr. N. A. Cullis and Mr. G. Dewar of the Electronics Centre, for their construction of various electronic elements, particularly the feedback circuit which formed such a crucial part of the interferometric arrangement;

- the foundation for Research and Development, for a PhD bursary and for generously covering the travel expenses to Poland

- the University of Natal, for a graduate assistantship bursary;

- the Technical University of Łódź, for the invitation to study at that university, and for providing accommodation and funds for the duration of my visit;

- and my family and friends, for their continued support and encouragement throughout.

LIST OF CONTENTS

Page

Page

LIST OF TABLES

Page

Page

Page

LIST OF FIGURES

LIST OF GRAPHS

Page

Part 1

SOME THEORETICAL STUDIES IN CRYSTAL OPTICS

Chapter 1

SYSTEMATIC EIGENVALUE APPROACH TO CRYSTAL OPTICS: AN ANALYTIC ALTERNATIVE TO THE GEOMETRIC ELLIPSOID MODEL

1.1 Introduction

A light wave propagating in a nonabsorbing dielectric may experience birefringence, be it linear or circular or both, which in general will vary with the direction of propagation. However, the classification into linear and circular is now known to be too coarse, with different types of each having been identified, with widely disparate characteristics (Argyres 1955; Graham and Raab 1983, 1990, 1991a; Graham, E. and Raab 1994; Graham, C. and Raab 1994). For instance, as long ago as 1878, Lorentz (1878) predicted the existence of a linear birefringence in certain cubic crystals and many years later reported its measurement in rock salt (Lorentz 1922). Others (Pastrnak and Vedam 1971; Pastrnak and Cross 1972) have also measured this effect in various cubic crystals, obtaining values of the order of 10^{-6}, compared with magnitudes of approximately 10^{-2}–10^{-1} in uniaxial crystals (e.g., quartz $n_o - n_e = -0.0091$ and calcite, $n_o - n_e = 0.172$ at $\lambda = 589.3$ nm (Jenkins and White 1976)). The existence in cubic crystals of this Lorentz birefringence, as it should be termed in his honour, was later confirmed on the basis of crystal symmetry, first by Lorentz himself (1922) and then by Condon and Seitz (1932), who pointed out certain incorrect

inferences on Lorentz's part. The origin of this birefringence cannot be explained in terms of anisotropy in the permittivity tensor, since this is isotropic for a cube. Lorentz presciently attributed the effect to the spatial nonuniformity, over the distance between scattering centres, of the electric field $\boldsymbol{E}$ of the light wave on account of its finite wavelength (Lorentz 1878). It is now known that Lorentz birefringence is due to the interaction between electric octopoles induced in matter and the second gradient of $\boldsymbol{E}$ and also between induced magnetic quadrupoles and the first gradient of the magnetic field $\boldsymbol{B}$ of the light (Graham and Raab 1990). While Lorentz birefringence and the familiar birefringence exhibited by uniaxial and biaxial crystals are both classified as linear, nevertheless there is a fundamental difference between them. The former is a manifestation of spatial dispersion, as the effect of nonuniformity of the light-wave field is now termed, whereas the latter arises from the interaction of $\boldsymbol{E}$, assumed to be uniform, with electric dipoles induced in matter. This will become evident in Section 1.2. As a consequence, the multipole descriptions of these two birefringences are quite different and so also are their orders of magnitude.

In addition to the above two types of linear birefringence, which exist relative to their respective fast and slow axes, there is the linear birefringence identified by Jones in the formulation of his optical calculus (Jones 1948). When this Jones birefringence exists, it does so in a macroscopically thin platelet of the crystal and is characterized by its fast and slow axes lying along the bisectors of those of a coexisting linear birefringence, which is manifest in another such platelet and without which the Jones birefringence would not be regarded as occurring. Theory has shown that Jones birefringence of electric-octopole–magnetic-quadrupole origin should be exhibited by certain nonmagnetic uniaxial and biaxial crystals quite independently of the normal linear birefringence in these crystals (Graham and Raab 1983; Graham, C. and Raab1994).

The first quantitative explanation of circular birefringence given by Gibbs (1882) was also in terms of spatial dispersion. The presently accepted theories of a range of optically active phenomena, including circular birefringence, all allow for spatial dispersion through the first gradient of $\boldsymbol{E}$ interacting with induced electric quadrupoles, while $\boldsymbol{B}$ interacts with induced magnetic dipoles (Nakano and Kimura 1969; Barron and Buckingham 1971; Buckingham and Dunn 1971; Raab and Cloete 1994). The typical order of magnitude of the circular birefringence $n_r - n_l$ in nonmagnetic crystals is 10^{-4}; for instance, in quartz it is 7.1×10^{-5} at $\lambda = 589.3$ nm for propagation along the optic axis (Jenkins and White 1976).

Just as there are distinct types of linear birefringence in terms of their different multipole descriptions, so there are also for circular birefringence. All ferromagnetic crystals exhibit this effect (Argyres 1955; Graham and Raab 1991a), which for them is of electric-dipole origin but involves a crystal property different from that of the electric-dipole tensor that describes the linear birefringence in nonmagnetic uniaxial and biaxial crystals (Graham and Raab 1991a). Furthermore, this circular birefringence, unlike that in nonmagnetic crystals, changes sign when the light path is reversed, as also happens in the Faraday effect. Such a nonreciprocal circular birefringence, as it is called, of even higher multipole order - namely, electric octopole–magnetic quadrupole - has been predicted for propagation along a body diagonal of certain antiferromagnetic cubic crystals, where it is the only effect to this multipole order (Graham and Raab 1991b).

In summary, the various birefringences and their orders of magnitude that may exist in a nonmagnetic crystal in terms of their induced multipole origins are classified in Table 1.1. Below a theory is presented, to the order of electric dipole, of the propagation of a plane monochromatic light wave in a nonmagnetic anisotropic dielectric. In the development and applications of this theory, no use is made of the ellipsoid model of crystal optics, to which the present approach is offered as an alternative. Furthermore, the context of this theory is the multipole description of optical effects in matter, which can be systematically extended to orders above electric dipole when this proves necessary for the explanation of certain effects in transmission, such as circular birefringence, both natural, discussed in Chapter 3, and electric-field-induced, described in Chapter 4. By contrast, the ellipsoid model, while it has its uses, is a dead end, which can be extended only approximately by treating higher-order effects as perturbations (Maldonado and Gaylord 1989). The multipole description, on the other hand, is an algebraic eigenvalue one that provides a direct means of determining, for an arbitrary propagation direction, the polarization eigenvectors that the medium supports, as well as their refractive indices. Furthermore, expressions for the various birefringences are generally analytic in form and, very desirably, are in terms of well-defined crystal properties, which then allow symmetry considerations to be applied to determine whether the particular effect exists in a crystal of given symmetry.

In Section 1.2 the basis of the multipole description of the effect of light-wave fields on matter is presented. This leads in Section 1.3 to the derivation, in the electric-dipole order, of the

Table 1.1 Multipole origin and order of magnitude of different birefringences in nonmagnetic crystals

Multipole origin	Birefringence type	Magnitude
Electric dipole	Linear (as in uniaxials and biaxials)	$\sim 10^{-1} - 10^{-2}$
Electric quadrupole–magnetic dipole	Circular	$\sim 10^{-4}$
Electric octopole–magnetic quadrupole	Linear (Lorentz in cubics; Jones)	$\sim 10^{-6}$

equation for wave propagation in a nonmagnetic anisotropic dielectric. Applications then follow in Sections 1.4 - 1.6, in which the effects of crystal symmetry on the light wave are analyzed.

1.2 Outline of the multipole approach

The wavelength of a plane monochromatic light wave, say, ~500 nm, is notably greater than the dimensions of a unit cell, typically 0.1 - 0.5 nm. In such a situation the use of an appropriate expansion is suggested. By Taylor-expanding the retarded vector potential $\mathbf{A}(\mathbf{r},t)$ at a point far from a finite distribution of time-changing currents, with the expansion being about an arbitrary origin inside the distribution, and by working in the long-wavelength limit, one can derive the multipole expansions of the $\boldsymbol{D}$ and $\boldsymbol{H}$ fields in Maxwell's equations (Graham *et al.* 1992). These are

$$D_\alpha = \varepsilon_o E_\alpha + P_\alpha - \tfrac{1}{2}\nabla_\beta Q_{\alpha\beta} + \tfrac{1}{6}\nabla_\gamma \nabla_\beta Q_{\alpha\beta\gamma} - \cdots, \tag{1.1}$$

$$H_\alpha = \mu_o^{-1} B_\alpha - M_\alpha + \tfrac{1}{2}\nabla_\beta M_{\alpha\beta} - \cdots. \tag{1.2}$$

Alternative derivations have also been reported (Rosenfeld 1951; Robinson 1973). In eqns. (1.1) and (1.2) Greek subscripts are used for Cartesian components of a tensor, with a repeated subscript denoting summation over the three components. Unless indicated otherwise, this convention is implied throughout this thesis. Also, $\boldsymbol{E}$ and $\boldsymbol{B}$ are the macroscopic electric and magnetic fields, respectively, of the light wave in the medium; P_α, $Q_{\alpha\beta}$, and $Q_{\alpha\beta\gamma}$ are the macroscopic electric-dipole, electric-quadruple, and electric-octopole moment densities, respectively; and M_α and $M_{\alpha\beta}$ are the corresponding quantities for magnetic dipole and quadrupole, respectively, as defined by Graham and Raab (1990). The multipole moment densities that arise from the same term in the expansion of $\mathbf{A}(\mathbf{r},t)$ have been paired in eqns. (1.1) and (1.2), and their contributions to a particular optical effect are thus of comparable magnitude.

Neither may be omitted.

At an instant of time the light wave at a macroscopic volume element of the medium comprises its $\boldsymbol{E}$ and $\boldsymbol{B}$ fields and also, to allow for spatial dispersion, their successive space derivatives. In addition, the wave possesses a series of time derivatives of each of these, but because of the harmonic condition in such terms as

$$\ddot{E}_\alpha = -\omega^2 E_\alpha, \quad \nabla_\beta \ddot{B}_\alpha = -\omega^2 \nabla_\beta \dot{B}_\alpha, \quad \text{etc.}, \tag{1.3}$$

where ω is the angular frequency of the light wave, only two of these successive time derivatives of a given field are independent. These may be taken to be the zeroth and the first. All the various space and time derivatives of the light-wave fields induce multipole moments in the volume element. For example, the electric-dipole moment density induced by a low-intensity light beam, for which nonlinear terms are negligible, may be written as

$$\begin{aligned} P_\alpha = {} & \alpha_{\alpha\beta} E_\beta + \frac{1}{\omega} \alpha'_{\alpha\beta} \dot{E}_\beta + \tfrac{1}{2} a_{\alpha\beta\gamma} \nabla_\gamma E_\beta + \frac{1}{2\omega} a'_{\alpha\beta\gamma} \nabla_\gamma \dot{E}_\beta \\ & + G_{\alpha\beta} B_\beta + \frac{1}{\omega} G'_{\alpha\beta} \dot{B}_\beta + \cdots, \end{aligned} \tag{1.4}$$

in which an established notation has been used (Buckingham 1967; de Figueiredo and Raab 1981; Barron 1982).

The quantities $\alpha_{\alpha\beta}$, $\alpha'_{\alpha\beta}$, $a_{\alpha\beta\gamma}$, . . . in eqn. (1.4) are well-defined macroscopic property tensors of the crystal, to each of which symmetry considerations may be applied to determine the number and nature of its components. Of these tensors the most familiar is the polarizability $\alpha_{\alpha\beta}$, which is related to the electric susceptibility $\chi_{\alpha\beta}$ by $\alpha_{\alpha\beta} = \varepsilon_o \chi_{\alpha\beta}$. Less well known are $a_{\alpha\beta\gamma}$ and $G'_{\alpha\beta}$, which together account for optical activity in nonmagnetic crystals (Graham and Raab 1990; Raab and Cloete 1994). The expression in eqn. (1.4) has an implicit multipole form, as may be formally seen from the quantum-mechanical expressions for its various property tensors (Graham and Raab 1991b; Appendix A) or, more intuitively, from the well-known interactions (Jackson 1975): (1) field with dipole moment and (2) first gradient of field with quadrupole moment.

Thus $\alpha_{\alpha\beta}$ and $\alpha'_{\alpha\beta}$ are of the order of electric dipole, $a_{\alpha\beta\gamma}$ and $a'_{\alpha\beta\gamma}$ of electric quadrupole, and $G_{\alpha\beta}$ and $G'_{\alpha\beta}$ of magnetic dipole. Since $\boldsymbol{P}$ in eqn. (1.4) is now seen to contain electric-quadrupole and magnetic-dipole terms, one should for consistency also include in eqns. (1.1) and (1.2) the induced forms of Q_{ij} and M_i, to the order of electric dipole, as the equivalent of eqn. (1.4).

However, as only electric-dipole terms are retained in this chapter, one has from eqns. (1.1), (1.2), and (1.4)

$$D_\alpha = \varepsilon_o E_\alpha + P_\alpha, \tag{1.5}$$

$$H_\alpha = \mu_o^{-1} B_\alpha, \tag{1.6}$$

$$P_\alpha = \alpha_{\alpha\beta} E_\beta + \frac{1}{\omega} \alpha'_{\alpha\beta} \dot{E}_\beta. \tag{1.7}$$

From the definition of the electric-dipole moment density

$$\boldsymbol{P} = \sum_n q\,\mathbf{r}/\Delta V, \tag{1.8}$$

where $\mathbf{r}$ is the displacement of charge q from an arbitrary origin inside the macroscopic volume element ΔV, it is evident that $\boldsymbol{P}$ is invariant under time reversal. So also from its definition is $\boldsymbol{E}$. It then follows from eqn. (1.7) that $\alpha_{\alpha\beta}$ is time-even and $\alpha'_{\alpha\beta}$ time-odd. Thus in terms of Neumann's principle (Birss 1966) the latter may not exist for a nonmagnetic medium, which by definition is time-even (Birss 1966).

The above discussion shows that the leading effect when a plane monochromatic light wave propagates in a nonmagnetic anisotropic medium is due to the polarizability $\alpha_{\alpha\beta}$, which is of electric-dipole order. This multipole order in such a medium is equivalent to the assumption that the electric field of the light wave is uniform over the volume element ΔV. Although the primary concern of this chapter is to derive the propagation characteristics of the wave in terms of the components of $\alpha_{\alpha\beta}$ for crystals of different symmetry, as an alternative to the ellipsoid model, the more general multipole approach has been outlined to indicate how the theory can be readily extended to explain other optical effects, such as circular, Lorentz, and Jones birefringences.

1.3 Wave equation in the electric-dipole order

It is convenient to express the electric field of a plane monochromatic light wave in the form

$$\boldsymbol{E} = \boldsymbol{E}^{(o)} \exp[-i\omega(t - n\,\mathbf{r}\cdot\sigma / c)], \tag{1.9}$$

where σ is the unit vector in the direction of propagation, which is along the wavefront normal, $\boldsymbol{E}^{(o)}$ is the field amplitude (in general, complex) for a particular polarization state, c is the vacuum speed of light, and n is the refractive index of the medium for the frequency, polarization, and direction of the light. As absorption is readily allowed for in the multipole approach, it is not neglected at this stage. Thus n may be assumed complex.

With eqn. (1.9) in the Maxwell equation

$$\nabla \times \boldsymbol{E} = -\dot{\boldsymbol{B}}, \tag{1.10}$$

one obtains the familiar result

$$\boldsymbol{B} = n\sigma \times \boldsymbol{E}/c. \tag{1.11}$$

Then substituting eqns. (1.5) - (1.7) with $\alpha'_{\alpha\beta} = 0$ for a nonmagnetic medium, eqn. (1.9), and eqn. (1.11) into the Maxwell equation for a source-free medium

$$\nabla \times \boldsymbol{H} = \dot{\boldsymbol{D}}, \tag{1.12}$$

one obtains

$$\left[n^2\sigma_\alpha\sigma_\beta - (n^2-1)\delta_{\alpha\beta} + \chi_{\alpha\beta}\right]E_\beta^{(o)} = 0. \tag{1.13}$$

In this the phase in eqn. (1.9) has been cancelled, $\delta_{\alpha\beta}$ is the Kronecker delta, and $\mu_o\varepsilon_o c^2 = 1$ and $\alpha_{\alpha\beta} = \varepsilon_o\chi_{\alpha\beta}$ were used.

Equation (1.13) is the wave equation, of the order of electric dipole, that describes the propagation in any direction of a low-intensity plane monochromatic light wave in a homogeneous nonmagnetic medium. With $\alpha = x, y$, and z in turn in eqn. (1.13), one obtains three linear and homogeneous equations in the unknown amplitude components $E_x^{(o)}$, $E_y^{(o)}$, and $E_z^{(o)}$, namely,

$$\left.\begin{aligned}
\left[n^2(\sigma_x^2-1)+1+\chi_{xx}\right]E_x^{(o)} + \left[n^2\sigma_x\sigma_y+\chi_{xy}\right]E_y^{(o)} + \left[n^2\sigma_x\sigma_z+\chi_{xz}\right]E_z^{(o)} &= 0,\\
\left[n^2\sigma_y\sigma_x+\chi_{yx}\right]E_x^{(o)} + \left[n^2(\sigma_y^2-1)+1+\chi_{yy}\right]E_y^{(o)} + \left[n^2\sigma_y\sigma_z+\chi_{yz}\right]E_z^{(o)} &= 0,\\
\left[n^2\sigma_z\sigma_x+\chi_{zx}\right]E_x^{(o)} + \left[n^2\sigma_z\sigma_y+\chi_{zy}\right]E_y^{(o)} + \left[n^2(\sigma_z^2-1)+1+\chi_{zz}\right]E_z^{(o)} &= 0.
\end{aligned}\right\} \tag{1.14}$$

These equations are relative to an arbitrary Cartesian frame and may be simplified by choosing principal axes for $\chi_{\alpha\beta}$. (This is possible since $\chi_{\alpha\beta}$ is a symmetric second-rank polar tensor, as its quantum-mechanical expression (Buckingham and Dunn 1971; Graham and Raab 1990; Appendix A) and its definition show. It may also be noted that the principal axes for $\chi_{\alpha\beta}$ coincide with the crystallographic axes for 27 of the 32 nonmagnetic point groups, the exceptions being the five triclinic and monoclinic symmetry classes (Birss 1966).) Equations (1.14) may be expressed as a matrix eigenvalue equation, which for principal axes has the form

$$\begin{bmatrix}
n^2(1-\sigma_x^2)-\chi_{xx} & -n^2\sigma_x\sigma_y & -n^2\sigma_x\sigma_z\\
-n^2\sigma_y\sigma_x & n^2(1-\sigma_y^2)-\chi_{yy} & -n^2\sigma_y\sigma_z\\
-n^2\sigma_z\sigma_x & -n^2\sigma_z\sigma_y & n^2(1-\sigma_z^2)-\chi_{zz}
\end{bmatrix}\begin{bmatrix}E_x^{(o)}\\E_y^{(o)}\\E_z^{(o)}\end{bmatrix} = \begin{bmatrix}E_x^{(o)}\\E_y^{(o)}\\E_z^{(o)}\end{bmatrix}. \tag{1.15}$$

Here the eigenvalues are unity, thus constraining n^2 to certain values for a given propagation direction. The polarization forms that may propagate, as described by the amplitude components $E_x^{(o)}$, $E_y^{(o)}$, and $E_z^{(o)}$, are then the eigenvectors corresponding to each n^2. Whatever the multipole order used in the theory, the wave equation can always be cast into an eigenvalue equation equivalent to eqn. (1.15) but with different multipole property tensors (Graham, C. and Raab 1994). The polarization eigenvectors are the only forms of the propagating wave that the medium supports for a given propagation direction. That these can be derived, to the required multipole order, from the corresponding eigenvalue equation is an advantage that the method offers.

Instead of solving eqn. (1.15), one may use the condition that for nontrivial solutions for the $E_i^{(o)}$ the determinant of their coefficients in the three eqns. (1.14) must vanish. For the principal axes for $\chi_{\alpha\beta}$ this condition is

$$\begin{vmatrix} n^2(\sigma_x^2-1)+1+\chi_{xx} & n^2\sigma_x\sigma_y & n^2\sigma_x\sigma_z \\ n^2\sigma_y\sigma_x & n^2(\sigma_y^2-1)+1+\chi_{yy} & n^2\sigma_y\sigma_z \\ n^2\sigma_z\sigma_x & n^2\sigma_z\sigma_y & n^2(\sigma_z^2-1)+1+\chi_{zz} \end{vmatrix} = 0. \qquad (1.16)$$

When multiplied out, this equation becomes

$$\begin{aligned} n^4(\varepsilon_x\sigma_x^2+\varepsilon_y\sigma_y^2+\varepsilon_z\sigma_z^2) - n^2[\varepsilon_x\varepsilon_y(\sigma_x^2+\sigma_y^2) \\ +\varepsilon_y\varepsilon_z(\sigma_y^2+\sigma_z^2)+\varepsilon_z\varepsilon_x(\sigma_z^2+\sigma_x^2)]+\varepsilon_x\varepsilon_y\varepsilon_z = 0, \end{aligned} \qquad (1.17)$$

where

$$\varepsilon_x = 1+\chi_{xx}, \quad \varepsilon_y = 1+\chi_{yy}, \quad \varepsilon_z = 1+\chi_{zz}. \qquad (1.18)$$

To the order of electric dipole, eqn. (1.17) has at most two distinct solutions for n^2 for an arbitrary propagation direction. (When the theory allows for higher multipole contributions, more than two roots of n^2 are possible. An example of this is given in eqn. (56) of the paper by Graham and Raab (1990) dealing with light propagation in cubic and other isotropic crystals. Such extra roots are associated with 'additional' rays, as they are termed, which have in fact been observed (Pekar 1983).) The two solutions of eqn. (1.17) are required on physical grounds to be real and positive in the absence of absorption. These two requirements must clearly be met by the formal approach of this thesis, which is embodied in eqn. (1.16), and it is shown that they are met in Appendix B.

For simplicity absorption is now neglected, as the ellipsoid model invariably does as well. Thus all the elements in the determinant in eqn. (1.16) are real, and as these are the coefficients of the

amplitude components in the three equations from which eqn. (1.16) is obtained, then the $E_i^{(o)}$ are also real. This implies from eqn. (1.9) that there are no phase differences between these components and thus that the electric-dipole theory presented here allows only linearly polarized beams to propagate. To find the particular polarization eigenvector that corresponds to a root of n^2, the value of n^2 is substituted into the three equations in $E_x^{(o)}$, $E_y^{(o)}$, and $E_z^{(o)}$ and these are solved for the $E_i^{(o)}$ components. For simple propagation directions the solution can usually be found by inspection of eqn. (1.16). This approach is applied in this Chapter in Sections 1.4 - 1.6 to crystals of different symmetry, of which there are three classes.

1.4 Crystals with equal principal components of $\chi_{\alpha\beta}$

Considered first are crystals whose symmetry is such that

$$\chi_{xx} = \chi_{yy} = \chi_{zz} = \chi. \tag{1.19}$$

From published tables of tensor components for the crystalline point groups (Birss 1966), it is evident that isotropy of $\chi_{\alpha\beta}$ occurs only for the five cubic classes, of which the point groups 23 and 432 are also optically active and thus fall outside the electric-dipole description. For an arbitrary propagation direction specified by σ, eqn. (1.17) yields two equal roots

$$n^2 = 1 + \chi = \varepsilon. \tag{1.20}$$

With this value in any one of the three equations on which eqn. (1.16) is based, one finds by inspection that

$$\sigma \cdot \boldsymbol{E}^{(o)} = 0. \tag{1.21}$$

Thus both eigenvectors propagate with transverse electric fields and, as shown in Section 1.3, are linearly polarized. Their relative orientation is not constrained by any result to this point. However, it can be shown algebraically that to the order of electric dipole the $\boldsymbol{D}$ fields of the two eigenpolarizations are mutually perpendicular for all σ (Yariv and Yeh 1984). Since to this multipole order $\boldsymbol{D} = \varepsilon \boldsymbol{E}$ for a cubic crystal, it follows that the two electric fields are also orthogonal for any propagation direction. Because eqn. (1.20) applies to both eigenpolarizations, no birefringence may occur for any propagation direction in cubic crystals when these are described by the present electric-dipole theory. This is not necessarily true to a higher multipole order. Indeed, one may note from tables of tensor components (Birss 1966) that for cubic crystals the tensors of rank 3 and 4 are not all isotropic. This admits the possibility that higher multipole contributions may give rise to birefringences for certain propagation directions, such as that found by Lorentz.

1.5 Crystals with two equal principal components of $\chi_{\alpha\beta}$

The two equal principal components of $\chi_{\alpha\beta}$ do not include the principal component corresponding to the axis of highest symmetry, which by crystallographic convention is taken to be the z-axis. Thus in this section

$$\chi_{xx} = \chi_{yy} \neq \chi_{zz}. \tag{1.22}$$

Tables (Birss 1966) show that eqn. (1.22) is satisfied for the hexagonal, trigonal, and tetragonal systems, which together contain 19 symmetry classes, including some optically active ones.

From eqns. (1.17), (1.18), and (1.22) the wave equation for an arbitrary propagation direction is

$$n^4\left[\varepsilon_x\left(1-\sigma_z^2\right)+\varepsilon_z\sigma_z^2\right]-n^2\varepsilon_x\left[\varepsilon_x\left(1-\sigma_z^2\right)+\varepsilon_z\left(1+\sigma_z^2\right)\right]+\varepsilon_x^2\varepsilon_z = 0. \tag{1.23}$$

Its solutions are

$$n_1^2 = \varepsilon_x, \tag{1.24}$$

$$n_2^2 = \frac{\varepsilon_x\varepsilon_z}{\varepsilon_x(1-\sigma_z^2)+\varepsilon_z\sigma_z^2}. \tag{1.25}$$

Thus the one ray travels with a refractive index that is independent of σ, called the ordinary or o-ray, while the other's refractive index depends, for a given medium, only on $\sigma_z = \cos\theta$, where θ is the angle between the propagation direction and the highest symmetry axis. This latter ray is the extraordinary or e-ray. Both rays are linearly polarized, as was shown in Section 1.3.

The electric-field amplitude, and hence the polarization form, of each of these rays is found from eqn. (1.16) by use of eqns. (1.24) and (1.25) in turn. For the o-ray the equations from which the first two rows of eqn. (1.16) are obtained yield by inspection

$$\sigma \cdot \boldsymbol{E}^{(o)} = 0, \tag{1.26}$$

while from the third row one finds

$$\varepsilon_x\sigma_x\sigma_z E_x^{(o)} + \varepsilon_x\sigma_y\sigma_z E_y^{(o)} + [\varepsilon_x(\sigma_z^2-1)+\varepsilon_z]E_z^{(o)} = 0. \tag{1.27}$$

With eqn. (1.26) this becomes

$$(\varepsilon_z - \varepsilon_x)E_z^{(o)} = 0, \tag{1.28}$$

so that $E_z^{(o)} = 0$. Thus for any given propagation direction the $\boldsymbol{E}$ field of the o-ray is purely transverse and polarized in the xy-plane, that is, in the plane perpendicular to the main symmetry axis. It follows from eqn. (1.26) that $E_x^{(o)}$ and $E_y^{(o)}$ are related by

$$\sigma_x E_x^{(o)} + \sigma_y E_y^{(o)} = 0. \tag{1.29}$$

Then

$$\boldsymbol{E}^{(o)} = E_x^{(o)}(1,\ -\sigma_x/\sigma_y,\ 0) = E_y^{(o)}(-\sigma_y/\sigma_x,\ 1,\ 0). \tag{1.30}$$

From the alternative forms in eqn. (1.30) for the linear polarization of the *o*-ray, we note that for *x*-propagation, $\sigma_x = 1$, $\sigma_y = 0$ and the $\boldsymbol{E}$ field vibrates parallel to the principal *y*-axis, while for *y*-propagation the wave is *x*-polarized. For *z*-propagation each of the three equations from which eqn. (1.16) is derived is satisfied by either of the transverse components $E_x^{(o)}$ and $E_y^{(o)}$. Accordingly, any polarization form propagates unchanged along the main symmetry axis, at least when higher multipole effects, including optical activity, are neglected. This conclusion also applies to *e*-ray propagation along the *z*-axis because eqns. (1.24) and (1.25) are identical when $\sigma_z = 1$.

The equivalent procedure for the *e*-ray yields from the equation corresponding to the third row of eqn. (1.16)

$$\varepsilon_x(\sigma_x E_x^{(o)} + \sigma_y E_y^{(o)}) + \varepsilon_z \sigma_z E_z^{(o)} = 0. \tag{1.31}$$

Adding and subtracting $\varepsilon_x\sigma_z E_z^{(o)}$, one finds

$$\varepsilon_x \sigma \cdot \boldsymbol{E}^{(o)} + (\varepsilon_z - \varepsilon_x)\sigma_z E_z^{(o)} = 0, \tag{1.32}$$

which shows that $\sigma\cdot\boldsymbol{E}^{(o)} \neq 0$ for the *e*-ray unless $\sigma_z = 0$ or $E_z^{(o)} = 0$. Thus the electric field of the *e*-ray is not transverse except when propagation is perpendicular to the axis of highest symmetry ($\sigma_z = 0$) or along this axis, since $E_z^{(o)} = 0$ for the latter direction, as shown above. Then substituting eqns. (1.25) and (1.31) into each of the equations on which the first two rows of eqn. (1.16) are based leads to the same result, namely,

$$\sigma_y E_x^{(o)} = \sigma_x E_y^{(o)}. \tag{1.33}$$

From eqns. (1.31) and (1.33)

$$E_z^{(o)} = -\frac{\varepsilon_x(\sigma_x^2 + \sigma_y^2)}{\varepsilon_z \sigma_x \sigma_z} E_x^{(o)} = -\frac{\varepsilon_x(\sigma_x^2 + \sigma_y^2)}{\varepsilon_z \sigma_y \sigma_z} E_y^{(o)}. \tag{1.34}$$

Then the amplitude of the electric field of an *e*-ray has components

$$\begin{aligned} \boldsymbol{E}^{(o)} &= E_x^{(o)}\left[1,\ \sigma_y/\sigma_x,\ -\varepsilon_x(\sigma_x^2 + \sigma_y^2)/(\varepsilon_z\sigma_x\sigma_z)\right] \\ &= E_y^{(o)}\left[\sigma_x/\sigma_y,\ 1,\ -\varepsilon_x(\sigma_x^2 + \sigma_y^2)/(\varepsilon_z\sigma_y\sigma_z)\right]. \end{aligned} \tag{1.35}$$

This represents a linear polarization that is perpendicular to that of the *o*-ray, as is evident from eqns. (1.30) and (1.35).

The acute angle ϕ between σ and the $\boldsymbol{E}$ field of an *e*-ray follows from

$$\sigma \cdot \boldsymbol{E}^{(o)} = E^{(o)} \cos\phi, \tag{1.36}$$

when eqns. (1.32), (1.34), and (1.35) are used. Then

$$\cos\phi = \sigma_z(\varepsilon_z - \varepsilon_x)\left[\frac{1-\sigma_z^2}{\varepsilon_x^2(1-\sigma_z^2)+\varepsilon_z^2\sigma_z^2}\right]^{\frac{1}{2}}. \tag{1.37}$$

As is required, $\phi = \pi/2$ for $\sigma_z = 0$ or $\sigma_z = 1$ or $\varepsilon_z = \varepsilon_x$. The angle between the Poynting vector $\boldsymbol{N} = \boldsymbol{E} \times \boldsymbol{H}$ (the ray direction) of the *e*-ray and σ is the complement of ϕ. This can be confirmed by evaluating $\boldsymbol{N}\cdot\sigma$ with eqns. (1.6), (1.11), and (1.35).

From eqns. (1.24) and (1.25) it is evident that only for propagation along the main symmetry axis does $n_1 = n_2$. A propagation axis for which no linear birefringence occurs is termed an optic axis. For this reason the crystals to which eqn. (1.22) applies are classed as uniaxial. However, this classification may not hold for higher multipole orders. Certain magnetic uniaxial classes exhibit linear birefringence along their main symmetry axis, owing to electric-quadrupole–magnetic-dipole contributions (Graham and Raab 1992), although no nonmagnetic uniaxial crystal loses its optic axis to this or even the next multipole order (Graham, C. and Raab 1994).

1.6 Crystals with three unequal principal components of $\chi_{\alpha\beta}$

Here principal axes are chosen such that

$$\chi_{xx} > \chi_{yy} > \chi_{zz}, \tag{1.38}$$

in which there is no ambiguity, since the three components may be taken as positive, as explained in Appendix B. From tables of tensor components (Birss 1966) it is evident that the principal components of $\chi_{\alpha\beta}$ are unequal for the orthorhombic, monoclinic, and triclinic systems. However, the ordering in eqn. (1.38) is not determined by symmetry, which is unable to assign magnitudes to quantities. From eqns. (1.18) and (1.38)

$$\varepsilon_x > \varepsilon_y > \varepsilon_z. \tag{1.39}$$

The two refractive indices for an arbitrary propagation direction can be determined from eqn. (1.17), and then their corresponding linearly polarized eigenvectors can be found from the three equations on which eqn. (1.16) is based. (An alternative solution for the eigenvectors is given in Appendix C). Despite the generality of this approach, it is possible to derive certain features of the transmission process that are characteristic of the crystal symmetries implied by eqn. (1.38).

To begin with, it is determined whether such crystals possess optic axes. For there to be no linear birefringence in a propagation direction specified by σ, the two roots of eqn. (1.17) must be equal. Thus from eqn. (B.1) in Appendix B

$$b^2 - 4ac = 0. \tag{1.40}$$

There are three possibilities to consider for σ.

1.6.1 None of σ_x, σ_y, σ_z is zero

It follows from eqns. (B.7), (B.12), and (B.14) that

$$b^2 - 4ac \neq 0. \tag{1.41}$$

Thus there is necessarily birefringence for such a propagation direction.

1.6.2 One of σ_x, σ_y, σ_z is zero

a. First take $\sigma_x = 0$, so that from eqn. (B.10)

$$\sigma_y^2 + \sigma_z^2 = 1. \tag{1.42}$$

Then from eqns. (B.6) - (B.9) and (1.42)

$$b^2 - 4ac = \left[\varepsilon_y(\varepsilon_x - \varepsilon_z)\sigma_y^2 + \varepsilon_z(\varepsilon_x - \varepsilon_y)\sigma_z^2\right]^2. \tag{1.43}$$

Because of eqn. (1.39) this cannot equal zero, thus implying that birefringence will occur when light propagates in the principal *yz*-plane.

b. For $\sigma_y = 0$ and from eqn. (B.10)

$$\sigma_x^2 + \sigma_z^2 = 1. \tag{1.44}$$

It follows from eqns. (B.6) - (B.9) and (1.44) that

$$b^2 - 4ac = \left[\varepsilon_x(\varepsilon_y - \varepsilon_z)\sigma_x^2 - \varepsilon_z(\varepsilon_x - \varepsilon_y)\sigma_z^2\right]^2. \tag{1.45}$$

Because of the ordering in eqn. (1.39), it is now possible for $b^2 - 4ac$ to vanish for certain propagation directions in the principal xz-plane. From eqn. (1.45) there are two such directions given by

$$\sigma_{oa} = \left\{ \left[\frac{\varepsilon_z(\varepsilon_x - \varepsilon_y)}{\varepsilon_y(\varepsilon_x - \varepsilon_z)} \right]^{\frac{1}{2}}, \; 0, \; \pm \left[\frac{\varepsilon_x(\varepsilon_y - \varepsilon_z)}{\varepsilon_y(\varepsilon_x - \varepsilon_z)} \right]^{\frac{1}{2}} \right\}, \tag{1.46}$$

in which eqn. (1.44) was used.

c. When $\sigma_z = 0$, it can be shown from eqns. (B.6) - (B.9) that, as for the case $\sigma_x = 0$, $b^2 - 4ac$ does not vanish.

1.6.3 Two of σ_x, σ_y, σ_z are zero

For each of the possibilities here it follows from eqns. (B.6) - (B.9) that eqn. (1.40) is not satisfied. Thus birefringence occurs for propagation along a principal axis, since such directions are implied by this example.

The above analysis shows that for crystals with three different principal components of $\chi_{\alpha\beta}$ there are, to the order of electric dipole, only two propagation directions that are free of linear birefringence. These are therefore the optic axes, and for the ordering in eqn. (1.38) they lie in the principal xz-plane with directions given by eqn. (1.46). Such crystals are said to be biaxial. To locate the two optic axes in the xz-plane, we note that the angle θ between either one, as specified by eqn. (1.46), and the unit vector $\hat{\mathbf{z}}$ along the positive z-axis is given by

$$\sigma_{oa} \cdot \hat{\mathbf{z}} = \cos\theta = \pm \left[\frac{\varepsilon_x(\varepsilon_y - \varepsilon_z)}{\varepsilon_y(\varepsilon_x - \varepsilon_z)} \right]^{\frac{1}{2}}. \tag{1.47}$$

Thus both the optic axes make the same acute angle θ with the z-axis.

The two identical refractive indices for propagation among an optic axis may be found from eqns. (B.1) - (B.3) and (1.46), which for both axes yield

$$n^2 = (b/2a) = \varepsilon_y. \tag{1.48}$$

Their corresponding eigenpolarizations are obtained by substituting eqns. (1.48) and (1.46) into the three equations from which eqn. (1.16) is derived and are

$$\boldsymbol{E}_1^{(o)} = (0,\ 1,\ 0), \tag{1.49}$$

$$\boldsymbol{E}_2^{(o)} = ([\varepsilon_z(\varepsilon_y - \varepsilon_z)]^{\frac{1}{2}},\ 0,\ \mp[\varepsilon_x(\varepsilon_x - \varepsilon_y)^{\frac{1}{2}}])[\varepsilon_z(\varepsilon_y - \varepsilon_z) + \varepsilon_x(\varepsilon_x - \varepsilon_y)]^{\frac{1}{2}}. \tag{1.50}$$

Each of these two linear polarizations has unit amplitude, and they are clearly orthogonal. It is also apparent that $\boldsymbol{E}_1^{(o)}$ is orthogonal to the propagation direction along either optic axis, given by eqn. (1.46), whereas $\boldsymbol{E}_2^{(o)}$ is not. If required, the angle between $\boldsymbol{E}_2^{(o)}$ and σ_{oa} can be found from $\boldsymbol{E}_2^{(o)} \cdot \sigma_{oa}$.

Consider now propagation in any principal plane, say, the *xy*-plane with

$$\sigma = (\sigma_x,\ \sigma_y,\ 0). \tag{1.51}$$

Then eqn. (1.16) becomes

$$\begin{vmatrix} n^2(\sigma_x^2 - 1) + \varepsilon_x & n^2\sigma_x\sigma_y & 0 \\ n^2\sigma_x\sigma_y & n^2(\sigma_y^2 - 1) + \varepsilon_y & 0 \\ 0 & 0 & -n^2 + \varepsilon_z \end{vmatrix} = 0, \tag{1.52}$$

in which eqns. (1.18) and (1.51) were used. Inspection of the third row of the determinant yields

$$n_1^2 = \varepsilon_z, \qquad \boldsymbol{E}_1^{(o)} = (0,\ 0,\ 1). \tag{1.53}$$

From the remaining 2 × 2 determinantal equation one finds

$$n_2^2 = \frac{\varepsilon_x\varepsilon_y}{\varepsilon_x\sigma_x^2 + \varepsilon_y\sigma_y^2}, \qquad \boldsymbol{E}_2^{(o)} = (\varepsilon_y\sigma_y,\ -\varepsilon_x\sigma_x,\ 0)[\varepsilon_x^2\sigma_x^2 + \varepsilon_y^2\sigma_y^2]^{-\frac{1}{2}}. \tag{1.54}$$

It is evident that the two linearly polarized eigenvectors, whose normalized amplitudes appear in eqns. (1.53) and (1.54), are orthogonal, as are $\boldsymbol{E}_1^{(o)}$ and σ but not $\boldsymbol{E}_2^{(o)}$ and σ in eqn. (1.51).

The eigenvector in eqn. (1.53) possesses two features that are characteristic of an *o*-ray in a uniaxial crystal: namely, that for an arbitrary propagation direction σ its refractive index is independent of σ and its polarization is perpendicular to σ. Because the eigenvector in eqns. (1.54) has neither of these properties, it resembles the *e*-ray in a uniaxial crystal. Conclusions similar to those for propagation in the *xy*-plane apply to the two other principal planes in a biaxial crystal.

It has been shown above that for any propagation direction in a principal plane of a biaxial crystal

the two eigenvectors are orthogonal. This is also true for uniaxial crystals for a quite general propagation direction. The question may then be asked, whether the eigenvectors in a biaxial crystal are mutually perpendicular for any propagation direction. A related question also arises: since one of the eigenvectors is orthogonal to σ for propagation in a principal plane of a biaxial crystal, as it is also in general for cubics and uniaxials, does this orthogonality apply for any propagation direction in a biaxial crystal? Appendix C shows that the answer to both of these is in the negative.

1.7 Discussion

The traditional explanation of optical effects in nonabsorbing crystals begins with Maxwell's equations and the assumed constitutive relations (Born and Wolf 1980)

$$D_\alpha = \varepsilon_{\alpha\beta} E_\beta, \tag{1.55}$$

$$H_\alpha = \mu^{-1} B_\alpha, \tag{1.56}$$

where $\varepsilon_{\alpha\beta}$ is the permittivity tensor and μ the permeability. Alternatively, for crystals that are neither ferromagnetic nor absorbing, the approximation is sometimes made that (Nye 1985)

$$\mu \approx \mu_o. \tag{1.57}$$

From either of these approaches the wave equation for a plane monochromatic light wave is then derived. The algebraic from of this equation is characteristic of an ellipsoid. Because of this the analytic description is invariably abandoned and instead the behaviour of a polarized light beam propagating in any given direction in a crystal is explained geometrically in terms of the properties of an ellipsoid. This approach raises a number of difficulties. First, the assumed relations in eqns. (1.55) and (1.56) contain the contradiction of a medium that is electrically anisotropic but magnetically isotropic, while the alternative involves the approximation in eqn. (1.57). Neither of these difficulties would arise if the ellipsoid model were recognized for what it is, namely, the electric-dipole description of light propagation. To this order, eqn. (1.56) is replaced by

$$H_\alpha = \mu_o^{-1} B_\alpha, \tag{1.58}$$

as eqns. (1.1) and (1.2) show, and the anomaly falls away. Second, the ellipsoid explanation of propagation effects, especially for an arbitrary direction in a biaxial crystal, becomes extremely complicated (see, for example, Figure 14.3 in Born and Wolf 1980), whereas, and admittedly this is a matter of opinion, an analytic approach is easier to follow and certainly lends itself to detailed calculation when this is required (see Appendix C and Chapter 2).

Perhaps the most serious difficulty associated with the ellipsoid model is, paradoxically, its very success in explaining the normal linear birefringence in uniaxial and biaxial crystals. Because of this it seems to be regarded as the basis for accounting for other birefringences, for instance, circular and field induced, as perturbations of the ellipsoid model (Maldonado and Gaylord 1988, 1989), whereas these can be treated analytically in the appropriate multipole theory. When the ellipsoid explanation is regarded in this way, it becomes the dead end referred to earlier, blocking the way to the proper description of these other effects.

No mention has been made so far of the impermeability tensor $\eta_{\alpha\beta}$ (Yariv and Yeh 1984). As the inverse of the permittivity tensor $\varepsilon_{\alpha\beta}$, it leads, by means of Maxwell's equations, to its own ellipsoid surface, known as the indicatrix. Various proofs exist, based on the symmetry of $\eta_{\alpha\beta}$, which derives from that of $\varepsilon_{\alpha\beta}$, of the orthogonality of the $\boldsymbol{D}$ fields of the two polarized eigenvectors (Ramachandran and Ramaseshan 1961; Yariv and Yeh 1984). In connection with one of these proofs appears a statement that the mutual orthogonality of the two $\boldsymbol{D}$ vectors and σ '*can be used as a coordinate system for the description of many physical phenomena, including optical activity*' (Yariv and Yeh 1984, page 75). However, optical activity is only properly described in the electric-quadrupole–magnetic-dipole order (Buckingham and Dunn 1971; Barron 1982; Raab and Cloete 1994) for which

$$D_\alpha = \varepsilon_{\alpha\beta} E_\beta , \tag{1.59}$$

where

$$\varepsilon_{\alpha\beta} = \varepsilon_o \delta_{\alpha\beta} + \alpha_{\alpha\beta} + \frac{in}{c} \sigma_\gamma [G'_{\alpha\delta} \in_{\beta\gamma\delta} + \tfrac{1}{2} \omega (a_{\alpha\beta\gamma} - a_{\beta\alpha\gamma})]. \tag{1.60}$$

Here, $\in_{\alpha\beta\gamma}$ is the Levi-Civita tensor. The electric-quadrupole and magnetic-dipole terms in eqn. (1.60), $a_{\alpha\beta\gamma}$ and $G'_{\alpha\beta}$, respectively, destroy the intrinsic symmetry of subscripts of $\varepsilon_{\alpha\beta}$ in eqn. (1.60), which $\varepsilon_{\alpha\beta}$ possesses in the electric-dipole order for a nonabsorbing medium. Consequently $\eta_{\alpha\beta}$ is not symmetric, nor, being complex, is it even Hermitian, so that the above proofs of the orthogonality of the two $\boldsymbol{D}$ eigenvectors do not apply in general to optical activity.

The birefringences that may be manifest in a crystal for a given propagation direction are a consequence of its point group symmetry. For instance, while quartz (point group 32) exhibits circular birefringence along its optic axis, among other directions, potassium dihydrogen phosphate ($\bar{4}2m$) does so for all directions except the optic axis (Nye 1985). And again: for cubic crystals with $m3m$ and $\bar{4}3m$ symmetry, Lorentz birefringence does not occur for propagation

along a cube edge, whereas it does in the cubic class $m3$ (Graham and Raab 1990). How does one predict such effects? The broad answer is to derive, in the appropriate multipole order, the wave equation that is equivalent to that in eqn. (1.16) and then from its two regular solutions for n_1^2 and n_2^2 for a given propagation direction to obtain an expression for the birefringence $n_1 - n_2$ in terms of components of multipole polarizability tensors. The point groups for which these components may exist can then be identified from tables. In this procedure it is imperative to work with valid property tensors (Birss 1966), otherwise symmetry considerations may not apply. (A property tensor is a constant of proportionality between specific physical *cause* and *effect* tensors, such as $\nabla_\gamma E_\beta$ and P_α in eqn. (1.4), for which $a_{\alpha\beta\gamma}$ is the relevant property tensor.) In eqn. (1.59) $\boldsymbol{D}$ is not a unique vector in general as can be seen by applying Helmoltz's theorem to Maxwell's equations. Accordingly, $\boldsymbol{D}$ is not a property tensor, nor therefore is $\varepsilon_{\alpha\beta}$ in eqn. (1.60), even though $\alpha_{\alpha\beta}$, $a_{\alpha\beta\gamma}$, and $G'_{\alpha\beta}$ in it are. It is evident that the use of a permittivity tensor to describe optical activity and other higher-order multipole effects may well lead to erroneous conclusions (Agranovich and Ginzburg 1984; Graham and Raab 1990).

Chapter 2

AN ALGEBRAIC DETERMINATION OF THE PRINCIPAL REFRACTIVE INDICES AND AXES IN THE ELECTRO-OPTIC EFFECT

2.1 Introduction

Transparent materials used in electro-optic devices are generally characterized by their field-free refractive indices relative to principal dielectric axes and also by their electro-optic coefficients at the wavelength of the light. These latter properties describe the dependence, usually of the impermeability tensor, on the first and, in some instances, the second power of either an applied uniform field or an alternating field whose frequency is such that the field is effectively constant in the material at an instant of time. Through its effect on the impermeability tensor of a dielectric the electric field may induce different optical behaviour; for example, a cubic crystal may be rendered biaxial (Kaminow and Turner 1966) with new principal dielectric axes rotated from the original ones (Namba 1961). A systematic means of determining the new principal refractive indices and axes in the presence of the field is a useful aid in the design and optimization of electro-optic devices. An algebraic theory, based on expressing the indicatrix equation in powers of the applied field, has been used to analyze the design requirements for modulating such properties as amplitude, phase, and frequency of a light wave in crystals of various symmetries (Kaminow and Turner 1966). Once the principal refractive indices and axes

of a crystal in the presence of the electric field are known, the polarization and refractive index for each of the two polarization eigenvectors that correspond to a particular propagation direction can be determined by standard procedures as done in Chapter 1 (see also Yariv and Yeh 1984). A general algebraic solution of this problem was given by Nelson (1975), which was also applied to other perturbations of the impermeability tensor but which for a biaxial crystal produces, by the author's admission, a complicated expression, incapable of simplification, for the refractive indices of the two eigenwaves. Similarly, Brandão Farla (1993a) considered in an algebraic treatment of the index ellipsoid approach the influence of an external perturbation on the refractive indices and axes of an isotropic medium. This was later generalized for the electro-optic effect (Brandão Farla 1993b), and examples were given for the linear electro-optic effect in biaxial and uniaxial crystals for specific field directions.

Numerous experimental values of the linear and quadratic electro-optic coefficients are reported in the literature for a variety of crystals (Landolt-Börnstein 1979, 1984). The most detailed attempt to date to use this information to determine, for any given crystal symmetry and field direction, the principal refractive indices and axes is that of Maldonado and Gaylord (1988). Their approach to this problem, which involves numerical processing of the experimental data, is claimed to be general to the extent that it is applicable to both the linear and quadratic electro-optic effects in cubic, uniaxial, and biaxial crystals in a field of arbitrary direction. However, the illustrations of their method are only for the linear effect in cubics and uniaxials and then for fields in simple directions. Being numerical rather than algebraic, the procedure suffers from certain drawbacks: it may require numerous iterations, as many as seven being reported in one example calculation and five in another; as will be apparent later, it does not distinguish between linear and quadratic field contributions to a principal refractive index and eigenvector, with the result that incorrect conclusions are drawn in some instances; and the calculations must be repeated for each different crystal of the same symmetry. By contrast, an algebraic treatment based on symmetry offers the considerable advantage that, even in the absence of experimental values for the refractive indices and electro-optic coefficients of a crystal of given symmetry, its optical nature to a given order in the field can nevertheless be determined.

The theory of an approach, which allows for the effects of symmetry, is presented in Section 2.2 and applied in later sections. This approach lends itself readily to analysis by algebraic means, yielding quantitative expressions, to a given order in the field, for the principal refractive indices

and their corresponding eigenvectors in terms of the applied field and of the relevant electro-optic coefficients. Instead of an expansion of the impermeability in powers of the field as in the work of Maldonado and Gaylord (1988), allowance is made for the perturbation by the field of the electric-dipole polarizability tensor. Although these procedures are equivalent in the present context, there are reasons for this preference: the use of various multipole polarizability tensors in theories of a range of optical effects is well established and successful. By contrast, the impermeability tensor and the index ellipsoid model based on it are incapable of explaining optical activity, both natural (Buckingham and Dunn 1971; Barron 1982; Raab and Cloete 1994) and electric-field-induced (Gunning and Raab 1997b; see also Chapter 4); Lorentz birefringence (Graham, C. and Raab 1994); light scattering in chiral systems (Barron 1982); etc., all of which require the inclusion in their theory of multipoles of higher order than electric dipole. An additional reason for the current preference is that quantum-mechanical expressions have been derived for many of the relevant optical polarizability tensors (Buckingham 1967; Graham and Raab 1991b; see also Appendix A), which provide useful information, in particular any permutation symmetry of tensor subscripts and relationships between different tensors.

2.2 Theory

The Fresnel ellipsoid model for describing the propagation of a plane monochromatic light wave in a homogeneous nonabsorbing dielectric can be derived from Maxwell's equations and the constitutive relations given in eqns. (1.5) and (1.6) (Nye 1985)

$$D_\alpha = \varepsilon_o E_\alpha + P_\alpha , \tag{2.1}$$

$$H_\alpha = \mu_o^{-1} B_\alpha , \tag{2.2}$$

where $\boldsymbol{E}$ and $\boldsymbol{B}$ are the electric and magnetic fields, respectively, of the light wave. The polarization $\boldsymbol{P}$ induced in a nonmagnetic medium by a low-intensity beam for which nonlinear effects are negligible, may be expressed as (see Section 1.2)

$$P_\alpha = \alpha_{\alpha\beta} E_\beta \tag{2.3}$$

in the absence of an applied field. In eqn. (2.3) $\alpha_{\alpha\beta}$ is the electric-dipole polarizability density at the frequency of the light, which is related to the electric susceptibility $\chi_{\alpha\beta}$ by

$$\alpha_{\alpha\beta} = \varepsilon_o \chi_{\alpha\beta} . \tag{2.4}$$

The quantum-mechanical expression for $\alpha_{\alpha\beta}$ (Buckingham 1967; Appendix A) shows that it is symmetric in its two subscripts, while from its definition in eqn. (2.3) it is a polar tensor, since $\boldsymbol{P}$ and $\boldsymbol{E}$ are. Thus principal axes may always be found for $\alpha_{\alpha\beta}$ (Birss 1966). Also, since $\alpha_{\alpha\beta}$, and

thus $\chi_{\alpha\beta}$, is a second-rank tensor, it may be represented by a 3 × 3 symmetric matrix whose elements are the nine tensor components.

Now let a weak uniform electric field **E** act in the medium such that there is only a linear perturbation. Then eqn. (2.3) becomes

$$P_\alpha = \alpha_{\alpha\beta}(\mathbf{E})E_\beta, \tag{2.5}$$

where $\alpha_{\alpha\beta}(\mathbf{E})$ is the polarizability in the presence of the field, which to first order in **E** may be expressed as (Buckingham and Pople 1955)

$$\alpha_{\alpha\beta}(\mathbf{E}) = \alpha_{\alpha\beta} + \tfrac{1}{2}\beta_{\alpha\beta\gamma}\mathrm{E}_\gamma + \cdots. \tag{2.6}$$

Known as the linear electro-optic coefficient or as the first hyperpolarizability tensor (Buckingham and Pople 1955), $\beta_{\alpha\beta\gamma}$ is a polar tensor, as eqns. (2.5) and (2.6) show, while from its quantum-mechanical expression it follows that (Buckingham and Longuet-Higgins 1968; Appendix A)

$$\beta_{\alpha\beta\gamma} = \beta_{\beta\alpha\gamma}. \tag{2.7}$$

Thus $\alpha_{\alpha\beta}(\mathbf{E})$ is also a symmetric polar tensor for which principal axes exist, although not necessarily the same as those for the unperturbed polarizability $\alpha_{\alpha\beta}$. In the absence of absorption, which we assume for simplicity, all quantities in eqn. (2.6) are real.

The principal refractive indices n_i, i = x, y, and z, of the field-free crystal are given by (Yariv and Yeh 1984)

$$n_i^2 = 1 + \chi_{ii} = 1 + \varepsilon_o^{-1}\alpha_{ii}, \quad i = x, y, z. \tag{2.8}$$

Thus n_i^2 - 1 are the eigenvalues of the real symmetric 3 × 3 matrix $[\varepsilon_o^{-1}\alpha_{\alpha\beta}]$, and the principal axes of $\alpha_{\alpha\beta}$ are its eigenvectors. The purpose of the present work is to determine the eigenvalues and eigenvectors of the field-perturbed 3 × 3 matrix $[\varepsilon_o^{-1}\alpha_{\alpha\beta}(\mathbf{E})]$, which is also real and symmetric and which, relative to principal axes for $\alpha_{\alpha\beta}$ and to first order in **E**, has the form

$$[\varepsilon_o^{-1}\alpha_{\alpha\beta}(\mathbf{E})] = \begin{bmatrix} n_x^2 - 1 + b_{xx\gamma}\mathrm{E}_\gamma & b_{xy\gamma}\mathrm{E}_\gamma & b_{xz\gamma}\mathrm{E}_\gamma \\ b_{xy\gamma}\mathrm{E}_\gamma & n_y^2 - 1 + b_{yy\gamma}\mathrm{E}_\gamma & b_{yz\gamma}\mathrm{E}_\gamma \\ b_{xz\gamma}\mathrm{E}_\gamma & b_{yz\gamma}\mathrm{E}_\gamma & n_z^2 - 1 + b_{zz\gamma}\mathrm{E}_\gamma \end{bmatrix}. \tag{2.9}$$

In deriving this eqns. (2.6) and (2.8) were used, and also introduced for convenience is the tensor $b_{\alpha\beta\gamma}$, defined below in eqn. (2.10), where its components are related to those of the electro-optic coefficient $r_{\alpha\beta\gamma}$ that describes the linear perturbation of the impermeability tensor by (Yariv and Yeh 1984)

$$b_{ijk} = (2\varepsilon_o)^{-1}\beta_{ijk} = -n_i^2 n_j^2 r_{ijk}. \tag{2.10}$$

For convenience in later sections we assume r_{ijk} to be positive, as indeed it is for most of the data presented in Yariv and Yeh (1984). The eigenvalues of the matrix in eqn. (2.9) may be written as

$$\lambda = n^2 - 1 \tag{2.11}$$

and found in the usual way from the determinantal equation

$$\left|\varepsilon_o^{-1}\alpha_{\alpha\beta}(\mathbf{E}) - \lambda I\right| = \begin{vmatrix} n_x^2 + b_{xx\gamma}E_\gamma - n^2 & b_{xy\gamma}E_\gamma & b_{xz\gamma}E_\gamma \\ b_{xy\gamma}E_\gamma & n_y^2 + b_{yy\gamma}E_\gamma - n^2 & b_{yz\gamma}E_\gamma \\ b_{xz\gamma}E_\gamma & b_{yz\gamma}E_\gamma & n_z^2 + b_{zz\gamma}E_\gamma - n^2 \end{vmatrix} = 0, \tag{2.12}$$

where I is the 3 × 3 unit matrix. Because of the form of eqn. (2.12), n^2 rather than n^2 - 1 may be regarded as the eigenvalues to be found. The eigenvectors **r** may then be determined by substituting in turn each eigenvalue into the three linear and homogeneous equations in the unknown components of **r**, whose coefficients are the elements of the determinant in eqn. (2.12), and then solving these three simultaneous equations. In simple cases the solution can be found by inspection. The **r** eigenvectors are the principal axes of $\alpha_{\alpha\beta}(\mathbf{E})$ relative to those of $\alpha_{\alpha\beta}$, and the angles between the two sets of axes may be determined readily from the scalar products of their respective direction unit vectors.

The solution of eqn. (2.12) may be simplified by exploiting the symmetry of the crystal, in particular, with regard to the allowed components of $\alpha_{\alpha\beta}$ and $b_{\alpha\beta\gamma}$. For instance, since $b_{\alpha\beta\gamma}$ is an odd-rank polar tensor, it vanishes identically for centrosymmetric crystals relative to axes with the origin at the centre. Crystal properties are generally referred to crystallographic Cartesian axes, for which tables of components of tensors up to rank four have been published for the 32 point groups of nonmagnetic crystals (Birss 1966), with the convention that the z-axis coincides with that of highest symmetry. These axes also serve as principal axes for $\alpha_{\alpha\beta}$ for all cubic and uniaxial crystals but not, with the exception of the orthorhombic classes, for biaxials. Thus although eqn. (2.12) applies to all symmetry classes, its $b_{\alpha\beta\gamma}$ components for the five monoclinic and triclinic point groups cannot be directly determined from tables such as those in Birss (1966). (Transformation from crystallographic to principal axes for $\alpha_{\alpha\beta}$ would be necessary.)

In Sections 2.3 - 2.6 the linear electro-optic behaviour of four different crystal symmetry classes is determined from eqn. (2.12) for certain simple field directions. The first three of these crystal

symmetries, and also the field configurations chosen, are those treated previously by Maldonado and Gaylord in their numerical procedure based on the general Jacobi method (Maldonado and Gaylord 1988). Whereas these authors offered no illustration of their procedure for a biaxial crystal, an application of the algebraic approach to the biaxial class of lowest symmetry, namely, 1 is presented in Section 2.6. A simple result is obtained for a field direction used in a recent experiment by Salvestrini *et al.* (1994).

To illustrate the applicability of the algebraic method to the quadratic electro-optic (or Kerr) effect, a single case study is analyzed in Section 2.7, where terms in both E and E^2 are included. This serves to demonstrate that erroneous conclusions may be reached when only contributions linear in E are included in the numerical approach.

2.3 The optically inactive cubic class $\bar{4}3m$

A well-known electro-optic crystal with this point group symmetry is gallium arsenide. From tables (Birss 1966) the only nonvanishing components of $\alpha_{\alpha\beta}$ and $b_{\alpha\beta\gamma}$ for this class are

$$\alpha_{xx} = \alpha_{yy} = \alpha_{zz}, \tag{2.13}$$

$$b_{xyz} = b_{yzx} = b_{zxy} = b_{xzy} = b_{zyx} = b_{yxz} = b. \tag{2.14}$$

Thus from eqn. (2.8),

$$n_x^2 = n_y^2 = n_z^2 = n_o^2. \tag{2.15}$$

Then eqn. (2.12) becomes

$$\begin{vmatrix} n_o^2 - n^2 & bE_z & bE_y \\ bE_z & n_o^2 - n^2 & bE_x \\ bE_y & bE_x & n_o^2 - n^2 \end{vmatrix} = 0. \tag{2.16}$$

2.3.1 First field direction

As in the work by Maldonado and Gaylord (1988) three different field directions are considered. The first field is taken to be

$$\mathbf{E} = (0, 0, E). \tag{2.17}$$

For it eqn. (2.16) reduces to

$$\begin{vmatrix} n_o^2 - n^2 & bE & 0 \\ bE & n_o^2 - n^2 & 0 \\ 0 & 0 & n_o^2 - n^2 \end{vmatrix} = 0. \tag{2.18}$$

By inspection the eigenvalues and corresponding normalized eigenvectors are exactly

$$n_1^2 = n_o^2 - bE, \qquad \mathbf{r}_1 = (-1,\ 1,\ 0)/\sqrt{2}, \tag{2.19}$$

$$n_2^2 = n_o^2, \qquad \mathbf{r}_2 = (0,\ 0,\ 1), \tag{2.20}$$

$$n_3^2 = n_o^2 + bE, \qquad \mathbf{r}_3 = (1,\ 1,\ 0)/\sqrt{2}. \tag{2.21}$$

Because the field-perturbed crystal has three different principal refractive indices, it is now biaxial. Its eigenvectors $\mathbf{r}_1$, $\mathbf{r}_2$, and $\mathbf{r}_3$ constitute, in that order, a right-handed mutually orthogonal set of unit vectors and serve as the axes of the Fresnel ellipsoid which describes the propagation of light through the crystal. Relative to these axes and with n_2 the intermediate of the three refractive indices, the two optic axes lie in the $\mathbf{r}_1\mathbf{r}_3$-plane and have the directions of the unit vectors (Klein 1970)

$$\sigma = \left(\left[\frac{n_3^2 (n_1^2 - n_2^2)}{n_2^2 (n_1^2 - n_3^2)} \right]^{\frac{1}{2}},\ 0,\ \pm \left[\frac{n_1^2 (n_2^2 - n_3^2)}{n_2^2 (n_1^2 - n_3^2)} \right]^{\frac{1}{2}} \right) \tag{2.22}$$

$$= \left(\left[(n_o^2 + bE)/2n_o^2 \right]^{\frac{1}{2}},\ 0,\ \pm \left[(n_o^2 - bE)/2n_o^2 \right]^{\frac{1}{2}} \right). \tag{2.23}$$

In the paper by Maldonado and Gaylord (1988) the acute angle θ is calculated between either optic axis and the principal axis associated with n_1^2 in eqn. (2.19), which is specified in its own reference frame as $\hat{\mathbf{X}} = (1,\ 0,\ 0)$, consistent with the choice implicit in eqn. (2.22). Then

$$\theta = \cos^{-1} \sigma \cdot \hat{\mathbf{X}} = \cos^{-1} \left[\frac{n_3^2 (n_1^2 - n_2^2)}{n_2^2 (n_1^2 - n_3^2)} \right]^{\frac{1}{2}} \tag{2.24}$$

$$= \cos^{-1} \left[(n_o^2 + bE)/2n_o^2 \right]^{\frac{1}{2}}. \tag{2.25}$$

Thus θ is not precisely 45°, which is the value reported by Maldonado and Gaylord (1988).

2.3.2 Second field direction

$$\mathbf{E} = (E,\ E,\ 0)/\sqrt{2}. \tag{2.26}$$

With this field in eqn. (2.16) one obtains

$$\begin{vmatrix} n_o^2 - n^2 & 0 & bE/\sqrt{2} \\ 0 & n_o^2 - n^2 & bE/\sqrt{2} \\ bE/\sqrt{2} & bE/\sqrt{2} & n_o^2 - n^2 \end{vmatrix} = 0. \tag{2.27}$$

Exact solutions of this are readily found; namely,

$$n_1^2 = n_o^2 - bE, \qquad \mathbf{r}_1 = (1,\ 1,\ -\sqrt{2})/2, \tag{2.28}$$

$$n_2^2 = n_o^2, \qquad \mathbf{r}_2 = (1,\ -1,\ 0)/\sqrt{2}, \tag{2.29}$$

$$n_3^2 = n_o^2 + bE, \qquad \mathbf{r}_3 = (1,\ 1,\ \sqrt{2})/2. \tag{2.30}$$

Here, also, the crystal is biaxial, with the eigenvectors forming a right-handed orthonormal system. When referred to the eigenvalues, the directions of the two optic axes are those in eqn. (2.23), and the acute angle θ between either optic axis and that associated with n_1^2 in eqn. (2.28) is given by eqn. (2.25).

2.3.3 Third field direction

$$\mathbf{E} = (E,\ E,\ E)/\sqrt{3}. \tag{2.31}$$

Equation (2.16) can be solved exactly for the field in eqn. (2.31), yielding

$$n_1^2 = n_o^2 - bE/\sqrt{3}, \qquad \mathbf{r}_1 = (1,\ -1,\ 0)/\sqrt{2}, \tag{2.32}$$

$$n_2^2 = n_o^2 - bE/\sqrt{3}, \qquad \mathbf{r}_2 = (1,\ 1,\ -2)/\sqrt{6}, \tag{2.33}$$

$$n_3^2 = n_o^2 + 2bE/\sqrt{3}, \qquad \mathbf{r}_3 = (1,\ 1,\ 1)/\sqrt{3}. \tag{2.34}$$

Because n_1^2 and n_2^2 are degenerate, their respective eigenvectors are not unique. Those in eqns. (2.32) and (2.33) were chosen for simplicity and such that $\mathbf{r}_1$, $\mathbf{r}_2$, and $\mathbf{r}_3$ form a right-handed orthonormal set. With two equal refractive indices the crystal in the field in eqn. (2.31) is uniaxial, its optic axis lying along $\mathbf{r}_3$, parallel to **E**. If, as for gallium arsenide, the sign of b is negative (Yariv and Yeh 1984), then the crystal is negative uniaxial.

For the three field directions used above, the expressions for the principal indices of refraction agree with those derived by Namba (1961) for the ellipsoid model. However, not all the corresponding eigenvectors are presented explicitly in the work by Namba to allow comparison.

2.4 The optically inactive uniaxial class 3*m*

An example of an electro-optic crystal that belongs to this class is lithium niobate. The only components of $\alpha_{\alpha\beta}$ and $b_{\alpha\beta\gamma}$ that exist for it are (Birss 1966)

$$\alpha_{xx} = \alpha_{yy}, \ \alpha_{zz}, \tag{2.35}$$

$$\left.\begin{aligned} &b_{yyy}, \ b_{zzz}, \ b_{xxy} = b_{xyx} = b_{yxx} = -b_{yyy}, \\ &b_{xxz} = b_{yyz}, \ b_{xzx} = b_{zxx} = b_{yzy} = b_{zyy}. \end{aligned}\right\} \tag{2.36}$$

Thus there are two independent components of $\alpha_{\alpha\beta}$ and four of $b_{\alpha\beta\gamma}$. From eqns. (2.8) and (2.35)

$$n_x^2 = n_y^2 = n_o^2 = 1 + \varepsilon_o^{-1}\alpha_{xx}, \tag{2.37}$$

$$n_z^2 = n_e^2 = 1 + \varepsilon_o^{-1}\alpha_{zz}, \tag{2.38}$$

where n_o and n_e are the refractive indices for the ordinary and extraordinary rays, respectively.

For an arbitrary field direction, eqn. (2.12) becomes

$$\begin{vmatrix} n_o^2 - b_1 E_y + b_3 E_z - n^2 & -b_1 E_x & b_4 E_x \\ -b_1 E_x & n_o^2 + b_1 E_y + b_3 E_z - n^2 & b_4 E_y \\ b_4 E_x & b_4 E_y & n_e^2 + b_2 E_z - n^2 \end{vmatrix} = 0, \tag{2.39}$$

where from eqns. (2.10) and (2.36)

$$b_1 = b_{yyy}, \ b_2 = b_{zzz}, \ b_3 = b_{xxz}, \ b_4 = b_{zxx}. \tag{2.40}$$

2.4.1 First field direction

The field is now applied in the three directions considered by Maldonado and Gaylord. The first is

$$\mathbf{E} = (0, 0, E). \tag{2.41}$$

Off-diagonal elements in eqn. (2.39) vanish for the field in eqn. (2.41). Exact eigenvalues and eigenvectors can then be found by inspection. These are

$$n_1^2 = n_o^2 + b_3 E, \qquad \mathbf{r}_1 = (1, 0, 0), \tag{2.42}$$

$$n_2^2 = n_o^2 + b_3 E, \qquad \mathbf{r}_2 = (0, 1, 0), \tag{2.43}$$

$$n_3^2 = n_e^2 + b_2 E, \qquad \mathbf{r}_3 = (0, 0, 1). \tag{2.44}$$

The eigenvectors $\mathbf{r}_1$ and $\mathbf{r}_2$ are not unique on account of the degeneracy of n_1^2 and n_2^2. Their orthonormal forms in eqns. (2.42) and (2.43) were chosen for simplicity. Because $n_1^2 = n_2^2 \neq n_3^2$, the field-perturbed crystal remains uniaxial with its optic axis given by $\mathbf{r}_3$ in eqn. (2.44), so that

it coincides with that of the field-free crystal. The refractive index expressions obtained from eqns. (2.42) - (2.44) agree to first order in **E** with those which follow from an algebraic expansion, for this specific field geometry, of the index ellipsoid (see, for example, Yariv and Yeh 1984).

2.4.2 Second field direction

This field direction is presented as

$$\mathbf{E} = (0, \mathrm{E}, 0). \tag{2.45}$$

For this field, eqn. (2.39) becomes

$$\begin{vmatrix} n_o^2 - b_1\mathrm{E} - n^2 & 0 & 0 \\ 0 & n_o^2 + b_1\mathrm{E} - n^2 & b_4\mathrm{E} \\ 0 & b_4\mathrm{E} & n_e^2 - n^2 \end{vmatrix} = 0. \tag{2.46}$$

Neglecting terms quadratic in **E** in the solution of the 2 × 2 determinantal equation contained in eqn. (2.46), namely,

$$\begin{vmatrix} n_o^2 + b_1\mathrm{E} - n^2 & b_4\mathrm{E} \\ b_4\mathrm{E} & n_e^2 - n^2 \end{vmatrix} = 0, \tag{2.47}$$

one obtains the following eigenvalues and their corresponding right-handed orthonormal eigenvectors:

$$n_1^2 = n_o^2 - b_1\mathrm{E}, \qquad \mathbf{r}_1 = (1,\ 0,\ 0), \tag{2.48}$$

$$n_2^2 = n_o^2 + b_1\mathrm{E}, \qquad \mathbf{r}_2 = \left(0,\ 1,\ \frac{b_4\mathrm{E}}{n_o^2 - n_e^2}\right), \tag{2.49}$$

$$n_3^2 = n_e^2, \qquad \mathbf{r}_3 = \left(0,\ -\frac{b_4\mathrm{E}}{n_o^2 - n_e^2},\ 1\right). \tag{2.50}$$

With three different refractive indices the crystal in the field in eqn. (2.45) is biaxial. These indices are numbered in eqns. (2.48) - (2.50) such that, for the experimental values of n_o, n_e, and b_1 that apply to lithium niobate for a wavelength of 632.8 nm (Yariv and Yeh 1984), the conventional order is followed; namely,

$$n_1 > n_2 > n_3. \tag{2.51}$$

Then eqn. (2.22) applies, with the angle θ between either optic axis and the principal axis associated with n_1^2 given by eqn. (2.24), which from eqns. (2.48) - (2.50) becomes

$$\theta = \cos^{-1}\left[\frac{-2n_e^2 b_1\mathrm{E}}{(n_o^2 + b_1\mathrm{E})(n_o^2 - b_1\mathrm{E} - n_e^2)}\right]^{\frac{1}{2}}. \tag{2.52}$$

2.4.3 Third field direction

The third field direction is

$$\mathbf{E} = (\mathrm{E}, 0, 0). \tag{2.53}$$

Here eqn. (2.39) reduces to

$$\begin{vmatrix} n_o^2 - n^2 & -b_1\mathrm{E} & b_4\mathrm{E} \\ -b_1\mathrm{E} & n_o^2 - n^2 & 0 \\ b_4\mathrm{E} & 0 & n_e^2 - n^2 \end{vmatrix} = 0. \tag{2.54}$$

Because the eigenvalues n^2 are not immediately evident from eqn. (2.54), we assume solutions to quadratic order in $\mathbf{E}$ that have the correct limiting forms for zero field; namely,

$$n_1^2 - (n_o^3 + a_1\mathrm{E} + a_2\mathrm{E}^2) = 0, \tag{2.55}$$

$$n_2^2 - (n_o^3 + a_3\mathrm{E} + a_4\mathrm{E}^2) = 0, \tag{2.56}$$

$$n_3^2 - (n_e^3 + a_5\mathrm{E} + a_6\mathrm{E}^2) = 0. \tag{2.57}$$

Then the product of the left-hand sides of eqns. (2.55) - (2.57), when compared with eqn. (2.54), yields

$$a_1 = -b_1, \; a_3 = b_1, \; a_5 = 0. \tag{2.58}$$

The same results are obtained when terms quadratic in $\mathbf{E}$, which are allowed by symmetry, are included in eqn. (2.6) and hence in eqn. (2.54). With the neglect of $\mathbf{E}^2$ contributions in eqns. (2.55) - (2.57), the eigenvalues and eigenvectors are then

$$n_1^2 = n_o^2 - b_1\mathrm{E}, \qquad \mathbf{r}_1 = k_1\left(1 - \frac{b_4^2\mathrm{E}}{2b_1(n_o^2 - n_e^2)}, \; 1, \; \frac{b_4\mathrm{E}}{n_o^2 - n_e^2}\right)\Big/\sqrt{2}, \tag{2.59}$$

$$n_2^2 = n_o^2 + b_1\mathrm{E}, \qquad \mathbf{r}_2 = k_2\left(-1 - \frac{b_4^2\mathrm{E}}{2b_1(n_o^2 - n_e^2)}, \; 1, \; -\frac{b_4\mathrm{E}}{n_o^2 - n_e^2}\right)\Big/\sqrt{2}, \tag{2.60}$$

$$n_3^2 = n_e^2, \qquad \mathbf{r}_3 = \left(-\frac{b_4\mathrm{E}}{n_o^2 - n_e^2}, \; 0, \; 1\right), \tag{2.61}$$

where

$$k_1 = \left[1 - \frac{b_4^2\mathrm{E}}{2b_1(n_o^2 - n_e^2)}\right]^{-\frac{1}{2}}, \tag{2.62}$$

and

$$k_2 = \left[1 + \frac{b_4^2\mathrm{E}}{2b_1(n_o^2 - n_e^2)}\right]^{-\frac{1}{2}}, \tag{2.63}$$

are normalization constants. These eigenvectors represent, to first order in the field, a system of orthogonal right-handed unit vectors. Thus in this field the crystal is biaxial and, with the same expressions for the principal refractive indices as those in eqns. (2.48) - (2.50), the angle θ is then also given by eqn. (2.52).

2.5 The nonenantiomorphous uniaxial class $\bar{4}2m$

Much studied members of this class are potassium dihydrogen phosphate (KDP) and its isomorphs, which form the subject of the experimental work in the second part of this thesis. They are known to exhibit optical activity for propagation along any direction except the optic axis. Linear birefringence also occurs for such directions, but as it is typically two orders of magnitude greater than circular birefringence (Table 1.1), we neglect the latter, as did Maldonado and Gaylord, in determining the principal refractive indices and axes for different field configurations.

The nonvanishing components of $\alpha_{\alpha\beta}$ and $b_{\alpha\beta\gamma}$ for the class $\bar{4}2m$ are (Birss 1966)

$$\alpha_{xx} = \alpha_{yy}, \ \alpha_{zz}, \tag{2.64}$$

$$b_{xyz} = b_{yxz}, \ b_{xzy} = b_{yzx} = b_{zxy} = b_{zyx}. \tag{2.65}$$

Because this symmetry class is uniaxial, eqns. (2.37) and (2.38) also apply to it. For the components in eqn. (2.65) and for the field in an arbitrary direction, eqn. (2.12) becomes

$$\begin{vmatrix} n_o^2 - n^2 & b_1 E_z & b_2 E_y \\ b_1 E_z & n_o^2 - n^2 & b_2 E_x \\ b_2 E_y & b_2 E_x & n_e^2 - n^2 \end{vmatrix} = 0. \tag{2.66}$$

Here

$$b_1 = b_{xyz}, \ b_2 = b_{xzy}. \tag{2.67}$$

2.5.1 First field direction

For KDP Maldonado and Gaylord considered five different field directions, and these are also treated here, particularly as a significant difference comes to light. The first of these field directions is

$$\mathbf{E} = (0, 0, E). \tag{2.68}$$

Equation (2.66) takes on a simple form which on inspection yields the following exact

eigenvalues and eigenvectors:

$$n_1^2 = n_o^2 - b_1 E, \qquad \mathbf{r}_1 = (1, -1, 0)/\sqrt{2}, \tag{2.69}$$

$$n_2^2 = n_o^2 + b_1 E, \qquad \mathbf{r}_2 = (1, 1, 0)/\sqrt{2}, \tag{2.70}$$

$$n_3^2 = n_e^2, \qquad \mathbf{r}_3 = (0, 0, 1). \tag{2.71}$$

Thus when the field is applied parallel to the optic axis, a crystal with $\bar{4}2m$ symmetry becomes biaxial. For the experimental values of n_o, n_e, and b_1 for KDP at a wavelength of 632.8 nm (Landolt-Börnstein 1979; Ghosh and Bhar 1982), the crystal's three principal refractive indices in eqns. (2.69) - (2.71) are ordered as in eqn. (2.51), and since they have the same expressions as those in eqns. (2.48) - (2.50), the angle θ which either optic axis makes with $\mathbf{r}_1$ is also given by eqn. (2.52).

2.5.2 Second field direction

This field direction is

$$\mathbf{E} = (0, E, 0). \tag{2.72}$$

Here eqn. (2.66) reduces to

$$\begin{vmatrix} n_o^2 - n^2 & 0 & b_2 E \\ 0 & n_o^2 - n^2 & 0 \\ b_2 E & 0 & n_e^2 - n^2 \end{vmatrix} = 0. \tag{2.73}$$

When terms quadratic in **E** are included in the calculation but only those linear in **E** are retained in the solution, one finds

$$n_1^2 = n_o^2, \qquad \mathbf{r}_1 = \left(1, 0, \frac{b_2 E}{n_o^2 - n_e^2}\right), \tag{2.74}$$

$$n_2^2 = n_o^2, \qquad \mathbf{r}_2 = (0, 1, 0), \tag{2.75}$$

$$n_3^2 = n_e^2, \qquad \mathbf{r}_3 = \left(-\frac{b_2 E}{n_o^2 - n_e^2}, 0, 1\right). \tag{2.76}$$

Thus in this approximation the field in eqn. (2.72) has no effect on the principal refractive indices, but, despite the degeneracy of n_1^2 and n_2^2, does lead to a system of unique right-handed orthonormal eigenvectors.

2.5.3 Third field direction

Consider the field

$$\mathbf{E} = (\mathrm{E},\ 0,\ 0). \tag{2.77}$$

Following an approach similar to that used for the field in eqn. (2.72), we obtain

$$n_1^2 = n_o^2, \qquad \mathbf{r}_1 = (1,\ 0,\ 0), \tag{2.78}$$

$$n_2^2 = n_o^2, \qquad \mathbf{r}_2 = \left(0,\ 1,\ \frac{b_2\mathrm{E}}{n_o^2 - n_e^2}\right), \tag{2.79}$$

$$n_3^2 = n_e^2, \qquad \mathbf{r}_3 = \left(0,\ -\frac{b_2\mathrm{E}}{n_o^2 - n_e^2},\ 1\right). \tag{2.80}$$

As before, $\mathbf{r}_1$, $\mathbf{r}_2$, and $\mathbf{r}_3$ constitute a right-handed orthonormal set of vectors.

2.5.4 Fourth field direction

Here the fourth field is taken to be

$$\mathbf{E} = (\mathrm{E},\ \mathrm{E},\ 0)/\sqrt{2}. \tag{2.81}$$

For this field eqn. (2.66) has the form

$$\begin{vmatrix} n_o^2 - n^2 & 0 & b_2\mathrm{E}/\sqrt{2} \\ 0 & n_o^2 - n^2 & b_2\mathrm{E}/\sqrt{2} \\ b_2\mathrm{E}/\sqrt{2} & b_2\mathrm{E}/\sqrt{2} & n_e^2 - n^2 \end{vmatrix} = 0. \tag{2.82}$$

Once again it can be proved that on neglecting terms quadratic in **E** the eigenvalues have their field-free values, so that the crystal remains uniaxial. By contrast, Maldonado and Gaylord indicate that it is biaxial in this field. An explanation of this difference is given in Section 2.7. The eigenvalues and orthonormal eigenvectors for this field geometry are

$$n_1^2 = n_o^2, \qquad \mathbf{r}_1 = (1,\ -1,\ 0)/\sqrt{2}, \tag{2.83}$$

$$n_2^2 = n_o^2, \qquad \mathbf{r}_2 = \left(1,\ 1,\ \frac{\sqrt{2}b_2\mathrm{E}}{n_o^2 - n_e^2}\right)\Big/\sqrt{2}, \tag{2.84}$$

$$n_3^2 = n_e^2, \qquad \mathbf{r}_3 = \left(-\frac{b_2\mathrm{E}}{n_o^2 - n_e^2},\ -\frac{b_2\mathrm{E}}{n_o^2 - n_e^2},\ \sqrt{2}\right)\Big/\sqrt{2}. \tag{2.85}$$

2.5.5 Fifth field direction

This field direction is given by

$$\mathbf{E} = (\mathrm{E},\ \mathrm{E},\ \mathrm{E})/\sqrt{3}\,. \tag{2.86}$$

Here eqn. (2.66) becomes

$$\begin{vmatrix} n_o^2 - n^2 & b_1\mathrm{E}/\sqrt{3} & b_2\mathrm{E}/\sqrt{3} \\ b_1\mathrm{E}/\sqrt{3} & n_o^2 - n^2 & b_2\mathrm{E}/\sqrt{3} \\ b_2\mathrm{E}/\sqrt{3} & b_2\mathrm{E}/\sqrt{3} & n_e^2 - n^2 \end{vmatrix} = 0. \tag{2.87}$$

For trial solutions of the same form as those in eqns. (2.55) - (2.57) it is straightforward to show that

$$a_1 = -b_1/\sqrt{3}\,,\ a_3 = b_1/\sqrt{3}\,,\ a_5 = 0. \tag{2.88}$$

Then retaining terms linear in **E** yields the eigenvalues and eigenvectors

$$n_1^2 = n_o^2 - b_1\mathrm{E}/\sqrt{3}\,, \qquad \mathbf{r}_1 = (1,\ -1,\ 0)/\sqrt{2}\,, \tag{2.89}$$

$$n_2^2 = n_o^2 + b_1\mathrm{E}/\sqrt{3}\,, \qquad \mathbf{r}_2 = \left(1,\ 1,\ \frac{2b_2\mathrm{E}}{\sqrt{3}(n_o^2 - n_e^2)}\right)\Big/\sqrt{2}\,, \tag{2.90}$$

$$n_3^2 = n_e^2\,, \qquad \mathbf{r}_3 = \left(-\frac{b_2\mathrm{E}}{\sqrt{3}(n_o^2 - n_e^2)},\ -\frac{b_2\mathrm{E}}{\sqrt{3}(n_o^2 - n_e^2)},\ 1\right). \tag{2.91}$$

so that the crystal is now biaxial. When n_1, n_2, and n_3 satisfy eqn. (2.51), the optic axes lie in the plane of $\mathbf{r}_1$ and $\mathbf{r}_3$ and make the same acute angle θ with $\mathbf{r}_1$, which from eqns. (2.24) and (2.89) - (2.91) is

$$\theta = \cos^{-1}\left[\frac{(n_o^2 - b_1\mathrm{E}/\sqrt{3})(-2b_1\mathrm{E}/\sqrt{3})}{(n_o^2 + b_1\mathrm{E}/\sqrt{3})(n_o^2 - b_1\mathrm{E}/\sqrt{3} - n_e^2)}\right]^{\frac{1}{2}}. \tag{2.92}$$

It follows from the above examples for the uniaxial class $\bar{4}2m$ that changes to the principal indices of refraction, which are linear in an applied field **E**, are induced only when **E** has a component along the main symmetry axis z. Perpendicular components of **E** on the other hand, cause the principal dielectric axes to rotate. These fundamental conclusions are not immediately evident from the numerical approach by Maldonado and Gaylord (1988).

2.6 The noncentrosymmetric biaxial class 1

The algebraic approach presented in this paper may also be applied to the biaxial classes, despite their low symmetry. To illustrate this the point group 1 is considered, which possesses no symmetry at all and therefore exhibits the linear electro-optic effect. A crystal belonging to this class, which received special attention recently on account of the very large linear electro-optic effect it displays, is rubidium hydrogen selenate (Salvestrini *et al.* 1994). This was studied experimentally in the field

$$\mathbf{E} = (0, \mathrm{E}, 0), \tag{2.93}$$

for which eqn. (2.12) is now solved for its linear electro-optic characteristics. Because of its total lack of symmetry, the class 1 has no zero components for $b_{\alpha\beta\gamma}$, as tables for crystallographic axes show (Birss 1966). Accordingly, relative to principal axes for $\alpha_{\alpha\beta}$ for which eqn. (2.12) applies, all 27 components of $b_{\alpha\beta\gamma}$ exist for an arbitrary optical wavelength, although some are related because of eqns. (2.7) and (2.10). For a biaxial crystal (Birss 1966)

$$\alpha_{xx} \neq \alpha_{yy} \neq \alpha_{zz}, \tag{2.94}$$

so that from eqns. (2.8), (2.12), and (2.93)

$$\begin{vmatrix} n_x^2 + b_1\mathrm{E} - n^2 & b_4\mathrm{E} & b_5\mathrm{E} \\ b_4\mathrm{E} & n_y^2 + b_2\mathrm{E} - n^2 & b_6\mathrm{E} \\ b_5\mathrm{E} & b_6\mathrm{E} & n_z^2 + b_3\mathrm{E} - n^2 \end{vmatrix} = 0. \tag{2.95}$$

In this section,

$$\left.\begin{aligned} b_1 &= b_{xxy},\ b_2 = b_{yyy},\ b_3 = b_{zzy}, \\ b_4 &= b_{xyy},\ b_5 = b_{xzy},\ b_6 = b_{yzy}. \end{aligned}\right\} \tag{2.96}$$

Taking trial solutions of the form of those in eqns. (2.55) - (2.57), one finds

$$a_1 = b_1,\ a_2 = b_2,\ a_3 = b_3. \tag{2.97}$$

Thus to first order in **E** the eigenvalues and their associated orthonormal eigenvectors are

$$n_1^2 = n_x^2 + b_1\mathrm{E}, \qquad \mathbf{r}_1 = \left(1,\ \frac{b_4\mathrm{E}}{n_x^2 - n_y^2},\ -\frac{b_5\mathrm{E}}{n_z^2 - n_x^2}\right), \tag{2.98}$$

$$n_2^2 = n_y^2 + b_2\mathrm{E}, \qquad \mathbf{r}_2 = \left(-\frac{b_4\mathrm{E}}{n_x^2 - n_y^2},\ 1,\ \frac{b_6\mathrm{E}}{n_y^2 - n_z^2}\right), \tag{2.99}$$

$$n_3^2 = n_z^2 + b_3\mathrm{E}, \qquad \mathbf{r}_3 = \left(\frac{b_5\mathrm{E}}{n_z^2 - n_x^2},\ -\frac{b_6\mathrm{E}}{n_y^2 - n_z^2},\ 1\right). \tag{2.100}$$

The eigenvalues in eqns. (2.98) - (2.100) illustrate a more general result: the off-diagonal elements in the first-order determinant in eqn. (2.12) for a biaxial crystal do not contribute to the first-order eigenvalues. Thus n_1^2, n_2^2, and n_3^2 may be found by inspection. This is the simple result referred to in Section 2.2.

2.7 The quadratic electro-optic effect in $\bar{4}2m$ crystals

To extend the theory in Section 2.2 to describe the quadratic electro-optic effect, the field-perturbed polarizability in eqn. (2.6) is expressed as (Buckingham and Pople 1955)

$$\alpha_{\alpha\beta}(\mathbf{E}) = \alpha_{\alpha\beta} + \tfrac{1}{2}\beta_{\alpha\beta\gamma}E_\gamma + \tfrac{1}{6}\gamma_{\alpha\beta\gamma\delta}E_\gamma E_\delta + \cdots . \tag{2.101}$$

In this $\gamma_{\alpha\beta\gamma\delta}$ is the quadratic electro-optic coefficient or second hyperpolarizability tensor (Buckingham and Pople 1955) and possesses the following intrinsic symmetry (Buckingham and Longuet-Higgins 1968):

$$\gamma_{\alpha\beta\gamma\delta} = \gamma_{\beta\alpha\gamma\delta} = \gamma_{\alpha\beta\delta\gamma} . \tag{2.102}$$

Then the three principal refractive indices n are found from the extension of eqn. (2.12):

$$\begin{vmatrix} n_x^2 + b_{xx\gamma}E_\gamma + c_{xx\gamma\delta}E_\gamma E_\delta - n^2 & b_{xy\gamma}E_\gamma + c_{xy\gamma\delta}E_\gamma E_\delta & b_{xz\gamma}E_\gamma + c_{xz\gamma\delta}E_\gamma E_\delta \\ b_{xy\gamma}E_\gamma + c_{xy\gamma\delta}E_\gamma E_\delta & n_y^2 + b_{yy\gamma}E_\gamma + c_{yy\gamma\delta}E_\gamma E_\delta - n^2 & b_{yz\gamma}E_\gamma + c_{yz\gamma\delta}E_\gamma E_\delta \\ b_{xz\gamma}E_\gamma + c_{xz\gamma\delta}E_\gamma E_\delta & b_{yz\gamma}E_\gamma + c_{yz\gamma\delta}E_\gamma E_\delta & n_z^2 + b_{zz\gamma}E_\gamma + c_{zz\gamma\delta}E_\gamma E_\delta - n^2 \end{vmatrix} = 0, \tag{2.103}$$

in which (Yariv and Yeh 1984)

$$c_{ijkl} = (6\varepsilon_o)^{-1}\gamma_{ijkl} = -n_i^2 n_j^2 g_{ijkl} , \tag{2.104}$$

where $g_{\alpha\beta\gamma\delta}$ is the quadratic equivalent of $r_{\alpha\beta\gamma}$.

As an example of its use, eqn. (2.103) is applied to a crystal of the class $\bar{4}2m$ in a field

$$\mathbf{E} = (E,\ E,\ 0)/\sqrt{2} ,$$

since it is for this situation that the finding of Maldonado and Gaylord differs qualitatively from that in Subsection 2.5.4. These authors conclude that the crystal becomes biaxial in the field, whereas this work finds it to be unaffected to first order in **E** and so remains uniaxial.

For this symmetry class one notes by means of tables (Birss 1966) that the only nonvanishing components of $c_{\alpha\beta\gamma\delta}$ that enter eqn. (2.103) for the applied field are

$$c_{xxxx} = c_{yyyy},\ c_{yyxx} = c_{xxyy},\ c_{xyxy},\ c_{zzxx} = c_{zzyy}. \tag{2.105}$$

Then from eqn. (2.66) it follows that eqn. (2.103) becomes

$$\begin{vmatrix} n_o^2 + c_1 E^2 - n^2 & c_2 E^2 & b_2 E/\sqrt{2} \\ c_2 E^2 & n_o^2 + c_1 E^2 - n^2 & b_2 E/\sqrt{2} \\ b_2 E/\sqrt{2} & b_2 E/\sqrt{2} & n_e^2 + c_3 E^2 - n^2 \end{vmatrix} = 0, \tag{2.106}$$

where

$$c_1 = \tfrac{1}{2}(c_{xxxx} + c_{yyxx}),\ c_2 = c_{xyxy},\ c_3 = c_{zzxx}. \tag{2.107}$$

The principal refractive indices and axes can then be determined from eqn. (2.106) and to second order in **E** are given by

$$n_1^2 = n_o^2 + \left[c_1 + c_2 + \frac{b_2^2}{n_o^2 - n_e^2} \right] E^2, \qquad \mathbf{r}_1 = k \left(1,\ 1,\ \frac{\sqrt{2} b_2 E}{n_o^2 - n_e^2} \right) \Big/ \sqrt{2}, \tag{2.108}$$

$$n_2^2 = n_o^2 + [c_1 - c_2] E^2, \qquad \mathbf{r}_2 = (-1,\ 1,\ 0)/\sqrt{2}, \tag{2.109}$$

$$n_3^2 = n_e^2 + \left[c_3 - \frac{b_2^2}{n_o^2 - n_e^2} \right] E^2, \qquad \mathbf{r}_3 = k \left(-\frac{b_2 E}{n_o^2 - n_e^2},\ -\frac{b_2 E}{n_o^2 - n_e^2},\ \sqrt{2} \right) \Big/ \sqrt{2}, \tag{2.110}$$

in which

$$k = \left[1 + \frac{b_2^2 E^2}{(n_o^2 - n_e^2)^2} \right]^{-\frac{1}{2}} \tag{2.111}$$

is a normalization constant. The unit vectors in eqns. (2.108) – (2.110) form a mutually orthogonal right-handed system, since $\mathbf{r}_1 \times \mathbf{r}_2 = \mathbf{r}_3$.

It is evident from the expressions for the n_i^2 in eqns. (2.108) – (2.110) that, to first order in the field, the crystal remains uniaxial but becomes biaxial, due to the quadratic terms. This serves to explain the difference in conclusion reached in this regard by Maldonado and Gaylord: in their matrix approach these authors included the numerical equivalent of our off-diagonal terms in $b_2 E/\sqrt{3}$, which, as eqns. (2.108) and (2.110) show, contribute in part to the quadratic terms which render the crystal biaxial. In addition, it follows from these equations that it is inconsistent to allow for the linear electro-optic coefficient whilst omitting the contributions of the quadratic electro-optic coefficient. In fact, for KDP the contributions of these two coefficients have comparable magnitude, as may be deduced from the following experimental values at a wavelength of 632.8 nm (Landolt-Börnstein 1979; Gosh and Bhar 1982; Górski *et al.* 1994;

Kucharczyk *et al.* 1995).

$$\left.\begin{aligned} &n_o = 1.5075,\ n_e = 1.4670,\ r_{xzy} = 8.7 \times 10^{-12}\ \mathrm{mV^{-1}},\\ &g_{xxxx} = -4.0 \times 10^{-20}\ \mathrm{m^2V^{-2}},\ g_{yyxx} = 0.2 \times 10^{-20}\ \mathrm{m^2V^{-2}},\\ &g_{zzxx} = -0.6 \times 10^{-20}\ \mathrm{m^2V^{-2}},\ g_{xyxy} = 1.4 \times 10^{-20}\ \mathrm{m^2V^{-2}}, \end{aligned}\right\} \quad (2.112)$$

Then from eqns. (2.10), (2.37), (2.38), (2.67), (2.104), and (2.107) one finds in units of $10^{-20}\ \mathrm{m^2V^{-2}}$ that

$$h_2^2/(n_o^2 - n_e^2) = 1.5,\ c_1 = 9.8,\ c_2 = -7.2,\ c_3 = 2.8. \quad (2.113)$$

The analysis in this section serves to show that the inclusion in the perturbed 3×3 matrix of off-diagonal elements linear in **E** may, in some instances, lead to inconsistencies unless terms in $\mathbf{E}^2$ are also included, and that the contributions of the latter are not necessarily negligible, as is evident from eqn. (2.113).

2.8 Discussion

When a uniform electric field is applied to a crystal, its principal refractive indices and axes are in general different from those of the field-free crystal. An algebraic theory presented in this paper shows how to derive analytic expressions for these perturbed properties to first order in the field, and also, by extension, to second order, for a crystal of any given symmetry in an arbitrary field. A numerical approach involving iterative diagonalization of the perturbed impermeability matrix has previously been reported in Maldonado and Gaylord (1988) and applied to certain crystals in fields with simple directions. Comparison of the results obtained by the two approaches is thus possible for these crystals and field configurations, using the same experimental data. The iterations described in Maldonado and Gaylord (1988) were performed on a calculator with 12-digit precision, with final refractive index values and corresponding eigenvectors being quoted to 8–10 digits.

In respect of gallium arsenide, as a representative of the cubic class of highest symmetry in which the linear electro-optic effect may occur, three field directions were considered, namely those in eqns. (1.17), (1.26), and (1.31). For two of these fields several iterations were required, with seven being reported for the field in eqn. (1.26). By contrast, the algebraic method yields immediate solutions, virtually by inspection. The greatest disagreement in the two approaches occurs in the principal refractive indices in the field (0, 0, E), which for the same data are

$$n_1 = 3.3895278. \qquad 3.3895161.$$

$$n_2 = 3.3895000. \qquad 3.3895000.$$

$$n_3 = 3.3894722. \qquad 3.3894839.$$

Our results calculated from eqns. (2.19) - (2.21) appear first. It may be that the above numbers in Maldonado and Gaylord (1988) are a misprint, in view of a later remark in that paper.

Numerical values for the principal refractive indices of lithium niobate in a field along its main symmetry axis (z) are not given in Maldonado and Gaylord (1988), presumably because, as eqn. (2.39) shows, there are no off-diagonal matrix elements to first order in E, so that the required refractive indices follow directly from the diagonal elements. Their values are quoted here for the record, using the data in Maldonado and Gaylord (1988) for a wavelength of 632.8nm: namely

$$n_o = 2.2885, \quad n_e = 2.2014,$$

$$r_{xz} = 8.6 \times 10^{-12}\ \mathrm{mV}^{-1}, \quad r_{zzz} = 30.8 \times 10^{-12}\ \mathrm{mV}^{-1}.$$

Then from eqns. (2.42) - (2.44), which also contain the corresponding eigenvectors, this work gives

$$n_1 = n_2 = 2.2884484, \qquad n_3 = 2.2012357.$$

For the other two field directions in lithium niobate our perturbed refractive index values differ from those in Maldonado and Gaylord (1988) to about one part in 10^8 for five of the six values, with even better agreement in the remaining one. However, in respect of the corresponding eigenvectors for the x and y field directions, there are marked differences: of those quoted in Maldonado and Gaylord (1988) and Section 2.4, only one has a simple closed form, whereas of the rest the majority of their Cartesian components differ from these in the range 1 - 80 parts in 10^4. The reason for this is that the iterations in Maldonado and Gaylord (1988) included the numerical counterparts of the off-diagonal matrix elements b_4E in eqns. (2.46) and (2.54), without consideration of the order in the applied field to which they contribute to the eigenvectors. The results of this Chapter, in keeping with the linear electro-optic approximation, include only terms linear in **E**.

In their analysis of KDP as a member of the symmetry class $\bar{4}2m$, Maldonado and Gaylord did not calculate the perturbed refractive indices and principal axes for fields parallel to the

crystallographic x- and y-axes, although they briefly referred to the diagonalization procedure for these fields. Consequently, no comparison with results in Subsections 2.5.2 and 2.5.3 is possible. For a field along the bisector of the x- and y-axes the different conclusion in Maldonado and Gaylord (1988) from those in Subsection 2.5.4 has already been considered in Section 2.7. In regard to the field $\mathbf{E} = (E, E, E)/\sqrt{3}$, here also no calculated values of the refractive indices appear in the paper by Maldonado and Gaylord (1988), while the numerical form of one of the two quoted eigenvectors has components which differ by about two parts in 10^4 from the solution in eqn. (2.91), when using the same experimental data as those in Maldonado and Gaylord (1988) at 550 nm. The other solution is exact and in agreement with that in eqn. (2.89). Finally, for a field along the main symmetry axis of KDP no calculated refractive indices or eigenvectors are given in Maldonado and Gaylord (1988), so because of their experimental relevance the former are evaluated below from the expressions in eqns. (2.69) - (2.71) using the experimental result $r_{xyz} = 11.7 \times 10^{-12}\,\mathrm{mV^{-1}}$ at a wavelength of 632.8 nm (Landolt-Börnstein 1979), in addition to those in eqn. (2.112). Then, for a field strength of $10^6\ \mathrm{Vm^{-1}}$,

$$n_1 = 1.5075190,$$

$$n_2 = 1.5074810,$$

and n_3 remains unchanged from n_e.

In this chapter there is a strong emphasis on the use of symmetry to obtain analytic expressions, to first and, if need be, second order in an applied field, for the perturbed principal refractive indices and axes of a crystal of given symmetry. This approach has the considerable advantage that the same expressions then apply to all crystals of the particular class and also, in some instances, to crystals of different symmetry, where their electro-optic coefficients have the same components, e.g. 422 and 622 (Yariv and Yeh 1984). By contrast, a numerical approach uses the experimental values of the relevant components for each crystal considered, as well as an assumed number for the field strength, in order to be able to write down the 3×3 matrix to be diagonalized. In this process the distinction between linear and quadratic field contributions is lost, as discussed in Section 2.7, with the possible consequence of erroneous conclusions and incorrect numerical values for the principal quantities being calculated.

Chapter 3

PHYSICAL IMPLICATIONS OF THE USE OF PRIMITIVE AND TRACELESS ELECTRIC-QUADRUPOLE MOMENTS

3.1 Introduction

Electric quadrupoles are encountered in a number of branches of physics and chemistry, particularly in their contribution to the interaction of electromagnetic radiation with matter. Many electromagnetic phenomena may be explained by means of a multipole theory, in which only the lowest order of multipoles necessary to explain the phenomenon is retained, based on the following relative magnitudes of their contributions (de Figueiredo and Raab 1981):

$$\text{electric dipole} >> \begin{cases}\text{electric quadrupole}\\ \text{magnetic dipole}\end{cases} >> \begin{cases}\text{electric octopole}\\ \text{magnetic quadrupole}\end{cases} >> \cdots \quad (3.1)$$

At the level of crystals and fluids the role of electric quadrupoles occurs principally in theories of chiral effects, both natural and induced, for example, circular birefringence and dichroism in a fluid of oriented molecules (Nakano and Kimura 1969; Buckingham and Dunn 1971), magnetic circular dichroism (Stephens 1970), circular intensity differential in light scattering, both natural (Barron and Buckingham 1971; Barron 1982) and electric-field-induced (Buckingham and Raab 1975), certain other light scattering effects (de Figueiredo and Raab 1981), and circular birefringence in nonmagnetic crystals (Graham and Raab 1990; Raab and Cloete 1994). Examples of nonchiral effects whose theories include quadrupole moments are gyrotropic and

various nonreciprocal birefringences in antiferromagnetic crystals (Hornreich and Shtrikman 1968; Graham and Raab 1992) and Jones birefringence in certain magnetic crystals (Graham and Raab 1983).

Despite its use in numerous papers, electric quadrupole moment is not consistently defined and several variants may be noted in the literature. Expressed in Cartesian tensor notation using Greek subscripts, some examples for a discrete charge distribution are:

(i) $n\sum q r_\alpha r_\beta$, $n = \frac{1}{2}$, (Rosenfeld 1951; Robinson 1973; Hanna *et al.* 1979),

$n = 1$, (Nakano and Kimura 1969; Stephens 1970; Raab 1975),

(ii) $n\sum q(3r_\alpha r_\beta - r^2\delta_{\alpha\beta})$, $n = \frac{1}{2}$, (Buckingham 1959; Buckingham and Dunn1971; Barron 1982),

$n = 1$, (Blatt and Weisskopf 1952; Jackson 1975),

(iii) $\sum q(r_\alpha r_\beta - r^2\delta_{\alpha\beta})$, (Binder and Reger 1992).

In these definitions **r** is the displacement of charge q from an arbitrary origin inside or near the distribution and the summation is over all charges in the distribution.

Of the above definitions the so-called primitive form

$$q_{\alpha\beta} = \sum q r_\alpha r_\beta \tag{3.2}$$

emerges naturally from the multipole expansions of a range of electromagnetic quantities: the electrostatic potential of a charge distribution (Buckingham 1959), the interaction energy of such a distribution with an electrostatic field (Buckingham 1959), the radiation field (Raab 1975; Landau and Lifshitz 1979), and the vector potential of a dynamic charge distribution (Graham *et al.* 1992). In some of these multipole expansions a rearrangement of terms permits the introduction of the traceless quadrupole moment (Buckingham 1959; Landau and Lifshitz 1979)

$$\theta_{\alpha\beta} = \tfrac{1}{2}(3q_{\alpha\beta} - q_{\gamma\gamma}\delta_{\alpha\beta}) = \tfrac{1}{2}\sum q(3r_\alpha r_\beta - r^2\delta_{\alpha\beta}). \tag{3.3}$$

This form has the advantage that it describes departures of the charge distribution from spherical symmetry (Buckingham 1959).

One essential test of the correctness of a theoretical expression for an observed effect is that it should be independent of the choice of origin used for the displacement vector **r** that appears in the definitions of multipole moments in general (Raab 1975), including those of the electric-

quadrupole moment in eqns. (3.2) and (3.3). Origin independence as a test procedure was first applied by Van Vleck (1932) and then used routinely by Buckingham and others in their various theories (Buckingham and Longuet-Higgins 1968; Stephens 1970; Barron and Buckingham 1971; Buckingham and Dunn 1971; Barron 1982; Graham and Raab 1990). In the theories of Buckingham and co-workers the traceless quadrupole moment in eqn. (3.3) was used and in all cases origin independence was established.

However, the use of traceless multipole moments has been questioned by a number of authors. Raab (1975) found that the traceless electric-octopole moment (Buckingham 1959; Fowler and Steiner 1990) is unable to describe the interaction of an octopolar molecule with an electromagnetic field, whereas the primitive moment

$$\sum q r_\alpha r_\beta r_\gamma$$

is able to. Further difficulties have been reported with the use of a traceless electric quadrupole moment density $\Theta_{\alpha\beta}$ in the multipole form of the electric displacement

$$D_\alpha = \varepsilon_0 E_\alpha + P_\alpha - \tfrac{1}{3}\nabla_\beta \Theta_{\alpha\beta} + \cdots, \tag{3.4}$$

first adopted by Buckingham and Dunn (1971). In this $\boldsymbol{P}$ is the electric-dipole moment density and $\Theta_{\alpha\beta}$ is defined by

$$\Theta_{\alpha\beta} = \theta_{\alpha\beta}/\Delta V, \tag{3.5}$$

where $\theta_{\alpha\beta}$ is the traceless quadrupole moment of the macroscopic volume element ΔV. Logan (1982) showed that the use of eqn. (3.4) in the context of a nonuniform electrostatic field leads to origin dependence of a Maxwell equation and also of the dielectric tensor of an ideal gas. The same difficulty arose when eqn. (3.4) was employed in a light transmission theory, based on Maxwell's equations, of the linear birefringence induced in a gas by an electric-field gradient (Imrie and Raab 1991). However, in both these theories the corresponding expressions were shown not to depend on origin when $\boldsymbol{D}$ was taken in the form (Rosenfeld 1951; Robinson 1973; Graham *et al.* 1992)

$$D_\alpha = \varepsilon_0 E_\alpha + P_\alpha - \tfrac{1}{2}\nabla_\beta Q_{\alpha\beta} + \cdots, \tag{3.6}$$

where

$$Q_{\alpha\beta} = q_{\alpha\beta}/\Delta V \tag{3.7}$$

is the primitive quadrupole moment density.

Against these findings, which seem to favour eqn. (3.6) over eqn. (3.4), are two contrary results.

In a theory based on light scattering, in which the traceless quadrupole moment in eqn. (3.3) was used, Buckingham and Longuet-Higgins (1968) derived an expression for the field-gradient-induced birefringence in a gas and showed that it was origin independent. Then in a theory of the optical activity of oriented molecules, which involved eqn. (3.4), Buckingham and Dunn (1971) established that the expression for this effect also did not depend on origin. In an attempt to resolve these inconsistencies for origin independence, depending on whether the traceless or primitive quadrupole moment is used in the theory, a different test was sought of the applicability of the two definitions. To this end the origin independence of Maxwell's two inhomogeneous equations was investigated using both eqn. (3.4) and eqn. (3.6) applied to a plane monochromatic light wave (Graham *et al.* 1992). It was found that this essential requirement for a law of physics, being a form of spatial invariance, was satisfied only when eqn. (3.6) was used with its primitive electric quadrupole moment density.

This last finding suggests that the traceless quadrupole moment in eqn. (3.3) and the form of $\boldsymbol{D}$ in eqn. (3.4) that is based on it are not generally applicable. If this is so, it is clearly of interest to revisit the problem treated by Buckingham and Dunn with a view to identifying why these authors found that the traceless form in eqn. (3.4) leads to origin independence.

3.2 The wave equation using the primitive quadrupole moment

An expression for the circular birefringence exhibited by an optically active medium may be derived by means of Maxwell's equations and appropriate constitutive relations. It has long been established that optical activity can be described in the electric-quadrupole–magnetic-dipole approximation (Nakano and Kimura 1969; Buckingham and Dunn 1971; Barron 1982; Graham and Raab 1990). To this multipole order the form of $\boldsymbol{D}$ in eqn. (3.6) is used which contains the primitive quadrupole moment. Consistent with this order is the $\boldsymbol{H}$ field in the form (Buckingham and Dunn 1971)

$$H_\alpha = \mu_o^{-1} B_\alpha - M_\alpha , \tag{3.8}$$

where $\boldsymbol{M}$ is the magnetic-dipole moment density defined by

$$\boldsymbol{M} = \left\{ \sum (q/2m)(\mathbf{r} \times \mathbf{p} + g\,\mathbf{s}) \right\} / \Delta V . \tag{3.9}$$

In this **r** is the displacement from an arbitrary origin inside ΔV of a particle of mass m, charge q, momentum **p**, g-factor g, and spin **s**.

The polarization densities in eqns. (3.6) and (3.8) that are induced in a nonmagnetic medium by a plane monochromatic light wave of angular frequency ω are, to the order of electric quadrupoles and magnetic dipoles (de Figueiredo and Raab 1981),

$$P_\alpha = \alpha_{\alpha\beta} E_\beta + \tfrac{1}{2} a_{\alpha\beta\gamma} \nabla_\gamma E_\beta + \frac{1}{\omega} G'_{\alpha\beta} \dot{B}_\beta , \tag{3.10}$$

$$Q_{\alpha\beta} = a_{\alpha\beta\gamma} E_\gamma , \tag{3.11}$$

$$M_\alpha = \frac{1}{\omega} G'_{\alpha\beta} \dot{E}_\beta . \tag{3.12}$$

In writing there equations, as in Chapter 1, time-odd tensors have been omitted for the nonmagnetic medium. Also, $\dot{\boldsymbol{E}} = \partial \boldsymbol{E}/\partial t$ and $\dot{\boldsymbol{B}} = \partial \boldsymbol{B}/\partial t$ and the polarizability tensors $\alpha_{\alpha\beta}$, $a_{\alpha\beta\gamma}$, etc. are macroscopic volume properties of the medium. By means of first-order perturbation theory quantum-mechanical expressions can be derived for these tensors which allow essential information to be determined, in particular any relationships between them, the intrinsic symmetry of their subscripts, and the effects of an origin shift. For no absorption, which is assumed for simplicity, these expressions are given in Appendix A. From these it follows from the hermiticity of the operators in eqns. (A.1)- (A.5) that

$$\alpha_{\alpha\beta} = \alpha_{\beta\alpha} , \quad a_{\alpha\beta\gamma} = a_{\gamma\alpha\beta} , \quad G'_{\alpha\beta} = -G'_{\beta\alpha} . \tag{3.13}$$

In addition,

$$a_{\alpha\beta\gamma} = a_{\alpha\gamma\beta} \tag{3.14}$$

because of the intrinsic symmetry of the quadrupole moment operator $Q_{\alpha\beta}$.

When eqns. (3.10) - (3.12) are substituted into eqns. (3.6) and (3.8), and eqns. (3.13) and (3.14) are used as well, the following constitutive relations are obtained

$$D_\alpha = \varepsilon_o E_\alpha + \alpha_{\alpha\beta} E_\beta + \tfrac{1}{2} (a_{\alpha\beta\gamma} - a_{\beta\alpha\gamma}) \nabla_\gamma E_\beta + \frac{1}{\omega} G'_{\alpha\beta} \dot{B}_\beta , \tag{3.15}$$

$$H_\alpha = \mu_o^{-1} B_\alpha + \frac{1}{\omega} G'_{\beta\alpha} \dot{E}_\beta . \tag{3.16}$$

It is convenient again to take the light-wave field in the complex form given in eqn. (1.9), i.e.

$$\boldsymbol{E} = \boldsymbol{E}^{(o)} \exp[-i\omega (t - n\, \mathbf{r} \cdot \sigma / c)], \tag{3.17}$$

in which c is the speed of light in a vacuum, **r** is the unit vector normal to the plane wave front,

and n is the refractive index for propagation in the direction of σ of the light beam, whose polarization state is described by the amplitude $\boldsymbol{E}^{(o)}$. By means of eqn. (3.17) and the Maxwell equation

$$\nabla \times \boldsymbol{E} = -\dot{\boldsymbol{B}}, \tag{3.18}$$

the various fields in $\boldsymbol{D}$ and $\boldsymbol{H}$ in eqns. (3.15) and (3.16) may be expressed in terms of $\boldsymbol{E}$. These $\boldsymbol{D}$ and $\boldsymbol{H}$ forms are then substituted into the Maxwell equation for a source-free medium

$$\nabla \times \boldsymbol{H} = \dot{\boldsymbol{D}} \tag{3.19}$$

to obtain the wave equation

$$\left\{[n^2\sigma_\alpha\sigma_\beta - (n^2-1)\delta_{\alpha\beta}] + [\chi_{\alpha\beta}] + \left[\frac{in}{\varepsilon_o c}U_{\alpha\beta}\right]\right\}E_\beta^{(o)} = 0. \tag{3.20}$$

In this the phase of $\boldsymbol{E}$ in eqn. (3.17) has been cancelled. Also, $\delta_{\alpha\beta}$ is the Kronecker delta, $\alpha_{\alpha\beta} = \varepsilon_o\chi_{\alpha\beta}$, and

$$U_{\alpha\beta} = \sigma_\gamma[G'_{\alpha\delta}\,\epsilon_{\beta\gamma\delta} - G'_{\beta\delta}\,\epsilon_{\alpha\gamma\delta} + \tfrac{1}{2}\omega(a_{\alpha\beta\gamma} - a_{\beta\alpha\gamma})] = -U_{\beta\alpha}, \tag{3.21}$$

where $\epsilon_{\alpha\beta\gamma}$ is the Levi-Civita tensor.

Equation (3.20) is the fundamental equation, equivalent to that derived in eqn. (1.13) but now within the electric-quadrupole–magnetic-dipole approximation, for describing the propagation of a plane monochromatic light wave in a nonabsorbing nonmagnetic medium, which is both anisotropic and devoid of sources. Of the three terms in brackets [...] in eqn. (3.20), the first applies to a vacuum, while the second allows for the effect of matter within the electric-dipole approximation and the third contains the contribution of electric quadrupoles and magnetic dipoles, as is evident from eqns. (3.21), (A.2), and (A.4).

Since eqn. (3.20) is the Maxwell vector equation (3.19) to the multipole order used, it comprises three equations in the unknown components $E_x^{(o)}$, $E_y^{(o)}$, and $E_z^{(o)}$ of the light-wave amplitude. When α in eqn. (3.20) is set equal to x, y, and z in turn, the matrix eigenvalue equation is obtained

$$\begin{bmatrix} n^2(1-\sigma_x^2) - t_{xx} & -n^2\sigma_x\sigma_y - t_{xy} & -n^2\sigma_x\sigma_z - t_{xz} \\ -n^2\sigma_y\sigma_x - t_{yx} & n^2(1-\sigma_y^2) - t_{yy} & -n^2\sigma_y\sigma_z - t_{yz} \\ -n^2\sigma_z\sigma_x - t_{zx} & -n^2\sigma_z\sigma_y - t_{zy} & n^2(1-\sigma_z^2) - t_{zz} \end{bmatrix} \begin{bmatrix} E_x^{(o)} \\ E_y^{(o)} \\ E_z^{(o)} \end{bmatrix} = \begin{bmatrix} E_x^{(o)} \\ E_y^{(o)} \\ E_z^{(o)} \end{bmatrix}, \tag{3.22}$$

where

$$t_{ij} = \chi_{ij} + \frac{in}{\varepsilon_o c} U_{ij}, \qquad i, j = x, y, z. \tag{3.23}$$

For a given propagation direction σ only those polarization states, as described by $E_x^{(o)}$, $E_y^{(o)}$, and $E_z^{(o)}$, may propagate that are eigenvectors of the matrix in eqn. (3.22) that represents the medium through the multipole tensors $\alpha_{\alpha\beta}$ and $U_{\alpha\beta}$. These eigenvectors, which the medium supports for the chosen propagation direction, emerge naturally from the theory without the need to assume their form in advance as has sometimes been done in the past (Buckingham and Dunn 1971; Graham and Raab 1983).

The requirement that the eigenvalues in eqn. (3.22) be unity constrains the refractive index for each polarization eigenvector to a particular expression in terms of $\alpha_{\alpha\beta}$ and $U_{\alpha\beta}$. An alternative approach to finding these refractive indices is to solve the secular equation based on eqn. (3.22), in which the determinant is obtained from the coefficients of $E_x^{(o)}$, $E_y^{(o)}$, and $E_z^{(o)}$, namely

$$\begin{vmatrix} n^2(\sigma_x^2 - 1) + 1 + t_{xx} & n^2\sigma_x\sigma_y + t_{xy} & n^2\sigma_x\sigma_z + t_{xz} \\ n^2\sigma_y\sigma_x + t_{yx} & n^2(\sigma_y^2 - 1) + 1 + t_{yy} & n^2\sigma_y\sigma_z + t_{yz} \\ n^2\sigma_z\sigma_x + t_{zx} & n^2\sigma_z\sigma_y + t_{zy} & n^2(\sigma_z^2 - 1) + 1 + t_{zz} \end{vmatrix} = 0. \tag{3.24}$$

In order to apply eqn. (3.24) a set of Cartesian axes must be chosen. The polarization of the light wave and its propagation direction are specified relative to laboratory axes, whereas the components of crystal property tensors are quoted in tables (for example, those by Birss 1966) for crystallographic axes, with the z-axis traditionally taken as that of highest symmetry. Accordingly, to be able to use such tables the laboratory and crystallographic axes are arranged to coincide.

3.3 Propagation in a uniaxial crystal

For the purpose of comparing the theoretical expressions obtained by using the primitive and traceless quadrupole moments, it is sufficient to consider a uniaxial crystal. Such a system includes, in effect, that treated by Buckingham and Dunn (1971), namely a fluid of oriented molecules with a macroscopic symmetry axis and isotropy about it.

To illustrate how the wave equation, or the secular equation in eqn. (3.24) that is based on it, enables the polarization eigenvectors and their refractive indices to be determined, propagation along the symmetry axis of the crystal is considered. Since the crystallographic axes of a uniaxial

crystal serve as principal axes for the symmetric second-rank polar tensor $\alpha_{\alpha\beta}$, its only nonzero components are (Birss 1966)

$$\alpha_{xx} = \alpha_{yy} \neq \alpha_{zz},$$

and this applies also to a fluid of oriented molecules. From eqn. (3.21)

$$U_{xx} = U_{yy} = U_{zz} = 0$$

in general, so that for all uniaxial systems eqn. (3.24) becomes

$$\begin{vmatrix} n^2(\sigma_x^2 - 1) + 1 + \chi_{xx} & n^2\sigma_x\sigma_y + \dfrac{in}{\varepsilon_0 c}U_{xy} & n^2\sigma_x\sigma_z + \dfrac{in}{\varepsilon_0 c}U_{xz} \\ n^2\sigma_y\sigma_x + \dfrac{in}{\varepsilon_0 c}U_{yx} & n^2(\sigma_y^2 - 1) + 1 + \chi_{yy} & n^2\sigma_y\sigma_z + \dfrac{in}{\varepsilon_0 c}U_{yz} \\ n^2\sigma_z\sigma_x + \dfrac{in}{\varepsilon_0 c}U_{zx} & n^2\sigma_z\sigma_y + \dfrac{in}{\varepsilon_0 c}U_{zy} & n^2(\sigma_z^2 - 1) + 1 + \chi_{zz} \end{vmatrix} = 0. \tag{3.25}$$

For propagation along the *z*-axis $\sigma = (0, 0, 1)$. From this and eqn. (3.21) it follows from Birss' tables that

$$U_{xz} = U_{yz} = 0, \tag{3.26}$$

so that eqn. (3.25) reduces to

$$\begin{vmatrix} -n^2 + 1 + \chi_{xx} & \dfrac{in}{\varepsilon_0 c}U_{xy} & 0 \\ -\dfrac{in}{\varepsilon_0 c}U_{xy} & -n^2 + 1 + \chi_{yy} & 0 \\ 0 & 0 & 1 + \chi_{zz} \end{vmatrix} = 0, \tag{3.27}$$

where

$$U_{xy} = G'_{xx} + G'_{yy} + \tfrac{1}{2}\omega(a_{xyz} - a_{yxz}). \tag{3.28}$$

(It should be noted that this expression for U_{xy} may simplify, depending on the particular point group symmetry of the uniaxial crystal, and in some cases will vanish.) The roots of eqn. (3.27) are given by

$$-n^2 + 1 + \chi_{xx} = \pm\frac{n}{\varepsilon_0 c}U_{xy}. \tag{3.29}$$

When these are substituted into the equation on which either the first or second row of the determinant in eqn. (3.27) is based, one obtains

$$E_y^{(o)} / E_x^{(o)} = \pm i \tag{3.30}$$

where the upper and lower signs in eqns. (3.29) and (3.30) are consistent.

The amplitude ratios in eqn. (3.30) are characteristic of circularly polarized light, with the upper sign describing left and the lower right, based on the sign choice for the phase in eqn. (3.17). Their respective refractive indices are denoted n_l and n_r. The circular birefringence follows from eqn. (3.29) and is given by

$$\begin{aligned} n_r - n_l &= \frac{1}{\varepsilon_0 c} U_{xx} \\ &= \frac{1}{\varepsilon_0 c}\left\{G'_{xx} + G'_{yy} + \tfrac{1}{2}\omega(a_{yxz} - a_{xxz})\right\}. \end{aligned} \tag{3.31}$$

By means of a similar approach to that above, the wave equation may be solved for any arbitrary propagation direction σ, so yielding the allowed forms of the field of the wave and their refractive indices.

3.4 The wave equation using the traceless quadrupole moment

The wave equation that was derived in Section 3.2 contains the contributions of the primitive electric-quadrupole moment defined in eqn. (3.2). When the traceless definition in eqn. (3.3) is adopted, expressions involving this moment will change. These are stated below against the equation number of the corresponding expression or equation based on the primitive quadrupole moment:

(3.6) : $$D_\alpha = \varepsilon_0 E_\alpha + P_\alpha - \tfrac{1}{3}\nabla_\beta \Theta_{\alpha\beta} \tag{3.4}$$

(3.10) : $$P_\alpha = \alpha_{\alpha\beta} E_\beta + \tfrac{1}{3} A_{\alpha\beta\gamma}\nabla_\gamma E_\beta + \frac{1}{\omega} G'_{\alpha\beta}\dot{B}_\beta \tag{3.32}$$

(3.11) : $$\Theta_{\alpha\beta} = A_{\alpha\beta\gamma} E_\gamma \tag{3.33}$$

(A.2) : $$A_{\alpha\beta\gamma} = 2\hbar^{-1}\Delta V \sum_j Z_{jn}\omega_{jn} Re\langle n|P_\alpha|j\rangle\langle j|\Theta_{\beta\gamma}|n\rangle \tag{3.34}$$

(3.13) : $$A_{\alpha\beta\gamma} = A_{\gamma\alpha\beta} \tag{3.35}$$

(3.15) : $$D_\alpha = \varepsilon_0 E_\alpha + \alpha_{\alpha\beta} E_\beta + \tfrac{1}{3}(A_{\alpha\beta\gamma} - A_{\beta\alpha\gamma})\nabla_\gamma E_\beta + \frac{1}{\omega} G'_{\alpha\beta}\dot{B}_\beta \tag{3.36}$$

$$(3.20)\ :\quad \left\{[n^2\sigma_\alpha\sigma_\beta-(n^2-1)\delta_{\alpha\beta}]+[\chi_{\alpha\beta}]+\left[\frac{in}{\varepsilon_o c}u_{\alpha\beta}\right]\right\}E_\beta^{(o)}=0 \tag{3.37}$$

$$(3.21)\ :\quad u_{\alpha\beta}=\sigma_\gamma[G'_{\alpha\delta}\in_{\beta\gamma\delta}-G'_{\beta\delta}\in_{\alpha\gamma\delta}+\tfrac{1}{3}\omega(A_{\alpha\beta\gamma}-A_{\beta\alpha\gamma})]=-u_{\beta\alpha}. \tag{3.38}$$

Since the wave equation determines the observable properties of a wave propagating in a medium, in particular the polarization eigenvectors and their respective refractive indices, the multipole terms in the wave equation should be independent of origin. This is considered in the next section.

3.5 Analysis of origin dependence

Let the origin be displaced by **R** from that used to specify **r** in the electric-dipole moment $\sum q\mathbf{r}$ and the moments in eqns. (3.2), (3.3), and (3.9). Then their densities change and so therefore may the various polarizability tensors of concern; those given in eqns. (A.1) - (A.5) and (3.34). The shifts in the tensors that appear in the wave eqns. (3.20) and (3.37) have been determined and are (Buckingham and Dunn 1971; Graham and Raab 1990)

$$\Delta\alpha_{\alpha\beta}=0 \tag{3.39}$$

$$\Delta a_{\alpha\beta\gamma}=-R_\gamma\alpha_{\alpha\beta}-R_\beta\alpha_{\alpha\gamma} \tag{3.40}$$

$$\Delta A_{\alpha\beta\gamma}=-\tfrac{3}{2}R_\beta\alpha_{\alpha\gamma}-\tfrac{3}{2}R_\gamma\alpha_{\alpha\beta}+R_\delta\alpha_{\alpha\delta}\delta_{\beta\gamma} \tag{3.41}$$

$$\Delta G'_{\alpha\beta}=\tfrac{1}{2}\omega\in_{\beta\gamma\delta}R_\gamma\alpha_{\alpha\delta}. \tag{3.42}$$

From eqn. (3.39) it may be seen that the electric-dipole term in both wave equations is origin independent. The electric-quadrupole–magnetic-dipole contributions to these equations enter via eqns. (3.21) and (3.38), the origin shifts of which can be shown from eqns. (3.40) - (3.42) to be

$$\Delta U_{\alpha\beta}=0 \tag{3.43}$$

$$\Delta u_{\alpha\beta}=\tfrac{1}{3}\omega\sigma_\gamma R_\delta(\alpha_{\alpha\delta}\delta_{\beta\gamma}-\alpha_{\beta\delta}\delta_{\alpha\gamma}). \tag{3.44}$$

Since $U_{\alpha\beta}$ contains the contributions of the primitive quadrupole moment, it is evident from eqn. (3.43) that the use of this moment ensures that the wave equation in eqn. (3.20) is independent of origin for any propagation direction σ. So, too, therefore, are the refractive indices calculated from this equation, as required of an observable. From eqn. (3.44) this is not generally the case when the traceless quadrupole moment is used. Nevertheless, when working with this moment

in their theory, Buckingham and Dunn (1971) established origin independence of their expression for the circular birefringence exhibited by a fluid of oriented molecules for light propagating along the symmetry axis. To explain their result in the light of eqn. (3.44), we note that for $\sigma = (0, 0, 1)$ the only nonvanishing components of $u_{\alpha\beta}$ in eqn. (3.38) are Birss (1966)

$$u_{xy} = G'_{xx} + G'_{yy} + \tfrac{1}{3}\omega(A_{xyz} - A_{yxz}) = -u_{yx}.$$

This expression for u_{xy} is the traceless equivalent of U_{xy} in eqn. (3.28), and in terms of it the circular birefringence is analogous to that in eqn. (3.31) and so is given by

$$n_r - n_l = \frac{1}{\varepsilon_0 c} u_{xy}.$$

From eqn. (3.44) the origin shift in u_{xy} is

$$\Delta u_{xy} = \tfrac{1}{3}\omega R_\delta(\alpha_{x\delta}\delta_{yz} - \alpha_{y\delta}\delta_{xz}) = 0.$$

Thus for propagation along the symmetry axis of an optically active uniaxial medium both the wave equation and the circular birefringence are independent of origin when the traceless quadrupole moment is used in the theory. This confirms the finding by Buckingham and Dunn.

However, a different conclusion regarding origin independence is reached when propagation is along the other crystallographic axes in certain uniaxial crystals, as is now demonstrated. Use of the 'traceless' wave eqn. (3.37) in conjunction with Birss' tables (Birss 1966) shows that x-propagation in crystals belonging to the optically active uniaxial point groups

$$4,\ \bar{4},\ 3,\ 6 \tag{3.45}$$

is described by the secular equation

$$\begin{vmatrix} 1+\chi_{xx} & 0 & \dfrac{in}{\varepsilon_0 c}u_{xz} \\ 0 & -n^2+1+\chi_{xx} & \dfrac{in}{\varepsilon_0 c}u_{yz} \\ -\dfrac{in}{\varepsilon_0 c}u_{xz} & -\dfrac{in}{\varepsilon_0 c}u_{yz} & -n^2+1+\chi_{zz} \end{vmatrix} = 0. \tag{3.46}$$

The origin shifts in the components u_{yz} and u_{xz} in this follow from eqn. (3.44) and for $\sigma = (1, 0, 0)$ are

$$\Delta u_{yz} = 0, \qquad \Delta u_{xz} = -\tfrac{1}{3}\omega R_z \alpha_{zz}. \tag{3.47}$$

On differentiating eqn. (3.46) with respect to u_{xz} one obtains

$$\Delta(n^2) = [2(\varepsilon_0 c)^{-2} n^2 (n^2 - 1 - \chi_{xx}) u_{xz}][\chi_{xx}(\chi_{xx} + \chi_{zz}) + (\varepsilon_0 c)^{-2}(1 + \chi_{xx})(u_{yz}^2 + u_{xz}^2) - 2n^2[1 + \chi_{xx} + (\varepsilon_0 c)^{-2} u_{xz}^2]]^{-1} \Delta u_{xz}. \quad (3.48)$$

As neither solution of eqn. (3.46) for n^2 has the value $1 + \chi_{xx}$, it is evident from eqns. (3.47) and (3.48) that the refractive indices of the two polarization eigenvectors for x-propagation in crystals described by the point groups in (3.45) depend on origin when the traceless quadrupole moment is used in the derivation of the wave equation.

An interesting association of properties is attributable to the two terms u_{xz} in eqn. (3.46). Not only do they give rise to the origin dependence of the wave equation, but their presence in the 1-3 and 3-1 positions in the determinant results in the light-wave eigenvectors for x-propagation having nonvanishing amplitude component $E_x^{(o)}$, so that for them $\nabla \cdot \boldsymbol{E} \neq 0$. This is apparent from the three homogeneous equations in $E_x^{(o)}$, $E_y^{(o)}$, and $E_z^{(o)}$, from which eqn. (3.46) is obtained. The same association of origin dependence and $\nabla \cdot \boldsymbol{E} \neq 0$ is found from the 'traceless' wave equation (3.37) when propagation is along the crystallographic y-axis in the classes in (3.45). For crystals belonging to the remaining optically active uniaxial classes (Nye 1985)

$$422,\ \bar{4}2m,\ 32,\ 622,$$

the wave eqn. (3.37) is origin independent and the light waves transverse for both x- and y-propagation.

Thus when the theory incorporates the traceless electric-quadrupole moment, the wave equation and properties derived from it, like refractive index, depend on origin for certain light paths through the optically active uniaxial crystals in (3.45). This defect does not occur when the primitive quadrupole moment is used, as eqn. (3.43) shows.

3.6 Discussion

Certain effects, which occur when an electromagnetic wave propagates through matter, require for their explanation the inclusion of electric-quadrupole moments in the theory. The origin independence of the expression for such an effect is assured if the primitive quadrupole moment in eqn. (3.2) is used. If the traceless definition in eqn. (3.3) is adopted instead, then it has been shown elsewhere (Graham *et al.* 1992) that Maxwell's equations depend on origin and, furthermore, the expressions for a number of electromagnetic effects suffer from the same difficulty (Logan 1982; Imrie and Raab 1991).

To these effects may now be added optical activity, since in this chapter it has been shown that for certain directions of propagation in optically active uniaxial crystals belonging to the classes in (3.45), the refractive indices of the propagating waves depend on origin when the traceless quadrupole moment is used but not when it is the primitive form. In the special case of propagation along the main symmetry axis of any optically active uniaxial medium, the origin dependence of the circular birefringence vanishes when the traceless moment is used in the theory. This result confirms the finding of Buckingham and Dunn (1971), who, working with traceless quadrupole moments, showed the origin independence of the circular birefringence of light propagating along the symmetry axis of a fluid of oriented molecules.

It is known that the primitive electric-quadrupole and higher moments emerge naturally in the multipole expansions of electrodynamic properties like the vector potential of a time-changing charge distribution (Graham *et al.* 1992) or the quantum-mechanical Hamiltonian for the interaction of a charge distribution with an electromagnetic field (Barron and Gray 1973; Raab 1975). While the traceless electric-quadrupole moment may replace the primitive moment in electrostatics, as in the potential and also the interaction energy of a charge distribution in a static field (Buckingham 1959), such replacement is not possible in all electrodynamic situations, even though it may be in some (Buckingham and Dunn 1971). This is the burden of the present chapter. A similar limitation has been found in respect of the definition of magnetic quadrupole moment: a form that is acceptable in magnetostatics (Buckingham and Stiles 1972) does not necessarily apply in electrodynamics (Raab 1975).

Under what circumstances may the primitive electric-quadrupole moment in an expression be replaced, within a constant factor, by the traceless moment? Equation (3.3) shows that this is permissible when the contribution of the isotropic term $q_{\gamma\gamma}\delta_{\alpha\beta}$ vanishes. This is known to occur for radiation fields (Landau and Lifshiftz 1979). That being so, one is led to ask: if light propagation in matter results from the coherent superposition in the forward direction of fields radiated by volume elements of matter in the path of the incident light wave (Barron 1982; Kauzmann 1957), why does the 'traceless' wave eqn. (3.37) depend in general on origin while the 'primitive' wave eqn. (3.20) does not? The answer to this is not simple. This is because, as found in Section 3.5, origin dependence seems to be associated with eigenvectors whose electric fields are not transverse, as they are for radiation. This matter bears further investigation.

Chapter 4

ELECTRIC-FIELD-INDUCED OPTICAL ACTIVITY IN NONMAGNETIC CRYSTALS

4.1 Introduction

Optical activity, the traditional but not the only manifestation of which is the ability of a medium to rotate the plane of linearly polarized light (Barron 1982), occurs as both a natural and a field-induced phenomenon. Naturally occurring optical activity is found in fluids whose molecules possess only rotation axes as their symmetry elements, in crystals with the same symmetry properties, and also in the four nonenantiomorphous crystal classes m, $mm2$, $\bar{4}$, and $\bar{4}2m$ (Nye 1985).

Magnetic optical activity is well known in the form of the Faraday effect. In this a rotation of the plane of linearly polarized light is induced by, and is proportional to, a uniform magnetic field acting along the light path. It may occur in any substance, irrespective of its symmetry. The equivalent electric effect is forbidden by time-reversal considerations in a fluid of randomly oriented molecules (Buckingham *et al.* 1971), while in crystalline media its existence is subject to certain symmetry requirements. It is these requirements for nonmagnetic crystals that are identified in this chapter by means of an electromagnetic theory of the effect, in which the linear electro-optic rotation is expressed in terms of crystal property tensors.

Theories of the effect have previously been published, in all of which symmetry has been used to determine the conditions for its existence. However, in none of these theories has a wave-propagation approach been adopted, which would allow the determination of accompanying effects for particular propagation and field directions in the crystal, such as a field-induced linear birefringence, and also, and most importantly, when the propagating waves have only transverse fields. In particular, Zheludev (1965) related the rotation per unit path length of a linearly polarized wave to the applied electric field by means of a third-rank axial tensor without regard to the form of the propagation. In this theory, crystals, for whose point groups the relevant components of this tensor may exist, were then predicted to exhibit a linear electro-optic rotation. A similar approach was followed by Anastassakis (1972), who went further by identifying some crystal symmetries that would allow the effect for particular field and light directions but still in the absence of other effects, both natural and field induced. In neither this theory nor Zheludev's was the physical origin of the responsible tensors considered. In their account of the linear electro-optic rotation, Buckingham *et al.* (1971) dealt only with propagation and field directions along the symmetry axis of uniaxial crystals, both magnetic and nonmagnetic. From their tensor expression for the effect these authors were able to predict the symmetry classes in which it should occur. Such an induced rotation in a magnetic crystal belonging to one of these predicted classes had previously been measured by O'Dell and White (1970). Finally, Churcher and Stedman (1982) also used symmetry considerations to determine the conditions for existence of the effect for different field and light-path geometries, but again the propagation characteristics of the light wave and coexisting effects, whether natural or induced, were not considered.

In the theory presented in this chapter, an eigenvalue wave equation is derived from Maxwell's equations, in which the various induced polarization densities are expressed in a consistent multipole form. This approach has been used before in theories of a number of naturally occurring optical effects (Graham and Raab 1990; Graham, C. and Raab 1994). In particular, circular birefringence and circular dichroism in fluids and crystals have been explained within the electric-quadrupole–magnetic-dipole approximation (Nakano and Kimura 1969; Buckingham and Dunn 1971; Barron 1982; Graham and Raab 1990; Raab and Cloete 1994). It is to this multipole order, allowing for the linear distortion by an applied electric field, that the present theory is worked. From the wave equation may be derived the wave characteristics for particular propagation and field directions in the crystal, leading, first, to an expression for the linear electro-optic rotation in terms of crystal property tensors, each having a specific physical origin,

and, second, to an indication of the existence of other effects that might adversely affect the polarization state of the light beam. The tensor expression for the linear electro-optic rotation allows a prediction to be made of the crystal point groups for which the effect may occur.

4.2 Eigenvalue wave equation

To derive an eigenvalue wave equation for light propagating through a source-free nonmagnetic medium in the presence of a uniform electric field, use is made of the two Maxwell equations

$$\nabla \times \boldsymbol{E} = -\dot{\boldsymbol{B}}, \tag{4.1}$$

$$\nabla \times \boldsymbol{H} = \dot{\boldsymbol{D}}. \tag{4.2}$$

The induction fields $\boldsymbol{H}$ and $\boldsymbol{D}$ in eqn. (4.2) can each be expressed in a multipole expansion (Rosenfeld 1951; Robinson 1973; Graham *et al.* 1992). The order to which these are carried is the lowest that is required for the theoretical explanation of the effect, based on the following relative magnitudes of the multipole contributions to a physical effect that results from the interaction of electromagnetic radiation with matter (de Figueiredo and Raab 1981):

$$\text{electric dipole} >> \begin{cases} \text{electric quadrupole} \\ \text{magnetic dipole} \end{cases} >> \begin{cases} \text{electric octopole} \\ \text{magnetic quadrupole} \end{cases} >> \cdots \tag{4.3}$$

Natural optical activity in its various manifestations can be accounted for in the electric-quadrupole–magnetic-dipole approximation (Nakano and Kimura 1969; Barron and Buckingham 1971; Buckingham and Dunn 1971; Barron 1982; Graham and Raab 1990). It will become apparent from the theory that follows that the linear electro-optic rotation in nonmagnetic crystals can be explained within the same approximation. Accordingly, we work to this multipole order, for which the $\boldsymbol{D}$ and $\boldsymbol{H}$ fields are (Graham *et al.* 1992)

$$D_\alpha = \varepsilon_o E_\alpha + P_\alpha - \tfrac{1}{2}\nabla_\beta Q_{\alpha\beta}, \tag{4.4}$$

$$H_\alpha = \mu_o^{-1} B_\alpha - M_\alpha. \tag{4.5}$$

The $\boldsymbol{D}$ field in eqn. (4.4) also satisfies the Maxwell equation

$$\nabla \cdot \boldsymbol{D} = 0$$

for a source-free medium (Graham *et al.* 1992). In eqns. (4.4) and (4.5) $\boldsymbol{E}$ and $\boldsymbol{B}$ are the light-wave electric and magnetic fields respectively, and P_α, $Q_{\alpha\beta}$, M_α are, respectively, the electric-dipole, the electric-quadrupole, and the magnetic-dipole moments per unit macroscopic volume. These densities are the averages per unit macroscopic volume of the following moments of a spinless charge distribution (Raab 1975):

$$\text{(electric dipole)} \quad p_\alpha = \sum q r_\alpha , \tag{4.6}$$

$$\text{(electric quadrupole)} \quad q_{\alpha\beta} = \sum q r_\alpha r_\beta , \tag{4.7}$$

$$\text{(magnetic dipole)} \quad m_\alpha = \sum (q/2m)(\mathbf{r} \times \mathbf{p} + g\mathbf{s})_\alpha , \tag{4.8}$$

where q is the charge, m the mass, **p** the linear momentum, g the g-factor, and **s** the spin of a particle that has displacement **r** from an arbitrary origin in the distribution.

The electric and magnetic fields of a plane monochromatic light wave passing through a material, and their space and time derivatives, induce multipole moments in each macroscopic volume element of the substance. For nonmagnetic media in the presence of a static, or low-frequency, uniform electric field **E** the induced multipole moment densities are, to the order of electric quadrupole and magnetic dipole (Buckingham *et al.* 1971; Imrie and Raab 1991),

$$\begin{aligned} P_\alpha = {} & \alpha_{\alpha\beta} E_\beta + \tfrac{1}{2} \beta_{\alpha\beta\gamma} E_\beta E_\gamma + \tfrac{1}{2} a_{\alpha\beta\delta} \nabla_\gamma E_\beta + \tfrac{1}{2} b_{\alpha\beta\gamma\delta} \nabla_\gamma E_\beta E_\delta \\ & + \frac{1}{\omega} G'_{\alpha\beta} \dot{B}_\beta + \frac{1}{\omega} J'_{\alpha\beta\gamma} \dot{B}_\beta E_\gamma , \end{aligned} \tag{4.9}$$

$$Q_{\alpha\beta} = a_{\alpha\beta\gamma} E_\gamma + d_{\alpha\beta\gamma\delta} E_\gamma E_\delta , \tag{4.10}$$

$$M_\alpha = \frac{1}{\omega} G'_{\alpha\beta} \dot{E}_\beta + \frac{1}{\omega} J'_{\alpha\beta\gamma} \dot{E}_\beta E_\gamma . \tag{4.11}$$

In these equations only terms up to the first power in **E** are retained. In addition, ω is the angular frequency of the light wave, and $\alpha_{\alpha\beta}$, $\beta_{\alpha\beta\gamma}$, etc., are polarizability tensors, which are field-free, macroscopic volume properties of the medium. For negligible absorption, which is assumed, the polarizabilities in eqns. (4.9) - (4.11) are real quantities.

Valuable information about a polarizability tensor can be obtained from its quantum-mechanical expression. This contains matrix elements of multipole moment density operators, thereby displaying the physical basis of the tensor. (See Appendix A for examples.) From such an expression any permutation symmetry of tensor subscripts that exists may be readily determined, as well as relationships with other tensors, and also an expression for the change in a tensor may be determined when the origin used to specify **r** in eqns. (4.6) - (4.8) is displaced. Quantum-mechanical expressions are known for only some of the polarizability tensors in eqns. (4.9) - (4.11) (Graham and Raab 1990), although the molecular equivalents have been reported for all of them (Buckingham and Longuet-Higgins 1968; Imrie and Raab 1991). The latter allow the

missing macroscopic expressions to be determined by analogy, and these are given in Appendix A. It can then be shown that

$$\begin{gathered}\alpha_{\alpha\beta} = \alpha_{\beta\alpha},\ \beta_{\alpha\beta\gamma} = \beta_{\beta\alpha\gamma},\ a_{\alpha\beta\gamma} = a_{\alpha\gamma\beta} = a_{\beta\gamma\alpha}, \\ b_{\alpha\beta\gamma\delta} = b_{\alpha\gamma\beta\delta} = d_{\beta\gamma\alpha\delta}, \\ G'_{\alpha\beta} = -G'_{\beta\alpha},\ J'_{\alpha\beta\gamma} = -J'_{\beta\alpha\gamma}.\end{gathered} \tag{4.12}$$

To obtain the propagation equation, it is convenient to describe the electric field of the plane light wave in the complex form of eqn. (1.9)

$$\boldsymbol{E} = \boldsymbol{E}^{(o)} \exp[-i\omega(t - n\,\mathbf{r}\cdot\sigma / c)]. \tag{4.13}$$

The plane-wave form for $\boldsymbol{B}$ that is obtained from eqns. (4.13) and (4.1) is readily shown to satisfy the remaining Maxwell equation

$$\nabla \cdot \boldsymbol{B} = 0.$$

Also by means of eqns. (4.13) and (4.l) it is possible to express the induced multipole moment densities in eqns. (4.9) - (4.11) in terms of $\boldsymbol{E}$ and, as a result, the expressions for $\boldsymbol{D}$ and $\boldsymbol{H}$ in eqns. (4.4) and (4.5) as well. The latter two expressions, when substituted into the Maxwell equation (4.2), yield the wave equation

$$\left[n^2\sigma_\alpha\sigma_\beta - (n^2-1)\delta_{\alpha\beta} + \chi_{\alpha\beta} + \frac{1}{2\varepsilon_o}\beta_{\alpha\beta\gamma}E_\gamma + \frac{in}{\varepsilon_o c}U_{\alpha\beta} + \frac{in}{\varepsilon_o c}T_{\alpha\beta\gamma}E_\gamma\right]E_\beta^{(o)} = 0, \tag{4.14}$$

where $\delta_{\alpha\beta}$ is the Kronecker delta tensor, $\alpha_{\alpha\beta} = \varepsilon_o\,\chi_{\alpha\beta}$, and

$$U_{\alpha\beta} = \sigma_\gamma\left[G'_{\alpha\delta}\,\epsilon_{\beta\gamma\delta} - G'_{\beta\delta}\,\epsilon_{\alpha\gamma\delta} + \tfrac{1}{2}\omega(a_{\alpha\beta\gamma} - a_{\beta\alpha\gamma})\right] = -U_{\beta\alpha}, \tag{4.15}$$

$$T_{\alpha\beta\gamma} = \sigma_\delta\left[J'_{\alpha\varepsilon\gamma}\,\epsilon_{\beta\delta\varepsilon} - J'_{\beta\varepsilon\gamma}\,\epsilon_{\alpha\delta\varepsilon} + \tfrac{1}{2}\omega(b_{\alpha\beta\delta\gamma} - b_{\beta\alpha\delta\gamma})\right] = -T_{\beta\alpha\gamma}, \tag{4.16}$$

where $\epsilon_{\alpha\beta\gamma}$ is the Levi-Civita tensor. In eqn. (4.14) the phase part of $\boldsymbol{E}$ in eqn. (4.13) has been cancelled, since it is not necessarily zero for all space and time. Also, the propagation unit vector σ, the applied field $\mathbf{E}$, and the electric-field amplitude $\boldsymbol{E}^{(o)}$ are specified in terms of a laboratory frame of Cartesian axes.

Equation (4.14) is the fundamental equation, within the electric-quadrupole–magnetic-dipole approximation, for describing light propagation in any source-free nonabsorbing nonmagnetic medium to which a weak uniform electric field is applied. Of the tensors in eqn. (4.14) that describe matter, the origin independence of $\alpha_{\alpha\beta}$ and $U_{\alpha\beta}$ has previously been established (Graham and Raab 1990; see also Chapter 3), while that of $\beta_{\alpha\beta\gamma}$ and $T_{\alpha\beta\gamma}$ can be shown to follow from eqn.

(4.16) and the quantum-mechanical results in Appendix A. The expression for $U_{\alpha\beta}$ agrees with that derived by Graham and Raab (1990) and is consistent with those of Barron (1982) and Buckingham and Dunn (1971); in the latter case, propagation only along the main symmetry axis was considered. This expression may be shown to account for the medium's natural optical activity in terms of the polarizability tensors $G'_{\alpha\beta}$ and $a_{\alpha\beta\gamma}$. The expression in eqn. (4.16) for $T_{\alpha\beta\gamma}$, which involves the polarizability tensors $J'_{\alpha\beta\gamma}$ and $b_{\alpha\beta\gamma\delta}$, is the leading electric-field perturbation of the tensor $U_{\alpha\beta}$ and is derived in this general form for the first time. It reduces to that derived by Buckingham *et al.* (1971), who considered the special case of light propagation and applied field both along the optic axis of a uniaxial crystal. As will become evident, the tensor $T_{\alpha\beta\gamma}$ accounts for the linear electric-field-induced optical activity of a nonmagnetic medium.

To the order of electric quadrupole and magnetic dipole, eqn. (4.14) is essentially the Maxwell vector equation (4.2) and, by setting α equal to x, y, and z in turn, may be written as a set of three linear homogeneous equations in the unknown components of $\boldsymbol{E}^{(o)}$. Arranged in an eigenvalue matrix form, these equations yield

$$\begin{bmatrix} n^2(1-\sigma_x^2)-t_{xx} & -n^2\sigma_x\sigma_y-t_{xy} & -n^2\sigma_x\sigma_z-t_{xz} \\ -n^2\sigma_y\sigma_x-t_{yx} & n^2(1-\sigma_y^2)-t_{yy} & -n^2\sigma_y\sigma_z-t_{yz} \\ -n^2\sigma_z\sigma_x-t_{zx} & -n^2\sigma_z\sigma_y-t_{zy} & n^2(1-\sigma_z^2)-t_{zz} \end{bmatrix} \begin{bmatrix} E_x^{(o)} \\ E_y^{(o)} \\ E_z^{(o)} \end{bmatrix} = \begin{bmatrix} E_x^{(o)} \\ E_y^{(o)} \\ E_z^{(o)} \end{bmatrix}, \tag{4.17}$$

in which the eigenvalues are unity and where

$$t_{ij} = \chi_{ij} + \frac{1}{2\varepsilon_o}\beta_{ij\gamma}E_\gamma + \frac{in}{\varepsilon_o c}U_{ij} + \frac{in}{\varepsilon_o c}T_{ij\gamma}E_\gamma, \quad i, j = x, y, z. \tag{4.18}$$

On account of eqns. (4.12), (4.15), and (4.16), and because the crystal tensors in eqn. (4.18) are real in the absence of absorption, it follows that

$$t_{ij} = t_{ij}^*. \tag{4.19}$$

Equation (4.17) has a physical significance: for any given propagation direction σ and applied field direction $\mathbf{E}$ the medium supports only those polarization forms whose amplitude components are, to the order of electric quadrupole and magnetic dipole, the eigenvectors of eqn. (4.17). Their associated refractive indices can be found from the constraint that the eigenvalues are unity. Alternatively, the condition that the three components of $\boldsymbol{E}^{(o)}$ have nontrivial solutions is that the determinant of their coefficients should vanish; that is,

$$\begin{vmatrix} n^2(\sigma_x^2-1)+1+t_{xx} & n^2\sigma_x\sigma_y+t_{xy} & n^2\sigma_x\sigma_z+t_{xz} \\ n^2\sigma_y\sigma_x+t_{yx} & n^2(\sigma_y^2-1)+1+t_{yy} & n^2\sigma_y\sigma_z+t_{yz} \\ n^2\sigma_z\sigma_x+t_{zx} & n^2\sigma_z\sigma_y+t_{zy} & n^2(\sigma_z^2-1)+1+t_{zz} \end{vmatrix} = 0. \qquad (4.20)$$

It is this secular equation that will be solved in this chapter to obtain the refractive index n of each of the polarization eigenvectors for light propagating through a nonabsorbing nonmagnetic crystal to which a uniform weak electric field is applied.

4.3 Application to nonmagnetic crystals

Equation (4.20) is specified relative to an arbitrary set of laboratory Cartesian axes x, y, and z. In practice this reference frame is chosen to coincide with a set of crystallographic Cartesian axes, since crystal property tensors are traditionally expressed relative to the latter. The crystal axes adopted in this work are those described by Birss (1966), of which the z-axis is taken to be that of highest symmetry. This choice allows use to be made of Birss' tables of tensor components for the different nonmagnetic symmetry point groups.

In the terminology of Graham and Raab (1990), a light wave whose electric field is perpendicular to its propagation direction is an **N**-(or normal) ray, while one lacking this geometry is an **S**-(or skew) ray. Because an **S**-ray has an electric field component along its propagation path, the concept of polarization is not strictly applicable to it, nor is the Jones calculus (Shurcliff 1962). Accordingly, in this paper we are concerned only with the propagation of **N**-rays through the crystal.

If the light path and the applied electric field are each taken to lie along a crystallographic axis, but not necessarily the same one, then the form of the determinant in eqn. (4.20) that is obtained for these two directions in a crystal having a particular point group symmetry allows immediate identification of whether or not an **N**-ray propagates. For example, for light propagating along the z-axis, that is, $\sigma = (0, 0, 1)$, an **N**-ray occurs when in eqn. (4.20)

$$t_{zx} = t_{zy} = 0, \qquad (4.21)$$

since then the z component of $\boldsymbol{E}^{(o)}$ necessarily vanishes. Also, as follows from eqn. (4.19),

$$t_{xz} = t_{yz} = 0. \qquad (4.22)$$

Thus for **N**-ray propagation along a crystallographic axis in the presence of the applied field, eqn. (4.20) reduces in general to the form

$$\begin{vmatrix} -n^2+1+a+b\mathrm{E} & c+ind \\ c-ind & -n^2+1+e+f\mathrm{E} \end{vmatrix} = 0. \tag{4.23}$$

In this, as is evident from eqns. (4.18), (4.15), and (4.16), a and e are the relevant principal components of $\chi_{\alpha\beta}$, for the light path chosen, b and f are, respectively, the corresponding components of $(2\varepsilon_o)^{-1}\beta_{\alpha\beta\gamma}$ and $c \pm ind$ represent the appropriate off-diagonal components of t_{ij} and are thus linear functions of **E**.

The approach developed by Jones (1948) in his calculus may be extended to determine the various optical effects experienced by the wave in its passage through a crystal. To this end, eqn. (4.23) is rewritten as

$$\begin{vmatrix} -n^2+1+\mathrm{A}+\mathrm{B} & c+ind \\ c-ind & -n^2+1+\mathrm{A}-\mathrm{B} \end{vmatrix} = 0, \tag{4.24}$$

where

$$\mathrm{A} = \tfrac{1}{2}(a+e)+\tfrac{1}{2}(b+f)\mathrm{E}, \tag{4.25}$$

$$\mathrm{B} = \tfrac{1}{2}(a-e)+\tfrac{1}{2}(b-f)\mathrm{E}. \tag{4.26}$$

It was shown by Jones that the total optical effect of a nondepolarizing medium on a polarized **N**-ray may be regarded as the superposition of separate effects, each occurring independently of the others in a different plate of the material that is infinitesimally thin on the macroscopic scale. The four distinct optical effects that were identified by Jones in a nonabsorbing medium may be obtained from eqn. (4.24) as follows:

4.3.1 Plate 1: A ≠ 0 and B = *c* = *d* = 0

Thus the wave equation in eqn. (4.24) becomes

$$\begin{vmatrix} -n^2+1+\mathrm{A} & 0 \\ 0 & -n^2+1+\mathrm{A} \end{vmatrix} = 0. \tag{4.27}$$

This has two equal roots for n that have the vacuum limit of $n = 1$ when $\mathrm{A} = 0$, namely,

$$n = (1+\mathrm{A})^{\frac{1}{2}}.$$

Their respective eigenvectors are, as eqn. (4.27) shows, orthogonal linear polarizations along the crystallographic axes that lie perpendicular to the propagation direction. Thus all polarization

forms in this plate experience isotropic refraction along the chosen light path in the presence of the field. This is the first of the effects described by Jones.

4.3.2 Plate 2: B ≠ 0 and A = c = d = 0

Here eqn. (4.24) reduces to

$$\begin{vmatrix} -n^2+1+\mathrm{B} & 0 \\ 0 & -n^2+1-\mathrm{B} \end{vmatrix} = 0, \tag{4.28}$$

the solutions of which are given by

$$n_1^2 = 1+\mathrm{B},$$

$$n_2^2 = 1-\mathrm{B}.$$

Again the two eigenvectors are orthogonal linear polarizations along crystallographic axes, but this time a linear birefringence is evident, which is the second of Jones' optical effects, namely,

$$n_1 - n_2 = \frac{2\mathrm{B}}{(n_1+n_2)}. \tag{4.29}$$

4.3.3 Plate 3: c ≠ 0 and A = B = d = 0

Then eqn.(4.24) assumes the form

$$\begin{vmatrix} -n^2+1 & c \\ c & -n^2+1 \end{vmatrix} = 0. \tag{4.30}$$

It is readily shown that the two eigenpolarizations in this plate are linear vibrations along the bisectors of the two crystallographic axes perpendicular to the light path and that, relative to these axes, designated plus and minus, occurs the linear birefringence

$$n_+ - n_- = \frac{2c}{(n_+ + n_-)}. \tag{4.31}$$

This effect was first identified by Jones (1948), has been named after him (Graham and Raab 1983), and has yet to be measured in a suitable crystal.

4.3.3 Plate 3: d ≠ 0 and A = B = c = 0

For this plate, eqn. (4.24) becomes

$$\begin{vmatrix} -n^2+1 & ind \\ -ind & -n^2+1 \end{vmatrix} = 0, \tag{4.32}$$

and here the eigenvectors are right- and left-circularly polarized light, for which the circular birefringence can be found from eqn. (4.32), and is

$$n_r - n_l = d, \tag{4.33}$$

where n_r and n_l are the refractive indices for right- and left-circularly polarized light, respectively. It is the field-induced component of d that gives rise to the linear electro-optic rotation of interest in this paper.

The above analysis indicates that the presence of terms B, c, and d in the determinant in eqn. (4.24) will give rise to the respective birefringences in eqns. (4.29), (4.31), and (4.33), each of which may be a combination of natural and induced effects. Thus inspection of the wave equation (4.20), when it describes **N**-ray propagation along a crystallographic axis in a crystal with a particular symmetry, allows immediate identification of whether the linear electro-optic rotation occurs and, if so, whether it is accompanied by other induced birefringences.

This chapter is concerned primarily with the field-induced part of the circular birefringence in eqn. (4.33), for this is what produces the linear electro-optic rotation. The tensor responsible for this effect is $T_{\alpha\beta\gamma}$, as is evident from eqns. (4.23), (4.20), and (4.18). On its own this tensor is not sufficient to determine whether **N**-ray propagation is allowed. To do this, it is necessary to evaluate the elements t_{ij} in the determinant in eqn. (4.20) to see whether the conditions for **N**-ray propagation, such as those given for z-propagation in eqns. (4.21) and (4.22), are met. This is readily done by means of Birss' tables. For the choice of crystallographic axes used by Birss, it is found that **N**-rays for which the linear electro-optic rotation occurs propagate only along the z- and x-axes in certain crystals, provided the applied field is parallel to the light path. These results are summarized in Table 4.1, which shows all the natural and induced birefringences, designated as $(\ )_0$ and $(\ )_E$, respectively, that occur for the given propagation and field direction. The symbols in the various entries in the table represent the crystal property tensors responsible for the particular effect, such as α representing $\alpha_{\alpha\beta}$, a representing $a_{\alpha\beta\gamma}$, etc.

Table 4.1 shows that for a number of symmetry classes the field-induced circular birefringence $(n_r - n_l)_E$ for propagation along a crystallographic axis coexists with one or more linear birefringences, natural and/or induced. Examples are the class 2 for z-propagation and 32 for x-propagation. In such cases a linearly polarized beam entering the crystal acquires ellipticity in addition to having its azimuth rotated, so that the crystal is unsuitable for use as an electro-optic

Table 4.1 Predicted existence, for applicable nonmagnetic point groups, of a linear electro-optic circular birefringence and other birefringences for **N**-ray propagation, within the electric-quadrupole–magnetic-dipole approximation

Symmetry	Propagation along crystallographic z-axis, **E** = (0, 0, E)					
Class	$(n_y-n_x)_0$	$(n_y-n_x)_E$	$(n_+-n_-)_0$	$(n_+-n_-)_E$	$(n_r-n_l)_0$	$(n_r-n_l)_E$
2	α	β	α	β	aG′	bJ′
2/m	α	0	α	0	0	bJ′
4	0	0	0	0	aG′	bJ′
$\bar{4}$	0	β	0	β	0	bJ′
4/m	0	0	0	0	0	bJ′
3	0	0	0	0	aG′	bJ′
$\bar{3}$	0	0	0	0	0	bJ′
6	0	0	0	0	aG′	bJ′
$\bar{6}$	0	0	0	0	0	bJ′
6/m	0	0	0	0	0	bJ′
Symmetry	Propagation along crystallographic x-axis, **E** = (E, 0, 0)					
Class	$(n_y-n_x)_0$	$(n_y-n_x)_E$	$(n_+-n_-)_0$	$(n_+-n_-)_E$	$(n_r-n_l)_0$	$(n_r-n_l)_E$
32	α	β	0	0	aG′	bJ′
$\bar{3}m$	α	0	0	0	0	bJ′

rotator of linearly polarized light. All the remaining classes in Table 4.1 apply to propagation along the z-axis, for which the induced circular birefringence may be accompanied by the corresponding natural property. As this latter effect will not alter the basic form of an incident linearly polarized beam, crystals of these classes could serve as electro-optic rotators of linearly polarized light and find application as modulators with this property. The expressions for the field-induced circular birefringence in these classes may be obtained from eqns. (4.33), (4.20), (4.18), and (4.16) and Birss' tables. In summary, when the propagation and electric-field directions are both along the highest symmetry axis in crystals belonging to the symmetry classes

$$4^{*},\ 4/m,\ 3^{*},\ \bar{3},\ 6^{*},\ \bar{6},\ 6/m \tag{4.34}$$

(the asterisk denotes natural optical activity), the linear electric-field-induced circular birefringence can be shown to be

$$n_r - n_l = \frac{1}{\varepsilon_o c}\left(2\mathrm{J}'_{xxz} + \omega b_{xyzz}\right)\mathrm{E}. \tag{4.35}$$

The angle ϕ through which the plane of a linearly polarized beam is rotated on passing through a length L of a medium exhibiting circular birefringence is (Jenkins and White 1976)

$$\phi = \frac{\pi L}{\lambda}(n_r - n_l), \tag{4.36}$$

where λ is the vacuum wavelength of the light. Equations (4.35) and (4.36) express the linear electro-optic rotation ϕ in crystals of the classes in list (4.34).

4.4 Discussion

This chapter presents an eigenvalue wave equation describing light propagation through a source-free nonmagnetic medium to which a uniform electric field is applied. In this approach, induced multipole moments to the order of electric quadrupole and magnetic dipole, and contributions thereto linear in the applied field, are consistently allowed for. The wave equation, when applied to nonmagnetic crystals, enables light-propagation characteristics to be determined in terms of crystal property tensors, and in particular an optical rotation linear in the applied field may be fully explained. Consequently, when crystal symmetry arguments are taken into account, nonmagnetic crystal classes may be identified that, for specific light-propagation and applied-field directions, exhibit an induced optical rotation for light waves that propagate with only transverse electric fields. Furthermore, other natural and field-induced birefringences, which coexist with the linear electro-optic rotation in these classes, may also be identified. These various birefringences are indicated in Table 4.1.

When comparing the results presented in this chapter with those of previous investigations, one finds that Zheludev (1965) predicts the existence of a linear electro-optic rotation in, *inter alia*, the cubic classes 23 and $m3$, without making specific mention of the light-propagation and applied-field configurations. Our approach shows, by means of eqn. (4.20) and Birss' tables, that for these two classes no such effect will occur if the light propagation and the applied field are directed along the same crystallographic axis, while for any other configuration there will be no effect for **N**-rays. Among the other results given by Zheludev, crystals belonging to the symmetry point group $\bar{4}$ are predicted to exhibit an electro-optic rotation without an accompanying linear electro-optic birefringence when the light path and the applied field are both along the optic axis. Results for $\bar{4}$ in Table 4.1 contradict this finding, in that both the normal and the Jones linear birefringences are induced for this particular experimental configuration. Zheludev also states that a crystal with $\bar{3}m$ symmetry would exhibit a linear electro-optic rotation in the absence of an induced linear birefringence. However, Table 4.1 shows that when this induced rotation

occurs for **N**-rays, it is accompanied by a natural linear birefringence, which is of much greater magnitude.

In his search for point groups that display a linear electro-optic rotation in the absence of linear birefringences, Anastassakis (1972) highlighted the symmetry classes 23, $m3$, and $\bar{4}$, for particular field and propagation directions. As discussed above, the classes 23 and $m3$ may not exhibit the effect for any configuration. However, our conclusions for the group $\bar{4}$, where the existence of a linear electro-optic rotation is predicted in the presence of the corresponding natural effect for z-propagation and the z-field, are in agreement with those of Anastassakis. Agreement is also found with the predictions of Buckingham *et al.* (1971), who treated propagation and applied-field directions only along the optic axis in uniaxial crystals. Because these authors did not consider the detailed propagation of the light wave, they were unable to predict for this configuration the existence of induced linear birefringences, such as in $\bar{4}$.

Finally, Churcher and Stedman (1982) give a comprehensive list of light-path–applied-field configurations for the existence of a linear electro-optic rotation in nonmagnetic point groups. They are not, however, concerned with the presence of other birefringences or **N**-ray propagation. For instance, they do not recognize the induced linear birefringences in classes 2, $\bar{4}$, and 32, which should accompany the linear electro-optic rotation, as Table 4.1 shows. Furthermore, the classes 222, $mm2$, $4mm$, 622, 23, and $m3$, among others, are listed as displaying the effect, but our approach reveals that it will not occur in these crystals for **N**-ray propagation.

Some of the differences in the findings mentioned above can be explained by our limiting consideration to **N**-rays, since only for them does polarization have a strict meaning.

Part 2

EXPERIMENTAL STUDIES OF THE QUADRATIC ELECTRO-OPTIC EFFECT IN KDP, ADP, AND DKDP

Chapter 5

THE QUADRATIC ELECTRO-OPTIC EFFECT IN KDP-TYPE CRYSTALS – REVIEW AND THEORY

5.1 Introduction

Chapters 5 – 11 describe the work undertaken in the second half of this thesis, which is concerned with the experimental investigation of the quadratic electro-optic effect in a number of crystals belonging to the potassium dihydrogen phosphate (KDP) family. This group comprises crystals of KDP and its isomorphs, such as: ammonium dihydrogen phosphate (ADP), deuterated KDP (DKDP), deuterated ADP (DADP), and rubidium dihydrogen phosphate (RDP). These crystals are well known for both their nonlinear properties and applications in the field of electro-optics. Also investigated in this experimental project was the electrostrictive effect in some of the same crystals.

Contained in this part of the thesis are the details and results of two separate experimental investigations of crystals of KDP, ADP, and DKDP. In the first, the coefficients g_{xxxx}, g_{yyxx}, and g_{zzxx} of the quadratic electro-optic effect in KDP and ADP crystals were determined, together with the electrostrictive coefficients γ_{xxyy} and γ_{xxzz}, by means of a Michelson interferometer assembled in the research laboratories at the University of Natal, Pietermaritzburg. The second investigation was conducted during a three-month visit to the Technical University of Łódź in Łódź, Poland.

In this work, the difference in the coefficients $|g_{xxxx} - g_{yyxx}|$ was evaluated in KDP, ADP, and DKDP crystals, and $|n_o^3 g_{xxxx} - n_e^3 g_{zzxx}|$ was measured in KDP and ADP, where n_o and n_e are the ordinary and extraordinary refractive indices respectively. These latter two sets of measurements were made by means of the dynamic polarimetric technique.

This chapter provides an introduction to the quadratic electro-optic effect in KDP-type crystals. Particular emphasis is given to previous work conducted in this field and the ensuing discussion establishes the motivation behind the present investigations. Also introduced is the electrostrictive effect in these crystals and results obtained previously are given. This effect, as will be seen, complements the quadratic electro-optic effect and any account of the latter must make full allowance for it.

5.2 Review of the electro-optic effect

The electro-optic effect manifests itself as a change in refractive index of the medium to which an electric field is applied. Such an effect was first revealed by Kerr (1875) when he observed that a glass plate to which a uniform static electric field was applied became birefringent. Further investigations by the same author, predominantly on nonconducting liquids, established the relationship between the observed effect and the applied field: this particular birefringence was proportional to the square of the electric field (Kerr 1880). Since named the Kerr effect in his honour, but also known as the quadratic electro-optic effect, this induced birefringence was further investigated by a number of researchers including Röntgen (1880), Kundt (1883), and Pockels (1906) who, in confirming its existence, went further to suggest the effect to be related to crystal structure and type. This effect is known to be universal in the sense that it occurs in every material, irrespective of its symmetry. The linear equivalent of the Kerr effect, that is an induced birefringence linear in the applied electric field, was observed some years after Kerr's discovery independently by Röntgen (1883) and Kundt (1883) in crystalline quartz and tourmaline, although at the time both these researchers attributed the birefringence to a consequence of the converse piezoelectic effect. It was Pockels (1906) who established after thorough investigation that the linear effect occurred as a result of a field-induced birefringence independent of any mechanical strains in the crystal. Unlike the quadratic effect, the existence of this linear electro-optic effect, also termed the Pockels effect, is subject to stringent symmetry requirements and only noncentrosymmetric media are found to display it.

Traditionally, the Pockels and Kerr electro-optic effects are described in terms of perturbations to the impermeability tensor $\eta_{\alpha\beta}$ linear and quadratic, respectively, in a static or low-frequency electric field **E**. Expressed in the form of an equation this is (Kaminow 1974):

$$\Delta\eta_{\alpha\beta} = \eta_{\alpha\beta}(\mathbf{E}) - \eta_{\alpha\beta}(0) = r_{\alpha\beta\gamma} E_\gamma + g_{\alpha\beta\gamma\delta} E_\gamma E_\delta + \cdots, \qquad (5.1)$$

where $r_{\alpha\beta\gamma}$ and $g_{\alpha\beta\gamma\delta}$ are defined as the linear and quadratic electro-optic coefficients respectively, and are those introduced in Chapter 2. This impermeability description is consistent with the analysis of optical properties of a medium in terms of its index ellipsoid or optical indicatrix (Yariv and Yeh 1984). By contrast, the description of the electro-optic effect introduced in Chapter 2 defines the coefficients of the linear and quadratic electro-optic effects in terms of electric-field-induced changes to the macroscopic polarizability or susceptibility, where the coefficients used in each of the approaches are related by eqns. (2.10) and (2.104). Thus in this latter description even the Pockels effect may be directly recognised as a nonlinear effect, inasmuch as the induced electric-dipole moment is proportional to the product of two fields: those of the light wave and of the static or low-frequency applied field. Being quadratic in **E**, the Kerr effect is clearly a nonlinear phenomena. This analysis of induced polarization rather than impermeability change allows additional nonlinear optical phenomena to be accounted for: such as the optical Kerr effect, where the electric interaction in this case involves fields with frequencies in the optical range. However, although the phenomenological description in terms of the induced polarization rather than impermeability change is used to derive the theoretical results in this work, the final expressions for the induced birefringences are given in terms of components of the coefficients $r_{\alpha\beta\gamma}$ and $g_{\alpha\beta\gamma\delta}$. The reason for this is that these coefficients find extensive use in the literature, so that expressing results obtained in the present experimental investigations in terms of these components allows comparisons to be made with previously published values.

KDP-type crystals at room temperature are paraelectric and belong to the nonmagnetic tetragonal symmetry point group $\bar{4}2m$. As a consequence, they lack a centre of inversion and display the Pockels effect for certain applied-field and light-propagation geometries. For this point group the third-rank polar tensor $r_{\alpha\beta\gamma}$ describing the linear electro-optic effect has, relative to crystallographic axes, only two nonvanishing independent components which can be determined from tables by Birss (1966). Similarly, relative to the same axes, the tensor $g_{\alpha\beta\gamma\delta}$ describing the quadratic electro-optic effect – a fourth-rank polar tensor – has only seven nonzero independent components. With the *z*-axis along that of highest symmetry in the crystal, these components for both coefficients are (Birss 1966):

$$\left.\begin{aligned} r_{xyz} &= r_{yxz},\ r_{xzy} = r_{yzx} = r_{zxy} = r_{zyx}, \\ g_{xxxx} &= g_{yyyy},\ g_{zzzz},\ g_{yyxx} = g_{xxyy},\ g_{xxzz} = g_{yyzz}, \\ g_{zzxx} &= g_{zzyy},\ g_{xyxy} = g_{yxyx} = g_{yxxy} = g_{xyyx}, \\ g_{xzxz} &= g_{yzyz} = g_{xzzx} = g_{zxxz} = g_{zxzx} = g_{zyzy} = g_{yzzy} = g_{zyyz}. \end{aligned}\right\} \qquad (5.2)$$

Both the linear and quadratic electro-optic responses of KDP-type crystals are fully accountable in terms of these tensor components.

The linear electro-optic effect in crystals of KDP and DKDP was first reported by Zwikker and Scherrer (1944), while the quadratic effect was studied in KDP by Jacquerod (1942). Since then the electro-optic properties of KDP-type crystals have attracted particular interest. This stems back to the late 1940's following the suggestion by Billings (1949) that electro-optic materials, in particular KDP and ADP, may have practical applications for the modulation of light and as optical shutters. In fact Billings (1949), and later Carpenter (1950), assembled and studied optical light shutters based on the linear electro-optic effect in both these crystals. Subsequently, the use of the electro-optic effect for technological applications developed into an important and extensive field in which the effect provides for the accurate and high speed manipulation of light without the need for moving parts. A few of the many applications are: in optical communications, where electro-optic modulators are generally used to impress a signal onto an optical carrier in the transmitting optics, while in the receiving optics electro-optic sensors - a field in themselves - decouple the signal; in electro-optic displays, which vary from liquid crystals to high-resolution image displays; in optical signal processors; and more recently, in optical computing and integrated optics.

The development of a large portion of these electro-optic devices is based on the application of an electric field in one of two configurations: either with the field parallel to the light-propagation direction or perpendicular to it, where these are termed longitudinal or transverse devices respectively. Detailed analysis (see, for example, Meintjes and Raab 1999) reveals that materials belonging to only two symmetry classes permit longitudinal devices utilizing the linear electro-optic effect free of both natural birefringence and optical activity. One of these, for light propagation along the optic axis, is the symmetry point group $\bar{4}2m$ to which KDP-type crystals belong in their room-temperature state. In this crystal family are found materials with a sizable

linear electro-optic effect and for which large strain-free crystals of high optical quality may be grown with relative ease. A consequence of this has been the extensive use of KDP-type crystals in electro-optic applications, resulting in widespread investigations of the electro-optic properties of these crystals with the specific intent to further the understanding of electro-optic effects so as to permit the development of newer and better devices for technological applications. The more pertinent of such earlier investigations are compiled in a text by Kaminow (1974). Evidence of the continuing importance of these crystals, both in longitudinal and transverse devices, is the fact that they are still actively marketed by major international suppliers of electro-optic materials (for example, Cleveland Crystals).

Further interest in electro-optic effects arises from the point of view of their relation to other nonlinear phenomena which in themselves have extensive commercial, and other, applications. In particular, the quadratic electro-optic effect (or dc Kerr effect) constitutes a third-order nonlinear optical process together with the optical Kerr effect, third-harmonic generation, Brillouin and Raman scattering, and optical phase conjugation. It has long been recognised that the electro-optic effect[1] may be considered to consist of two parts related to separate microscopic interactions (Kaminow and Johnston 1967, 1969). The one part, a lattice or ionic contribution, accounts for the interaction of the applied electric field with the crystal lattice where the field-induced lattice displacements modify the electronic polarizability, and the other part, which is electronic in nature, stems directly from the interaction of the electric field with the electronic polarizability. Considering specifically the coefficient of the quadratic electro-optic effect, one may express these separate components in the form of an equation as

$$g_{\alpha\beta\gamma\delta}^{\text{primary}} = g_{\alpha\beta\gamma\delta}^{\text{ion}} + g_{\alpha\beta\gamma\delta}^{\text{elec}}, \tag{5.3}$$

where $g_{\alpha\beta\gamma\delta}^{\text{ion}}$ and $g_{\alpha\beta\gamma\delta}^{\text{elec}}$ are the ionic and electronic parts respectively.

One distinct type of nonlinear phenomenon may be recognised as a consequence purely of the interaction of the electric field with the medium in the absence of lattice displacements. This arises at frequencies of the perturbing field in the optical range where the medium's lattice motions are unable to follow the field reversals, so that ionic or lattice contributions to the electronic susceptibility fall away. The electronic part of the quadratic electro-optic effect in this

[1] We are concerned in the present discussion with the so-called *true* or *primary* electro-optic effect; that without any contributions arising from piezoelectric and electrostrictive strains.

case is associated with the third-order optical susceptibility $\chi^{(3)}_{ijkl}$ by the equation (Yariv and Yeh 1984)

$$g^{elec}_{ijkl} = -\frac{12\chi^{(3)}_{ijkl}}{\varepsilon_{ii}\varepsilon_{jj}}. \qquad (5.4)$$

where the tensor components are relative to principal axes and ε_{ii} is a principal component of the dielectric constant of the medium. Since this describes individual components, summation over repeated subscripts is not implied. This susceptibility is in itself related to further nonlinear phenomena, such as third-harmonic generation and four-wave mixing (Yariv 1975). A second group of third-order nonlinear phenomena, associated with the ionic part of the electro-optic effect, is known to be associated with second-order Raman scattering, hyper-Raman scattering, and electric-field-induced Raman scattering.

It is evident therefore that examining the quadratic electro-optic effect is relevant from the point of acquiring an understanding of electro-optic effects, given the role they play in a variety of applications, and also considering its relationship to a number of important phenomena in nonlinear optics.

5.3 Review of published results for coefficients of the quadratic electro-optic effect in KDP, ADP, and DKDP

With the attention KDP and its isomorphs have received in the past, a variety of experimental results for the nonlinear properties of these crystals has been published. In particular, the linear electro-optic effect, described by the third-rank tensor $r_{\alpha\beta\gamma}$, has been extensively investigated by means of numerous techniques. Based on these investigations, values obtained for the two independent linear electro-optic coefficients r_{xyz} and r_{xzy} for KDP-type crystals, and their temperature and wavelength dependences, are largely agreed upon and thoroughly tabulated by Landolt-Börnstein (1979, 1984).With regard to the quadratic electro-optic effect, similar experimental determinations of these coefficients have been conducted spanning a period from the early 1960's up to the present decade. A summary of these results for crystals of KDP, ADP, and DKDP is given in Table 5.1, which contains the coefficient or combination of coefficients investigated, the value of the coefficient determined, and the means by which the measurements

Table 5.1 Previous results for the quadratic electro-optic coefficients of KDP, ADP, and DKDP crystals. These values (in units of 10^{-20} m^2V^{-2}) were determined at room temperature and in the wavelength range from 550 - 633 nm

Crystal	Coefficient	Value	Method	Reference
KDP	$\lvert g_{xxxx} - g_{yyxx}\rvert$	260	SP	Perfilova and Sonin (1967)
	$\lvert g_{xxxx} - g_{yyxx}\rvert$	230	SP	Jamroz *et al.* (1979)
	$\lvert g_{xxxx} - g_{yyxx}\rvert$	< 10	DP	Jamroz and Karniewicz (1979)
	$\lvert g_{xxxx} - g_{yyxx}\rvert$	2.5 ± 0.5	DP	Górski and Kucharczyk (1987b)
	$g_{xxxx} - g_{yyxx}$	- 4.2 ± 0.6	DI	Kucharczyk *et al.* (1995)
	g_{xxxx}	- 4.0 ± 0.6	DI	Kucharczyk *et al.* (1995)
	g_{yyxx}	+ 0.2 ± 0.2	DI	Kucharczyk *et al.* (1995)
	$\lvert n_o^3 g_{xxxx} - n_e^3 g_{zzxx}\rvert$	1350	SP	Perfilova and Sonin (1967)
	$n_o^3 g_{xxxx} - n_e^3 g_{zzxx}$	- 12 ± 3	DI	Kucharczyk *et al.* (1995)
	g_{zzxx}	- 0.6 ± 0.3	DI	Kucharczyk *et al.* (1995)
	$\lvert n_e^3 g_{zzzz} - n_o^3 g_{xxzz}\rvert$	3100	DS	Perfilova and Sonin (1967)
	g_{zzzz}	≤ 0.24	DM	Grib *et al.* (1975)
	$\lvert g_{xyxy}\rvert$	94	SP	Perfilova and Sonin (1967)
	$\lvert g_{xyxy}\rvert$	1.4 ± 0.3	DP	Górski *et al.* (1994)
ADP	$\lvert g_{xxxx} - g_{yyxx}\rvert$	170	SP	Perfilova and Sonin (1967)
	$\lvert g_{xxxx} - g_{yyxx}\rvert$	53	SP	Lomova and Sonin (1968)
	$\lvert g_{xxxx} - g_{yyxx}\rvert$	4.7 ± 1.0	DP	Górski and Kucharczyk (1987b)
	$\lvert n_e^3 g_{zzzz} - n_o^3 g_{xxzz}\rvert$	2400	SP	Perfilova and Sonin (1967)
	$\lvert n_o^3 g_{xxxx} - n_e^3 g_{zzxx}\rvert$	1650	SP	Perfilova and Sonin (1967)
	$\lvert g_{xxxx} - g_{zzxx}\rvert$	605.7 ± 14	SP	Perfilova (1967)
	$\lvert g_{xxzz} - g_{zzzz}\rvert$	294.2 ± 2	SP	Perfilova (1967)
	$\lvert g_{xyxy}\rvert$	6000	SP	Perfilova and Sonin (1967)
DKDP	$\lvert g_{xxxx} - g_{yyxx}\rvert$	300	SP	Perfilova and Sonin (1967)
	$\lvert g_{xxxx} - g_{yyxx}\rvert$	250	SP	Jamroz *et al.* (1979)
	$\lvert g_{xxxx} - g_{yyxx}\rvert$	< 10	DP	Jamroz and Karniewicz (1979)
	$\lvert n_o^3 g_{xxxx} - n_e^3 g_{zzxx}\rvert$	1270	SP	Perfilova and Sonin (1967)
	$\lvert n_o^3 g_{xxxx} - n_e^3 g_{zzxx}\rvert$	10.4 ± 0.6	DP	Ledzion *et al.* (1999)
	$\lvert n_e^3 g_{zzzz} - n_o^3 g_{xxzz}\rvert$	4700	SP	Perfilova and Sonin (1967)
	$\lvert g_{xyxy}\rvert$	15	SP	Perfilova and Sonin (1967)

SP - static polarimetric; DP - dynamic polarimetric; DI - dynamic interferometric; and DM - deflection method.

were made. These results were all evaluated by optical means, either polarimetric (both static and dynamic), interferometric, or in the case of Grib *et al.* (1975) by a light deflection method. In addition to the value for g_{zzzz} for KDP given in Table 5.1 determined by Grib *et al.*, these authors also established that the coefficient g_{xxzz} was at least two orders of magnitude smaller ($\sim 10^{-20} m^2 V^{-2}$) than coefficients determined by Perfilova and Sonin (1967).

Upon viewing the results listed in Table 5.1 one is immediately aware that, in contrast to the agreement found in the linear electro-optic investigations, there are large discrepancies in the values determined for components of the quadratic electro-optic effect coefficients. These inconsistencies, which in several instances are up to two orders of magnitude even for the same electro-optic coefficients (for example, $|g_{xxxx} - g_{yyxx}|$ for both KDP and ADP), have been well noted in the literature (see, for example, Kucharczyk and Górski 1983; Górski and Kucharczyk 1987b; and Górski *et al.* 1994). The conclusion reached is that the spread in these values cannot be explained in terms of either measurement error (Kucharczyk and Górski 1983) or a temperature dependence of the coefficients since all the readings were recorded at approximately the same temperature. Likewise, attributing the difference in the results to a wavelength dependence of the coefficients can be ruled out because, although the readings span the range from 550 - 633 nm, these coefficients are known to have only a small dependence on wavelength in the visible region of the spectrum (Kucharczyk 1992). However, a pattern clearly evident in the tabulated results in Table 5.1 is that coefficients determined by the static polarimetric method, which involve the use of a dc electric field applied to the investigated material, are consistently larger than those measured by the other methods, all of which used a low-frequency perturbing electric field. In fact, this discrepancy between static and low-frequency measurements even extends to determinations of fourth-order electro-optic coefficients in KDP-type crystals where again the static values are found to be several orders of magnitude larger than the dynamic ones (Górski and Kucharczyk 1990). More recently, it has been proposed that it is specifically the results determined by means of static polarimetric methods, the favoured approach in the earlier investigations, that are overestimated, while those measured by dynamic techniques give a true indication of the effect (Górski and Kucharczyk 1987a).

5.4 Theory of the quadratic electro-optic effect in crystals of symmetry $\bar{4}2m$

Although optical properties of transparent media are usually described in terms of the impermeability tensor and the associated ellipsoid model (Yariv and Yeh 1984), a multipole approach was introduced in the first part of this thesis as a suitable analytic alternative. This has the advantage of not being limited to the order of electric dipole, as is the ellipsoid model, and can be invoked to account fully for higher-order multipole effects such as chirality. Illustrations of this method within the context of the electric-dipole order, and in the absence of applied fields, are given in Chapter 1 for nonmagnetic crystals of any symmetry. In addition, formulated on the same multipole basis and also to the order of electric dipole, the second chapter of this thesis describes the analytic determination of the principal indices and axes of a nonmagnetic medium in the electro-optic effect. Specifically, the quadratic electro-optic effect in crystals of symmetry $\bar{4}2m$ is dealt with in Section 2.7, albeit for only one particular field direction. It is these methods that will be applied in the study of the quadratic electro-optic effect in KDP-type crystals in the present experimental work. Such crystals, which belong to a nonenantiomorphous class, will in principle exhibit optical activity for any propagation direction off the optic axis. However, in the presence of the natural birefringence which exists for these propagation directions, this optical activity is found theoretically, and in practice (for KDP), not to be significant (Meintjes and Raab 1999; Kobayashi *et al.* 1988). Accordingly, in the following theoretical discussion KDP-type crystals are, to a good approximation, assumed to be optically inactive. This is in line with previous theoretical discussions of the electro-optic effect in KDP-type media (see, for instance, Carpenter 1950).

Investigations of the quadratic electro-optic effect in noncentrosymmetric media are usually conducted for those applied-field and light-propagation directions for which the linear electro-optic effect does not in principle occur (Perfilova and Sonin 1965), and the present inquiry is no exception. This enables the measurement of the quadratic electro-optic effect in the absence of the linear effect, which is considerably larger in magnitude and would complicate the investigation. Furthermore, it may be shown that for the nonmagnetic symmetry point group $\bar{4}2m$, to which KDP-type crystals belong in their room-temperature paraelectric phase, each of the seven independent components of the quadratic electro-optic coefficient in eqn. (5.2) which exist for it may be measured separately, and in the absence of the linear electro-optic

effect, for particular applied-field and light-propagation configurations and linear polarization states (Gunning *et al.* 1999). The crystals of KDP, ADP, and DKDP available for investigation in this research permitted two such configurations with light propagation, in turn, along the crystallographic *y*- and *z*-axes for a field in the *x*-direction. These alignments, for a linearly polarized probing beam, allowed measurement of the quadratic electro-optic coefficients g_{xxxx}, g_{yyxx}, and g_{zzxx} to be made separately, in the case of the interferometric technique, and in combination, in the polarimetric investigation. Given in this section is a theoretical study of the propagation of monochromatic light in a nonmagnetic medium of symmetry $\bar{4}2m$ for the particular field and propagation directions specified above for the crystals available, which relates the observed electro-optic effect to the separate electro-optic coefficients mentioned.

Equation (2.103) in Section 2.7 is the general expression, to the order of electric dipole, which may be solved for a nonmagnetic crystal of any symmetry, to which a static or low-frequency uniform electric field of arbitrary direction is applied, to determine the principal indices of refraction and associated axes of the medium. It includes the third- and fourth-rank tensors $b_{\alpha\beta\gamma}$ and $c_{\alpha\beta\gamma\delta}$, related to $r_{\alpha\beta\gamma}$ and $g_{\alpha\beta\gamma\delta}$, and $\beta_{\alpha\beta\gamma}$ and $\gamma_{\alpha\beta\gamma\delta}$, by eqns. (2.10) and (2.104) respectively, which describe, in turn, perturbations of the polarizability linear and quadratic in the field (eqn. 2.101). For convenience, eqn. (2.103) is reproduced below, since it serves as the starting point for the derivations in this chapter.

$$\begin{vmatrix} n_x^2 + b_{xx\gamma}\mathrm{E}_\gamma + c_{xx\gamma\delta}\mathrm{E}_\gamma\mathrm{E}_\delta - n^2 & b_{xy\gamma}\mathrm{E}_\gamma + c_{xy\gamma\delta}\mathrm{E}_\gamma\mathrm{E}_\delta & b_{xz\gamma}\mathrm{E}_\gamma + c_{xz\gamma\delta}\mathrm{E}_\gamma\mathrm{E}_\delta \\ b_{xy\gamma}\mathrm{E}_\gamma + c_{xy\gamma\delta}\mathrm{E}_\gamma\mathrm{E}_\delta & n_y^2 + b_{yy\gamma}\mathrm{E}_\gamma + c_{yy\gamma\delta}\mathrm{E}_\gamma\mathrm{E}_\delta - n^2 & b_{yz\gamma}\mathrm{E}_\gamma + c_{yz\gamma\delta}\mathrm{E}_\gamma\mathrm{E}_\delta \\ b_{xz\gamma}\mathrm{E}_\gamma + c_{xz\gamma\delta}\mathrm{E}_\gamma\mathrm{E}_\delta & b_{yz\gamma}\mathrm{E}_\gamma + c_{yz\gamma\delta}\mathrm{E}_\gamma\mathrm{E}_\delta & n_z^2 + b_{zz\gamma}\mathrm{E}_\gamma + c_{zz\gamma\delta}\mathrm{E}_\gamma\mathrm{E}_\delta - n^2 \end{vmatrix} = 0, \tag{5.5}$$

where

$$n_\mathrm{i}^2 = 1 + \chi_{\mathrm{ii}} = 1 + \varepsilon_\mathrm{o}^{-1}\alpha_{\mathrm{ii}}, \qquad \mathrm{i} = x,\ y,\ z.$$

Of relevance to the experimental work in this thesis is the orientation of the principal refractive indices and axes for a crystal belonging to the nonmagnetic symmetry point group $\bar{4}2m$ in the presence of the field $\mathbf{E} = (\mathrm{E}, 0, 0)$. For this field direction, and by means of tables given by Birss (1966), the only nonvanishing components of $b_{\alpha\beta\gamma}$ and $c_{\alpha\beta\gamma\delta}$ that enter eqn. (5.5) for this point group are

$$\left.\begin{aligned} b_{xzy} &= b_{yzx} = b_{zxy} = b_{zyx}, \\ c_{xxxx} &= c_{yyyy},\ c_{yyxx} = c_{xxyy},\ c_{zzxx} = c_{zzyy}. \end{aligned}\right\} \tag{5.6}$$

Thus for this field direction eqn. (5.5) becomes

$$\begin{vmatrix} n_o^2 + c_1 E^2 - n^2 & 0 & 0 \\ 0 & n_o^2 + c_2 E^2 - n^2 & bE \\ 0 & bE & n_e^2 + c_3 E^2 - n^2 \end{vmatrix} = 0, \tag{5.7}$$

where

$$\left.\begin{aligned} b = b_{xzy},\ c_1 = c_{xxxx},\ c_2 = c_{yyxx},\ c_3 = c_{zzxx}, \\ n_x^2 = n_y^2 = n_o^2,\ n_z^2 = n_e^2. \end{aligned}\right\} \tag{5.8}$$

Solving this equation for the principal indices of refraction and corresponding eigenvectors to terms second-order in the applied field, as is done in the similar analysis in Section 2.7, one obtains

$$n_1^2 = n_o^2 + c_1 E^2, \qquad \mathbf{r}_1 = (1,\ 0,\ 0), \tag{5.9}$$

$$n_2^2 = n_o^2 + \left[c_2 + \frac{b^2}{n_o^2 - n_e^2} \right] E^2, \qquad \mathbf{r}_2 = k\left(0,\ 1,\ \frac{bE}{n_o^2 - n_e^2} \right), \tag{5.10}$$

$$n_3^2 = n_e^2 + \left[c_3 - \frac{b^2}{n_o^2 - n_e^2} \right] E^2, \qquad \mathbf{r}_3 = k\left(0,\ -\frac{bE}{n_o^2 - n_e^2},\ 1 \right), \tag{5.11}$$

where the normalization constant k is

$$k = \left[1 + \frac{b^2 E^2}{(n_o^2 - n_e^2)^2} \right]^{-\frac{1}{2}}. \tag{5.12}$$

Alternatively, these equations may be rewritten in terms of the traditional electro-optic coefficients $r_{\alpha\beta\gamma}$ and $g_{\alpha\beta\gamma\delta}$ by making use of the expressions

$$b_{ijk} = -n_i^2 n_j^2 r_{ijk} \quad \text{and} \quad c_{ijkl} = -n_i^2 n_j^2 g_{ijkl}$$

in eqns. (2.10) and (2.104) of Chapter 2 respectively. This gives

$$n_1^2 = n_o^2 - n_o^4 g_{xxxx} E^2, \qquad \mathbf{r}_1 = (1,\ 0,\ 0), \tag{5.13}$$

$$n_2^2 = n_o^2 - n_o^4 \left[g_{yyxx} - \frac{n_e^4 r_{xzy}^2}{n_o^2 - n_e^2} \right] E^2, \qquad \mathbf{r}_2 = k \left(0,\ 1,\ -\frac{n_o^2 n_e^2 r_{xzy} E}{n_o^2 - n_e^2} \right), \tag{5.14}$$

$$n_3^2 = n_e^2 - n_e^4 \left[g_{zzxx} + \frac{n_o^4 r_{xzy}^2}{n_o^2 - n_e^2} \right] E^2, \qquad \mathbf{r}_3 = k \left(0,\ \frac{n_o^2 n_e^2 r_{xzy} E}{n_o^2 - n_e^2},\ 1 \right), \tag{5.15}$$

in which

$$k = \left[1 + \frac{n_o^4 n_e^4 r_{xzy}^2 E^2}{(n_o^2 - n_e^2)^2} \right]^{-\frac{1}{2}}. \tag{5.16}$$

These results give an important insight into the behaviour of crystals of the class $\bar{4}2m$ in the presence of the field $\mathbf{E} = (E, 0, 0)$. As the expressions for n_1^2 in eqns. (5.13) - (5.15) show, this point group becomes biaxial due to terms quadratic in the field, a conclusion in agreement with findings by Perfilova *et al.* (1966) in their study of this symmetry point group. In addition, these results show that, despite being quadratic in the field, changes to the refractive indices from their field-free values include contributions from both the linear and quadratic electro-optic coefficients. The field-dependent principal axes of the new system, relative to which the determinant in eqn. (5.7) is diagonalized, are given by the orthogonal set of axes $\mathbf{r}_1$, $\mathbf{r}_2$, and $\mathbf{r}_3$ in eqns. (5.13) - (5.15). These describe a rotation, dependent on the applied field, in the *yz*-plane about the field-free crystallographic *x*-axis.

The angle θ by which the field-perturbed principal axes are rotated about the *x*-axis follows from eqns. (5.14) and (5.15) and is given by

$$\theta = \tan^{-1} \left[\frac{n_o^2 n_e^2 r_{xzy} E}{n_o^2 - n_e^2} \right]. \tag{5.17}$$

This angle is typically very small. In fact, using values quoted in eqns. (2.112) for n_o, n_e, and r_{xzy} for KDP at a wavelength of 632.8 nm, and assuming an electric field strength of 5×10^5 Vm^{-1} - a typical value in this and other investigations of the quadratic electro-optic effect in KDP-type crystals (Perfilova 1967; Kucharczyk and Górski 1983) - one obtains from eqn. (5.17)

$$|\theta| \approx 0.01°. \tag{5.18}$$

Experimentally, the present investigation is concerned specifically with light propagation along

crystallographic axes, rather than the field-perturbed axes of the crystal in the presence of an applied electric field. Alignment relative to the latter would be especially difficult on account of their field-dependent nature and very slight deviation from the crystallographic axes. Having said this, given the very small and experimentally almost indistinguishable difference in alignment between the two sets of axes, one may be tempted to treat the two sets as equivalent, and thus to take as the refractive indices of the polarization eigenvectors of light propagating along crystallographic axes those in eqns. (5.13) - (5.15) for the principal axes perpendicular to the propagation direction σ; in other words, to assume:

For $\sigma = (0, 1, 0)$

$$n_1^2 = n_o^2 - n_o^4 g_{xxxx} E^2, \qquad \mathbf{r}_1 = (1, 0, 0), \tag{5.19}$$

$$n_2^2 = n_e^2 - n_e^4 \left[g_{zzxx} + \frac{n_o^4 r_{xzy}^2}{n_o^2 - n_e^2} \right] E^2, \qquad \mathbf{r}_2 = (0, 0, 1). \tag{5.20}$$

For $\sigma = (0, 0, 1)$

$$n_1^2 = n_o^2 - n_o^4 g_{xxxx} E^2, \qquad \mathbf{r}_1 = (1, 0, 0), \tag{5.21}$$

$$n_2^2 = n_o^2 - n_o^4 \left[g_{yyxx} - \frac{n_e^4 r_{xzy}^2}{n_o^2 - n_e^2} \right] E^2, \qquad \mathbf{r}_2 = (0, 1, 0). \tag{5.22}$$

The above assumption is now tested by determining the actual refractive indices corresponding to the eigenvectors for propagation along the crystallographic *y*- and *z*-axes, in order to compare with those in eqns. (5.19) - (5.22). This is achieved by an extension of the theory in Chapter 1 to allow for the electro-optic effect.

As in the case of eqn. (2.101) in Section 2.7, perturbations linear and quadratic in the electric field are allowed for by writing the polarizability as (Buckingham and Pople 1955)

$$\alpha_{\alpha\beta}(\mathbf{E}) = \alpha_{\alpha\beta} + \tfrac{1}{2}\beta_{\alpha\beta\gamma} E_\gamma + \tfrac{1}{6}\gamma_{\alpha\beta\gamma\delta} E_\gamma E_\delta + \cdots. \tag{5.23}$$

Hence, taking this field-perturbed polarizability into account in the theory given in Sections 1.2 and 1.3, one may rewrite the wave equation that appears in eqn. (1.13) as (Górski *et al.* 1994)

$$\left[n^2 \sigma_\alpha \sigma_\beta - (n^2 - 1)\delta_{\alpha\beta} + \chi_{\alpha\beta} + b_{\alpha\beta\gamma} E_\gamma + c_{\alpha\beta\gamma\delta} E_\gamma E_\delta \right] E_\beta^{(o)} = 0, \tag{5.24}$$

in which $\delta_{\alpha\beta}$ is the Kronecker delta, $\alpha_{\alpha\beta} = \varepsilon_o \chi_{\alpha\beta}$, as defined previously, and again for simplicity, as in the derivation of eqn. (2.103), we set:

$$b_{ijk} = (2\varepsilon_o)^{-1}\beta_{ijk} \quad \text{and} \quad c_{ijkl} = (6\varepsilon_o)^{-1}\gamma_{ijkl}.$$

This modified wave equation, whilst still to the order of electric dipole as is eqn. (1.13), now describes the propagation in any direction of a low-intensity plane monochromatic light wave in a homogeneous nonmagnetic medium to which a static or low-frequency uniform electric field **E** is applied.

The three homogeneous equations obtained from eqn. (5.24) by setting $\alpha = x, y$, and z, in turn, yield a matrix eigenvalue equation equivalent to that in eqn. (1.15), but now allowing for linear and quadratic perturbations in the field. The requirement for nontrivial solutions of this equation is the condition

$$\begin{vmatrix} n^2(\sigma_x^2 - 1) + 1 + t_{xx} & n^2\sigma_x\sigma_y + t_{xy} & n^2\sigma_x\sigma_z + t_{xz} \\ n^2\sigma_y\sigma_x + t_{yx} & n^2(\sigma_y^2 - 1) + 1 + t_{yy} & n^2\sigma_y\sigma_z + t_{yz} \\ n^2\sigma_z\sigma_x + t_{zx} & n^2\sigma_z\sigma_y + t_{zy} & n^2(\sigma_z^2 - 1) + 1 + t_{zz} \end{vmatrix} = 0, \qquad (5.25)$$

where

$$t_{ij} = \chi_{ii}\delta_{ij} + b_{ij\gamma}E_\gamma + c_{ij\gamma\delta}E_\gamma E_\delta. \qquad (5.26)$$

As in the case of eqn. (1.16), this equation is relative to crystallographic axes. It is this secular equation that will be used in the following analysis to solve for the refractive indices and corresponding eigenvectors for light propagation along the crystallographic y- and z-axes of KDP-type crystals in the presence of a field parallel to the crystallographic x-axis.

Consider a general propagation direction in the yz-plane for which $\sigma = (0, \sigma_y, \sigma_z)$. For the point group $\bar{4}2m$ in the presence of the field **E** = (E, 0, 0), the nonvanishing components of $b_{\alpha\beta\gamma}$ and $c_{\alpha\beta\gamma\delta}$ are given in eqn. (5.6). Thus eqn. (5.25) for this symmetry class and propagation direction becomes

$$\begin{vmatrix} n_o^2 + c_1E^2 - n^2 & 0 & 0 \\ 0 & n_o^2 + c_2E^2 - n^2\sigma_z^2 & n^2\sigma_y\sigma_z + bE \\ 0 & n^2\sigma_y\sigma_z + bE & n_e^2 + c_3E^2 - n^2\sigma_y^2 \end{vmatrix} = 0. \qquad (5.27)$$

In this equation n_o, n_e, b, c_1, c_2, and c_3 are as defined in eqn. (5.8). Solving this equation for n^2, and immediately expressing the results in terms of the linear and quadratic electro-optic coefficients $r_{\alpha\beta\gamma}$ and $g_{\alpha\beta\gamma\delta}$ (related to $b_{\alpha\beta\gamma}$ and $c_{\alpha\beta\gamma\delta}$ by eqns. (2.10) and (2.104) respectively), one obtains the two solutions:

$$n_1^2 = n_o^2 - n_o^4 g_{xxxx} E^2, \tag{5.28}$$

$$n_2^2 = \frac{n_o^2 n_e^2}{n_o^2 \sigma_y^2 + n_e^2 \sigma_z^2} + \frac{2 n_o^4 n_e^4 \sigma_y \sigma_z r_{xzy} E}{(n_o^2 \sigma_y^2 + n_e^2 \sigma_z^2)^2} - \frac{n_o^4 n_e^4 \sigma_y^2 g_{zzxx} E^2 + n_e^4 n_o^4 \sigma_z^2 g_{yyxx} E^2}{(n_o^2 \sigma_y^2 + n_e^2 \sigma_z^2)^2} - \frac{n_o^4 n_e^4 r_{xzy}^2 E^2}{n_o^2 \sigma_y^2 + n_e^2 \sigma_z^2} + \frac{4 n_o^6 n_e^6 \sigma_y^2 \sigma_z^2 r_{xzy}^2 E^2}{(n_o^2 \sigma_y^2 + n_e^2 \sigma_z^2)^3} + \cdots, \tag{5.29}$$

in which only terms up to second-order in the field are retained. The refractive indices in eqns. (5.28) and (5.29) are those of the two polarization eigenvectors of a light wave propagating in an arbitrary direction $\sigma = (0, \sigma_y, \sigma_z)$ in a crystal of the nonmagnetic class $\bar{4}2m$, to which a field along the crystallographic x-axis in applied. It is evident that the one refractive index is independent of the propagation direction and contains a term quadratic in the field. On the other hand, the refractive index of the second polarization eigenvector contains terms both linear and quadratic in the field, which all depend on the propagation direction. The term linear in the field vanishes for light paths along either the crystallographic y- or z-axes. Thus choosing such propagation directions allows the determination of the quadratic electro-optic effect without interference from the linear equivalent.

Expressions for the refractive indices for propagation along the crystallographic y- and z-axes may be obtained from eqns. (5.28) and (5.29) by setting $\sigma = (0, 1, 0)$ and $(0, 0, 1)$ respectively, to yield:

For $\sigma = (0, 1, 0)$

$$n_1^2 = n_o^2 - n_o^4 g_{xxxx} E^2, \qquad \mathbf{r}_1 = (1, 0, 0), \tag{5.30}$$

$$n_2^2 = n_o^2 - n_e^4 \left[g_{zzxx} + n_o^2 r_{xzy}^2 \right] E^2, \qquad \mathbf{r}_2 \approx k_2 \left(0, -n_o^2 r_{xzy} E, 1 \right), \tag{5.31}$$

For $\sigma = (0, 0, 1)$

$$n_1^2 = n_o^2 - n_o^4 g_{xxxx} E^2, \qquad \mathbf{r}_1 = (1, 0, 0), \tag{5.32}$$

$$n_2^2 = n_e^2 - n_o^4 \left[g_{yyxx} + n_e^2 r_{xzy}^2 \right] E^2, \qquad \mathbf{r}_2 \approx k_1 \left(0, 1, -n_e^2 r_{xzy} E \right), \tag{5.33}$$

where the normalization constants are

$$k_1 = \left[1 + n_o^4 r_{xzy}^2 E^2 \right]^{-\frac{1}{2}} \text{ and } k_2 = \left[1 + n_e^4 r_{xzy}^2 E^2 \right]^{-\frac{1}{2}}.$$

The eigenvector for each of these refractive indices was obtained by substituting the corresponding refractive index expression back into the equations from which the determinant

was derived for the particular propagation direction. Notably, in each of these cases one of the eigenvectors, that not parallel to the crystallographic x-axis, has a component in the direction of the light path; it is thus an **S**-ray (see definition and discussion thereof in Section 4.3). However, using the known values of r_{xy}, n_o, and n_e (Yariv and Yeh 1984; Landolt-Börnstein 1979, 1984) for KDP, ADP, and DKDP, and a field of approximately 5×10^5 Vm^{-1}, it is possible to calculate that in both instances this component is about 10^{-5} of the component perpendicular to the propagation direction. Accordingly, to a good approximation, these eigenvectors may be assumed to be polarized perpendicular to the propagation path, and parallel to the crystallographic axes (Górski *et al.* 1994).

From the refractive indices in eqns. (5.19) - (5.22) and (5.30) - (5.33) it is immediately evident that the seemingly acceptable approximation suggested in the discussion leading to eqns. (5.19) - (5.22), namely that the refractive indices in eqns. (5.13) - (5.15) corresponding to the field-perturbed principal axes may be regarded as those of the eigenvectors of the light wave propagating along the crystallographic y- or z-axis, is not valid given the true refractive indices in eqns. (5.30) - (5.33) for propagation along the crystallographic y- or z-axes. The difference lies in the terms in $(r_{xy})^2$ which are quadratic in the field. For the values of r_{xy}, n_o, and n_e for KDP, ADP, and DKDP, one calculates that these terms differ by a few orders of magnitude. For instance, for KDP (using values given in eqns. (2.112)) the $(r_{xy})^2$ terms in the n_2^2 expressions of eqns. (5.20) and (5.22) are approximately 1×10^{-20} m^2V^{-2}, while in the corresponding expressions in eqns. (5.31) and (5.33) they are about 8×10^{-22} m^2V^{-2}. Hence, in the first instance this term is comparable in magnitude to the quadratic electro-optic term (about 10^{-19} - 10^{-20} m^2V^{-2} for the dynamic results in Table 5.1), while in the second, not.

To complete this analysis one should now determine n_2^2 in eqn. (5.29) for propagation along each of the field-perturbed principal axes in eqns. (5.14) and (5.15). Consider, for argument's sake, propagation along the direction given by $\mathbf{r}_3$ in eqn. (5.15). For this field-dependent propagation direction the expressions for n_1^2 and n_2^2 in eqns. (5.28) and (5.29) reduce to

$$n_1^2 = n_o^2 - n_o^4 g_{xxxx} E^2, \qquad \mathbf{r}_1 = (1,\ 0,\ 0), \tag{5.34}$$

$$n_2^2 = n_o^2 - n_o^4 \left[g_{yyxx} - \frac{n_e^4 r_{xzy}^2}{n_o^2 - n_e^2} \right] E^2, \qquad \mathbf{r}_2 = k \left(0\ ,\ 1,\ -\frac{n_o^2 n_e^2 r_{xy} E}{n_o^2 - n_e^2} \right), \tag{5.35}$$

where k is given below eqns. (5.15). Hence, as would be expected, the results in the two

treatments are in agreement. Closer inspection reveals that since $\mathbf{r}_3$ is a field-dependent propagation path, the $r_{xzy}E$ term in the expression for n_2^2 in eqn. (5.29), which contains $\sigma_y\sigma_z$, becomes a term in $(r_{xzy}E)^2$. This combines with the other $(r_{xzy}E)^2$ term in that equation to form that in eqn. (5.35), different from the one in eqn. (5.31) which is for a field-independent propagation direction along a crystallographic axis. This result for the form of n_2^2 for propagation directions along a field-perturbed principal axis has some important consequences when one considers the manner in which the investigation of the quadratic electro-optic effect in KDP-type crystals is conducted. Section 5.5 considers this point further.

From the expressions in eqns. (5.30) - (5.33), one may obtain the difference in the refractive indices between the field and field-free conditions for each polarization eigenvector.

For $\sigma = (0, 1, 0)$

$$\Delta n_1 = n_1 - n_0 = -\tfrac{1}{2} n_o^3 g_{xxxx} E^2, \qquad \Delta n_2 = n_2 - n_e = -\tfrac{1}{2} n_e^3 \left[g_{zzxx} + n_o^2 r_{xzy}^2 \right] E^2, \quad (5.36)$$

For $\sigma = (0, 0, 1)$

$$\Delta n_1 = n_1 - n_o = -\tfrac{1}{2} n_o^3 g_{xxxx} E^2, \qquad \Delta n_2 = n_2 - n_o = -\tfrac{1}{2} n_o^3 \left[g_{yyxx} + n_e^2 r_{xzy}^2 \right] E^2, \quad (5.37)$$

in which the assumption was made that

$$n(0) \approx \tfrac{1}{2} \left[n(\mathbf{E}) + n(0) \right]. \quad (5.38)$$

For a field applied along the crystallographic x-axis these equations describe the field-induced changes in refractive index of the polarization eigenvectors which the medium supports for the specified propagation direction. These eigenvectors are, to a good approximation, parallel to the crystallographic axes perpendicular to the propagation direction. The leading field-induced changes in the refractive indices are those that are quadratic in the applied field, and are accountable for in terms of the linear electro-optic coefficient r_{xzy} and the quadratic electro-optic coefficients g_{xxxx}, g_{yyxx}, and g_{zzxx}. With the neglect of the linear electro-optic term in eqns. (5.36) and (5.37), these results are in agreement with those determined by means of the index ellipsoid method, in which contributions due to the linear electro-optic tensor are usually not considered since, for these light-propagation and field conditions, they do not lead to a contribution linear in the field, and their contribution quadratic in the field is not considered significant (Górski *et al.* 1994). It is clear from eqns. (5.36) and (5.57), however, that this tensor does contribute, in part, to the quadratic effect, and for the sake of consistency will be retained at this stage.

For propagation along the crystallographic z-axis in a KDP-type crystal with **E** along the x-axis

the electro-optic effect is quadratic in the field, as eqn. (5.37) shows, and so also is the electrostrictive effect (see Section 5.6). The applied field thus constitutes a very small perturbation, which is not experimentally significant except in difference effects such as Δn_i in eqns. (5.36) and (5.37). This provides the basis for certain assumptions in the derivation of a further result to be used in this experiment. To derive this expression, consider a linearly polarized beam entering the crystal along its optic axis (the z-axis), with its polarization plane at an angle α to the applied field in the x-direction. Because of the very slightly different refractive indices n_1 and n_2 in the eqns. (5.32) and (5.33) for light linearly polarized along the x- and y-axes, the beam may be assumed to retain its state of linear polarization and to propagate with an average refractive index $n(\alpha)$ which lies between n_1 and n_2. The electric field of the wave in the crystal is then taken as

$$\boldsymbol{E} = \boldsymbol{E}^{(o)}\cos\theta,$$

where $\theta = \omega(t\text{-}n(\alpha)z/c)$. Strictly, however, the beam propagates as its two eigenpolarizations along the x- and y-axes, their respective fields being

$$\boldsymbol{E}_x = \boldsymbol{E}^{(o)}\cos\alpha\cos\theta_x \quad \text{and} \quad \boldsymbol{E}_y = \boldsymbol{E}^{(o)}\sin\alpha\cos\theta_y,$$

where

$$\theta_i = \omega(t - n_i z/c), \qquad i = x,\ y.$$

The energies or intensities in the approximate and exact descriptions must be the same. Thus

$$\boldsymbol{E}^2 = \boldsymbol{E}_x^2 + \boldsymbol{E}_y^2. \tag{5.39}$$

Then by taking differential elements on both sides of eqn. (5.39) and setting θ, θ_x, and θ_y to be equal except when differences in the elements ΔE, ΔE_x, and ΔE_y matter, it can readily be shown that

$$\Delta n(\alpha) = \Delta n_x \cos^2\alpha + \Delta n_y \sin^2\alpha. \tag{5.40}$$

Hence, from eqns. (5.37),

$$\Delta n(\alpha) = -\tfrac{1}{2} n_o^3 \left[g_{xxxx}\cos^2\alpha + \left(g_{yyxx} + n_e^2 r_{xzy}^2 \right)\sin^2\alpha \right] E^2. \tag{5.41}$$

This result includes Δn_1 and Δn_2 in eqns. (5.37) as special cases and with eqns. (5.36) provides the theoretical basis for determining the quadratic electro-optic coefficients measured in this project. An expression comparable to eqn. (5.41) for propagation along an axis perpendicular to the optic axis cannot be derived on account of the accompanying natural birefringence, the magnitude of which would invalidate the assumption used to obtain eqn. (5.41).

The results derived in this section for both the refractive indices of the polarization eigenvectors for propagation along the crystallographic *y*- and *z*-axes of a KDP-type crystal in the presence of a field in the *x*-direction, and for the influence of this field on the principal crystallographic axes, are in agreement with those derived previously (see, for instance, Perfilova *et al.* 1966; Górski *et al.* 1994; Kucharczyk *et al.* 1995). However, the eigenvalue analysis leading to eqns. (5.28) and (5.29) for propagation in the *yz*-plane offers some new insight into the different electro-optic coefficient contributions to the refractive indices of the polarization eigenvectors for propagation off the crystallographic axes. In particular, the contribution of the linear electro-optic coefficient to the terms both linear and quadratic in the field is noted even for very small propagation directions off the crystallographic axes. As eqn. (5.29) shows, a linear coefficient contributes a term linear in **E** which, if unrecognised, may seriously affect the results of an experiment to measure the quadratic coefficients when propagation is not exactly along a crystallographic axis. Before undertaking an experimental investigation into the quadratic electro-optic effect in KDP-type crystals, these matters need to be suitably addressed.

5.5 Experimentally determining the quadratic electro-optic effect

As mentioned in the previous section, optical determinations of the quadratic electro-optic effect in KDP-type crystals are typically undertaken for those light-path and applied-field directions for which the linear electro-optic effect is, in principle, not exhibited. Yet, despite this, it has been shown (Kucharczyk and Górski 1983; Górski and Kucharczyk 1987a) that for the experimental conditions which accurately meet the theoretical requirements forbidding the effect, the linear electro-optic contribution to the measured field-induced birefringence or refractive index change may well compete with the quadratic electro-optic effect and adversely influence its determination.

The basis for this argument is that in any real experiment the physical conditions which forbid the existence of the linear electro-optic effect are in a practice not likely to be met perfectly. For instance, there is always a limit to the accuracy with which the crystal can be aligned with the light path and also to the precision with which the crystal can be cut relative to its crystallographic axes (Kucharczyk and Górski 1983). This latter limitation also has an impact on how the electric field is oriented with respect to the crystal axes, since two parallel plane faces of the crystal under

investigation are usually coated with a conducting material to act as electrodes. A further consideration, for which allowance is not ordinarily made in a theoretical analysis, is the possibility of a small angular divergence of the probing light beam. Under these conditions, a contribution to the refractive indices of the principal eigenvectors linear in the field may exist (Kucharczyk and Górski 1983; Górski and Kucharczyk 1987a). An example of this may be seen in eqn. (5.29) in which the refractive index expression n_2^2 contains a term first-order in **E** for propagation at an angle to the crystallographic *y*- or *z*-axis in the *yz*-plane. Since the linear electro-optic effect is so much larger than the quadratic effect in these crystals ($r_{ijk}E_k \sim 10^{-7}$ compared with $g_{ijkl}E_kE_l \sim 10^{-10}$ for $E = 5 \times 10^5$ Vm^{-1}), the linear contribution may well be comparable to, or possibly larger than, the quadratic term, even for very small off-axis propagation angles. For instance, if the light path in the *yz*-plane diverges by 0.2° from the *z*-axis, then the term in **E** in eqn. (5.29) is about 36 times greater than the largest of the $\mathbf{E}^2$ terms in this equation. Similar conclusions have been reached by Kucharczyk and Górski (1983) and Górski and Kucharczyk (1987a), who applied a numerical analysis to the polarimetric experiment for the same light path configurations as that used in the above calculation, and who, in addition, allowed for nonparallelism of the laser beam and small misalignments in the field direction in determining contributions due to the linear effect to the induced birefringence quadratic in the field. The large effect measured in such situations is termed the *apparent* quadratic electro-optic effect, and was been shown to be comparable in magnitude to results measured by means of the static polarimetric method. Accordingly, measurement practices that take steps to eliminate contributions from the linear effect are highly necessary.

Without going into the details of the polarimetric technique, since these will be covered in Chapter 9, it is important to realise that the static method is concerned with the determination of the absolute change in birefringence of a crystal, in the polarimetric arrangement, as a function of the applied dc electric field. For example, to measure the quadratic electro-optic coefficients $|g_{xxxx} - g_{zzxx}|$ and $|g_{xxzz} - g_{zzzz}|$ in ADP, Perfilova (1967) determined the induced birefringence as a function of the square of the applied field for two different crystal orientations in which the linear electro-optic effect was considered nonexistent; in the one instance with the field in the *y*-direction for the light path along the crystallographic *x*-axis, and in the other the field along the optic axis for propagation in the *y*-direction. From this assumed dependence the quadratic electro-optic coefficients of interest were determined. In this case both were of the order of 10^{-18} m^2V^{-2}. However, crucial to such an investigation procedure, is that the change in birefringence is due

only to the quadratic electro-optic effect. In such determinations no allowance was made for the possible contribution of the linear electro-optic coefficients, as in eqn. (5.29), to a change in birefringence.

On the other hand, the dynamic approach, both polarimetric and interferometric, for measuring the quadratic electro-optic effect involves the use of a sinusoidal electric field of known frequency applied to the crystal. Thus, through the use, for example, of a lock-in amplifier an harmonic analysis of the resulting modulated emerging light intensity from the optical arrangement is possible. Results for the field-induced change in birefringence (polarimetric method) or refractive index (interferometric technique) determined from this light intensity change may thus be evaluated at the second harmonic of the modulated applied field frequency, and from these the necessary quadratic electro-optic coefficients were evaluated. Therefore induced effects which are purely quadratic in the field are measured, and any effect linear in the field is filtered out. In addition to distinguishing between contributions linear and quadratic in the field, when it comes to sensitivity and noise reduction, a modulation technique offers a decided advantage over a static method.

Besides a contribution first-order in the linear electro-optic coefficient, terms quadratic in $r_{\alpha\beta\gamma}$ may also contribute to the induced refractive index changes in KDP-type crystals, as eqn. (5.29) shows. In the previous section, much was made of the two seemingly inconsistent results in eqns. (5.19) - (5.22) and (5.30) - (5.33) before this difference was explained. This discussion is justified if one considers, as an example, the experimental arrangement to which eqn. (5.29) applies in which a static electric field is used in an investigation for the applied-field and light-propagation configurations of interest in this project this. For this field, the directions of the principal axes of the field-perturbed system given by eqns. (5.13) - (5.15) are fixed in the crystal, and only slightly different from the crystallographic axes. Thus because of the experimental difficulty in ensuring a precise light propagation path, a beam directed along a crystallographic axis may unintentionally end up along one of these principal axes in its near vicinity. In this situation the contribution of $(r_{xzy}E)^2$ to the observed refractive index change is very different from that for propagation along the intended crystallographic axis. Calculation for KDP (see Section 5.4) shows that it is two orders of magnitude larger. By contrast, the dynamic method employs an alternating electric field, which thus changes the orientation of the principal axes of the perturbed crystal with time, in step with the field. For a fixed propagation direction therefore, there is no possibility of accidentally

orientating the light path along one of the principal axes of the perturbed crystal, and the propagation condition leading to the larger contribution in $(r_{xy}E)^2$ cannot be met.

Not surprisingly, the literature provides convincing evidence and argument in favour of a dynamic measurement procedure over a static one (Kucharczyk and Górski 1983; Górski and Kucharczyk 1987a). Yet, despite this, it is largely the static results for KDP-type crystals that are quoted in the literature (see, for example, Yariv and Yeh 1984; Landolt-Börnstein 1979, 1984). Thus the remeasurement of quadratic electro-optic coefficients by dynamic means is important, not only to establish reliable values of these coefficients in KDP-type crystals, but also to correct perceptions regarding their magnitude. This experimental project focuses particularly on the quadratic electro-optic coefficients g_{xxxx}, g_{yyxx}, and g_{zzxx} in KDP, ADP, and DKDP crystals.

5.6 Electrostriction in KDP-type crystals

Although this thesis concentrates on optical phenomena in crystals, it is important to realise in an experimental investigation of the quadratic electro-optic effect that electrostriction - the deformation of a crystal quadratic in the applied field - like the quadratic electro-optic effect, is described by a fourth-rank polar tensor (Nye 1985). Consequently, this effect may occur in crystals of all symmetry classes, and the point group symmetry properties of its tensor are precisely those of the quadratic electro-optic coefficient. Inasmuch as electrostriction coexists with the quadratic electro-optic effect, an investigation of the latter must make full allowance for possible influences of electrostriction. With this in mind, room-temperature values of some components of the electrostrictive tensor of crystals of KDP and ADP are given in Table 5.2, since it will be seen that in the interferometric investigation outlined later that electrostriction plays a role. As in Table 5.1 for the quadratic electro-optic coefficients, note is also made of the method of measurement.

With two exceptions, the results in Table 5.2 are as they appear in the various published articles, and in these cases were measured by a direct method. The exceptions are the values quoted for Troussant *et al.* (1988) and Sysoev (1992), which are not tabulated as they appear in the literature but were recalculated from the reported data. The former of these gave results for the electrostrictive coefficients Q_{zzzz} and Q_{xxzz} defined in terms of the induced polarization rather than

Table 5.2 Reported values (in units of 10^{-20} m^2V^{-2}) for some components of the electrostrictive tensor $\gamma_{\alpha\beta\gamma\delta}$ in some KDP and ADP at room temperature

Crystal	Coefficient	Value	Method	Reference
KDP	$\lvert\gamma_{xxxx}\rvert$	400	SI	Madhu Mohan and Haranadh (1995)
	$\lvert\gamma_{xxxx}\rvert$	38	SI	Górski (1987)
	γ_{xxzz}	0.8	DT	Troussant *et al.* (1988)
	$\lvert\gamma_{zzxx}\rvert$	1.5	RM	Sysoev (1992)
	γ_{zzzz}	0.9	DT	Troussant *et al.* (1988)
	$\lvert\gamma_{xxxx} + \gamma_{zzzz} - 2\gamma_{xyyz}\rvert$	2	RM	Sysoev (1992)
ADP	$\lvert\gamma_{xxxx}\rvert$	200	SI	Górski (1987)
	$\lvert\gamma_{xxxx}\rvert$	2.3	DI	Zaitseva and Fotchenkov (1967)
	$\lvert\gamma_{xxzz}\rvert$	79	SI	Hruška (1965)
	$\lvert\gamma_{xxzz}\rvert$	79	SI	Madhu Mohan and Haranadh (1995)
	$\lvert\gamma_{xxzz}\rvert$	12	DI	Zaitseva and Fotchenkov (1967)
	$\lvert\gamma_{yyxx} + \gamma_{zzxx}\rvert$	19	SI	Hruška (1965)

SI - static interferometric; DI - dynamic interferometric; DT - coupled neutron and gamma diffraction technique; RM - resonance method.

electric field. Through the use of the relation (Kaminow 1974)

$$\gamma_{iijj} = \varepsilon_o^2(\varepsilon_{jj} - 1)^2 Q_{iijj}, \tag{5.42}$$

where ε_o is the permittivity of free space, ε_{jj} is the principal component of the low-frequency dielectric constant of the medium, and summation over the indices is not implied, the coefficients in Table 5.2 in terms of the electric field were calculated. The results given by Sysoev (1992) were determined in the vicinity of the phase transition temperature T_c (122K for KDP). In the range of $0.04\ K < T - T_c < 30\ K$ these were given (in units of 10^{-20} m^2V^{-2}) as

$$\gamma_{zzxx} = \left[(3.09 \pm 0.12) \times 10^{-20}\right]\tau^{-2.01}$$

$$\gamma_{xxxx} + \gamma_{zzzz} - \gamma_{yyzz} = \left[(4.179 \pm 0.12) \times 10^{-20}\right]\tau^{-1.99}$$

where

$$\tau = \left[T - T_c\right]/T_c .$$

Assuming linearity of these results to higher temperature ranges, one may calculate the given values in Table 5.2 at room temperature.

As is evident from the values listed in Table 5.2, the magnitude of the electrostrictive coefficients

in KDP and ADP crystals, like the quadratic electro-optic coefficients, are subject to wide disagreement. It was decided, therefore, that where necessary, values required for particular electrostrictive coefficients in this investigation would be determined experimentally, so as not to have to rely on the uncertain values given above.

5.7 Contributions from the electrostrictive effect

Although the electrostrictive effect is proportional to the square of the field, there are experimental situations in which it is not manifested (see below). However, when it does coexist with the quadratic electro-optic effect, and the latter's contribution is sought, it becomes necessary to distinguish the two effects. The *true* quadratic electro-optic effect exhibited by a material is that which does not include an electrostrictive contribution; it is the effect which would be measured if the perturbing electric field was at a frequency above the range of acoustic resonances of the crystal being investigated, since at these frequencies the crystal is not free to follow the field-induced strains and is effectively considered to be *clamped*. This is the same coefficient that would be measured if the sample was physically restrained from following the induced strains. If, on the other hand, the frequency of the electric field applied to the crystal is well below the fundamental frequency of mechanical resonance of the specimen, which like the acoustic resonance frequency depends on the sample dimensions, then it is considered to be mechanically free. In this case strains will be induced in the material by the applied field via the electrostrictive effect (see, for example, Kaminow 1974).

For the present investigation the frequency of the field was well below the frequencies of mechanical resonance of the different crystal specimens. They were, therefore, subject to a field-induced strain on account of the electrostrictive effect. The implications of this strain may, broadly speaking, be divided into three parts:

(i) it leads to a physical increase or decrease in the crystal's dimensions,

(ii) it forms part of an elasto-optic–electrostrictive contribution to the measured electro-optic effect, and

(iii) it contributes to an attraction or repulsion of the material's electrodes.

Each of these effects is of significance in an actual experiment and allowance should also be made for it in order to understand the precise nature of the observed quadratic electro-optic effect.

5.7.1 Strain-induced changes to the crystal dimensions

The electric field-induced strain $S_{\alpha\beta}$ due to the electrostrictive effect is given by (see, for example, Nye 1985)

$$S_{\alpha\beta} = \gamma_{\gamma\delta\alpha\beta} E_\gamma E_\delta , \tag{5.43}$$

where $\gamma_{\gamma\delta\alpha\beta}$ is the fourth-rank polar tensor describing the electrostrictive effect, and **E** is the applied electric field. This strain induced in a crystal results in a change in its length in the i^{th} direction, ΔL_i, given by (see, for example, Nye 1985)

$$\Delta L_\alpha = S_{\alpha\beta} L_{\alpha\beta} . \tag{5.44}$$

It is the change in the crystal's dimension in the direction of light propagation which is important in experiments involving interferometric techniques. Together with the electro-optic effect, this variation in crystal length contributes to a change in the optical path length experienced by the probing light wave. Since optical investigations are usually based on the measurement of these path length changes in their determination of electro-optic effects, the contribution due to electrostriction should be allowed for. For an applied electric field parallel to the crystallographic *x*-axis, the relevant changes in sample length in the crystallographic *y*- and *z*- directions are, from eqns. (5.43) and (5.44), given by:

$$\Delta L_y = \gamma_{xxyy} L_y E^2 , \tag{5.45}$$

$$\Delta L_z = \gamma_{xxzz} L_z E^2 . \tag{5.46}$$

In the derivation of these expressions use was made of the fact that $\gamma_{\gamma\delta\alpha\beta}$, being a fourth-rank polar tensor like $g_{\alpha\beta\gamma\delta}$, possesses the same nonvanishing components as does $g_{\alpha\beta\gamma\delta}$, in particular those in eqn. (5.2) for the class $\bar{4}2m$. These expressions for the field-induced variations in crystal length will find application in Section 8.1 where equations are derived for the total optical path-length change induced by the quadratic electro-optic and electrostrictive effects in an interferometric investigation. It may also be noted that in the case of *relative* measurements, such as those performed in the polarimetric method (i.e. in the determination of the magnitude of the difference between two electro-optic coefficients), this electrostrictive induced path-length change does not contribute to the measured birefringence change.

5.7.2 Elasto-optic-electrostrictive contributions to the electro-optic effect

The coefficient of the quadratic electro-optic effect determined when the crystal is unable to follow field-induced strains (i.e. when it is not subject to electrostrictive effects) is referred to as

the *true*, or *primary*, quadratic electro-optic effect. Coefficients measured in these conditions are usually designated $g^{s}_{\alpha\beta\gamma\delta}$, where the superscript *s* signifies the coefficient is determined at constant stress. In this experiment, however, the quadratic electro-optic coefficients are determined for a frequency of the applied field well below the sample's mechanical resonance frequencies, which are typically of the order of 1 MHz. When measured in these conditions where the sample is free to follow field-induced strains, and is thus considered *unclamped*, the coefficients are designated $g'_{\alpha\beta\gamma\delta}$, as they are measured at constant strain. These two coefficients - those of constant stress (clamped) and constant strain (unclamped) - differ by an amount that is due to an elasto-optic-electrostrictive contribution (see, for example, Kaminow 1974). Expressed in an equation:

$$g^{t}_{\alpha\beta\gamma\delta} - g^{s}_{\alpha\beta\gamma\delta} = p_{\alpha\beta\lambda\mu}\gamma_{\lambda\mu\gamma\delta}, \tag{5.47}$$

where $p_{\alpha\beta\lambda\mu}$ and $\gamma_{\lambda\mu\gamma\delta}$ are the elasto-optic and electrostrictive coefficients respectively.

Thus when determining the quadratic electro-optic effect at low frequencies, the contribution of the elasto-optic and electrostrictive effects is present which may lead to the observed electro-optic effect being either greater or less than the true quadratic electro-optic effect. This contribution needs to be recognised and allowed for in order to evaluate the true effect.

5.7.3 Electrostrictive attraction of the electrodes

A further physical process, besides the electro-optic effect, results in an electric field-induced change in refractive index of the medium being investigated. This arises due to the stress induced in the sample on account of the electrostatic attraction of the electrodes and the piezoelectric effect, and is described, for example, by Bohatý and Haussühl (1977). Under these conditions there is a contribution to the measured electro-optic coefficient given in terms of the piezo-optic and mechanical stress tensors $q_{\alpha\beta\gamma\delta}$ and $\sigma_{\alpha\beta}$ respectively.

Thus under these conditions, taking the discussions in Subsections 5.7.2 and 5.7.3 into account, one may relate the coefficient of the quadratic electro-optic effect measured in this experiment g'_{ijkl} to the true coefficient g^{s}_{ijkl} by

$$g^{t}_{ijkl} = g^{s}_{ijkl} + p_{ijmn}\gamma_{klmn} + \frac{q_{ijmn}\sigma_{mn}}{E_k E_l}. \tag{5.48}$$

In order to determine the true electro-optic coefficient, each additional tensor on the right-hand side of eqn. (5.48) needs to be known, from which g^{s}_{ijkl} may be determined in this experiment.

Chapter 6

NOTES ON THE INTERFEROMETRIC INVESTIGATION

6.1 Introduction

A light wave that propagates through a medium exhibiting both the quadratic electro-optic and electrostrictive effects will experience a change in optical path length dependent on the applied field. This variation in path length is a consequence of the two field-induced effects: the quadratic electro-optic effect which leads to a change in refractive index of the medium, Δn, and the material's electrostrictive strain, which alters its length by ΔL. This is given by the expression

$$\Delta d = \left[L\Delta n + (n - n_a)\Delta L \right]. \tag{6.1}$$

In this equation n_a is the refractive index of the environment surrounding the affected material, L is the field-free length of the medium in the direction of light propagation, and n is similarly its field-free refractive index for the particular propagation path and polarization state of the light wave. This change in optical path length, if introduced between the two light waves of an interferometer, will lead to a shift in the phase of the interference pattern emerging from the system.

On account of its sensitivity to small optical path-length changes, such as those given in eqn. (6.1), laser interferometry suggests itself as being ideally suited to the measurement of birefringence changes due to the electro-optic effect and also of dilations of the medium resulting from piezoelectric-type strains. Such measurements would allow the responsible effects to be

determined themselves. Indeed, numerous investigations of the sort are reported in the literature, and this is precisely the method proposed for the present inquiry. In some respects the interferometric examination presented in this thesis is a continuation of work submitted in the dissertation *An interferometric investigation of the quadratic electro-optic effect in KDP* by Gunning (1995) for the degree of Master of Science. That project, describing a study of single-crystal KDP by means of a Michelson interferometer, determined the sign and magnitude of the quadratic electro-optic coefficients g_{xxxx}, g_{yyxx}, and g_{zzxx} by a compensation method. Notably, those results also included a small undetermined, and largely unknown, contribution due to the electrostrictive effect. The only known examination of its sort into the quadratic electro-optic properties of KDP-type crystals, this method of investigation offered promising possibilities for further, more extensive, inquiries into these crystals, and it was this that prompted the present continuation of the research. Although the work reported here makes use of the original interferometer developed in the initial project, numerous modifications to the apparatus were made which led to a significant improvement in its sensitivity and stability. Furthermore, these modifications also led to a more accurate determination of the piezoelectric constant of the reference material used for compensation purposes in both instances.

The development of the interferometer used in this research, and the procedure by which the investigations were conducted, were always with the two-fold aim of this inquiry in mind: to obtain a measure of the sign and magnitude of various quadratic electro-optic coefficients of mechanically-free samples of KDP and ADP single-crystals at room temperature; and also to obtain an estimate of the electrostrictive coefficients of these crystals which coexist and contribute, to an extent, to the observed field-induced optical path-length change under the same conditions. This particular chapter considers the manner in which these effects displayed by KDP-type crystals might be investigated interferometrically; introduced are many of the thoughts and ideas behind the interferometer used in this work. These may, broadly speaking, be divided into three main areas: the type of interferometer decided upon; the means by which the induced optical path-length changes, and consequently the results of interest, were determined; and also, the employment of a means of active stabilization. Since the field of optical interferometry is so vast, the references given here are largely those pertaining to investigations of electro-optic, piezoelectric, and electrostrictive effects. All these examinations encompass the same fundamental idea - that of measuring small field-induced optical path-length changes - and it is within this context that the apparatus for the present study was developed.

6.2 On the principle of optical interferometry

Before considering the methods adopted to investigate the quadratic electro-optic and electrostrictive effects by interferometric means in this work, it is necessary to give some background into the principle of optical interferometry. Results derived here are referred to in later sections.

Laser interferometry has as its basis the well-known phenomenon of interference, which occurs when two coherent superimposed monochromatic light waves meet at a point. The intensity at the point depends on the extent of cancellation of the two waves. For a point with co-ordinate **r**, the resultant electric field of the two interfering waves linearly polarized in the same plane and propagating in the same direction is

$$\boldsymbol{E} = \boldsymbol{E}_1 + \boldsymbol{E}_2 = \exp\left[-i\omega n\,\mathbf{r}\cdot\sigma/c\right]\left\{\boldsymbol{E}_1^{(o)}\exp\left[-i\phi_1\right] + \boldsymbol{E}_2^{(o)}\exp\left[-i\phi_2\right]\right\}, \tag{6.2}$$

where $\boldsymbol{E}_i^{(o)}$ is an amplitude, possibly complex, and ϕ_i a phase angle. Hence, the corresponding light intensity is given by (Born and Wolf 1980)

$$\begin{aligned} I = k|\boldsymbol{E}|^2 &= k\left[|\boldsymbol{E}_1|^2 + |\boldsymbol{E}_2|^2 + 2\boldsymbol{E}_1\boldsymbol{E}_2\right] \\ &= I_1 + I_2 + 2(I_1 I_2)^{\frac{1}{2}}\cos\Delta\phi, \end{aligned} \tag{6.3}$$

where I_1 and I_2, respectively, are the intensities of each individual wave, $\Delta\phi$ is the phase difference between them, and k is a constant of proportionality. In an optical interferometer the interfering waves emanate from a common light source, so the phase difference between the waves may be expressed in terms of the variation in optical path length, Δd, travelled by the two waves before forming the interference pattern. In this case

$$\Delta\phi = \frac{2\pi\Delta d}{\lambda}, \tag{6.4}$$

where λ is the wavelength of the light. Accordingly, it follows from eqns. (6.3) and (6.4) that the intensity at a point P on the resulting interference pattern, expressed in terms of the optical path-length difference Δd, is

$$I = I_1 + I_2 + 2(I_1 I_2)^{\frac{1}{2}}\cos\left(\frac{2\pi\Delta d}{\lambda}\right). \tag{6.5}$$

This equation shows the first result of importance in this section: that a change in optical path length between two waves which travel down separate arms of an optical interferometer leads to a variation in the interference intensity at a point on the pattern. The dependence expressed

by this equation of interference intensity against optical path-length difference is depicted in Figure 6.1.

Equation (6.5) may be taken a step further by re-expressing it in terms of the maximum and minimum intensities in the interference pattern. These intensities, obtained for particular path-length differences, are respectively (Born and Wolf 1980; Hariharen 1992)

$$I_{max} = I_1 + I_2 + 2(I_1 I_2)^{\frac{1}{2}} \text{ when } \Delta d = 0,\ \lambda,\ 2\lambda,\ 3\lambda,\ \cdots \tag{6.6}$$

and

$$I_{min} = I_1 + I_2 - 2(I_1 I_2)^{\frac{1}{2}} \text{ when } \Delta d = \tfrac{1}{2}\lambda,\ \tfrac{3}{2}\lambda,\ \tfrac{5}{2}\lambda,\ \cdots. \tag{6.7}$$

Substituted into eqn. (6.5), these give the result (see, for example, Pan and Cross 1989):

$$I = \tfrac{1}{2}\left(I_{max} + I_{min}\right) + \tfrac{1}{2}\left(I_{max} - I_{min}\right)\cos\left(\frac{2\pi\Delta d}{\lambda}\right). \tag{6.8}$$

Following on from eqn. (6.8), one may derive an expression for the sensitivity of the interference intensity at a point to small changes in the optical path-length difference. This is given by

$$\frac{\partial I}{\partial \Delta d} = \left| \frac{\pi}{\lambda}\left(I_{max} - I_{min}\right)\sin\left(\frac{2\pi\Delta d}{\lambda}\right) \right|. \tag{6.9}$$

It is thus evident that as the path-length difference Δd changes, the sensitivity at a point varies between a maximum value of $\pi(I_{max} - I_{min})/\lambda$ and a minimum of zero, and that furthermore the situation for maximum sensitivity is satisfied for the specific condition that

$$\Delta d = \frac{\lambda}{4}(2n+1), \quad n = 0,\ 1,\ 2,\ \cdots, \tag{6.10}$$

Additionally, at this point of maximum sensitivity the interference pattern intensity is given by

$$I_o = \tfrac{1}{2}\left(I_{max} + I_{min}\right). \tag{6.11}$$

This means that maximum sensitivity of an interferometer's interference pattern to small changes in the optical path length between the waves, occurs at a point half way between the positions of maximum and minimum intensity of the pattern. Points satisfying this condition are those such as A and B on the intensity curve in Figure 6.1, and when employing an interferometer to measure optical path-length changes, it is desirable, in the interests of maximizing the apparatus' sensitivity, to operate at these points.

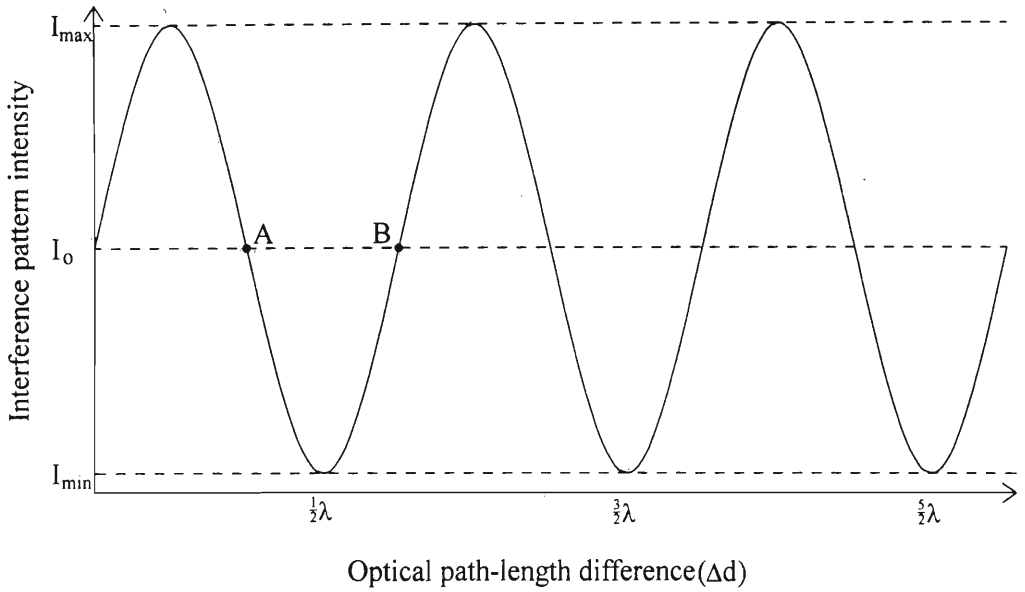

Figure 6.1 Diagram of the variation in intensity of the fringe pattern with a change in optical-path length between the interfering waves

A further important result in optical interferometry is that described by Fotchenkov (1957). It gives a direct relationship between a small optical path-length shift introduced between the two waves forming the interference pattern and the resulting intensity change, when the pattern is positioned at a point half way between maximum and minimum intensity. To complete the relationship, knowledge of the maximum and minimum light intensities of the interference pattern and the wavelength of the light propagating through the interferometer are also required. That many workers have made use of this result to evaluate, amongst others, the electro-optic and piezoelectric-type effects of materials, is testimony to its significance. Given the usefulness of the result, and the role it plays in this work, it is of some interest to study the mechanism behind it.

If the interferometer is operated at its most sensitive point and sufficiently stabilized against environmental noise influences to the extent that their contribution may be neglected, then the optical path-length difference between the two waves forming the interference pattern may be written as

$$\Delta d = \Delta d_{effect} + \frac{\lambda}{4}(2n+1), \tag{6.12}$$

where Δd_{effect} is the small optical path-length change introduced in the interferometer as a consequence of an effect being investigated (for instance, an electro-optic or piezoelectric-type effect). If d_{effect} is very much smaller than the wavelength of the light propagating in the interferometer, then substituting eqn. (6.12) into eqn. (6.8) yields

$$I \approx \tfrac{1}{2}(I_{max} + I_{min}) \pm \tfrac{1}{2}(I_{max} - I_{min})\left(\frac{2\pi\Delta d_{effect}}{\lambda}\right). \tag{6.13}$$

The approximation that $\sin(2\pi\Delta d_{effect}/\lambda) \approx 2\pi\Delta d_{effect}/\lambda$ is valid, for a wavelength of 632.8 nm, within 1% for $|d_{effect}|$ values of less than 13 nm (Zhang *et al.* 1988). Thus the light intensity detected at the interferometer output consists of two parts: one, a static term equal to $\frac{1}{2}(I_{max} + I_{min})$, where intuitively this may be seen as a consequence of the interferometer being stabilized at the most sensitive point; and another, which varies linearly with the small induced change in the optical path length between the two waves. Hence, this second component is that responsible for a small variation of the interference intensity from the intensity at the most stable point, given by

$$\Delta I_{effect} = \pm(I_{max} - I_{min})\left(\frac{\pi\Delta d_{effect}}{\lambda}\right). \tag{6.14}$$

Rewritten in terms of Δd, this becomes (Fotchenkov 1957)

$$\left|\Delta d_{\text{effect}}\right| = \frac{\lambda \Delta I_{\text{effect}}}{\pi\left(I_{\text{max}} - I_{\text{min}}\right)}. \tag{6.15}$$

With the interferometer operated at its most sensitive point, and with the magnitude of the maximum and minimum light intensities of the interference pattern and the wavelength of the light all known, the induced optical path-length difference may be determined from eqn. (6.15) by measuring the change in light intensity of the interference pattern. It is this result that finds widespread use in the literature (for instance, Haesen and Kwaaitaal 1976; Zhang *et al.* 1988).

6.3 Some interferometric determinations of field-induced optical path-length changes

The use of interferometric techniques to measure electric-field-induced optical path-length changes of the same order of magnitude as those expected in this investigation (~1 Å) is by no means new. Many such determinations are reported in the literature in the measurement of piezoelectric and electrostrictive coefficients, as well as coefficients of the linear and quadratic electro-optic effects, and it is from this wealth of information that many ideas for the present investigation were drawn. Since the basis of the interferometric techniques to determine both the linear and quadratic effects is the same, some of the more relevant of these approaches are mentioned here to establish a background for the method of the present electro-optic inquiry. In the ensuing discussion, published values for quadratic electro-optic and electrostrictive coefficients are quoted to demonstrate the feasibility of interferometric techniques in determining induced optical path-length changes due to coefficients of the same order of magnitude (10^{-20} m^2V^{-2}) as those expected for KDP and ADP in the present interferometric work (see Tables 5.1 and 5.2).

Zook *et al.* (1967) made use of a Michelson interferometer to measure the sign, magnitude, and temperature dependence of various linear electro-optic coefficients of single-crystal lithium niobate ($LiNbO_3$). These results were obtained from measurements of the shift in phase of the interferometer's interference pattern arising from the electric-field-induced change in refractive index of a sample placed in one arm of the interferometer. Of particular interest was the use in this experiment of a vibrating mirror in the so-called *reference* arm of the interferometer (that without the sample under investigation) to sweep through the optical path length linearly with

time. The purpose of this was two-fold: first, to overcome random phase shifts due to environmental noise and, second, to vary the interference pattern intensity detected at the interferometer output sinusoidally with time in order to determine the magnitude of the field-induced phase shift. When a modulated voltage was applied to the $LiNbO_3$ crystal in the *probing* arm of the interferometer, the optical path-length shift induced in that arm resulted in a small time-changing displacement of the intensity curve detected at the interferometer output. The magnitude of this change relative to the sine wave variation derived from the vibrating mirror, the period of which corresponded to a path difference of one wavelength between the beams in either arm, gave a measure of the induced phase shift. This method is, however, restricted in its sensitivity by the accuracy with which the displacement of the intensity curve could be resolved (Onuki *et al.* 1972). Despite this, a very similar approach was applied by Fujii and Sakudo (1970) to investigate the quadratic electro-optic effect in cubic strontium titanate ($SrTiO_3$), but on this occasion a Mach-Zehnder interferometer was employed and the optical path length in the reference arm was varied by means of a rotating glass plate. For two different crystal configurations – in the one with the electric field along the crystallographic *z*-axis, and in the other along the bisector of the *yz*-axes, but in both cases with the light propagating in the *x* direction – the sign and magnitude of three independent quadratic electro-optic coefficients were determined. The results obtained in this way at room temperature for a wavelength of 632.8 nm were: $g_{xxxx} = 14 \times 10^{-19}$ m^2V^{-2}, $g_{xxyy} = 4 \times 10^{-19}$ m^2V^{-2}, and $g_{yzyz} = 7 \times 10^{-19}$ m^2V^{-2} (These were calculated from the published results, which were quoted in terms of induced polarization, using a value for the low-frequency dielectric constant ε_{ii} given in the same paper).

Also favouring a Mach-Zehnder interferometer were Onuki *et al.* (1972) who determined the linear electro-optic coefficients of a number of crystals, including KDP. Notably, this approach moved away from that of Zook *et al.* (1967) and Fujii and Sakudo (1970) by determining the sign and magnitude of the modulated field-induced phase shift by a null method, where the induced effect in the sample under investigation was determined relative to the known linear electro-optic response exhibited by a reference material placed in the same arm of the interferometer. The reference samples used in this instance were DKDP and lithium tantalate ($LiTaO_3$), for which the linear electro-optic effect had been determined previously by the approach of Fujii and Sakudo (1970). This method of measurement, found to be more suitable for the determination of small induced phase shifts (Onuki *et al.* 1972), was also employed by Haussühl and Walda (1971) to measure the quadratic electro-optic effect in lithium fluoride (LiF) and α-$TlAl(SO_4)_2.12H_2O$

using the linear electro-optic coefficient r_{xyz} of KDP as a reference. Their results for the quadratic electro-optic coefficients determined for various light-propagation and modulated applied-field configurations, in units of 10^{-20} m^2V^{-2}, are: for LiF $g_{xxxx} = -0.256$, $g_{xxyy} = -0.214$, and $g_{xyxy} = -0.007$; and α-$TlAl(SO_4)_2.12H_2O$ $g_{xxxx} = 0.701$, $g_{xxyy} = 0.613$, $g_{xxzz} = 0.625$, and $g_{xyxy} = -0.038$. Again, all these values were found at room temperature and for a wavelength of 632.8 nm, and the applied field was modulated at a frequency of 500 Hz. These measured coefficients are those of the unclamped electro-optic effect, and include an elasto-optic-electrostrictive contribution, as well as an additional term due to the attraction of the electrodes, both of which must be allowed for, as mentioned previously in Section 5.7.

A further important interferometric method for determining field-induced optical path-length variations of much less than the wavelength of the interferometer light, is that described by Fotchenkov (1957). The theory of this method was dealt with in detail in Section 6.2, culminating in the derivation of eqn. (6.15). It allows the determination of induced path-length changes directly from a measure of the variation in intensity of the interferometer's interference pattern, and finds extensive application in the determination of phase shifts due to electro-optic, piezoelectric, and electrostrictive effects. Fotchenkov himself (Fotchenkov 1957) and Kwaaitaal (1974) used this method to investigate the piezoelectric effect in quartz by means of Michelson interferometers. In these approaches either the mirror in the probing arm of the interferometer was attached to the quartz sample under investigation, or the sample itself was polished to provide a mirror surface. Consequently, any variation of the specimen dimension perpendicular to the light beam incident upon it resulted in a change in optical path length in that arm of the interferometer and a shift in phase between the beams in the two arms. The measurement of this path-length change thus allowed the sample's dilation to be determined and related to the piezoelectric effect responsible for it. Similarly, Zheludev and Fotchenkov (1958) employed this approach to measure the electrostrictive effect in quartz and sodium chloride (NaCl) samples. Their results for NaCl, again in units of 10^{-20} m^2V^{-2}, are $\gamma_{xxxx} = 0.3$, $\gamma_{xxyy} = -0.15$, and $\gamma_{xyxy} = 0.05$. The same procedure was used by Luymes (1982) in his determination of the electrostrictive coefficient γ_{xxxx} in samples of quartz, diamond, and LiF. Values reported in that work were all of the order of 10^{-21} m^2V^{-2}. Further electrostrictive coefficients were measured by Zhongyan *et al.* (1988), once more with the use of a Michelson interferometer and the approach described above. Here, results for a number of electrostrictive coefficients were reported to be of the order of 10^{-21} m^2V^{-2} in crystals of calcium fluoride (CaF_2), strontium fluoride (SrF_2), and barium fluoride

(BaF_2). To give some examples of the use of this method to determine the magnitude of electro-optic effects in crystals: it was invoked by Massey *et al.* (1980) and more recently Bierlein and Arweiler (1986) to measure various linear electro-optic coefficients of potassium titanate phosphate (KTP) at 632.8 nm. Both of these investigations made use of a Mach-Zehnder interferometer. Likewise Pan and Jang (1990) also employed a Mach-Zehnder interferometer in a similar investigation of the linear electro-optic coefficient r_{zzz} of $LiNbO_3$.

Still other interferometric methods for determining electro-optic and piezoelectric-type effects rely on the interference formed between light reflections at the polished faces of investigated samples. By studying the interference pattern arising between light transmitted through and reflected within $LiNbO_3$ and $LiTaO_3$ crystals, Takizawa and Okada (1982) were able to deduce the magnitude of the effective linear electro-optic coefficients r_{zzz} and r_{xxz} which included a small piezoelectric contribution. The same authors later investigated the linear electro-optic coefficient $|r_{xyz}|$ and the piezoelectric coefficient $|d_{zxy}|$ in KDP and ADP crystals by the same method (Takizawa and Okada 1985). These coefficients were determined for an applied field along the crystallographic z-axis and for light propagation along the bisector of the x- and y-axes. Wang and Liu (1992) measured three independent coefficients of the linear electro-optic effect in KTP using a Fizeau interferometer in conjunction with a Faraday cell. The interference pattern in this apparatus was formed between two equal light components reflected from the front and back surfaces of the crystal sample, and the variation in the light intensity due to the electro-optic effect was nulled by a known amount by means of the Faraday cell arrangement. Tan and Arndt (1996) also relied on reflection within the crystal and from its outer face in a Fabry-Perot interferometer in their investigation of the piezoelectric effect in quartz and electrostriction in SiO_2 glass.

6.4 Means of interferometric stabilization

The sensitivity of interferometric measurement techniques has been greatly enhanced since their advent through the use of photodetectors to detect the intensity of the interference pattern, converting the optical signal into an electronic one, and modulation techniques used in conjunction with lock-in detection methods. This is equally true for any design of interferometer. In fact, in the case of a Michelson interferometer, and using a photodiode as a detector, Sizgoric and Gundjian (1969) report a theoretical limit to the sensitivity of 10^{-4} Å, where the limiting

factor was taken to be the shot noise of the photodiode. But, in practice, it is noted (Kwaaitaal 1974) that before any theoretical limit to the sensitivity is reached, an interferometer will fall under the influence of environmental noise which is typically low-frequency in nature and may be attributed to a wide variety of causes: for instance, acoustic noise, mechanical and building vibrations, thermal drift, and field-induced strains, amongst others. Under these conditions the sensitivity of an interferometer is limited by its susceptibility to these influences before an ideal theoretical limit is reached. Accordingly, to harness the potential sensitivity of an optical interferometer, means to detach the apparatus from adverse influences must be sought.

There are many conventional means to isolate optical interferometers from detracting environmental influences. Probably the more common of these, to provide isolation from building and mechanical vibrations, is to assemble the apparatus on a sufficiently massive optical table which is then supported by, and pneumatically isolated from, a secondary support table (Doswell and Kunov 1990). In other instances, the interferometer may be operated in a temperature controlled environment (Allensworth 1980), or have its components assembled from materials specifically chosen for their low thermal expansion coefficients. Yet these measures are often expensive, in some instances wholly impractical, and in the end usually provide only a degree of noise insolation. For this reason, alternative means to actively stabilize interferometers against noise have been developed and reported in the literature. These active stabilization techniques may be categorized into two main groups (Kwaaitaal *et al.* 1980): those in which stabilization is achieved by an electronic feedback system, and those stabilized by optical arrangements. Both these methods offer the attractive possibility of considerable noise isolation without the need for expensive apparatus or extensive modification. An outline of these approaches, within the context of determining small path-length changes, particularly those induced by a field, is given here. It is worth noting that the majority of the more relevant work concerned with the determination of optical path-length changes due to electro-optic and piezoelectric-type effects by means of Mach-Zehnder and Michelson interferometers involves the use of one or other of these active stabilization approaches.

6.4.1 Electronically stabilized interferometers

Although they take on a variety of practical forms, the fundamental principles of electronically stabilized interferometers, as described by Kwaaitaal (1974), are basically similar. Consider an interferometer in which an optical path-length change, of magnitude far less than the wavelength

of the laser light, is induced in the probing arm of the interferometer by an effect under investigation. In such a situation the optical path-length difference between the two waves forming the interference pattern may be seen as consisting of three distinct parts given by the following expression (Doswell and Kunov 1990):

$$\Delta d = (d_1 - d_2) + d_{effect} + d_{noise}. \tag{6.16}$$

In this equation d_1 and d_2 are the constant (or static) distances along either arm of the interferometer, d_{effect} is the small optical path-length change, usually modulated, which is introduced by the effect being investigated, and d_{noise} represents the sum of all time-changing optical path-length changes due to noise effects. To establish an interferometer at its point of maximum sensitivity, the condition for which is given in eqn. (6.10), the static optical path-length difference is adjusted until

$$(d_1 - d_2) + d_{noise} = \frac{\lambda}{4}(2n+1), \quad n = 0,\ 1,\ 2,\ \cdots, \tag{6.17}$$

such that the near-static phase difference between the two waves is

$$\Delta\phi = \frac{2\pi}{\lambda}\left[(d_1 - d_2) + d_{noise}\right] = \frac{\pi}{2}(2n+1). \tag{6.18}$$

Hence, the interferometer will be balanced at either of the equivalent points A or B in Figure 6.1. However, in a real experiment the noise contribution to Δd, and hence to $\Delta\phi$, tends not to be zero. Its presence upsets this point of balance at A or B on account of its time-changing nature and adversely affects the accurate determination and evaluation of the desired contribution d_{effect}. This is where the stabilization of an interferometer comes into effect, which has the aim of nulling, or minimizing, potential noise contributions to the phase difference.

In an electronically stabilized interferometer this is achieved as follows: a photodetector is used to detect the light intensity at a point on the interference pattern, and in this way an electronic signal, usually a voltage output, proportional to the intensity at that point is obtained. This voltage output is then monitored and, knowing the voltage which corresponds to the interference pattern intensity at the maximum sensitivity points, as given by eqn. (6.11), any variation in the voltage representing a shift from this balance condition is discernible. In fact, the magnitude of the voltage difference gives a measure of the extent of the disturbance from balance. This voltage deviation then influences an active element within the interferometer which further modifies the phase difference to null the voltage deviation and in this way drive the interferometer back to the point of maximum sensitivity. This constitutes the electronic control of an interferometer.

There exists a number of ways to actively alter the phase difference between the two waves. As can be seen from eqn. (6.18), these methods involve the variation of either the wavelength of the light used, or the static optical path-length difference where this, in turn, may be achieved by varying the relative path lengths of the interferometer arms or, equivalently, changing the refractive index of the medium through which the light propagates. Arguably the more common and most practical of these (especially in the framework of piezoelectric and electro-optic effect determinations) is to vary the relative path lengths of each arm of the interferometer. For instance, Vlasov and Medvedev (1972) altered the voltage applied to a piezoelectric transducer which actively drove the mirror in the reference arm of their Michelson interferometer, and in doing so reported a sensitivity for their apparatus of 3 Å[1]. Kwaaitaal (1974) and Haesen and Kwaaitaal (1976) stabilized their Michelson interferometers through the active driving of a mirror mounted upon a condensor microphone in the reference arm. The former stated a sensitivity of 10^{-3} Å, as did Luymes (1983) who, in his measurement of electrostrictive strains, employed a mirror mounted upon a piezoelectric transducer in the one interferometric arm. Doswell and Kunov (1990) describe the stabilization of a Mach-Zehnder interferometer by means of driving the reference mirror mounted upon a piezoelectric plate, and Pan and Jang (1990) used a similar process, but now with a servo-transducer, in their determination of the linear electro-optic effect in a $LiNbO_3$ crystal. Pan and Cross (1989) employed the same method to investigate high-frequency piezoelectric and electrostrictive strains. In fact, the list could go on to include Schneider and Robertson (1979), Yasuda *et al.* (1980), White and Emmony (1985), Halloway and Emmony (1988), Zang *et al.* (1988), Zhonyan *et al.* (1988), and van Sterkenburg *et al.* (1990), amongst many others, all of whom actively varied the path length in one arm of their interferometer in the interests of stability, by means of either condensor microphones or speakers, piezoelectric transducers, or servo transducers. In a slight variation of this approach, but with the same end in mind, Jackson *et al.* (1980) and Fritsch and Adamovsky (1981) changed the optical

---

[1] To be perfectly correct, this earlier work by Vlasov and Medvedev operated on a slightly different basis from that described above. The output interference pattern was split by means of a beam splitter and the two patterns thus formed were then viewed by separate photomultipliers, but displaced by a quarter of the interference pattern relative to each other. The electronic balance circuit then stabilized the interference pattern detected by one of the photomultipliers at either maximum or minimum intensity and thus the other photomultiplier, the measurement photomultiplier, theoretically viewed the interference pattern at its most sensitive point. However, the interference pattern's position not being particularly responsive to optical path-length changes at its peaks restricted the sensitivity of this method.

path length in the one interferometer arm by straining optical fibres wound rigidly around a piezoelectric cylinder and through which the light in their interferometers travelled.

The method of stabilizing an optical interferometer by adaptive tuning of the laser wavelength to compensate for optical path-length differences arising from noise influences, was suggested by Shajenko and Green (1980) who described the approach for application in a Michelson interferometer. This method was then realized by Olsson *et al.* (1980), who employed an electro-optically tuned laser and reported a sensitivity to optical path-length changes of the order of 10^{-2} Å. However, this approach is acknowledged to be both more expensive and complicated than those mentioned above (White and Emmony 1985).

In view of the other options to alter the phase difference for the purpose of stabilization, the third approach - that of varying the refractive index of the medium through which the light in the interferometer propagates - is debatably the least appropriate or practical. As far as is known, there are few examples of its utilization. Although Onuki *et al.* (1972) in their determination of linear electro-optic coefficients used a pair of optical wedges which were translated perpendicular to the light propagating in the one arm of the interferometer, effectively changing the refractive index over that optical path length, and in this way positioning the interferometer at its most sensitive point, this method did not incorporate any electrical feedback system. Despite this a sensitivity of about 10^{-1}Å was reported. It may be thought that the refractive index changes induced in a crystal by the electro-optic or piezo-optic effects could be used to effect active stabilization of an interferometer, but the small magnitude of these changes is unlikely to null noise perturbations.

6.4.2 Optically stabilized interferometers

The concept of an optically stabilized interferometer, known also as a phase quadrature or quadrature-dual interferometer, as proposed by Peck and Obetz (1953), involves a phase shift of $90°$ being introduced between the two perpendicular components of the light wave in one arm of the interferometer. For instance, Vilkomerson (1976) in measuring ultrasound pulses responsible for an optical path-length displacement of magnitude 10^{-2} Å achieved this by placing a $\frac{\lambda}{8}$ - plate in the one arm of a Michelson interferometer, whereas Allensworth (1980) obtained the same result by placing a $\frac{\lambda}{4}$ - plate in the arm of a Mach-Zehnder interferometer in an investigation of sample strains. On recombining the two beams which travel down the separate

arms of the interferometer, this phase difference gives rise to two discrete interference patterns which are in phase quadrature. These may be differentiated by means of a polarizing beam splitter and detected by individual photodetectors.

In this case, as can be expected, the induced optical path-length change in the one arm of the interferometer due to the effect being studied leads to an intensity variation in each of these interference patterns. However, on account of the 90° phase difference between the two orthogonal components of the light in the one arm of the interferometer, these two intensity shifts are in phase quadrature, and one displays a sine-function dependence on the optical path-length difference and the other a cosine dependence. Thus although both these induced signals fluctuate with a change in optical path length brought about by noise influences, the sum of the squares of these signals is always constant, independent of the optical path length, and the square root of this signal gives a measure of the amplitude of the effect to be determined. Although a measurement sensitivity of the order of those accepted for electronically stabilized interferometers is reported in the literature (10^{-2} Å by Vilkomerson 1976), the application of optically stabilized interferometers in the measurement of small field-induced optical path-length changes is far less common than the electronic equivalent. This is despite there being no obvious disadvantage in the use of the method. In the present work, both were given equal consideration.

6.5 On the interferometer developed for the present investigation

6.5.1 Choice of interferometer

It is evident from the discussion in Section 6.3, that there are a number of sophisticated interferometric designs and approaches for the determination of electro-optic and electrostrictive coefficients, the more common of which are based on the Mach-Zehnder and Michelson methods. The interferometric processes mentioned in the last paragraph of that section, which rely on reflections from the surfaces of the medium under investigation, require specially prepared samples with reflective and/or semi-reflective faces (Tan and Arndt 1996). Since the KDP and ADP crystals available for this research were not so prepared, the interference patterns formed by these methods were of poor quality and not suitable for accurate investigations by these techniques. Consequently, such interferometric designs were ruled out. Turning to the Mach-Zehnder and Michelson arrangements, both were tested during the initial stages of this

work, but neither method was found to be clearly favourable to the other for the present application. It is noted, however, that the Mach-Zehnder interferometer is often more complicated to align (Hariharan 1992) and has difficulties associated with it due to the limited coherence length of a laser beam (see, for example, Pan and Cross 1989). This is particularly evident when implementing the active stabilization technique, mentioned in Subsection 6.4.1, of varying the length of one arm of the interferometer. But perhaps of greater significance, the Michelson interferometer allows the probing light wave to pass twice through the medium under investigation, and thus be influenced two-fold by the effect to be measured. When determining small field-induced path-length changes this is a noticeable advantage. It was this fact, more than any other, which led to a Michelson interferometer being favoured over the Mach-Zehnder type for the present application.

6.5.2 Determination of both the quadratic electro-optic and electrostrictive effects by transmission

All investigations in this work were conducted by way of the transmission of light through the crystals being studied and did not involve reflection from the sample surfaces, as is inevitably the case to obtain piezoelectric-type results (Kwaaitaal 1974; Luymes 1983; Zhang *et al.* 1988). It was desirable to achieve all the necessary results for both the quadratic electro-optic and electrostrictive coefficients independently through transmission alone.

It may be noted in eqn. (6.1), which relates the induced optical path-length difference to the refractive index change, electro-optically induced in this case, and also to the medium's change in length, due in this instance to the electrostrictive effect, that the contribution of this latter part is dependent on the difference between the refractive indices of the crystal and of the environment in which it is placed. Ideally, for the determination solely of electro-optic effects, one would like to place the crystal in an environment of matching refractive index, thereby eliminating any electrostrictive contribution to the induced optical path-length change entering eqn. (6.1). However in practice, finding such a match is inherently difficult, especially if one considers that for a uniaxial medium the refractive index depends on the incident light's polarization angle relative to the principal crystallographic axes for propagation directions off the optic axis. The MSc project by Gunning (1995) initiating this work endeavored to minimize the electrostrictive contribution by placing the KDP crystal under investigation in silicon oil,

whose refractive index was very similar to both the ordinary and extraordinary refractive indices of KDP. However, even in this case the electrostrictive contribution to the change in optical path length was not negligible, and contributed to uncertainty in the quoted results for the quadratic electro-optic coefficients.

The proposal for this project to measure both the quadratic electro-optic and electrostrictive effect contributions, was to determine the induced optical path-length change in the crystal, for the particular light-propagation and polarization directions of interest, in two media of distinctly different refractive indices. Thus the electrostrictive contribution would differ in each case and, if sufficiently large, could be determined. The environments chosen for this investigation were those of silicon oil and air. In this way combining the results for the induced optical path-length change for the two different crystal environments permitted the evaluation of both the quadratic electro-optic and electrostrictive effect coefficients. For the KDP and ADP crystals in this work, the quadratic electro-optic coefficients g_{xxxx}, g_{yyxx}, and g_{zzxx} could be separately determined, as could the two electrostrictive coefficients γ_{xxzz} and γ_{xxyy}.

6.5.3 Determination of optical path-length changes induced in the interferometer

Of the approaches mentioned previously for the interferometric determination of small field-induced optical path-length changes, the two which are most apt for the Michelson interferometer used in this research, are: (1) the compensation method, and (2) that which determines the induced path-length change from a measure of the variation in light intensity of the interferometer's interference pattern when the system is balanced at its most sensitive point.

In some respects, the latter of these approaches could be considered the more direct, and consequently more desirable, procedure; it does not rely on an accurately calibrated material against which to compensate. However, included in the expression applying to this method, namely eqn. (6.15), is the term $(I_{max} - I_{min})$. This means that in order to apply eqn. (6.15), the difference between maximum to minimum intensity of the interference pattern must be measured, as well as the small change in intensity due to the induced optical path-length variation from the effect being investigated. However, with any one of the crystal samples investigated in this work placed in the probing arm of the interferometer, the interference pattern was of diminished

intensity, and (I_{max} - I_{min}) was small in magnitude. Consequently, the electronic signal obtained by photodetector of this intensity was small and subject to a large signal-to-noise ratio. It was also observed to fluctuate slowly with time as the experiment proceeded. Because this intensity difference must be known accurately for use in eqn. (6.15), this technique was not regarded as suitable. On the other hand, the compensation approach does not involve the determination of the difference between maximum and minimum intensity of the fringe pattern. The only intensity change required is that resulting from the optical path-length variation due to the effect being investigated. Although very much smaller in magnitude, this could be determined accurately by means of a lock-in amplifier and modulation techniques, which did much to assist with noise reduction.

Thus after inquiring into both possibilities, the method decided upon to evaluate the various quadratic electro-optic and electrostrictive coefficients of KDP and ADP crystals in this work, was the former compensation technique. Notably, this is the same choice as was made in the MSc project initiating this research (Gunning 1995).This approach, similar in many respects to that by Haussühl and Walda (1971), amongst others, involved the nulling of the field-induced path-length shift due to the effect under investigation by a path-length difference of known sign and magnitude. The known path-length variation in this project was achieved through the use of a piezoceramic reference plate of well-established piezoelectric response to which the mirror in one arm of the interferometer was securely attached through an inelastic bond. The application of an electric field to this reference material resulted in a known dilation of the sample, and thus a known translation of the attached mirror. This was related precisely to a change in optical path length in the arm of the interferometer of which the reference material and mirror formed part.

In this compensation approach, a modulating voltage of fixed amplitude was applied to the crystal sample under investigation, so inducing, by means of the quadratic electro-optic and electrostrictive effects, an alternating shift in the optical path length of the beam propagating through the crystal in the probing arm of the interferometer. Consequently there was an oscillating shift in the intensity of the interference pattern. On account of the quadratic nature of the two effects being investigated, this intensity variation was modulated at twice the frequency ω of the voltage applied to the crystal. To compensate for the path-length shift induced in the crystal, a voltage was applied to the piezoelectric reference plate modulated at a frequency, and with a phase, such that the optical path-length change it induced, through the dilation of the

ceramic and the consequent motion of the attached mirror, was at precisely the frequency of the crystal's resulting optical path-length change but in antiphase with it. Thus by adjusting the amplitude of the voltage applied across the reference plate the intensity variation of the interference pattern at twice the fundamental frequency ω could be monitored, and the voltage applied to the reference plate for which it became zero determined. This point corresponded to the condition that the two induced optical path lengths were of the same magnitude, the unknown path-length shift originating in the crystal having been compensated by the well-established piezoelectric response. Since the path-length change induced by the reference plate was known both in sign and magnitude relative to the voltage applied across it, the path-length difference induced for a particular voltage applied to the crystal was established. The various coefficients of interest - those of the quadratic electro-optic and electrostrictive effects - could then be determined from knowledge of the relationship between these effects and the sign and magnitude of the induced optical path-length variation, for the particular crystal orientation and applied field in question.

It is worth noting that other reference materials for use as compensators were also investigated. In one instance this involved a polished quartz disc, and in another a longitudinal Pockels cell containing a DKDP crystal. Thus the induced optical path-length variation of the investigated effect could be determined relative to the piezoelectric coefficient d_{xxx} of quartz and the linear electro-optic coefficient r_{xyz} of DKDP, respectively. However, neither of these approaches was as satisfactory in achieving reproducible and consistent results as that involving the piezoceramic. The Pockels cell in particular was most unsuitable, being susceptible to inconsistencies even for slight reorientations of the cell or different propagation paths through the DKDP crystal.

6.5.4 Stabilization of the interferometer

One of the requirements of the present experimental investigation was that the apparatus should permit the plane of linear polarization of the light wave propagating through the crystal under study to be set at selected angles. The reason behind this was: first, to allow the various coefficients of the quadratic electro-optic and electrostrictive effects to be determined individually, and, second, to enable the quadratic effect exhibited by the material to be studied for a range of polarization angles of the light incident upon the crystal to ensure the effect being investigated does, in fact, obey the dependence on polarization angle that the quadratic effect

should, as derived in Section 5.4 (see also, for example, Kucharczyk *et al.* 1995). This being the case, the method of optical stabilization mentioned in Section 6.4, which derives its stability from the known manipulation of polarized light, does not readily lend itself to use in this experiment. To allow for investigating the quadratic electro-optic and electrostrictive effects for varying incident polarization angles when using the optical stabilization method, it would be necessary to modify the approach, either by adding further optical components, which would increase spurious reflections and adversely affect the quality of the interference pattern in a set-up already containing an abundance of optical elements, or by rotating the crystal itself about the light path. The latter procedure was regarded as impractical on account of the relatively large dimensions of the crystal, and hence of the box in which it is mounted. Conversely, the method of electronic stabilization offers no such restriction to the polarization of the light incident on the crystal, and involves a simpler optical arrangement with fewer optical components. In view of this, the choice to utilize electronic stabilization, as opposed to the optical equivalent, was an obvious one. The method of electronic stabilization invoked in this experiment involved actively controlling the path length of the reference arm of the interferometer by means of a feedback circuit manipulating the voltage applied across a piezoelectric transducer to which the mirror in that arm was attached. The principle of the method adopted follows that outlined in Section 6.4, and details of the various components used in its operation are given in the next chapter.

6.5.5 Calibration of the piezoceramic reference sample

In order that the piezoelectric response of the ceramic plate be used as a reference to offset, or null, the path-length change introduced by the crystal, it is imperative that its response to the applied voltage be accurately established. The manner in which this was accomplished in this project stands out as one of the more significant differences from the original MSc work (Gunning 1995) on which it follows. Since the two calibration approaches used in each case led to conflicting results, some explanation needs to be given.

The calibration of the piezoceramic plate's response was accomplished in the initial MSc work by observing its behaviour in the presence of a static electric field. This involved measuring the voltage applied to the reference material which induced a shift of one complete fringe of the interference pattern, equivalent to a path-length difference of precisely one wavelength. Hence, knowing the piezoelectric response for this voltage, the ceramic material was taken to be calibrated for lesser voltages and also for low-frequency fields. However, this procedure makes

two unsubstantiated assumptions: first, that the field-induced response of the piezoelectric material is the same at low frequencies as it is for dc fields; and, second, that the response to an applied voltage is linear from low voltages (0 - 15 V rms), used to null the crystal's induced path-length changes (see tabulated results in Chapter 8), up to 1063 V dc required for the optical path-length shift of one wavelength used in the calibration. Both these assumptions are questionable. To start with, a piezoceramic material in the presence of a modulated electric field is known to have certain characteristic resonance frequencies for which the amplitude of the induced dilation of the medium is greater than in the dc case. A sample's fundamental resonance frequency coincides with the condition that the wavelength of the modulated electric field is twice the distance between the electrode plates on adjacent surfaces of the material. For the piezoceramic plate used in this work, this fundamental resonance frequency occurrs at approximately 167 Hz. Other resonance harmonics of successively smaller magnitude, but still corresponding to larger amplitude dilations than the dc case, are observed at higher frequencies. Thus, taking the resonance nature of a piezoceramic material into account, it seems sensible that, even though the frequency of use may not correspond precisely to a resonance harmonic, the response to the electric field should be determined at the frequency of use, and not merely assumed to be equivalent to the dc case. Another important consideration concerns the linearity of the response of a piezoelectric ceramic material to electric fields, since the calibration procedure mentioned above assumes linearity from the order of a few volts right up to those 1000 times larger. It is well known that on account of their ferroelectric nature, piezoelectric materials in the presence of strong electric fields exhibit nonlinearity and hysteresis in their expansion. Thus, it seems reasonable that the response of the piezoceramic should be established for the magnitude of voltages used in the experiment, and the linearity in this range confirmed.

The calibration procedure adopted in the present work presupposed neither of the assumptions of the initial project; it involved the piezoelectric response of the reference plate being established at the same frequency, and over the same voltage range, as that used in the research. This calibration method was based on determining field-induced optical path-length differences from a measure of the resulting change in intensity of the interference pattern when balanced at its most sensitive point. When calibrating the piezoceramic the crystal, and the box in which it was placed, were removed from the interferometer, thus allowing considerably shorter static optical path lengths in either arm of the interferometer, and a more well-defined interference pattern. The difference between the maximum and minimum intensity of the interference pattern

was thus larger than with the crystal present, and the signal output from the photodetector corresponding to this change in incident light intensity was more substantial and less susceptible to noise. It could be easily and accurately established through the use of a digital oscilloscope.

In the analysis of the piezoelectric response of the reference sample, all that is needed is the change in the material's dimension perpendicular to the incident light as a function of the applied voltage, since this leads to an equivalent shift in the optical path length in the arm of the interferometer in which the mirror rigidly attached to the piezoceramic was placed; this is all the information required for the compensation approach. No in-depth investigation of the mechanism behind the piezoelectric response (i.e. the particular components of the piezoelectric tensor responsible for the induced strain) is called for. With this in mind, an expression for the change in piezoceramic sample dimension ΔL, responsible for the displacement of the affixed mirror, in terms of the voltage V applied across its electrode plates, is

$$\Delta L^{ref} = dV^{ref}. \tag{6.19}$$

In this equation d is a constant related to an unspecified coefficient, or even coefficients, of the material's piezoelectric response for the particular direction of the applied field. Hereafter, this constant d will be referred to as the piezoelectric calibration constant, or calibration constant for short, of the material. The application of a voltage across the reference material leads to a variation in the optical path length in the Michelson interferometer given, in terms of the above equation, by

$$\Delta d^{ref} = 2\Delta L^{ref} = 2dV^{ref}. \tag{6.20}$$

Thus substituting this equation into eqn. (6.15), and assuming a photodetector output voltage proportional to the incident light intensity, one has

$$\frac{\lambda \Delta V}{\pi (V_{max} - V_{min})} = \left|\Delta d^{ref}\right| = 2dV^{ref}, \tag{6.21}$$

where ΔV is the change in photodetector output for a voltage applied to the reference sample, corresponding to the small change in intensity from that at the point of maximum stability, and V_{max} and V_{min} represent the maximum and minimum output voltages from the photodetector respectively. To calibrate the piezoelectric reference sample in this work, the induced change in the photodetector output was determined as a function of the voltage applied to the ceramic. Hence, having a measure of both (V_{max} - V_{min}) and ΔV allowed a graph to be plotted of the field-induced change in optical path length versus the voltage applied to the piezoceramic to be plotted. The gradient of this plot gave the value of d, the calibration constant. Importantly, this

calibration was conducted at the frequency of modulation, and over the same voltage range used to null the crystal's induced optical path-length variation. The results of this procedure are given in Subsection 8.2.4.

Chapter 7

DESCRIPTION OF THE INTERFEROMETRIC INVESTIGATION

7.1 Introduction

After the discussion in the previous chapter of a number of relevant examples of the application of interferometric techniques in determining electro-optic and piezoelectric-type effects and the method adopted in this project, this chapter describes in detail the Michelson interferometer developed in this research for determining particular coefficients of the quadratic electro-optic and electrostrictive effects of KDP and ADP single crystals. Enhanced through the use of modulation and lock-in techniques, along with an electronic feedback system to eliminate environmental noise, the sensitivity of this apparatus was such that modulated optical path-length changes with an amplitude of the order of 10^{-1} Å were detectable. This interferometric arrangement is shown schematically in Figure 7.1; included are all optical and electronic components for the compensation and electronic stabilization methods.

7.2 Components of the Michelson interferometer

7.2.1 The optical bench

All the optical components constituting the interferometer used in this research were securely mounted on a heavy cast iron optical bench. This bench consisted of four separate arms fastened

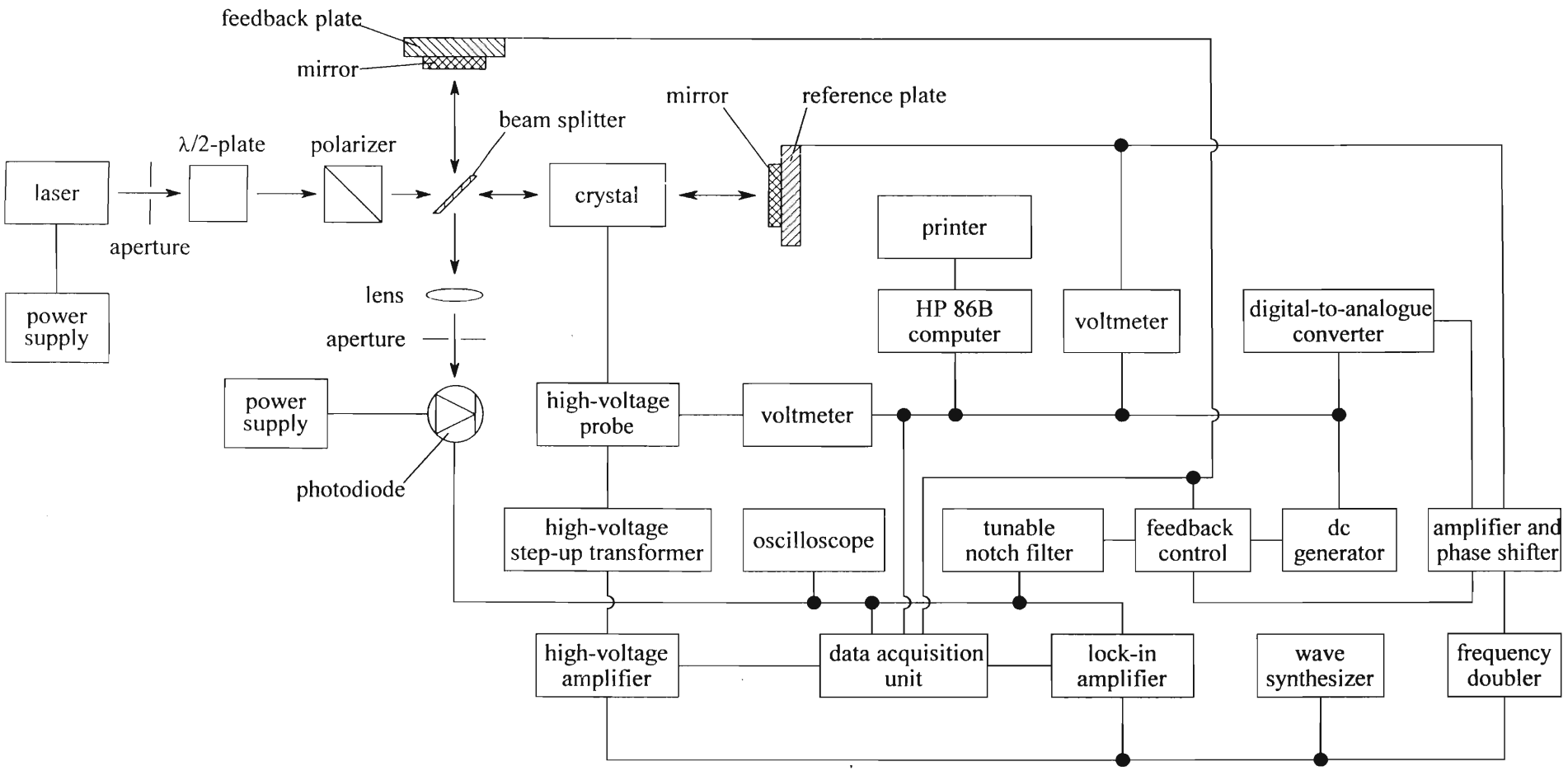

Figure 7.1 Schematic diagram depicting the interferometric arrangement with all the optical and electronic components used in its application

together in the same plane in the form of a cross with adjacent arms perpendicular to one another. To give an idea of its dimensions: three of the four arms were approximately 500 mm in length, the fourth was about 1000 mm in length, and the rectangular cross-section of each arm measured 150 mm × 100 mm. Each optical component, with the exception of the laser, was individually mounted on the bench by means of a single stand of adjustable height, on which a screw gauge allowed for the accurate lateral alignment of the component across the arm of the optical bench. In the case of the laser two such stands were used, one supporting either end. Mounted in this way, the components could be independently positioned, and optimally aligned, in their respective places along the particular arm of the interferometer. To keep the total optical path length of the interferometer to an absolute minimum, separate components in each arm were mounted as close to one another as practical.

7.2.2 Source of linearly polarized monochromatic light

Providing the source of linearly polarized monochromatic light for the interferometer was a Spectra-Physics model 107B-2 He-Ne laser. With a wavelength of 632.8 nm, the output beam from this laser had an intensity of 25 mW and was found not to diverge appreciably over the length of the interferometer - a distance, typically, of 1000 mm from the laser output aperture, down either interferometer arm, and to the aperture of the photodiode. Furthermore, the coherence length of this beam was far greater than the difference in the static optical path lengths between the two interferometer arms. By careful adjustment of the stands mounting the laser on the optical bench, the laser's output beam was aligned at a set height above the bench's horizontal plane and travelling parallel with the bench in each arm when viewed from above.

7.2.3 Optical components

Various optical components were used to control the light traversing the interferometer. An important requirement for this investigation was the accurate rotational manipulation of the plane of linear polarization of the light beam. This was achieved by placing a $\frac{\lambda}{2}$ - plate immediately after the laser on the optical bench which could be rotated until the plane of polarization of the beam entering the interferometer was at the desired angle relative to the crystallographic or laboratory axes. In this way as much of the light intensity as possible was retained from the laser, thereby improving the quality of the fringe pattern formed. This $\frac{\lambda}{2}$ - plate was a 25 mm disc cut

from clear mica, selected for 632.8 nm, and to facilitate its accurate rotational alignment was mounted in a divided circle of resolution of 2' of arc. Although the light transmitted through this $\frac{\lambda}{2}$ - plate was essentially linearly polarized, as a precaution it was then passed through a Glan-Taylor polarizing prism similarly mounted in a divided circle and oriented with its fast axis at the desired polarization angle. The sole purpose of this polarizing prism was to remove any doubt about possible ellipticity of the light entering the interferometric assembly.

The beam splitter, mounted at the intersection of the arms of the optical bench, was a semi-transparent plane-parallel plate, slightly silvered on the reverse side, which served in principle to direct light beams of equal intensity down both arms of the interferometer. It then recombined them after traversing the two arms and directed them towards the photodiode. In practice it was found that a slight difference existed between the intensity of light directed down the two arms of the interferometer, which depended on the plane of polarization of the incident beam. Consequently, anisotropy in the beam splitter was suspected, having the probable effect that vertical and horizontal polarization components of the light were transmitted and reflected to different extents. If this were so, there might be possible implications on the polarization of the light transmitted through the beam splitter down the measurement arm. Experimentally it was established that light of either vertical or horizontal polarization relative to the laboratory frame was transmitted through the beam splitter without any depolarization, whilst light polarized at some intermediate angle was in fact depolarized to a small extent. In an attempt to resolve this problem various other beam splitters were tried, including several cubic beam splitters and semi-transparent plate beam splitters silvered on the reverse side to different extents. However, all these exhibited the same anomaly, and in the end the beam splitter selected was that which displayed the least anisotropy.

As a check, though very weak in comparison to the polarized part, only the depolarized component of the incident beam was permitted to propagate through the crystal and the experiment was run in the usual manner. This light intensity was not observed to lead to any detectable induced variation in the interference pattern intensity, even for electric fields applied to the investigated crystals of far greater strength than those typically used in measurements. Thus, to a good approximation the very slight depolarizing effect of the beam splitter was neglected. At this stage further sources of depolarization in the interferometer's

probing arm were considered: the crystal itself, the windows of the box, and the silicon oil or air surrounding the crystal, through all of which the beam passed; and the mirror in the probing arm which reflects the beam back through the crystal. But, it was established experimentally that these possible sources did not in practice contribute to any detectable depolarization of the beam.

Polished glass plates, flash-coated with 99.8% pure aluminium, served as the mirrors at the end of each arm of the interferometer. These were mounted on the plane surfaces of a piezoelectric ceramic plate and a piezoelectric transducer element in the probing and reference arms respectively. Through the use of adjustable holders, these mirrors and the piezoelectric materials to which they were attached were finely oriented so that each mirror's reflective surface was perpendicular to the interferometer beam incident upon it. Furthermore, the holders could be translated along their respective arms of the optical bench, and in doing so permit the careful setting of the length of each interferometer arm. In practice the static optical path length of these was set to be within a few millimetres of each other, and kept as short as possible. Typically this was some 500 mm when the crystal was present in the apparatus, and as short as 80 mm when the crystal was absent and the piezoceramic reference plate was being calibrated. The electric control and manipulation of each of these mirrors by means of the separate piezoelectric elements are described in more detail later in this chapter.

7.2.4 Light detection system

The two beams emerging from the interferometer were oriented to coincide over the aperture of a silicon photodiode, so forming an interference pattern at that point. In converting the optical signal into an electronic one, the photodiode provided a voltage output proportional to the light intensity incident on its aperture. This proportionality was confirmed by Malus' law over the range of intensities encountered in this investigation. A preamplifier which formed an integral part of the photodiode permitted amplification of the output signal by factors of 1, 5, 10, and 50.

Two different means were used to detect the output signal from the photodiode: for larger intensity changes of the interference pattern, such as those encountered during the calibration of the piezoceramic reference material, a digital oscilloscope was used (for the most part a Philips model PM 3350A), while the smaller voltage modulations experienced in the electro-optic studies or reference plate calibration were detected by a Brookdeal Electronics EG & G Princeton

Applied Research model 5205 lock-in amplifier. Special care was taken to screen the output from the photodiode to avoid spurious signals radiated from other sources. To this end, commercially available audio-frequency coaxial cable, specifically designed to provide a high degree of screening over this frequency range, was used to carry the signal from the photodiode to the lock-in amplifier. For the same reason, this cable was kept as short as possible and routed in such a way as to keep it well away from the power supplies, amplifiers, and high-voltage step-up transformer.

To ensure that the photodiode viewed only an area of the interference pattern of near-uniform intensity, the fringe pattern was manipulated so that the spacing between fringes was much larger than the aperture of the photodiode. This was achieved through the adjustment of the static optical path lengths, set to be as near to one another as possible by the careful alignment of the mirrors at the end of either arm of the interferometer, and by placing a converging lens, of focal length 38 mm, just before the photodiode in the path of the emerging beams. The spacing of the fringe pattern thus achieved was typically 8 mm, which compares with the square aperture of the photodiode of 1.5 mm × 1.5 mm.

7.3 The crystal specimens

7.3.1 General properties

Available for investigation in this interferometric research project were three KDP-type single crystals, one of which was KDP and the remaining two ADP. Each specimen was right-parallelepiped in shape with the plane faces cut in the *xy*-, *xz*-, and *yz*-planes of the crystallographic axes; to avoid ambiguity of this description, it is shown in Figure 7.2. The accuracy with which these crystals were cut relative to their crystallographic axes was estimated to be: less that 0.3 ° for the *z*-axis, and within 3 ° for the *x*- and *y*-directions. These best estimates were made using a conoscopic cross arrangement and also establishing the maximum and minimum response of the electro-optic effects of the crystals with polarization angle in the polarimetric arrangement. Approximate dimensions of these crystals were 50 mm × 50 mm × 5 mm for the KDP and larger ADP specimen and 35 mm × 35 mm × 7 mm for the smaller ADP single crystal. To facilitate the application of an electric field to these samples, each was prepared with a thin coating of conducting paint on the two faces in the *yz*-plane, so forming

(a)

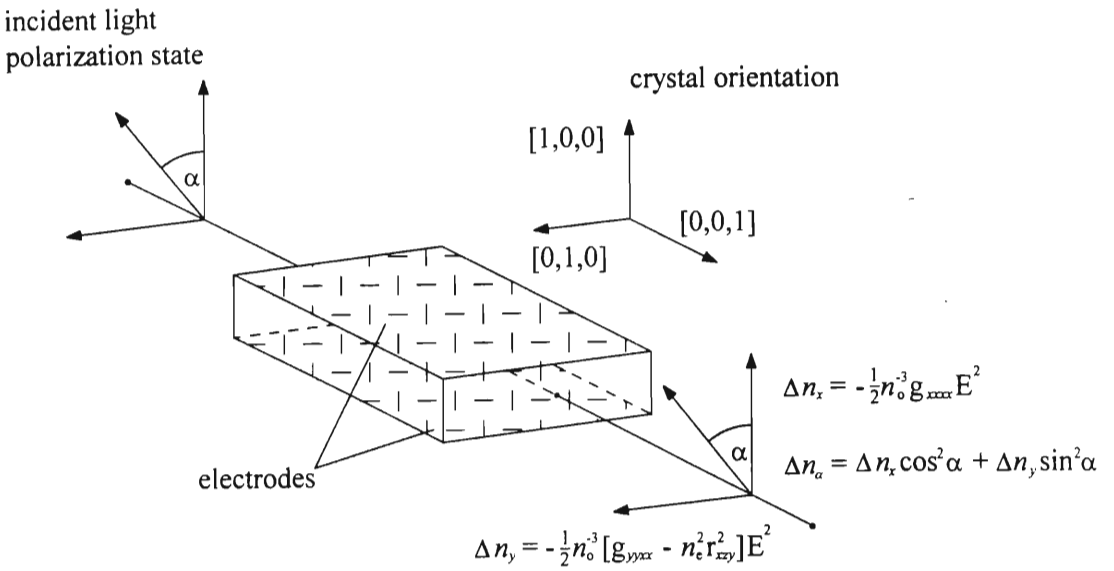

(b)

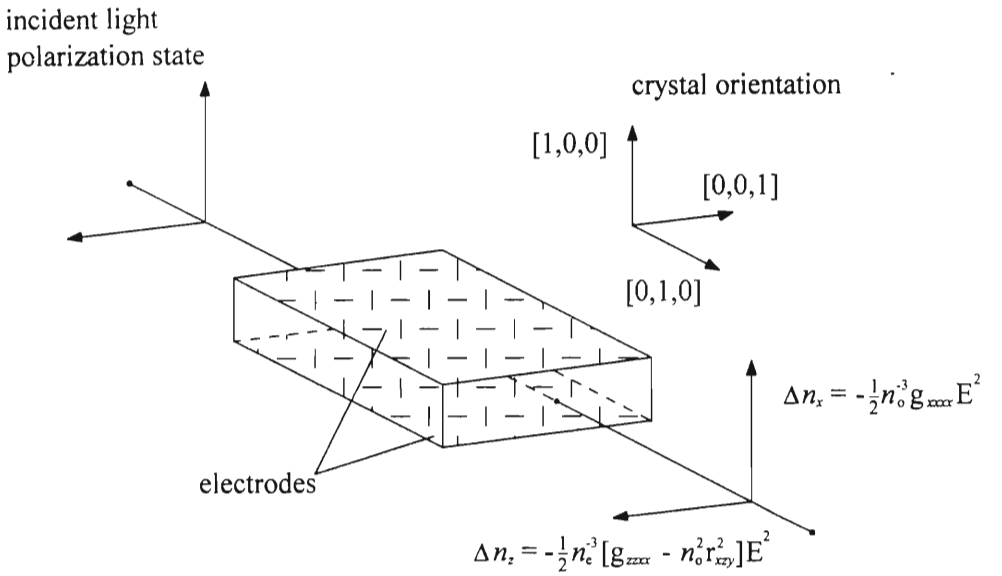

Figure 7.2 Diagram of the crystal orientation relative to crystallographic axes, and the light propagation and polarization states involved in this work for the investigation of the quadratic electro-optic coefficients: (a) g_{xxxx} and g_{yyxx}, (b) g_{xxxx} and g_{zzxx}.

an electrode surface either side of the crystal. Accordingly, to the accuracy with which a specimen's *yz*-plane faces were cut relative to the crystallographic axes, a field applied between these surfaces was taken to be parallel to the crystallographic *x*-axis. Since the resistivity of KDP- type crystals is large, typically in the region of $10^{12}\,\Omega$m for KDP and ADP, strong electric fields could be applied to them with no appreciable flow of current, which would have led to heating of the medium and instability in the field. For the particular geometry of these crystals light propagation along the crystallographic *y*- or *z*-axes was therefore possible for an applied field in the *x*-direction. For these configurations, the relationships have been established in Chapter 5 for the field-induced changes in refractive index of the polarization eigenvectors, which propagate for these directions, in terms of the quadratic electro-optic effect, and also for the change in sample dimensions on account of the electrostrictive effect. Also shown in Figure 7.2, therefore, are the field-induced changes in refractive index in terms of particular coefficients of the quadratic electro-optic effect, derived in Section 5.4, for the specific propagation directions and polarization angles of interest.

7.3.2 Mounting of the crystals

A perspex box measuring 100 mm × 60 mm in length and width and 50 mm in depth was used to house the crystals under investigation in the probing arm of the interferometer. Free transmission of the laser beam through this container in two perpendicular directions was enabled by windows made of thin microscope cover slides mounted centrally and free of strain on the four vertical sides of the box. At any one time, the specimen under investigation was placed in this container with its electrode surfaces approximately in the horizontal plane of the optical bench, with support beneath it being provided by separate perspex mounts on each corner. So situated, the investigated sample was in the path of the light beam set to travel through the crystal approximately half way between the electrode surfaces. Resting freely in this manner, the crystal was taken to be mechanically free to respond to the applied electric field.

Since KDP-type crystals are hygroscopic, special attention had to be paid during the project to ensure that the environments in which the experimental specimens were placed - in the one instance silicon oil and the other air - were moisture free. Thus, there was a lid for this container, also made of perspex, which could be bolted into place with a gasket between it and the box effectively sealing off the interior environment. Then, in the instance where the crystals were

investigated in an air environment, silica crystals were placed in the box with the crystal (but well out of the way of the light beam) to provide a dry atmosphere with the container lid securely fastened. An optically inactive silicon diffusion pump oil was used as the alternative environment for the crystals.

7.3.3 Orientation of the crystals

To allow the particular components of the quadratic electro-optic and electrostrictive coefficients of interest to be determined, careful attention had to be paid to the alignment of the crystals to ensure the desired light-propagation and polarization geometries were achieved. These entailed the accurate propagation of the light along, in turn, the crystallographic y- and z- axes, and the known linear polarization of the light relative to the x- and z-, and x- and y-axes, for these propagation directions respectively. To facilitate these requirements, the solution invoked was to align the crystallographic x-, y-, and z-axes relative to a set of established, and well defined, laboratory axes x', y', and z'. This laboratory frame was specified as follows: the perpendicular above the plane of the optical bench was the x' direction, and the direction of the light beam, preadjusted to propagate at a set height above the optical bench and parallel to the interferometer's probing arm, was taken to be the z'-axis. In order to enable the accurate rotation of the container about three mutually orthogonal axes, and thereby to facilitate the orientation of the crystal relative to the laboratory frame, the mounting which secured the crystal box in place on the optical bench permitted its adjustment through the use of two independent screw gauges and a divided circle in the plane of the bench. An outline of the crystal alignment process is given as follows:

Stage 1: Alignment of the optic axis relative to the z′-axis of the laboratory frame

The first step in the alignment of the crystal under investigation was to orient the specimen so that the light-propagation direction, the laboratory z′-axis, coincided with the crystallographic z-axis. This was accomplished through the use of the familiar interference figure formed by light passing along the optic axis of a uniaxial crystal placed between crossed polarizers. An explanation of this effect for monochromatic light may be found in most optics text books (see, for example, Born and Wolf 1980). With the stand holding the piezoceramic plate and associated mirror temporarily removed from the interferometer, a second Glan-Taylor polarizing prism was placed on the optical bench directly after the crystal mounting box with its fast axis rotated

orthogonal to the arbitrary plane of linear polarization of the light incident upon the crystal. In practice, the beam splitter was left in its place on the optical bench between the first polarizer and the crystal, since removing it from the arrangement resulted in a slightly different propagation path of the light through the crystal, and it was the propagation path with the beam splitter present that was of interest. So situated, the crystal was effectively between two crossed polarizers and the light transmitted through this system was allowed to fall upon a plane screen. This produced the well-known optical phenomenon for a uniaxial crystal of a conoscopic image (Born and Wolf 1980) which, for light travelling along the optic axis, consists of alternate light and dark circular fringes with a black cross centred on them. The spacing of these fringes and definition of the central cross depend on the birefringence and the optical path lengths of the sample investigated; for those used in this work, the fringe pattern and cross were clearly defined. By adjusting the two screw gauges and divided circle, which served to tilt and rotate the crystal box, the specimen was aligned until the centre of this conoscopic image was positioned over the centre of the beam position in the absence of the additional crossed polarizing prism. When this condition was met, the light wave was propagating exactly along the optic axis of the crystal and thus this axis, the crystallographic z-axis, coincided precisely with the z'-axis of the laboratory frame.

Stage 2: Alignment of the crystallographic x-axis relative to the laboratory x'-axis

Once the initial z-orientation process was complete, the second stage of the crystal alignment procedure was to orient the crystallographic x-axis relative to the laboratory frame. It was desired to have this axis aligned parallel to the direction vertical to the optical bench, the x'-axis, which would leave the crystallographic yz-plane in the plane of the optical bench. This was achieved through a second temporary modification to the experimental arrangement in which again the mirror assembly after the crystal box was replaced by a Glan-Taylor prism crossed relative to the first polarizing prism. Also included after the crystal, but before the second polarizing prism, was a $\frac{\lambda}{4}$ - plate oriented with its fast and slow axes at 45° to the linearly polarized beam incident upon the crystal, and a photodiode was used to detect the total light intensity passing through this system. In effect one had the polarimetric arrangement shown in Figure 7.3.

A known result for this particular arrangement for KDP-type crystals to which a modulated electric field of fixed amplitude is applied, is that the oscillating intensity of the emerging light

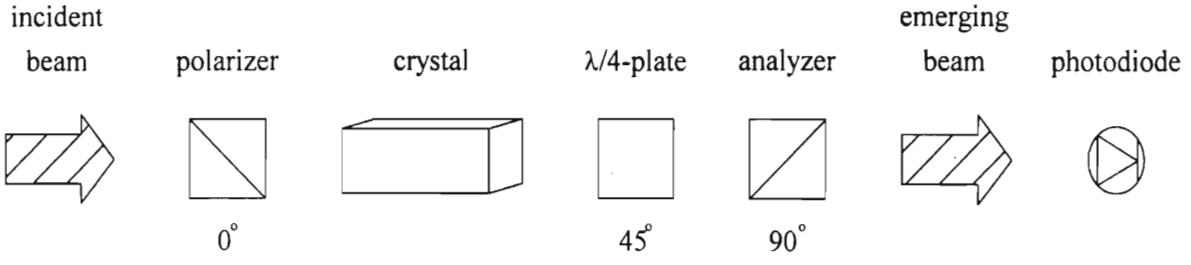

Figure 7.3 The polarimetric arrangement involved in aligning the crystallographic x-axis with the laboratory x'-axis

varies in magnitude relative to the constant background intensity as the plane of polarization of the first polarizer, and hence the polarization of the light incident upon the crystal, is rotated, keeping the fast and slow axes of the second polarizer and $\frac{\lambda}{4}$-plate at $90°$ and $45°$ to the polarization plane of the first polarizer, respectively. This is a consequence of the electro-optic effects displayed by KDP-type crystals for these symmetry conditions. In the presence of an electric field applied along the crystallographic x-axis, the light intensity modulated at the second harmonic of the applied field frequency has a minimum when the incident light is linearly polarized parallel to the crystallographic x- or y-axes (Górski *et al.* 1994). In practice this modulated intensity change could be accurately established, relative to the dc background signal, through the use of the lock-in amplifier in conjunction with the photodiode.

To orient the crystallographic x-axes relative to the laboratory x'-axis, knowing roughly the x-crystallographic direction since this is the applied field direction between the electrode plates, the polarization plane of the light incident upon the crystal was fixed at precisely $0°$ to the x'-axis of the laboratory reference frame. Then, while the amplitude of the light intensity modulation at the second harmonic relative to the dc background signal was observed, the crystal to which a voltage of fixed amplitude was applied was rotated about the light-propagation direction, which is also the optic axis of the crystal, by means of the screw gauges on the crystal mounting box until the minimum of this modulated intensity at the second harmonic of the emerging light was found. The crystal so oriented was aligned in such a way that the crystallographic x-, y-, and z-axes now coincided with the laboratory x'-, y'-, and z'-axes.

Stage 3: Propagation of light along the crystallographic y-axis

At this stage, the light was set to propagate along the optic axis of the particular crystal under investigation, and the polarization plane of the light incident upon the sample was known relative to the x and y crystal directions, which coincided with the laboratory x'- and y'-axes. It still remained to allow light propagation along the crystallographic y-axis for a known linear polarization relative to the x- and z-axes of the crystal. A method similar to the conoscopic cross arrangement used in Stage 1 above is not readily applicable for light propagation along the crystallographic y-axis of a uniaxial crystal, since no such clearly defined pattern is evident for

this propagation path[1]. Thus this alignment was realised in this project by rotating the aligned crystal box accurately through 90° about the x-axis of the crystal in the crystallographic yz-plane. This was possible only because the laboratory and crystal frames had been brought into coincidence.

To enable this, use was made of the divided circle upon which the crystal box assembly was mounted, by accurately aligning the rotation plane of this component in the plane of the optical bench through the use of an engineer's level and screw gauges on the stand which attached it to the bench. This divided circle, the same as those mounting the $\frac{\lambda}{2}$ - plate and polarizing prisms, had a rotational resolution of 2' of arc. Rotation of this divided circle pivoted the crystal box assembly about the x'-axis of the laboratory frame. Thus once the crystal had been aligned relative to the laboratory axes in Stages 1 and 2 above, with the light propagating along the z-axis, the crystal could be revolved about its x-axis through precisely 90° so that the light then traversed the crystallographic y-axis, and the plane of linear and horizontal polarizations of the light relative to the optical bench were then parallel to the x- and z-axes respectively.

Each of these orientation stages was repeated at regular intervals during the project to ensure that misalignment had not occurred.

7.3.4 The voltage applied to the crystal

Given the small magnitude of the quadratic electro-optic and electrostrictive coefficients of KDP-type crystals (see Tables 5.1 and 5.2), relatively large electric fields had to be applied to the specimens under investigation in order for a measurable effect to be induced. In previous such investigations on these crystals the typical amplitude of the applied field was of the order of 10^5 - 10^6 Vm^{-1} (Perfilova 1968; Kucharczyk and Górski 1983; and Górski and Kucharczyk 1987b).

In this experiment the modulated applied voltages were the result of a three-stage configuration: an initial small sinusoidal signal being amplified twice before being applied across the crystal

---

[1]Although in the polarimetric investigation described in Chapter 9 use was made of the conoscopic pattern formed for this propagation path, it was not as clearly defined as that for propagation along the optic axis. In this part of the experimental work, an alternative solution to this alignment was found.

under investigation. Providing the source of the initial input signal was a Philips model PM 5141 LF wave synthesizer which served to generate a sinusoidal signal of amplitude 50 mV rms. This signal then formed the input for a variable high-voltage amplifier, the output from which was further amplified by a high-voltage step-up transformer. By means of a feedback circuit, integral with the step-up transformer and high-voltage amplifier, the output from this configuration was maintained to within 0.1 % of the value preset by the variable amplifier. In this way, a stable voltage output from the transformer in the range 0 - 15 kV rms could be applied across the crystal. However, to guard against possible electrical breakdown between the crystal's electrode surfaces, the applied voltages in this work were limited to less than 4.3 kV rms. For the dimensions of the KDP and ADP samples investigated this translates to fields of amplitude up to 1.2×10^6 Vm^{-1}. To measure the applied voltages of this magnitude, a Fluke model 80K-6 high-voltage probe was used which was rated to measure ac voltages up to 4.3 kV rms. This probe was wired permanently in the circuit in parallel with the crystal and provided 1000:1 attenuation of the measured voltage, its output being read by a HP 3478A digital multimeter.

The frequency of the signal applied to the crystals under investigation had to satisfy two constraints: first, that it was well below the frequencies of mechanical resonance of the particular specimens, thus ensuring they could be treated as mechanically free (Section 5.7), and second, that it was away from the line frequency of 50 Hz. For convenience the frequency chosen for this investigation was 391 Hz, but other frequencies in the near vicinity were also tested with no discernible influence on the measured results. For this frequency of the modulated signal read by the probe, and for the specified precision of the multimeter used in this range, the voltages applied across the crystal could be determined to within 1% accuracy in accordance with the probe manufacturer's rating.

In laying out the apparatus, the high-voltage amplifier and step-up transformer were kept well away from all other electrical instruments to avoid interference effects from the high fields they generated. Furthermore, the output from the high-voltage transformer was connected to the Fluke probe and the crystal mounting box via a coaxial cable. Two sealed plug sockets in the lid of the crystal box assembly, to which the high-voltage cable was connected, allowed for the application of the voltage to the crystal while preventing interaction between the interior and exterior atmospheres. Inside the crystal box, short copper wires completed the circuit from the plug

sockets in the container lid to either electrode surface of the crystal. Thus, through the use of the coaxial cable and short wires to the crystals, stray fields in its vicinity were kept to a minimum. In addition to these precautions, the entire crystal box assembly was screened with a grounded metal foil, with a small aperture on each of the vertical faces of the box coinciding with the side windows, to allow the free transmission of the light beam. In practice, changes in the position of the high-voltage cable relative to the crystal sample were found to have no effect on the results.

7.4 The piezoceramic reference plate

7.4.1 General

The piezoceramic plate to which the mirror in the probing arm of the interferometer was securely attached, and which served as the reference material for this work, was especially selected on account of the large, repeatable, piezoelectric response it exhibited. This disc-shaped piezoceramic was approximately 16 mm in diameter and 3 mm thick, and the application of an electric field to it was enabled by conducting surfaces which coated the two plane parallel faces. On one of these plane surfaces was mounted the small polished mirror, with a surface area of about 8 mm^2, of the probing arm of the interferometer. The other surface was attached to an insulating perspex mounting plate, which itself formed part of an interferometer mirror holder enabling the precise alignment of the mirror surface perpendicular to the beam incident upon it. Besides this alignment, the holder could also be translated along the length of the particular arm of the optical bench thereby facilitating the control of the static length of that interferometer arm. A voltage applied across the electrode surfaces of this reference plate established, via the material's piezoelectric response, a change in the sample's thickness perpendicular to the plane faces. As a consequence, there was a displacement of the mirror surface and a change in the optical path length in the probing arm of the interferometer of which the reference material and attached mirror formed part. This relationship, for a piezoceramic plate dilation perpendicular to the interferometer beam, is given in eqn. (6.20) in terms of the piezoceramic calibration constant.

7.4.2 Application of the voltage to the reference plate

A necessary condition for the modulated voltage applied to the piezoceramic reference plate was that this signal should be variable in both its phase and magnitude, and also at precisely twice the frequency of the voltage applied to the crystal. This was essential in order to permit the compensation of the induced optical path length in the interferometer, arising from the signal applied to the crystal, by that induced by the reference plate. In the experimental arrangement for this project the same 50 mV rms output signal from the Philips model PM 5141 wave synthesizer, which provided the input for the high-voltage amplifier, also formed the basis of the voltage applied to the reference material. This signal, of frequency 391 Hz, was passed initially through a frequency doubler and then an amplifier and phase shifter contained in an integral unit, before being applied across the electrode surfaces of the piezoceramic. Thus, by means of this set-up, modulated voltages of frequency 782 Hz, amplitude 0 - 15 V rms, and of any phase could be applied to the reference material. To enable automation of the measurement process, an explanation of which is given later in Section 7.7, a digital-to-analogue converter was used to provide a dc reference for the voltage amplifier and phase-shifter unit. The amplitude of the amplifier output was proportional to this dc signal. The digital-to-analogue converter could be addressed, and its dc output manipulated, by a computer, which thus had direct control over the amplitude of the modulated voltage applied to the piezoceramic plate.

As in the case of the crystal, the voltage was applied to the piezoceramic by means of a coaxial cable and short electrode wires, thus keeping stray fields to a minimum and also not imposing any mechanical force on the sample which would inhibit its response to the field. Here also, the relative change in position of these cables led to no difference in the response of the material.

7.4.3 Calibration of the reference plate

Relevant components of the apparatus used for the calibration of the piezoceramic are shown schematically in Figure 7.4. For this purpose the interferometer was assembled in the usual manner, but with the crystal and its box removed from the instrument. The absence of these components allowed considerably shorter optical path lengths in the arms of the interferometer, with 40 mm being the norm from the beam splitter to either mirror surface, and a considerable improvement in the clarity of the interference pattern emerging from the system. A measure of

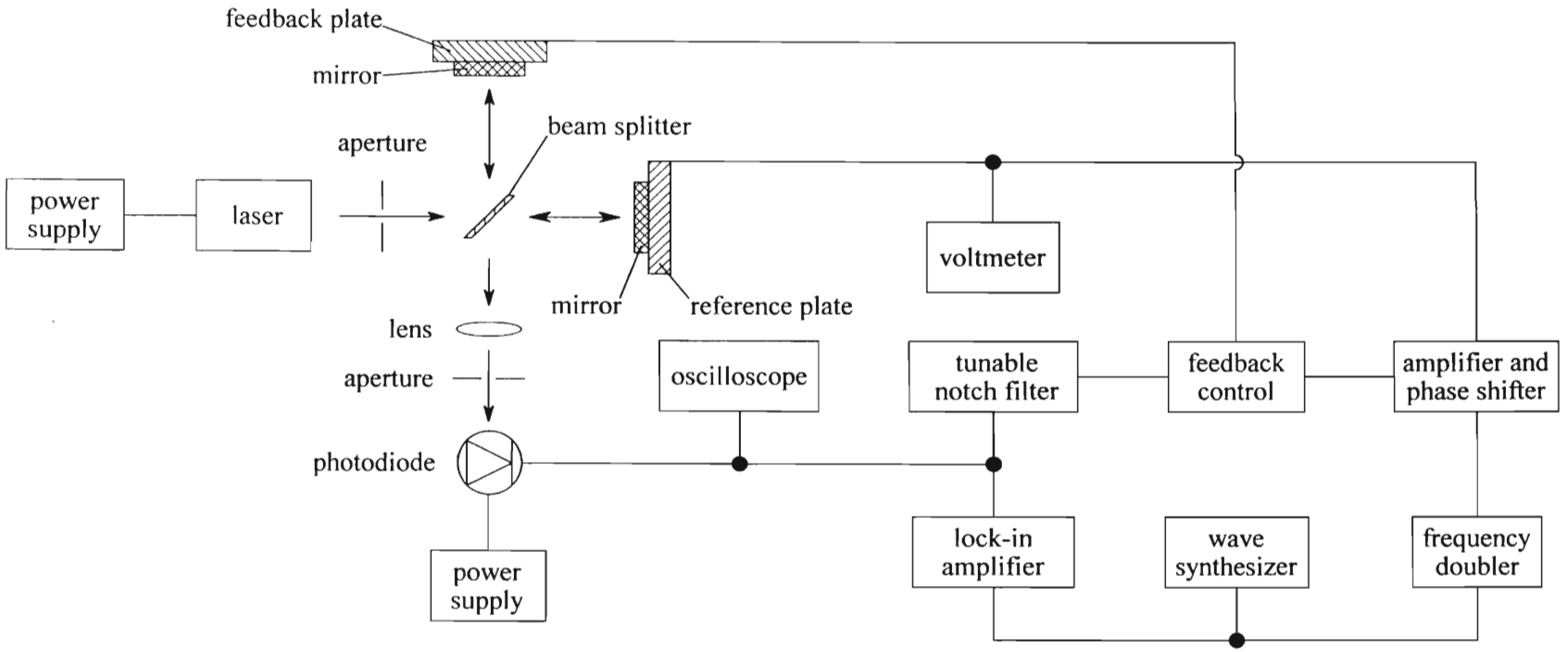

Figure 7.4 Diagram of the interferometric apparatus, including all necessary optical and electronic components, for the calibration of the piezoceramic reference plate

the light intensity at a point on this interference pattern was obtained in the usual manner by the photodiode, the output voltage from which was detected by both the Philips digital oscilloscope and the lock-in amplifier. These served to determine, respectively, a measure of the difference between maximum and minimum output voltage on account of a shift on one complete fringe of the interference pattern, and the small modulated voltage change due to the field applied to the piezoceramic material. Throughout this calibration procedure the interferometer was operated at its point of maximum sensitivity, and kept balanced at that point by means of the feedback circuit explained in the next section.

In the calibration of the piezoceramic, a modulated voltage of variable amplitude, but at a frequency of precisely 782 Hz, was applied to its electrodes in the usual manner via the frequency doubler, amplifier, and phase-shifter unit. When required, a modulated signal of nominal frequency (391 Hz) was also applied to the piezotransducer element which actively drove the mirror in the other arm of the interferometer. The amplitude of this latter voltage was such that through the displacement of the mirror it shifted the optical path length in that arm by precisely one wavelength, thereby varying the interference pattern by a complete fringe, with the intensity being observed by the photodiode. A digital oscilloscope, set to read peak-to-peak voltages, was used to determine the voltage change from the photodiode which corresponded to this variation in intensity of the interference pattern of one complete wavelength. This facilitated the determination of the difference between the maximum and minimum intensity of the interference pattern, which was required for the calibration process (see eqn. (6.21)), and only while establishing this difference was a modulated voltage applied to the piezotransducer. Typically these readings were taken over an average of 8 or 16 cycles to overcome random fluctuations of the photodiode output signal. With a voltage applied across the piezoceramic reference material, the small variation in voltage of the photodiode signal so induced was determined by means of the lock-in amplifier using modulation techniques.

In the calibration process both these voltages, and consequently the change in optical path length induced by the reference plate related to them by eqn. (6.21), were measured for known voltages of up to15 V rms applied to the piezoceramic. From the relationship of induced optical path length to voltage applied to the reference ceramic (eqn. 6.20), the calibration constant d of the piezoceramic was determined from the gradient of the best-fit line. A summary of these results

is tabulated in Table 8.3, and a sample graph is given in Graph 8.1 to show the linearity of the piezoceramic's response to the applied voltage field in this range. As expected, all results were found to be independent of the angle of linear polarization of the beam propagating through the interferometer.

7.5 Stabilization of the interferometer

7.5.1 Passive stabilization

Isolation of the interferometer from external noise influences was of paramount importance to enable the determination of the very small field-induced optical path-length changes in this experiment. With this in mind, various measures were taken in the construction of the apparatus to ensure a degree of inherent stability. The optical bench was a heavy cast-iron structure to which all the optical components were securely fastened. To provide isolation from mechanical and building vibrations the bench was placed upon an anti-vibration mat, which in turn rested on a slate slab measuring 1200 mm × 900 mm × 50 mm supported by five air cushions on a concrete table. Once assembled, the apparatus was operated independently in a room well-removed from any machinery. Measures against acoustic noise were taken by building a robust wooden enclosure which encased most of the interferometer, and which was padded on the outside with high-density closed-cell foam. Only the laser and the corresponding arm of the optical bench were kept outside this enclosure, the beam passing through an opening in the one side, since heat generated by the laser would have lead to excessive heating of the enclosed atmosphere with consequential detrimental effects. The sound enclosure itself was securely fixed to the concrete table on which the slate slab and optical bench were positioned, and did not come into contact with either.

The use of an airconditioner to control the temperature of the laboratory was considered since thermal expansion of the interferometer components was seen as a possible cause of slow variations in the optical path lengths of the interferometer arms and consequently of a drift in the interference pattern. However, the vibrations generated by the unit available, together with the subsequent air drafts it caused, affected for the worse the apparatus's stability and sensitivity, so that no advantage was gained by the more stable thermal environment. Over the period of the investigation, the room temperature was observed to be in the range of 15 - 24 °C with an average of about 21 °C.

Further steps taken for the purpose of isolation included the use of the thin flexible copper wires already mentioned, about 0.14 mm in diameter and between 50 mm to 100 mm in length, to form electrical contacts to the electrode surfaces of the piezoceramic reference plate and the crystal, as well as the piezoelectric transducer. These wires ensured that there was the least amount of mechanical force applied to the respective material and that there was isolation of the material from the coaxial cable supplying the necessary voltage. Both these measures were necessary since in the first instance the response of the samples must not be restricted in any way, and secondly Coulomb forces along the lengths of the coaxial cables can cause them to vibrate. By means of a microscope, tests were conducted during the experiment to see if the copper wires themselves vibrated, but even for the highest voltages used during the research, no vibrations were observed.

7.5.2 The piezoelectric transducer element

The mirror at the end of the interferometer's so-called reference arm was mounted on a piezoelectric transducer element so as also to allow its manipulation by means of an applied electric field. Forming an integral part of the active electronic stabilization process utilized in this project, this transducer was one such as those often found commercially comprising the moving element in high-frequency tweeters or alarm speakers. It was appealing for use in this work in that it was inexpensive, yet offered an efficient and sensitive response for low applied voltages. This transducer element consisted of a thin circular brass base-plate, supported around its periphery by a plastic mounting secured in turn to an interferometer mirror holder, and a thin disc of piezoelectric ceramic material coating the one side. A voltage applied across the piezoelectric induced a stress in the material which in turn caused a flexing of the brass plate, either convex or concave depending on the polarity of the applied voltage. Thus a mirror attached to the centre of the piezotransducer element could be displaced on the application of an electric field. For the element used in this work a voltage of 700 mV, supplied by way of the feedback circuit, was sufficient to displace the mirror enough to shift the interferometer's interference pattern by one complete fringe, corresponding to a shift in optical path length in that arm of a wavelength.

7.5.3 Active stabilization

In this project it was found that the various passive stabilization steps employed, though beneficial, were not in themselves sufficient to eliminate all noise influences, and the interference pattern was still observed to drift slowly with time away from the point of maximum sensitivity as read by the photodiode. Although in the short term readings could be taken, in the long run constant readjustment of the apparatus was necessary to bring the interference intensity back to the point of maximum sensitivity. To achieve long-term stability of the interferometer, essential in obtaining a large number of readings on a given crystal, a means of electronic stabilization was adopted in this project to provide isolation against low-frequency noise (< 10 Hz). Shown schematically in Figure 7.5 are all the components associated with the active electronic feedback system used for this experiment, the principle of which follows that outlined in Subsection 6.4.1.

When providing a measure of the intensity at a point on the interference pattern, the photodiode output voltage may be seen as consisting of three separate signals representing the distinctive parts of the optical path-length difference given in eqn. (6.16): a static signal depending on the relative position of the interference pattern seen by the photodiode, a measurement signal, and a low-frequency noise signal. The overall idea behind the feedback control of the apparatus in this work was to monitor the dc and low-frequency output from the photodiode and keep the dc output component constant at a point corresponding to maximum sensitivity of the interference pattern, eqn. (6.11), whilst eliminating all low-frequency noise contributions. This was achieved by regulating the voltage applied to the piezotransducer element, which determined the reference arm's optical path length, and thus controlling the interference pattern and the signal detected by the photodiode.

In the feedback part of the circuit, the photodiode output was passed initially through a good quality tunable notch filter which was accurately set to eliminate the measurement part of the signal, which had a constant frequency of 782 Hz, and yet not to introduce any phase shift in the higher and lower frequency components of the signal. These requirements were both important since, first, it was essential that the feedback system not view the measurement signal and in any way try to null it, and, second, introducing a phase shift in the signal seen by the feedback circuit was detrimental to the prompt response of the system to noise. What remained of the photodiode

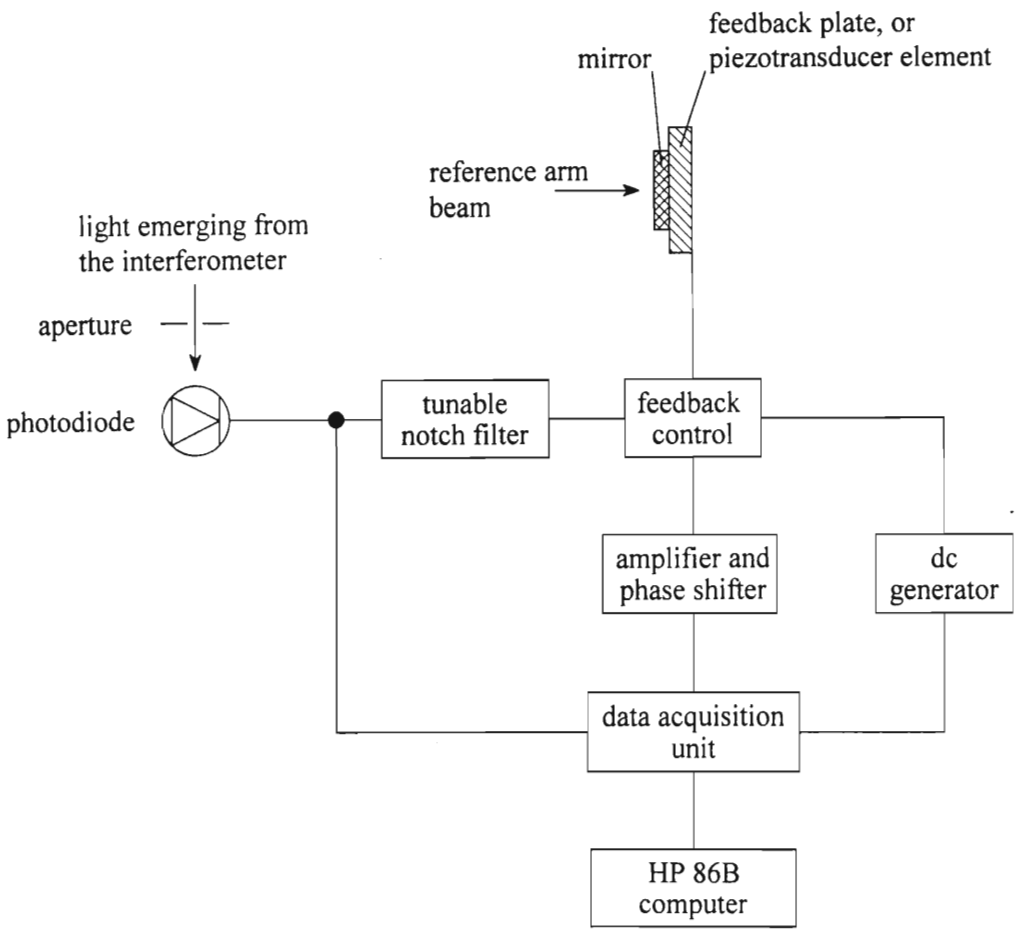

Figure 7.5 Diagram of the various optical and electronic components involved in the active stabilization of the interferometer against low-frequency noise influences

output signal, the dc and noise components, was then fed into the feedback control box, a unit specially designed and built by the University of Natal Electronics Centre, the circuit diagram of which is given in Appendix D. The principle of operation of this control circuit was the comparison of the low-frequency component of the photodiode voltage (<10 Hz), obtained after filtering the input signal, with an adjustable 0 - 10 V dc reference signal by means of a differential amplifier. Obtained was a voltage which gave a measure of the difference between the dc part of the photodiode output and the dc reference, and also of the low-frequency noise contained on the photodiode signal. This voltage so established was amplified, inverted in phase, and then applied across the piezoelectric transducer. Hence there was an induced change in the optical path length of the reference arm, a subsequent variation in the intensity of the interference pattern detected by the photodiode, and an alteration in the voltage fed into the feedback circuit. Thus a feedback loop was established which ideally stabilized for the condition when the voltage output from the photodiode was the same as the reference dc voltage supplied by the feedback circuit, and contained no low-frequency component. This controlled the interference intensity, as read by the photodiode, at a fixed preset value, and also eliminated all low-frequency noise contributions.

In this work the dc reference voltage was adjusted so that the position of the interference pattern read by the photodiode was that most sensitive to small changes in optical path length, as described in Section 6.2. To accomplish this a sinusoidal voltage of fixed amplitude was applied, during the configuration stage of the experiment, to the piezotransducer by means of the amplifier and phase-shifter unit via the feedback circuit, such that the optical path length in the reference arm was modulated by precisely one wavelength in the same manner as when calibrating the piezoceramic reference plate. When this occurred the dc reference voltage of the feedback circuit was adjusted until the light intensity variation detected by the photodiode and displayed on the digital oscilloscope was observed to vary sinusoidally from maximum to minimum intensity. The interferometer so configured was stabilized with the most sensitive portion of the intensity pattern falling upon the photodiode aperture, and the intensity of the pattern read at this point was precisely

$$I_o = \tfrac{1}{2}(I_{max} + I_{min}),$$

where I_{max} and I_{min} are respectively the maximum and minimum intensities as defined in Section 6.2. Any clipping of the signal when viewed by the digital oscilloscope, or a signal not purely

sinusoidal, was indicative of the interferometer not balanced at the point I_0. Corresponding to the intensity I_0 viewed by the photodiode, was an output voltage V_0. If the photodiode signal was kept within the range 0.8 - 1.2 V_0 (which corresponds to the range 0.8 - 1.2 I_0) then the sensitivity of the apparatus to small changes in optical path length, $\partial I/\partial \Delta d$ given by eqn (6.9), was confined within 2% of maximum (White and Emmony 1985).

In practice, the feedback circuit had an adjustable gain which was maximised to ensure the elimination of noise, and also that the feedback loop did not over-compensate and send the system into oscillation (Doswell and Kunov 1990). As a result the photodiode output was maintained at the preset value V_0. This was, however, usually a delicate task, since it was very easy to set the system oscillating, and typically the gain was set just under optimum. Thus during the experimental work on this project a very slow drift away from the point of balance was still observed. To overcome this problem, when a set of readings was initiated during the experiment, the computer recorded, by means of a data acquisition/control unit, the dc voltage output V_0 from the photodiode which corresponded to the light intensity I_0 falling upon the aperture. Then at regular intervals during the experiment the dc voltage from the photodiode was remeasured automatically and compared with that recorded initially. If any discrepancy was evident, indicating a drift in the interference point, the dc reference voltage contained in the feedback circuit was adjusted by the computer by means of a dc voltage supplied from a Philips model PM 5190 generator until the difference fell within an acceptable range. Once this condition was met the experiment was continued. In this work a typical balance voltage V_0 was of the order of 3.00 V, and readings were only taken when the system was balanced within 0.05 V of this condition. Thus the sensitivity limit adopted was always safely within 2% of maximum.

Also, there was a maximum voltage, namely |20| V, which could be applied to the piezotransducer to maintain the system at its balance point. Furthermore, as the voltage reached this limit there was a nonlinear response of the mirror displacement to the voltage applied by the feedback circuit, which had implications for the effectiveness of the feedback system since the gain of the loop was no longer linear. In this work, the computer was set to configure and balance the apparatus so that the feedback voltage was within the range 0 - |2| V dc at the beginning of an experimental run. In practice the voltage at the end of a run was never more than |10| V.

7.6 Signal measurement and data aquisition

The two signals fed into the respective inputs on the lock-in amplifier were those of a 391 Hz reference from the Philips model PM 5141 signal generator and the measurement voltage output from the photodiode. The lock-in amplifier available for use in this work, the Brookdeal Electronics EG & G Princeton Applied Research model 5205, allowed its various functions to be controlled by means of selection switches on the front panel. Throughout this work the 2f mode was selected because of the second-harmonic nature of the effects of interest induced in the crystal, and the doubling in frequency of the signal applied to the piezoceramic. Further to this, there was a choice of in-line filters on the input signal channel: either a low pass, band pass, or notch filter. That selected for this work was the band pass filter tuned manually to 782 Hz so as to allow the measurement signal through unopposed, and yet significantly attenuate higher and lower frequency contributions. Depending on the stability of the apparatus when conducting a set of readings, a time constant setting of 1 s was usually selected, but occasionally, when the measured signal was very small in magnitude and subject to a large amount of noise, a setting of 3 s was necessary. The sensitivity range of the unit is from 1 μV to 5 V rms full scale deflection, but was generally set at 10 mV rms except, again, for very small signals when the 1 mV rms range was used. For this choice of settings the maximum dynamic reserve of the lock-in amplifier was 60 db. By means of other selection keys on this instrument, the phase difference between the reference and input signals could be adjusted coarsely in steps of 90°, or finely in 0.025° steps.

A significant difference between the experimental procedure adopted in this project and that of the initial MSc work on which it is based (Gunning 1995), was the use of a computer to acquire all the necessary readings and, to an extent, automate the experiment. This was with the primary objective of enabling a considerable number of readings to be accumulated over a large period of time, so as to reduce noise contributions and achieve a better statistical average. The control system used consisted largely of Hewlett-Packard equipment, the central units being an HP 86B computer and an HP model 3421A data acquisition/control unit. Each of these had an IEEE interface which enabled the main equipment used in the experiment (HP digital multimeters, digital-to-analogue converter, and Philips model PM 5190 generator) to be addressed.

Data recorded in this experiment included the output signal from the Fluke high-voltage probe, which was read by an HP 3478A five-digit multimeter, and the piezoceramic applied voltage measured by a second HP 3478A five-digit multimeter connected in parallel with the piezoceramic plate. Both these multimeters were addressed directly by the HP 86B computer via IEEE interfaces. Additional results were gathered by the computer via the data acquisition/control unit, which contained a multiplexer card with eight multimeter and two relay channels. A dc signal from an output on the front panel of the lock-in amplifier provided a linear measure of the detected measurement signal. This voltage, in the range of -10 - 10 V dc corresponding to -100% - 100% scale deflection on the output signal channel for the chosen sensitivity range, was measured by one of the multiplexer multimeter channels of the data acquisition/control unit. A further two multiplexer multimeter channels recorded the dc photodiode current and the dc component of the piezotransducer element voltage respectively. Both these voltages were monitored during the course of the experiment, as part of the computer's role in controlling the feedback unit, as described in Subsection 7.5.3. When necessary, the dc voltage output from the Philips PM 5190 generator was adjusted by the computer, via an IEEE interface, effecting an alteration on the feedback unit's dc reference voltage to maintain the interferometer at the balance point.

A final function of the data acquisition/control unit was the use of one of the relay switches on the multiplexer card to control the power to the high-voltage amplifier. Throughout the course of the investigation, the HP 86B computer monitored the voltage applied to the crystal. If there was an unacceptable fluctuation of this signal, more than 10 V, indicating an electrical breakdown across the specimen, or through the coaxial cable, or some other fault in the high-voltage circuitry, the computer, via the relay switch, cut the power to the high-voltage amplifier. This was purely a precautionary function, and the voltage to the crystal sample could only be re-established by manually reconfiguring the high-voltage amplifier and reactivating the relay switch.

7.7 Experimental procedure

When an experimental run was commenced, the $\frac{\lambda}{2}$ - plate and Glan-Taylor polarizing prism were rotated to give the desired angle of linearly polarized light propagating through the

interferometer, and all the optical components were optimally aligned to produce a well-defined interference pattern over the aperture of the photodiode. A voltage to a maximum of 4.3 kV rms was applied across the crystal, and the phase of the reference signal at the lock-in amplifier adjusted until the measure of the photodiode signal given by the lock-in amplifier was at a maximum, indicating the two signals were in phase. The phase of the voltage applied across the piezoceramic reference plate was then set so that the intensity variation signal it generated was precisely in antiphase to that resulting from the crystal. Furthermore, the feedback circuit was configured to establish the interference pattern viewed by the photodiode at its most sensitive point.

Listed in Appendix E, is the code for the HP 86B program used for the control of the experiment and the accumulation of the results employing the compensation technique. Once the experiment was set up in the manner described, the approximate voltage to be applied to the piezoceramic to null the effect induced in the crystal was established manually, by altering the voltage applied to the reference material. Then, with the HP 86B control program initiated, this approximate compensation voltage was entered into the computer together with the time constant setting of the lock-in amplifier. All other data required for the calculation of the results by the computer in the compensation method were contained in the program code and updated depending on the crystal being investigated and the chosen propagation direction. The computer would then run the experiment to establish accurately the correct balance condition using the approximate value entered as a reference. In this procedure voltages controlled by the computer via the digital-to-analogue converter were applied to the piezoceramic in the range of zero to twice the approximate balance voltage, but never exceeding 15 V rms. In all, twelve voltages spaced at even intervals were applied nonsequentially over this range, and, for each of these, 25 lock-in amplifier dc output channel and applied ceramic voltages were measured and the average of each recorded. In each case, before such a set of lock-in amplifier output readings was recorded, the computer paused for an interval greater than the lock-in amplifier time constant setting so as to allow a period for the system to stabilize. Once a run of twelve readings was completed, the computer established the best-fit straight line for the plot of piezoceramic voltage against lock-in amplifier output. The intercept of this graph gave the voltage applied to the piezoceramic for which the optical path length it induced precisely nulled that of the crystal sample. The following information: the crystal voltage, the null voltage, the correlation coefficient r of the best-fit line

of the plot of ceramic voltage against lock-in amplifier output, and a calculated value of the combined quadratic electro-optic and electrostrictive effects was then printed by an HP printer.

This entire process was repeated until terminated manually by human intervention. Chapter 8 gives an analysis of all results obtained for the investigations on the various KDP and ADP crystals. Depending on the stability of the interferometer when the readings were conducted, or whether it was necessary for the computer to intervene with the stabilization process, such an experimental run to determine a single null point took approximately 10 minutes.

Chapter 8

RESULTS OF THE INTERFEROMETRIC INVESTIGATION

8.1 Introduction

The changes in refractive indices and dimensions of a crystal, that result from the application of an electric field, may be related to the electro-optic and piezoelectric-type tensors respectively. In particular for the KDP-family of crystals and for the light paths and field directions chosen, the changes are quadratic in the field. This was shown in Chapter 5. For this situation eqn. (6.1), which describes the change in optical path length Δd of the light wave propagating through a medium, may be rewritten as

$$\Delta d = \left[L f(r_{ijk}, g_{ijkl}) + (n - n_a) f(\gamma_{ijkl}) \right] E^2. \tag{8.1}$$

In this equation $f(r_{ijk}, g_{ijkl})E^2$ and $f(\gamma_{ijkl})E^2$ are the appropriate field-induced expressions for the changes in refractive index and dimension, respectively, in eqns. (5.36), (5.41), (5.45), and (5.46) for the two particular experimental configurations of interest, L and n are the crystal's field-free length and refractive index, respectively, for the propagation direction and polarization state of the light, and n_a is the refractive index of the atmosphere surrounding the crystal. If one assumes a modulated field given by

$$E = E^{(o)} \cos\omega t, \tag{8.2}$$

where $E^{(o)}$ is the amplitude and ω the frequency, then

$$E^2 = \tfrac{1}{2}\left(E^{(o)}\right)^2 (1 + \cos 2\omega t). \tag{8.3}$$

Thus, the induced optical path-length variation of the light propagating through the crystal includes a static term, as well as one modulated at the second harmonic of the field frequency. For the present dynamic investigation it is the latter term that is of interest, which may be expressed as

$$\Delta d(2\omega) = \tfrac{1}{2}\left[Lf(r_{ijk}, g_{ijkl}) + (n - n_a) f(\gamma_{ijkl})\right]\left(E^{(o)}\right)^2 \cos 2\omega t. \tag{8.4}$$

The resulting modulated change in the optical path length $\Delta d^{crystal}$ in the probing arm of the Michelson interferometer is

$$\Delta d^{crystal} = 2\Delta d(2\omega) = \left[Lf(r_{ijk}, g_{ijkl}) + (n - n_a) f(\gamma_{ijkl})\right]\left(E^{(o)}\right)^2 \cos 2\omega t. \tag{8.5}$$

Similarly, the optical path-length variation induced in the interferometer by the dilation of the piezoceramic reference plate due to an applied voltage

$$V = V^{(o)} \cos 2\omega t, \tag{8.6}$$

where $V^{(o)}$ is the amplitude and ω the modulation frequency, is from eqn. (6.20)

$$\Delta d^{ref} = 2\Delta L^{ref} = 2dV^{(o)} \cos 2\omega t. \tag{8.7}$$

In this equation d is the piezoelectric calibration constant defined in eqn. (6.19).

At the point of compensation between the two modulated optical path-length changes induced in the same arm of the interferometer by the crystal and piezoceramic plate, respectively:

$$\left[Lf(r_{ijk}, g_{ijkl}) + (n - n_a) f(\gamma_{ijkl})\right]\left(E^{(o)}\right)^2 \cos 2\omega t = -2dV^{(o)} \cos(2\omega t + \phi), \tag{8.8}$$

where ϕ is the constant phase shift introduced in the voltage applied to the piezoceramic necessary to achieve compensation. Hence, making use of eqns. (5.36), (5.41), (5.45) and (5.46) together with this relation, one may express the relevant components of the quadratic electro-optic and electrostrictive coefficients in terms of known, and measurable, quantities when compensation is achieved. Furthermore, with knowledge of the constant phase ϕ, relative to the phase of the voltage applied to the crystal, the sign of these components, or combination thereof, may also be ascertained. For the particular light-propagation directions and polarization states used for the study of KDP-type crystals in this work, and to which a field was applied along the crystallographic x-axis, these expressions are:

1. For light propagating along the y-axis of the crystal, linearly polarized parallel to the crystallographic x- and z-axes respectively:

$$g_{xxxx} - 2(n_o - n_a)n_o^{-3}\gamma_{xxyy} = \frac{2\sqrt{2}dV^{null}t^2}{n_o^3 L_y (V^{crystal})^2}, \tag{8.9}$$

$$g_{zzxx} + n_o^2 r_{xy}^2 - 2(n_e - n_a)n_e^{-3}\gamma_{xxyy} = \frac{2\sqrt{2}dV^{null}t^2}{n_e^3 L_y (V^{crystal})^2}, \tag{8.10}$$

2. For light propagating along the optic axis of the crystal, linearly polarized at an angle α relative to the crystallographic *x*-axis:

$$g_{xxxx}\cos^2\alpha + \left(g_{yyxx} + n_e^2 r_{xy}^2\right)\sin^2\alpha - 2(n_o - n_a)n_o^{-3}\gamma_{xxzz} = \frac{2\sqrt{2}dV^{null}t^2}{n_o^3 L_z (V^{crystal})^2}. \tag{8.11}$$

In these expressions: $V^{crystal}$ and V^{null} are the rms voltages applied to the crystal and reference plate, respectively, when compensation is achieved; L_i, i = *y*, *z*, is the field-free length of the specimen in the direction of light propagation; t is the distance between the electrode surfaces of the crystal; and n_o, n_e, and n_a are the ordinary, extraordinary, and surrounding atmosphere refractive indices. Also, use was made of the well-known relation $E^{(o)} = V^{crystal}/t$ to express the electric field in the crystal in terms of the applied voltage amplitude and the distance t between the electrodes surfaces.

The three eqns. (8.9) - (8.11) contain three independent quadratic electro-optic coefficients, namely

$$g_{xxxx},\ g_{yyxx},\ \text{and}\ g_{zzxx},$$

and two such electrostrictive coefficients

$$\gamma_{xxzz},\ \text{and}\ \gamma_{xxyy}.$$

All other quantities in these equations can be measured separately. At first sight it might seem that the five unknown coefficients cannot be determined from three equations. However, eqn. (8.11) can be recast in two forms which describe straight-line graphs (see eqns. (8.14) and (8.15)), the slopes (which are the same in magnitude, but opposite in sign) and intercepts of which yield experimental values for

$$g_{yyxx} - g_{xxxx} + n_e^2 r_{xy}^2$$

$$g_{xxxx} - 2(n_o - n_a)n_o^{-3}\gamma_{xxzz}$$

$$g_{yyxx} + n_e^2 r_{xy}^2 - 2(n_o - n_a)n_o^{-3}\gamma_{xxzz}.$$

Alternatively, for *z*-propagation through the crystal particular polarizations of the incident light, e.g. parallel to the crystallographic *x*- and *y*-axes, may be used in turn to give experimental

values for

$$g_{xxxx} - 2(n_o - n_a)n_o^{-3}\gamma_{xxzz}$$

$$g_{yyxx} + n_e^2 r_{xzy}^2 - 2(n_o - n_a)n_o^{-3}\gamma_{xxzz}.$$

Thus only one more independent measurable involving the five unknown coefficients is required. In practice, this can be obtained from one of the eqns. (8.9) - (8.11) by taking the appropriate measurements using a different crystal environment of refractive index n_a, for instance silicon oil in the place of air.

8.2 The experimental variables

8.2.1 Refractive indices and the linear electro-optic coefficient r_{xzy}

To determine for KDP and ADP the five unknown electro-optic and electrostrictive coefficients in eqns. (8.9) - (8.11), one requires the ordinary and extraordinary refractive indices of each crystal for the wavelength and temperature of the experiment, as well as the refractive indices of silicon oil and dry air for the same conditions. Other results required are those for the linear electro-optic coefficient r_{xzy} of each crystal respectively, also for the same experimental conditions.

Values used in this project for the ordinary and extraordinary refractive indices were calculated from the Sellmeier equations and tabulated Sellmeier coefficients given by Ghosh and Bhar (1982) for KDP and ADP, while recommended values for the coefficient r_{xzy} were obtained from tables in Landolt-Börnstein (1979). All these results, given in Table 8.1, are for 632.8 nm and room temperature (21 °C). With the use of a refractometer, the refractive index of the silicon oil was determined at room temperature to be 1.5572 for 589.9 nm, and dispersion from this wavelength to 632.8 nm was assumed to be negligible. Finally, the refractive index of dry air for 632.8 nm and 21 °C was taken to be 1.0003 (Kaye and Laby 1986).

Table 8.1 Values used for n_o, n_e, and r_{xzy} for KDP and ADP at 632.8 nm and 21 °C

Crystal	n_o	n_e	r_{xzy} (10^{-12} mV^{-1})
KDP	1.5075	1.4670	8.7
ADP	1.5222	1.4773	23.4

8.2.2 Dimensions of the crystals

The dimensions of the one KDP and two ADP crystals investigated in this research were determined with the use of a travelling microscope. The results for the distance t between the electrode surfaces and the crystal lengths L_y and L_z in the two orthogonal directions are given in Table 8.2. To obtain an accurate measure of each crystal's dimensions these readings were taken over the entire surface of the crystal, and in presenting the results the mean of these determinations is quoted together with the standard error σ_m in the mean. The latter is defined by the expression

$$\sigma_m = \sqrt{\frac{\sum (x_i - \bar{x})^2}{n(n-1)}}, \tag{8.12}$$

where $\bar{x}$ is the mean of a set of n readings of x_i. This standard error is taken as being a measure of the maximum uncertainty in the dimension.

Table 8.2 The dimensions of the crystals

Crystal	$t \pm \sigma_m$ (mm)	$L_y \pm \sigma_m$ (mm)	$L_z \pm \sigma_m$ (mm)
KDP	4.99 ± 0.01	50.05 ± 0.02	49.77 ± 0.02
ADP (larger)	5.01 ± 0.02	50.27 ± 0.02	51.22 ± 0.02
ADP (smaller)	7.06 ± 0.02	34.58 ± 0.04	35.54 ± 0.02

8.2.3 The measured voltages

The two voltages that enter eqns. (8.9) - (8.11) are the null voltage V^{null} applied to the piezoelectric plate and the voltage across the crystal $V^{crystal}$. The former of these was measured directly by an HP five-digit multimeter which, for the range and frequency of voltages used, has an accuracy of 0.4%. Also, since an identical meter was used to measure the piezoceramic voltage in its calibration, this is the same uncertainty as that entering the ceramic voltage used in eqn. (6.21) to calibrate the reference plate. The crystal voltage was determined via a Fluke high-voltage probe in conjunction with an HP five-digit multimeter. As discussed in Subsection 7.3.4, the maximum uncertainty in this measurement was 1%. The final voltages required in the calibration of the piezoceramic, were the peak-to-peak voltage output from the photodiode and the small modulated voltage change in this output signal for the induced ceramic path-length variation. Again, the determination of these has been described previously in Subsection 7.4.3.

Measured by the EG&G lock-in amplifier in conjunction with an HP five-digit multimeter, the small modulated voltage variation was established to an accuracy of 0.4% for the frequency and voltage range in question. The peak-to-peak voltage, determined by means of a Philips PM3350A digital oscilloscope, was known to within 2% in accordance with the oscilloscope's rating. It is this last uncertainly, more than any other, that accounts for the largest portion of the uncertainty in the final results. This was unfortunate, but the only other digital oscilloscope available for use in this work also had a similar uncertainly in its peak-to-peak voltage measurement.

8.2.4 Calibration constant *d* of the piezoceramic reference plate

At various stages of the experiment, null voltages in the range of 0.1 - 15 V rms were applied to the piezoceramic plate, with the balance being found typically between 500 mV and 5 V rms (see, for example, Tables 8.4, 8.6 - 8.10, and 8.12 - 8.19). Hence, in the calibration of the reference plate by the procedure outlined in Subsection 7.4.3, voltages in the same range were applied to the piezoceramic. In each calibration the induced optical path-length change in the interferometer was determined with the use of eqn. (6.21) for ten equally spaced, and nonsequential, voltages applied to the ceramic plate. The magnitude of the calibration constant d was obtained by a least-squares analysis of this data, given the linear relationship in eqn. (6.20). On each occasion that the constant was determined, readings were repeated a number of times and the mean of the set established together with the standard error (eqn. (8.12)) in this mean. The results for all the calibrations of the ceramic given in Table 8.3. Also given in the last row of this table is the mean of all the individual means and the standard error in this mean. This error is regarded as inclusive of all alignment errors occurring between individual sets of determinations of the calibration constant.

Since a known characteristic of ceramic piezoelectrics is the logarithmic decay over a long time of their piezoelectric response, it was important that the calibration constant of the reference plate used in this work be established at regular intervals throughout the investigation. For the period of this study there was no observed change in the constant, nor a trend indicating a decay in the response, and based on all results obtained, this constant was taken to be

$$d = -(2.542 \pm 0.073) \times 10^{-10}\ \mathrm{mV}^{-1}. \tag{8.13}$$

The maximum uncertainty in this final result is inclusive of the individual uncertainties arising at different stages in the calibration procedure. It includes the uncertainties in the measurement of the applied ceramic voltage, modulation signal output from the photodiode, and peak-to-peak

Table 8.3 Results for the calibration constant d of the piezoceramic reference plate

Number of determinations	$\lvert d \rvert \pm \sigma_m$ (10^{-10} mV^{-1})
20	2.537 ± 0.005
6	2.528 ± 0.007
18	2.546 ± 0.004
17	2.545 ± 0.004
28	2.545 ± 0.003
11	2.536 ± 0.004
10	2.549 ± 0.004
15	2.548 ± 0.004
10	2.563 ± 0.002
12	2.542 ± 0.004
16	2.534 ± 0.004
8	2.521 ± 0.004
15	2.549 ± 0.003
12	2.543 ± 0.005
16	2.542 ± 0.003
6	2.548 ± 0.010
9	2.528 ± 0.002
13	2.530 ± 0.006
16	2.557 ± 0.003
mean	2.542 ± 0.001

photodiode output, all of which enter eqn. (6.21) from which the calibration constant was calculated, and also includes the statistical error in the mean of the results listed in Table 8.3. The maximum relative uncertainty in the final quoted result is the square root of the sum of the square these individual relative uncertainties. In addition, the sign quoted for the result in eqn. (8.13) was determined by noting the direction of the shift induced in the interference pattern for a large static electric field applied to the piezoceramic material. A positive voltage was observed to lead to a lengthening of the probing arm of the interferometer or, equivalently, a decrease in the thickness of the reference plate.

Furthermore, in Graph 8.1 is given an example of the piezoceramic's response to the applied electric field at a frequency of 782 Hz and over the range of voltages experienced in this work. As is evident from this graph, the linearity in the field is excellent and typically, when

Graph 8.1 Example plot of the optical path-length variation induced in the interferometer versus the rms voltage, at 782 Hz, applied to the piezoceramic reference plate to display the linearity of the response over the voltage range used in this work

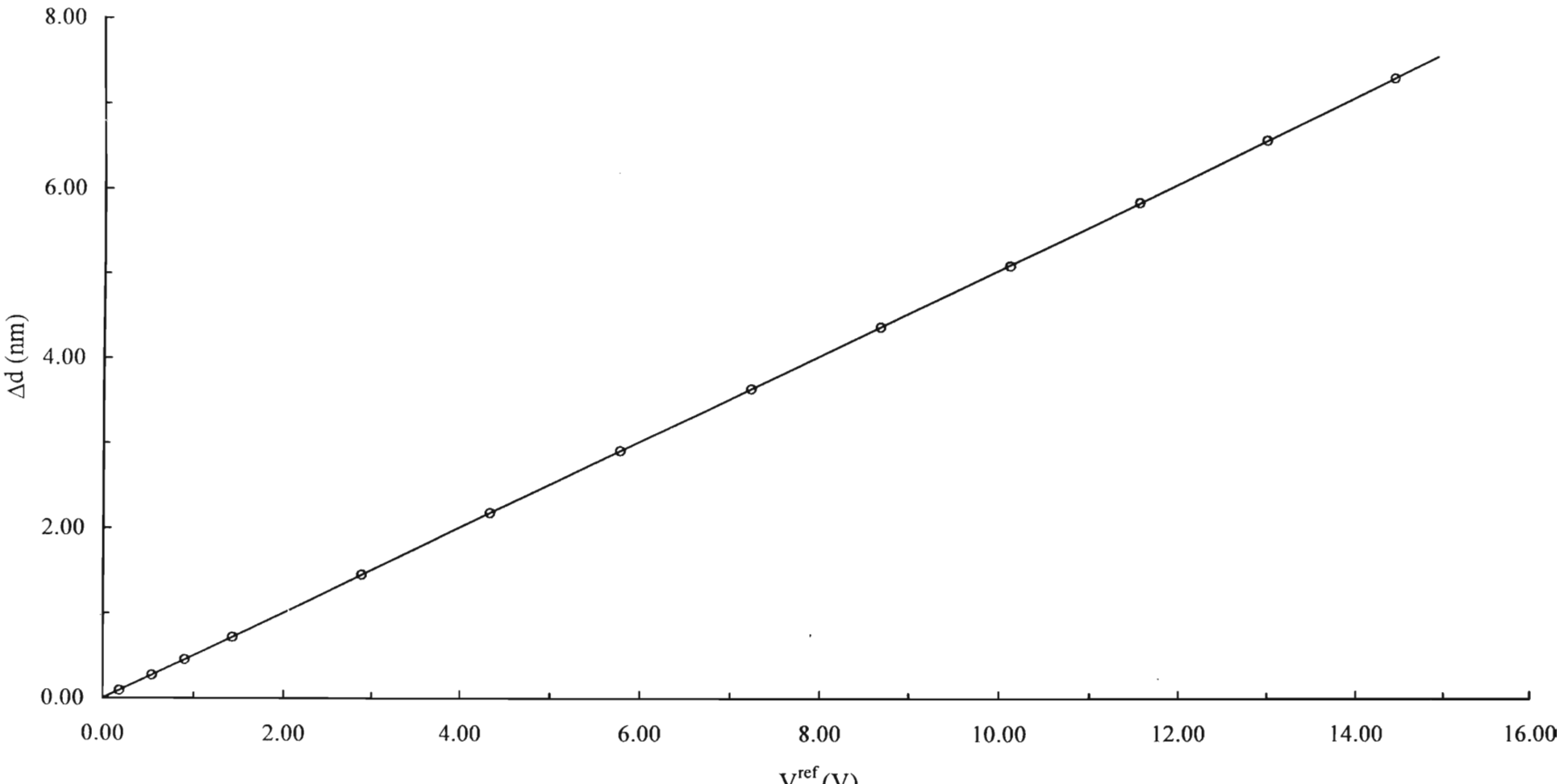

determining the calibration constants given in Table 8.3 from similar plots, the correlation coefficient for the best-fit line was better than 0.999. In addition, no hysteresis in the piezoceramic's response was observed and for the voltages used the induced optical path-length variation was less than 13 nm, as required for the 'small angle' approximation of eqn. (6.13). The calibration constant determined in this manner was found, as expected, to be independent of the angle of linear polarization of the light traversing the interferometer.

8.3 Uncertainty in the electro-optic and electrostrictive results

To assess the accuracy to which the final results for the quadratic electro-optic and electrostrictive coefficients in this research may be quoted, the uncertainty in each measured observable entering eqns. (8.9) - (8.11), from which they were calculated, had to be accounted for, as did the spread in the experimental results achieved by the null method. This section discusses the treatment of these uncertainties.

Determination of the null point in this interferometric work was achieved through the use of the HP 86B program presented in Appendix E and which is described in Section 7.7. This program, in its determination of the applied ceramic voltage necessary to satisfy the null condition for a particular voltage applied across the crystal, relied on a least-squares analysis of the collected data consisting of voltage changes at the second harmonic of the photodiode output signal and applied ceramic voltages. For each determination of a null point the correlation coefficient r was also calculated to give an indication of the stability of the analysis, and the result for a particular null determination was only included in the final quoted results if r was found to be better that 0.995. In each experimental run undertaken in this project, with a particular voltage applied to the crystal, the null point was established a number of times, and for each of these the combination of particular components of the quadratic electro-optic and electrostrictive coefficients established depending on the light-propagation direction and angle of polarization of the probing light. These values, reported as the effective quadratic electro-optic-electrostrictive response G^{eff}, follow from the right-hand side of eqns. (8.9) - (8.11) depending on the specific experimental conditions for the investigation in question. Quoted in the tabulated list of results for a particular investigation is the mean, for an experimental run consisting of a number of determinations, of the value of both G^{eff} and the null voltage from

which it follows. Also quoted is the standard error, defined in eqn. (8.12), in the mean of G^{eff}. These are the values given in the tabulated results in Tables 8.4, 8.6 - 8.10, and 8.12 - 8.19.

One would expect the final average of the means from each of the many sets of data to equal the average of the individual means weighted by the inverse square of their corresponding σ_m values (see, for example, Barford 1967). In other words: those results known to a greater certainly (with less standard error about the mean) would have a greater weight in the average. However, for the results obtained for the quadratic electro-optic-electrostrictive contributions (Tables 8.4, 8.6 - 8.10, and 8.12 - 8.19), the difference between the average of all results for the same experimental conditions in a particular table and an individual mean of a set is typically greater than the standard error in that individual mean. From this one may conclude that the reconfiguring of the apparatus between a set of null point determinations, which changed the light path through the crystal and the position of the piezoceramic plate, as well as other seemingly minor and unavoidable factors, affected to some extent the mean of each set. In quoting the uncertainty in the final average of the results, this affect needs to be allowed for since it would not be reflected by the uncertainty in any of the individual sets of readings. Accordingly, for the results quoted in each case in the final rows of Tables 8.6 - 8.9, and 8.12 - 8.19, and in each of the entries of the summary Tables 8.5 and 8.11, the means are given equal weight and treated as separate entities, with the average of the means being quoted together with its standard error. This uncertainty is taken as being representative of the random error due to noise, as well as the error arising from the slightly different experimental conditions between each set of results.

For some experimental configurations the final results for particular combinations of components of the quadratic electro-optic and electrostrictive coefficients for that specific arrangement were established directly from the tabulated results with no further analysis. This was not the case for the results for *z*-propagation through the KDP and larger ADP crystals in an air environment. In these two instances a graphical treatment of the tabulated results was undertaken. This involved graphs of G^{eff} versus $\sin^2\alpha$ and G^{eff} versus $\cos^2\alpha$ being plotted, from which results for particular quadratic electro-optic-electrostrictive contributions were obtained from the gradient and intercept by means of the appropriate linear relationships (see eqns. (8.14) and (8.15)). The linearity of these graphs confirmed the validity of the theory in Section 5.4 relating $\Delta n(\alpha)$ to the

polarization angle α and on which eqn. (8.11) is based. This equation also permitted an analysis of results for the full range of polarization angles. The statistical uncertainly in these results was reflected by the error in the least-squares determination of the gradient and intercept.

In the final presentation of the results for the different combinations of the quadratic electro-optic and electrostrictive coefficients in each subsection, the maximum uncertainty quoted in a result represents both the experimental error in determining the null points and the uncertainty in each measured observable entering the equations from which the value was calculated. In this case, the maximum relative uncertainty was the square root of the sum of the square of each individual relative uncertainty.

8.4 Results

This section contains the results for the different combinations of components of the quadratic electro-optic and electrostrictive coefficients obtained by means of interferometric measurements on KDP and ADP in this research. Each subsection gives details and tabulated data for a particular propagation direction and polarization state of the light wave probing the crystal, chosen to give a result for a specific combination of coefficients. From these results, for each of the different experimental configurations, values for the individual coefficients of the quadratic electro-optic and electrostrictive effects could be determined.

The KDP results were obtained from the single crystal that was available, while for ADP two crystals were studied as detailed in Subsection 7.3.1. Of these ADP crystals the larger was investigated only in air. To determine the relevant electrostrictive coefficients of ADP, the smaller crystal was investigated in both air and silicon oil, working with simple configurations in which the light was kept at a fixed polarization along the crystallographic x-axis. For each set of measurements on a crystal, a different propagation path was taken, covering most of the width of the crystal. Of the three crystals investigated, the larger ADP specimen was found to be particularly sensitive to the light path through the crystal, and the differences in the measured results for this crystal are largely due to this.

8.4.1 Results for z-propagation through the KDP crystal in air

Equation (8.11), applicable for z-propagation through KDP-type crystals, may be rewritten as

$$(g_{yyxx} - g_{xxxx} + n_e^2 r_{xy}^2)\sin^2\alpha + g_{xxxx} - 2(n_o - n_{air})n_o^{-3}\gamma_{xxzz} = \frac{2\sqrt{2}dV^{null}t^2}{n_o^3 L_z (V^{crystal})^2}, \quad (8.14)$$

$$(g_{xxxx} - g_{yyxx} - n_e^2 r_{xy}^2)\cos^2\alpha + g_{yyxx} + n_e^2 r_{xy}^2 - 2(n_o - n_{air})n_o^{-3}\gamma_{xxzz} = \frac{2\sqrt{2}dV^{null}t^2}{n_o^3 L_z (V^{crystal})^2}. \quad (8.15)$$

In this work a number of measurements were made of the null voltage V^{null} for each of a range of voltages $V^{crystal}$ applied to the KDP crystal for a specific angle α of the incident light's polarization plane relative to the x-axis of the crystal. From these results and the known values tabulated in Tables 8.1 and 8.2 and in eqn. (8.13), the right-hand side of eqn. (8.14) (the same as the right-hand side of eqn. (8.15)) was evaluated and entered with the results as G^{eff}, the effective quadratic electro-optic-electrostrictive contribution for that polarization angle. The relevant results for each set of determinations are tabulated in Table 8.4. Also included in this table, and similar tables for other investigations, are the values for the electric field strength for each set of null determinations. This latter value is included soley to give an idea of the magnitude of the applied field in each instance. The averages of the results for G^{eff} for the different polarization states are presented in Table 8.5. It should be noted that the field-induced optical path-length variation in KDP for light polarized at $|80°|$ relative to the crystal's x-axis was too small to be established, while that for $|90°|$ was opposite in sign to those determined for the other angles. This indicates that the quadratic electro-optic and electrostrictive response of KDP in an air environment and for z-propagation, passes through zero for the incident light linearly polarized at an angle in the vicinity of $|80°|$ relative to the x-axis.

From Table 8.5, Graphs 8.2 and 8.3 of G^{eff} versus $\sin^2\alpha$ and G^{eff} versus $\cos^2\alpha$, respectively, were plotted, and from the least-squares gradient and intercept of these graphs, the theoretical linearity of which is evident from eqns. (8.14) and (8.15), the following results were obtained:

$$g_{yyxx} - g_{xxxx} + n_e^2 r_{xy}^2 = (3.22 \pm 0.03) \times 10^{-20}\,m^2V^{-2}, \quad (8.16)$$

$$g_{xxxx} - 2(n_o - n_{air})n_o^{-3}\gamma_{xxzz} = -(3.13 \pm 0.02) \times 10^{-20}\,m^2V^{-2}, \quad (8.17)$$

$$g_{yyxx} + n_e^2 r_{xy}^2 - 2(n_o - n_{air})n_o^{-3}\gamma_{xxzz} = (0.09 \pm 0.02) \times 10^{-20}\,m^2V^{-2}. \quad (8.19)$$

In the determination of the results for the intercept and gradient of Graphs 8.2 and 8.3 by a least-squares method (Barford 1967), the G^{eff} values known to a greater certainty (i.e. with a smaller standard error) were given more weight in the calculation. This was deemed necessary since, as is evident from Table 8.5, the G^{eff} values for the smaller polarization angles α are known to a

greater relative precision than those for the larger angles. The reason for this was because G^{eff} for these larger angles is considerably smaller in magnitude, and thus more difficult to measure accurately, given the limited precision of the apparatus. Clearly less importance can be placed on these results. The motivation for plotting two separate graphs was to allow the results in eqns. (8.17) and (8.18) to be obtained directly from intercepts of the respective graphs, rather than indirectly through a calculation, involving the value for the gradient, as this would have had implications on the uncertainty quoted for the respective values. As it stands, the maximum uncertainty in the values in eqns. (8.16) to (8.18) is representative of the statistical error in the calculation of the gradient and the intercept of Graphs 8.2 and 8.3.

In quoting the final results for this crystal orientation, the uncertainty in the measured quantities used in the calculation of G^{eff} must also be included. Taking these uncertainties into account, one may express the final results for the combination of quadratic electro-optic and electrostrictive coefficients for this orientation as:

$$g_{yyxx} - g_{xxxx} + n_e^2 r_{xzy}^2 = (3.22 \pm 0.21) \times 10^{-20}\,m^2V^{-2}, \tag{8.19}$$

$$g_{xxxx} - 2(n_o - n_{air})n_o^{-3}\gamma_{xxzz} = -(3.13 \pm 0.20) \times 10^{-20}\,m^2V^{-2}, \tag{8.20}$$

$$g_{yyxx} + n_e^2 r_{xzy}^2 - 2(n_o - n_{air})n_o^{-3}\gamma_{xxzz} = (0.09 \pm 0.02) \times 10^{-20}\,m^2V^{-2}. \tag{8.21}$$

Table 8.4 Results for *z*-propagation through the KDP crystal in air

Polarization angle α	Number of null determinations	$V^{crystal}$ (V)	E (10^5 Vm^{-1})	V^{null} (V)	$G^{eff} \pm \sigma_m$ (10^{-20} m^2V^{-2})
0°	14	3571	7.156	3.847	−3.170 ± 0.014
	17	1794	3.595	0.962	−3.139 ± 0.013
	18	1607	3.220	0.775	−3.152 ± 0.013
	16	1924	3.856	1.107	−3.142 ± 0.007
	14	2093	4.194	1.312	−3.146 ± 0.015
	7	2407	4.824	1.763	−3.198 ± 0.019
	10	2438	4.886	1.824	−3.225 ± 0.020
	18	2341	4.691	1.634	−3.132 ± 0.012
	9	3303	6.619	3.310	−3.188 ± 0.019
10°	13	1992	3.992	1.129	−2.990 ± 0.010
	16	1606	3.218	0.764	−3.111 ± 0.011
	7	2912	5.836	2.476	−3.068 ± 0.020
	17	2008	4.024	1.180	−3.075 ± 0.010
	7	2408	4.826	1.712	−3.103 ± 0.007
	21	2232	4.473	1.467	−3.094 ± 0.010
	11	3209	6.431	3.045	−3.107 ± 0.014
	14	3456	6.926	3.509	−3.087 ± 0.019
−10°	11	1992	3.992	1.152	−3.051 ± 0.008
	13	1606	3.218	0.752	−3.063 ± 0.007
	25	2008	4.024	1.186	−3.091 ± 0.016
	15	2490	4.990	1.838	−3.115 ± 0.018
	26	2249	4.507	1.460	−3.033 ± 0.009
	15	2619	5.248	2.017	−3.089 ± 0.009
	10	3216	6.445	3.023	−3.071 ± 0.021
20°	11	2541	5.092	1.649	−2.684 ± 0.008
	10	2129	4.267	1.186	−2.749 ± 0.009
	24	1577	3.160	0.655	−2.766 ± 0.013
	15	2878	5.768	2.149	−2.727 ± 0.013
	21	2533	5.076	1.713	−2.804 ± 0.028
	26	3264	6.541	2.765	−2.727 ± 0.007
−20°	11	2541	5.092	1.688	−2.747 ± 0.004
	20	1924	3.856	0.963	−2.733 ± 0.012
	22	3050	6.112	2.488	−2.810 ± 0.005
	11	3559	7.132	3.296	−2.734 ± 0.009
	11	2765	5.541	1.991	−2.736 ± 0.008
	14	2372	4.754	1.469	−2.743 ± 0.005
	28	2248	4.505	1.332	−2.769 ± 0.011

continued

continued from previous page

Polarization angle α	Number of null determinations	$V^{crystal}$ (V)	E (10^5 Vm^{-1})	V^{null} (V)	$G^{eff} \pm \sigma_m$ (10^{-20} m^2V^{-2})
30°	16	1924	3.856	0.821	-2.330 ± 0.007
	13	2582	5.174	1.445	-2.278 ± 0.016
	14	3217	6.447	2.188	-2.221 ± 0.004
	4	2407	4.824	1.257	-2.280 ± 0.004
	24	2256	4.521	1.104	-2.279 ± 0.015
	9	3119	6.251	2.179	-2.354 ± 0.005
	10	2879	5.770	1.778	-2.253 ± 0.008
	17	2181	4.371	1.054	-2.328 ± 0.011
-30°	25	2541	5.092	1.377	-2.240 ± 0.005
	20	1924	3.856	0.797	-2.263 ± 0.006
	16	2584	5.178	1.500	-2.360 ± 0.025
	11	3218	6.449	2.300	-2.333 ± 0.011
	16	2221	4.451	1.068	-2.275 ± 0.006
	7	2728	5.467	1.631	-2.303 ± 0.004
40°	17	1793	3.593	0.516	-1.686 ± 0.009
	16	3507	7.028	1.953	-1.669 ± 0.006
	14	3192	6.397	1.632	-1.683 ± 0.005
	9	2863	5.737	1.293	-1.657 ± 0.014
	20	2499	5.008	1.002	-1.686 ± 0.010
	11	2583	5.176	1.126	-1.773 ± 0.004
	9	3315	6.643	1.815	-1.735 ± 0.007
-40°	13	1793	3.593	0.512	-1.673 ± 0.006
	12	3217	6.447	1.738	-1.764 ± 0.011
	27	2425	4.860	0.968	-1.729 ± 0.007
	9	2891	5.794	1.404	-1.765 ± 0.008
	22	2334	4.677	0.880	-1.697 ± 0.008
	9	3537	7.088	2.082	-1.749 ± 0.009
50°	13	2869	5.749	0.876	-1.118 ± 0.005
	15	2922	5.856	0.907	-1.116 ± 0.014
	5	2405	4.820	0.672	-1.220 ± 0.009
	19	2203	4.415	0.527	-1.141 ± 0.009
	12	2562	5.134	0.730	-1.168 ± 0.017
	27	2385	4.780	0.639	-1.180 ± 0.014
	17	3300	6.613	1.177	-1.136 ± 0.011
-50°	13	2922	5.856	0.953	-1.172 ± 0.007
	28	1844	3.695	0.347	-1.073 ± 0.011

continued

continued from previous page

Polarization angle α	Number of null determinations	$V^{crystal}$ (V)	E (10^5 Vm^{-1})	V^{null} (V)	$G^{eff} \pm \sigma_m$ (10^{-20} m^2V^{-2})
-50°	14	3312	6.637	1.234	-1.182 ± 0.005
	8	2414	4.838	0.635	-1.145 ± 0.004
	32	2375	4.760	0.629	-1.172 ± 0.008
	12	2682	5.375	0.794	-1.160 ± 0.005
	11	2539	5.088	0.706	-1.151 ± 0.002
60°	8	2689	5.389	0.443	-0.644 ± 0.005
	13	1992	3.992	0.255	-0.674 ± 0.011
	16	3662	7.339	0.803	-0.629 ± 0.011
	23	2562	5.134	0.427	-0.683 ± 0.023
	32	2386	4.782	0.381	-0.703 ± 0.009
	7	3316	6.645	0.704	-0.672 ± 0.015
-60°	12	2602	5.214	0.404	-0.627 ± 0.011
	5	1852	3.711	0.206	-0.631 ± 0.008
	12	3445	6.904	0.740	-0.655 ± 0.008
	9	3507	7.028	0.821	-0.702 ± 0.008
	21	2203	4.415	0.307	-0.664 ± 0.004
	17	2376	4.762	0.373	-0.694 ± 0.006
	21	2891	5.794	0.533	-0.670 ± 0.003
70°	8	3702	7.419	0.412	-0.316 ± 0.004
	14	3377	6.768	0.335	-0.309 ± 0.004
	4	2407	4.824	0.195	-0.353 ± 0.043
	14	3011	6.034	0.240	-0.278 ± 0.008
	10	2932	5.876	0.253	-0.309 ± 0.006
	9	2888	5.788	0.245	-0.309 ± 0.006
	17	3644	7.303	0.397	-0.314 ± 0.005
-70°	12	3724	7.463	0.443	-0.336 ± 0.006
	16	3176	6.365	0.313	-0.326 ± 0.009
	21	3378	6.770	0.315	-0.290 ± 0.016
	14	2721	5.453	0.217	-0.308 ± 0.002
	22	2454	4.918	0.179	-0.312 ± 0.006
	17	3168	6.349	0.296	-0.310 ± 0.004
	11	2755	5.521	0.224	-0.310 ± 0.007
90°	16	3931	7.878	0.083	0.057 ± 0.004
	13	3886	7.788	0.234	0.163 ± 0.013
	17	4020	8.056	0.301	0.196 ± 0.010
	12	3585	7.184	0.109	0.089 ± 0.005

continued

continued from previous page					
Polarization angle α	Number of null determinations	$V^{crystal}$ (V)	E (10^5 Vm^{-1})	V^{null} (V)	$G^{eff} \pm \sigma_m$ (10^{-20} m^2V^{-2})
90°	11	4313	8.643	0.141	0.080 ± 0.004
-90°	11	4014	8.044	0.103	0.067 ± 0.005
	8	3893	7.802	0.095	0.066 ± 0.004
	11	4173	8.363	0.164	0.099 ± 0.002
	14	4049	8.114	0.135	0.087 ± 0.001

Table 8.5 Summary of results contained in Table 8.4 for the various polarization angles of incident light for *z*-propagation through the KDP crystal in air

Polarization angle α	$\cos^2\alpha$	$\sin^2\alpha$	$G^{eff} \pm \sigma_m$ (10^{-20} m^2V^{-2})
0°	1.000	0.000	-3.166 ± 0.011
10°	0.970	0.030	-3.079 ± 0.014
-10°	0.970	0.030	-3.073 ± 0.010
20°	0.883	0.117	-2.743 ± 0.017
-20°	0.883	0.117	-2.753 ± 0.011
30°	0.750	0.250	-2.291 ± 0.016
-30°	0.750	0.250	-2.296 ± 0.018
40°	0.587	0.413	-1.698 ± 0.015
-40°	0.587	0.413	-1.729 ± 0.015
50°	0.413	0.587	-1.154 ± 0.014
-50°	0.413	0.587	-1.151 ± 0.014
60°	0.250	0.750	-0.668 ± 0.011
-60°	0.250	0.750	-0.663 ± 0.011
70°	0.117	0.883	-0.313 ± 0.008
-70°	0.117	0.883	-0.313 ± 0.005
90°	0.000	1.000	0.117 ± 0.024
-90°	0.000	1.000	0.080 ± 0.008

Graph 8.2 Plot of G^{eff} versus $\sin^2\alpha$ for z -propagation through KDP in air

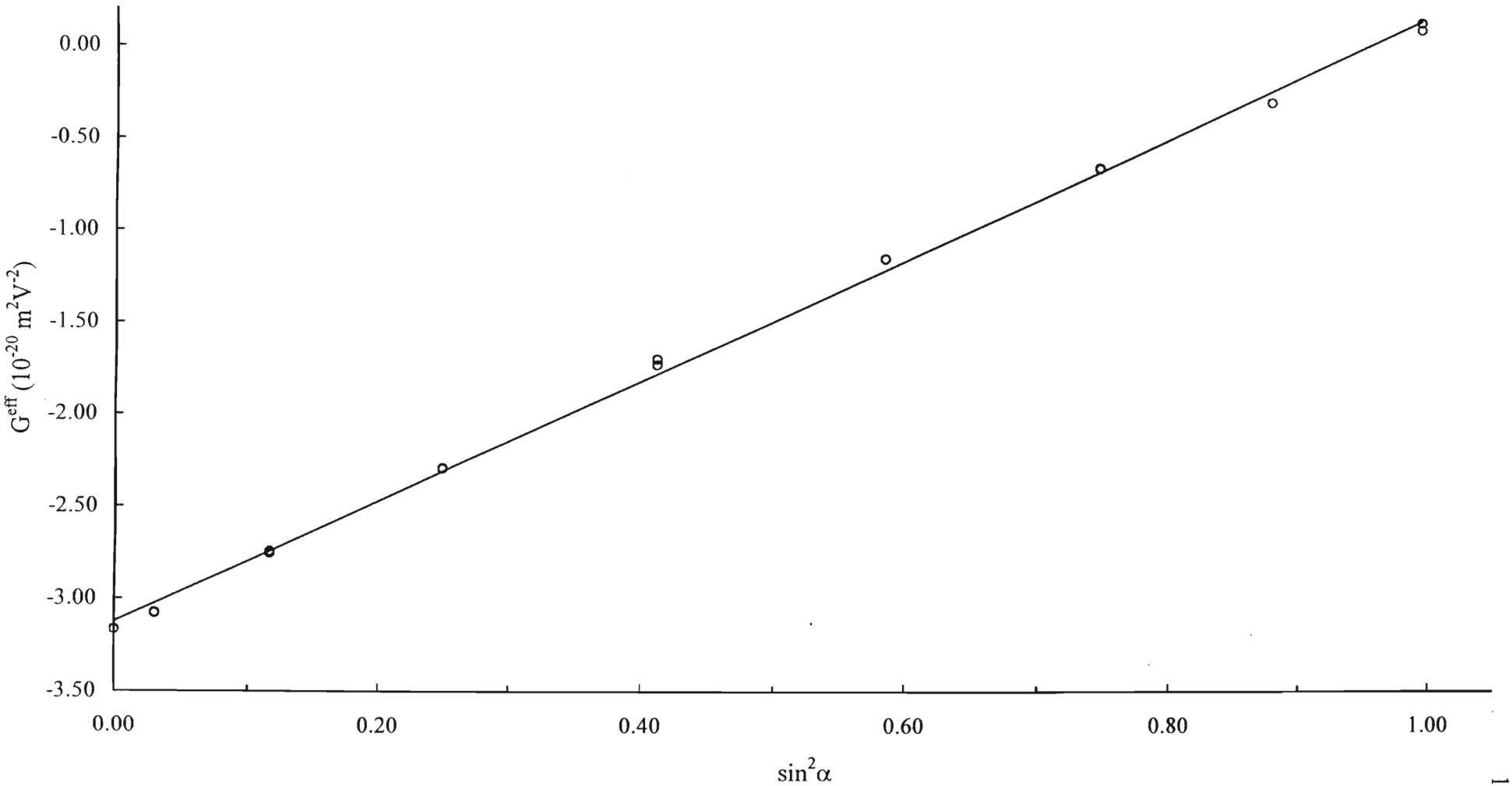

Graph 8.3 Plot of G^{eff} versus $\cos^2\alpha$ for z -propagation through KDP in air

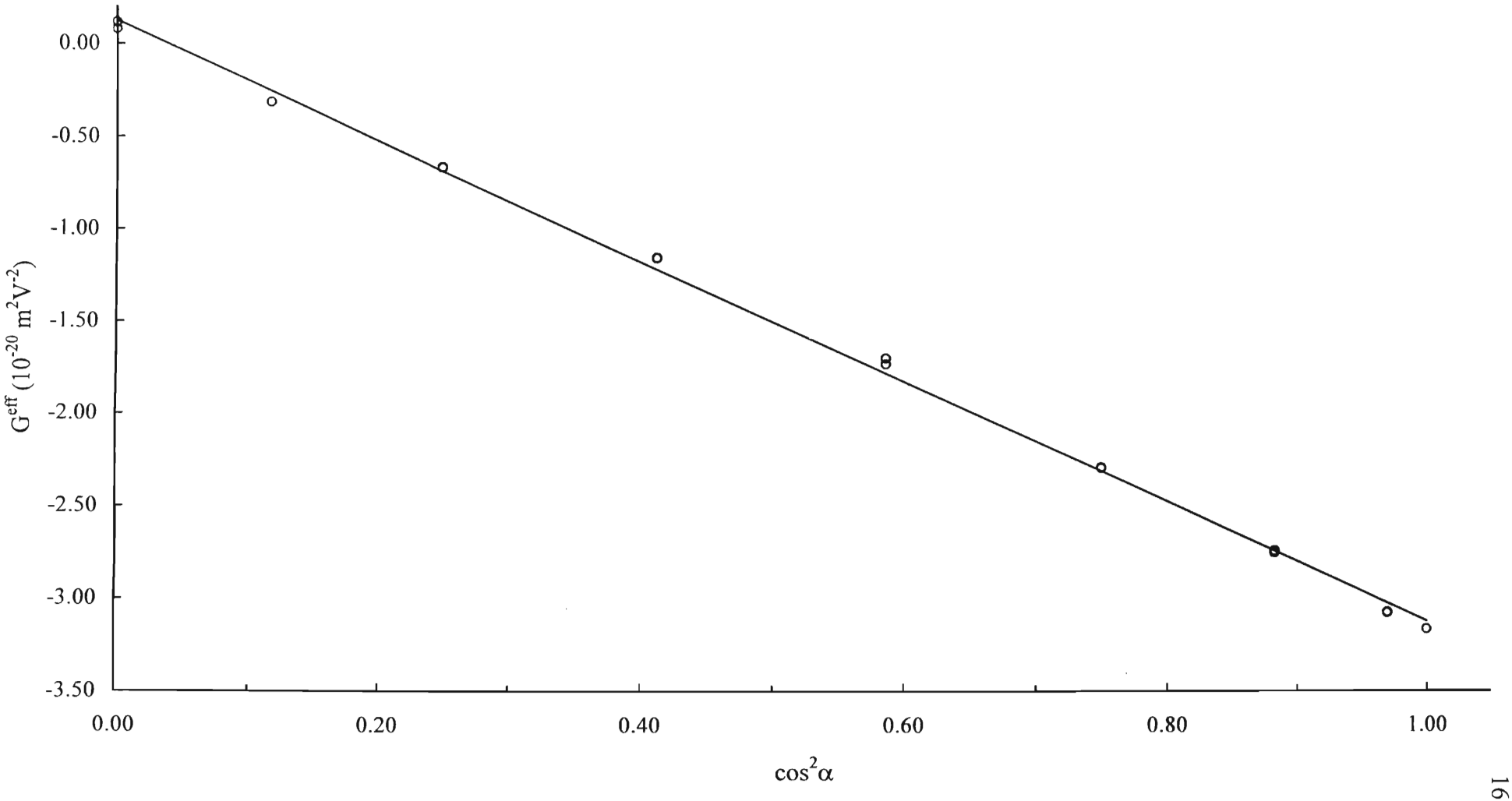

8.4.2 Results for *y*-propagation through the KDP crystal in air

Measurements for this configuration were obtained for the incident light polarized in turn at 0° and |90°| relative to the crystallographic *x*-axis. Values for these two angles of V^{null}, $V^{crystal}$, and consequently of the induced quadratic electro-optic-electrostrictive contribution, G^{eff}, given by the right-hand side of eqns. (8.9) and (8.10), are tabulated in Tables 8.6 and 8.7 respectively. On taking the uncertainty in the measured quantities into account, as well as the statistical spread in the null determinations, one may calculate from these values:

$$g_{xxxx} - 2(n_o - n_{air})n_o^{-3}\gamma_{xxyy} = -(3.87 \pm 0.23) \times 10^{-20}\,m^2V^{-2}, \qquad (8.22)$$

$$g_{zzxx} + n_o^2 r_{xzy}^2 - 2(n_e - n_{air})n_e^{-3}\gamma_{xxyy} = -(1.16 \pm 0.08) \times 10^{-20}\,m^2V^{-2}. \qquad (8.23)$$

Table 8.6 Results for *y*-propagation through the KDP crystal in air and the incident light polarized at 0° relative to the crystallographic *x*-axis

Number of null determinations	$V^{crystal}$ (V)	E (10^5 Vm^{-1})	V^{null} (V)	$G^{eff} \pm \sigma_m$ (10^{-20} m^2V^{-2})
19	2820	5.651	2.963	−3.893 ± 0.010
16	2105	4.218	1.642	−3.873 ± 0.003
10	2595	5.200	2.488	−3.860 ± 0.004
15	2059	4.126	1.565	−3.857 ± 0.011
12	1855	3.717	1.270	−3.856 ± 0.006
17	2166	4.341	1.745	−3.886 ± 0.007
12	1825	3.657	1.240	−3.890 ± 0.004
20	2024	4.056	1.513	−3.860 ± 0.007
13	1732	3.471	1.103	−3.841 ± 0.002
12	1803	3.613	1.202	−3.863 ± 0.020
14	2173	4.355	1.739	−3.848 ± 0.016
			mean	−3.866 ± 0.005

Table 8.7 Results for *y*-propagation through the KDP crystal in air and the incident light polarized at |90°| relative to the crystallographic *x*-axis

Number of null determinations	$V^{crystal}$ (V)	E (10^5 Vm^{-1})	V^{null} (V)	$G^{eff} \pm \sigma_m$ (10^{-20} m^2V^{-2})
12	2801	5.613	0.8173	−1.181 ± 0.018
11	2735	5.481	0.7550	−1.144 ± 0.004
7	2956	5.924	0.9068	−1.177 ± 0.010
8	3220	6.453	1.0656	−1.165 ± 0.014
18	2053	4.114	0.4082	−1.098 ± 0.013
16	2844	5.699	0.8099	−1.135 ± 0.013
11	2679	5.369	0.7376	−1.165 ± 0.024
17	2542	5.094	0.6820	−1.197 ± 0.016
12	2434	4.878	0.6202	−1.187 ± 0.008
17	2805	5.621	0.7865	−1.133 ± 0.011
17	2566	5.142	0.6773	−1.166 ± 0.017
			mean	−1.159 ± 0.009

8.4.3 Results for *z*-propagation through the KDP crystal in silicon oil

In this instance results for V^{null}, $V^{crystal}$, and thus G^{eff}, calculated from the right-hand side of eqn. (8.11), were determined for the incident light beam linearly polarized parallel to the crystallographic *x*-axis only. These results are shown in Table 8.8 and, when uncertainties in the relevant quantities entering eqn. (8.11) are accounted for, lead to:

$$g_{xxxx} - 2(n_o - n_{oil})n_o^{-3}\gamma_{xxzz} = -(3.46 \pm 0.22) \times 10^{-20}\,m^2\,V^{-2}. \qquad (8.24)$$

Table 8.8 Results for *z*-propagation through the KDP crystal in silicon oil and the incident light polarized at 0° relative to the crystallographic *x*-axis

Number of null determinations	$V^{crystal}$ (V)	E (10^5 Vm^{-1})	V^{null} (V)	$G^{eff} \pm \sigma_m$ (10^{-20} m^2V^{-2})
11	2677	5.365	2.362	−3.463 ± 0.004
8	2336	4.681	1.816	−3.497 ± 0.009
9	2452	4.914	2.008	−3.508 ± 0.006
10	2881	5.774	2.676	−3.388 ± 0.034
17	2726	5.463	2.432	−3.439 ± 0.021
10	2349	4.707	1.808	−3.443 ± 0.010
			mean	−3.456 ± 0.018

8.4.4 Results for *y*-propagation through the KDP crystal in silicon oil

Again, as in the previous case, only polarization parallel to the crystallographic *x*-axis was considered, but now for propagation in the *y*-direction. The relevant results obtained are tabulated in Table 8.9, with the value for G^{eff} calculated from the right-hand side of eqn. (8.9). From these results, and the uncertainties in the measured quantities,

$$g_{xxxx} - 2(n_o - n_{oil})n_o^{-3}\gamma_{xxyy} = -(3.40 \pm 0.21) \times 10^{-20}\,m^2V^{-2}. \qquad (8.25)$$

Table 8.9 Results for *y*-propagation through the KDP crystal in silicon oil and the incident light polarized at 0° relative to the crystallographic *x*-axis

Number of null determinations	$V^{crystal}$ (V)	E (10^5 Vm^{-1})	V^{null} (V)	$G^{eff} \pm \sigma_m$ (10^{-20} m^2V^{-2})
18	2458	4.926	1.944	-3.362 ± 0.017
14	2727	5.465	2.429	-3.412 ± 0.005
9	2836	5.683	2.620	-3.404 ± 0.005
5	2419	4.848	1.905	-3.402 ± 0.002
19	2372	4.754	1.846	-3.428 ± 0.012
			mean	-3.402 ± 0.011

8.4.5 Results for *z*-propagation through the larger ADP crytal in air

This investigation was conducted on the larger of the ADP crystals. As for the equivalent investigation on KDP detailed in Subsection 8.4.1, eqns. (8.14) and (8.15) are applicable and graphs of the effective electro-optic-electrostrictive contribution (G^{eff}) versus $\sin^2\alpha$ and $\cos^2\alpha$ may be plotted, from which the necessary results may be established. Data recorded in this instance are tabulated in Table 8.10, and a summary of the results for the various polarization angles is given in Table 8.11 from which Graphs 8.4 and 8.5 were plotted. Again, as in the treatment of KDP, the points on these graphs were weighted in accordance with the uncertainty in G^{eff}, with those known to a greater accuracy carrying more importance in the least-squares calculations of the intercept and gradient. From these graphs, the following results were obtained:

$$g_{yyxx} - g_{xxxx} + n_e^2 r_{xzy}^2 = (5.75 \pm 0.05) \times 10^{-20}\,m^2V^{-2}, \qquad (8.26)$$

$$g_{xxxx} - 2(n_o - n_{air})n_o^{-3}\gamma_{xxzz} = -(7.07 \pm 0.03) \times 10^{-20}\,m^2V^{-2}, \qquad (8.27)$$

$$g_{yyxx} + n_e^2 r_{xzy}^2 - 2(n_o - n_{air})n_o^{-3}\gamma_{xxzz} = -(1.32 \pm 0.03) \times 10^{-20}\,m^2V^{-2}. \qquad (8.28)$$

Table 8.10 Results for *z*-propagation through the larger ADP crystal in air

Polarization angle α	Number of null determinations	$V^{crystal}$ (V)	E (10^5 Vm^{-1})	V^{null} (V)	$G^{eff} \pm \sigma_m$ (10^{-20} m^2V^{-2})
0°	7	2131	4.253	3.203	-7.018 ± 0.006
	30	1833	3.659	2.358	-6.982 ± 0.027
	14	1927	3.846	2.612	-6.999 ± 0.020
	10	2305	4.601	3.905	-7.313 ± 0.029
	19	1779	3.551	2.302	-7.238 ± 0.023
	15	2508	5.006	4.578	-7.241 ± 0.015
	7	3200	6.387	7.539	-7.325 ± 0.024
	32	2386	4.762	4.283	-7.486 ± 0.049
	5	2691	5.371	5.418	-7.444 ± 0.025
	18	2489	4.968	4.529	-7.273 ± 0.063
10°	9	2901	5.790	5.766	-6.816 ± 0.022
	11	1848	3.689	2.308	-6.723 ± 0.013
	4	2644	5.277	4.936	-7.025 ± 0.007
	14	2387	4.764	4.136	-7.222 ± 0.039
	20	2489	4.968	4.446	-7.140 ± 0.082
-10°	20	2320	4.631	3.682	-6.806 ± 0.009
	19	2269	4.529	3.529	-6.819 ± 0.113
	13	1849	3.691	2.329	-6.777 ± 0.016
	22	2491	4.972	4.213	-6.755 ± 0.026
	12	2401	4.792	4.076	-7.035 ± 0.083
	15	2508	5.006	4.448	-7.035 ± 0.007
	11	2387	4.764	4.141	-7.230 ± 0.022
	10	2489	4.968	4.377	-7.029 ± 0.018
20°	13	2406	4.802	3.633	-6.243 ± 0.029
	18	2133	4.257	2.806	-6.136 ± 0.027
	16	2644	5.277	4.508	-6.415 ± 0.009
	10	3200	6.387	6.550	-6.364 ± 0.009
	18	2386	4.762	3.861	-6.747 ± 0.009
	8	2501	4.992	4.148	-6.597 ± 0.008
-20°	19	2245	4.481	3.177	-6.271 ± 0.017
	12	2491	4.972	3.848	-6.170 ± 0.020
	19	2160	4.311	3.054	-6.512 ± 0.006
	14	2752	5.493	4.915	-6.457 ± 0.012
	10	2655	5.299	4.628	-6.532 ± 0.008
	17	3200	6.387	6.586	-6.398 ± 0.032
	18	2387	4.764	3.823	-6.675 ± 0.027

continued

continued from previous page

Polarization angle α	Number of null determinations	$V^{crystal}$ (V)	E (10^5 Vm^{-1})	V^{null} (V)	$G^{eff} \pm \sigma_m$ (10^{-20} m^2V^{-2})
	10	2501	4.992	4.146	-6.595 ± 0.004
30°	12	2797	5.583	4.279	-5.442 ± 0.038
	11	2780	5.549	4.379	-5.637 ± 0.023
	8	2036	4.064	2.239	-5.373 ± 0.013
	12	2644	5.277	3.905	-5.557 ± 0.012
	16	2426	4.842	3.376	-5.707 ± 0.011
	9	2387	4.764	3.377	-5.897 ± 0.007
	13	2489	4.968	3.539	-5.684 ± 0.044
-30°	31	2132	4.255	2.527	-5.531 ± 0.033
	14	2143	4.277	2.577	-5.582 ± 0.014
	9	1825	3.643	1.887	-5.638 ± 0.024
	11	2654	5.297	4.017	-5.653 ± 0.009
	8	2489	4.968	3.517	-5.648 ± 0.015
40°	16	2850	5.689	3.561	-4.361 ± 0.040
	10	2851	5.691	3.623	-4.435 ± 0.021
	27	1747	3.487	1.358	-4.426 ± 0.017
	12	2143	4.277	2.034	-4.407 ± 0.020
	9	2776	5.541	3.455	-4.460 ± 0.020
	11	2644	5.277	3.295	-4.690 ± 0.015
	9	2426	4.842	2.816	-4.760 ± 0.011
	12	2279	4.549	2.457	-4.707 ± 0.007
	12	2244	4.479	2.407	-4.756 ± 0.049
	9	2499	4.988	2.979	-4.745 ± 0.043
-40°	12	2851	5.691	3.639	-4.454 ± 0.029
	9	2851	5.691	3.631	-4.444 ± 0.009
	15	2143	4.277	2.094	-4.537 ± 0.015
	15	2160	4.311	2.157	-4.599 ± 0.022
	12	2244	4.479	2.321	-4.587 ± 0.021
	14	1865	3.723	1.609	-4.603 ± 0.028
	15	3025	6.038	4.372	-4.754 ± 0.012
	7	2387	4.764	2.818	-4.920 ± 0.014
	10	2500	4.990	3.036	-4.834 ± 0.061
50°	27	1926	3.844	1.303	-3.496 ± 0.050
	18	2302	4.595	1.959	-3.678 ± 0.010
	11	2426	4.842	2.178	-3.681 ± 0.021
	19	2401	4.792	2.107	-3.637 ± 0.038

continued

continued from previous page

Polarization angle α	Number of null determinations	$V^{crystal}$ (V)	E (10^5 Vm^{-1})	V^{null} (V)	$G^{eff} \pm \sigma_m$ (10^{-20} m^2V^{-2})
50°	11	2341	4.673	2.111	-3.833 ± 0.013
	15	2500	4.990	2.308	-3.674 ± 0.044
-50°	11	1682	3.357	0.983	-3.457 ± 0.018
	9	2268	4.527	1.761	-3.407 ± 0.046
	9	2940	5.868	2.927	-3.369 ± 0.011
	12	2473	4.936	2.255	-3.668 ± 0.027
	18	2507	5.004	2.225	-3.522 ± 0.010
	14	3200	6.387	3.718	-3.613 ± 0.012
	3	2386	4.762	2.167	-3.786 ± 0.007
	10	2500	4.990	2.359	-3.755 ± 0.052
60°	19	2688	5.365	1.909	-2.629 ± 0.027
	9	2746	5.481	2.184	-2.882 ± 0.011
	14	2341	4.673	1.530	-2.777 ± 0.066
	15	2971	5.930	2.553	-2.877 ± 0.018
	23	3059	6.106	2.654	-2.822 ± 0.022
	5	2386	4.762	1.670	-2.918 ± 0.011
	7	2500	4.990	1.708	-2.718 ± 0.003
-60°	11	2991	5.970	2.244	-2.496 ± 0.018
	10	2473	4.936	1.639	-2.666 ± 0.014
	10	2747	5.483	2.061	-2.718 ± 0.014
	13	2507	5.004	1.716	-2.716 ± 0.018
	20	3059	6.106	2.627	-2.793 ± 0.007
	11	2500	4.990	1.760	-2.801 ± 0.011
	8	3136	4.531	2.078	-2.102 ± 0.029
	8	3164	4.766	2.103	-2.090 ± 0.023
	17	3183	5.162	1.901	-1.867 ± 0.051
70°	27	2270	6.259	1.081	-2.088 ± 0.036
	14	2388	6.315	1.155	-2.015 ± 0.020
	10	2586	6.353	1.320	-1.964 ± 0.023
	5	2386	4.762	1.276	-2.229 ± 0.005
	11	2500	4.990	1.352	-2.152 ± 0.013
-70°	11	2655	5.299	1.395	-1.969 ± 0.006
	11	2397	4.784	1.065	-1.844 ± 0.009
	14	2455	4.900	1.110	-1.832 ± 0.020
	19	2159	4.309	0.912	-1.947 ± 0.017
	11	2728	5.445	1.460	-1.951 ± 0.018

continued

continued from previous page					
Polarization angle α	Number of null determinations	$V^{crystal}$ (V)	E (10^5 Vm^{-1})	V^{null} (V)	$G^{eff} \pm \sigma_m$ (10^{-20} m^2V^{-2})
-70°	16	2511	5.012	1.336	-2.109 ± 0.021
	12	2211	4.413	1.038	-2.112 ± 0.009
	10	2500	4.990	1.344	-2.140 ± 0.008
80°	20	2909	5.806	1.499	-1.762 ± 0.022
	18	2388	4.766	0.868	-1.514 ± 0.027
	28	1825	3.643	0.425	-1.269 ± 0.028
	14	2399	4.788	0.802	-1.387 ± 0.023
	15	3058	6.104	1.338	-1.424 ± 0.024
	7	2500	4.990	1.135	-1.806 ± 0.011
-80°	13	2656	5.301	1.148	-1.618 ± 0.017
	8	2991	5.970	1.384	-1.539 ± 0.016
	10	2159	4.309	0.773	-1.651 ± 0.012
	12	2472	4.934	0.914	-1.487 ± 0.045
	9	3077	6.142	1.164	-1.223 ± 0.018
	3	2386	4.762	1.042	-1.821 ± 0.023
	18	2500	4.990	1.066	-1.697 ± 0.072
90°	10	2644	5.277	1.067	-1.519 ± 0.009
	16	2906	5.800	1.319	-1.554 ± 0.035
	11	2491	4.972	0.761	-1.220 ± 0.013
	11	2564	5.118	0.799	-1.210 ± 0.017
	22	2172	4.335	0.479	-1.010 ± 0.013
	2	2386	6.259	0.948	-1.657 ± 0.001
	6	2501	4.762	1.065	-1.694 ± 0.037
	12	3136	4.992	1.338	-1.354 ± 0.017
-90°	10	2491	4.972	0.741	-1.187 ± 0.019
	18	2115	4.222	0.665	-1.480 ± 0.016
	18	2615	5.220	0.679	-0.989 ± 0.016
	9	2500	4.990	1.092	-1.738 ± 0.055

Table 8.11 Summary of results contained in Table 8.10 for the various polarization angles of incident light for *z*-propagation through the larger ADP crystal in air

Polarization angle α	$\cos^2(\alpha)$	$\sin^2(\alpha)$	$G^{eff} \pm \sigma_m$ (10^{-20} m^2V^{-2})
0°	1.000	0.000	-7.232 ± 0.057
10°	0.970	0.030	-6.985 ± 0.095
-10°	0.970	0.030	-6.936 ± 0.060
20°	0.883	0.117	-6.417 ± 0.092
-20°	0.883	0.117	-6.451 ± 0.059
30°	0.750	0.250	-5.614 ± 0.066
-30°	0.750	0.250	-5.610 ± 0.021
40°	0.587	0.413	-4.575 ± 0.053
-40°	0.587	0.413	-4.637 ± 0.055
50°	0.413	0.587	-3.666 ± 0.044
-50°	0.413	0.587	-3.572 ± 0.056
60°	0.250	0.750	-2.803 ± 0.039
-60°	0.250	0.750	-2.698 ± 0.046
70°	0.117	0.883	-2.063 ± 0.040
-70°	0.117	0.883	-1.988 ± 0.043
80°	0.030	0.970	-1.527 ± 0.088
-80°	0.030	0.970	-1.577 ± 0.071
90°	0.000	1.000	-1.402 ± 0.086
-90°	0.000	1.000	-1.348 ± 0.164

The final results for this crystal, with due allowance for the uncertainties in the measured quantities, are:

$$g_{yyxx} - g_{xxxx} + n_e^2 r_{xy}^2 = (5.75 \pm 0.40) \times 10^{-20}\,m^2V^{-2}, \tag{8.29}$$

$$g_{xxxx} - 2(n_o - n_{air})n_o^{-3}\gamma_{xxzz} = -(7.07 \pm 0.46) \times 10^{-20}\,m^2V^{-2}, \tag{8.30}$$

$$g_{yyxx} + n_e^2 r_{xy}^2 - 2(n_o - n_{air})n_o^{-3}\gamma_{xxzz} = -(1.32 \pm 0.11) \times 10^{-20}\,m^2V^{-2}. \tag{8.31}$$

Graph 8.4 Plot of G^{eff} versus $\sin^2\alpha$ for *z* -propagation through the larger ADP in air

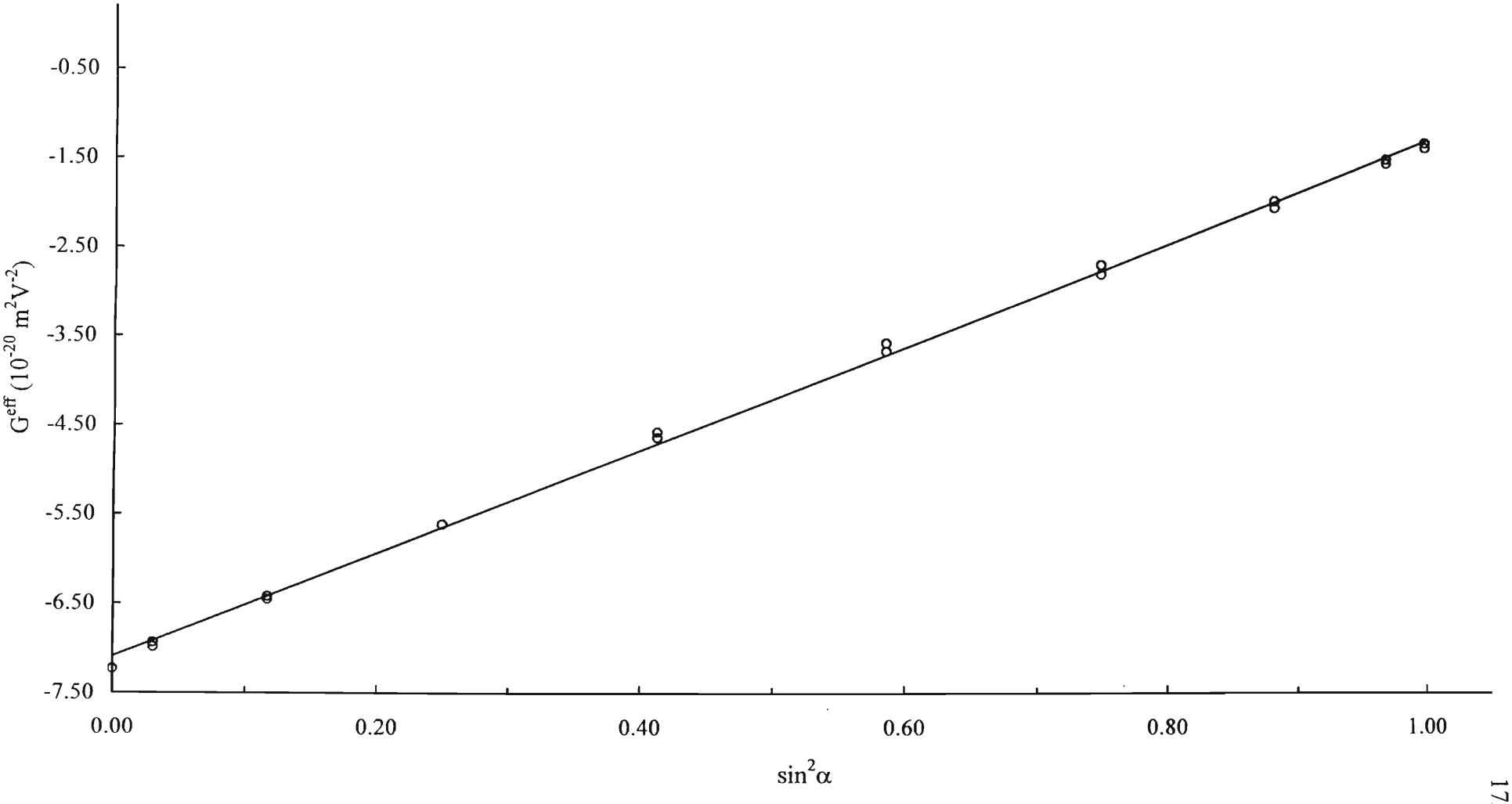

Graph 8.5 Plot of G^{eff} versus $\cos^2\alpha$ for *z* -propagation through the larger ADP in air

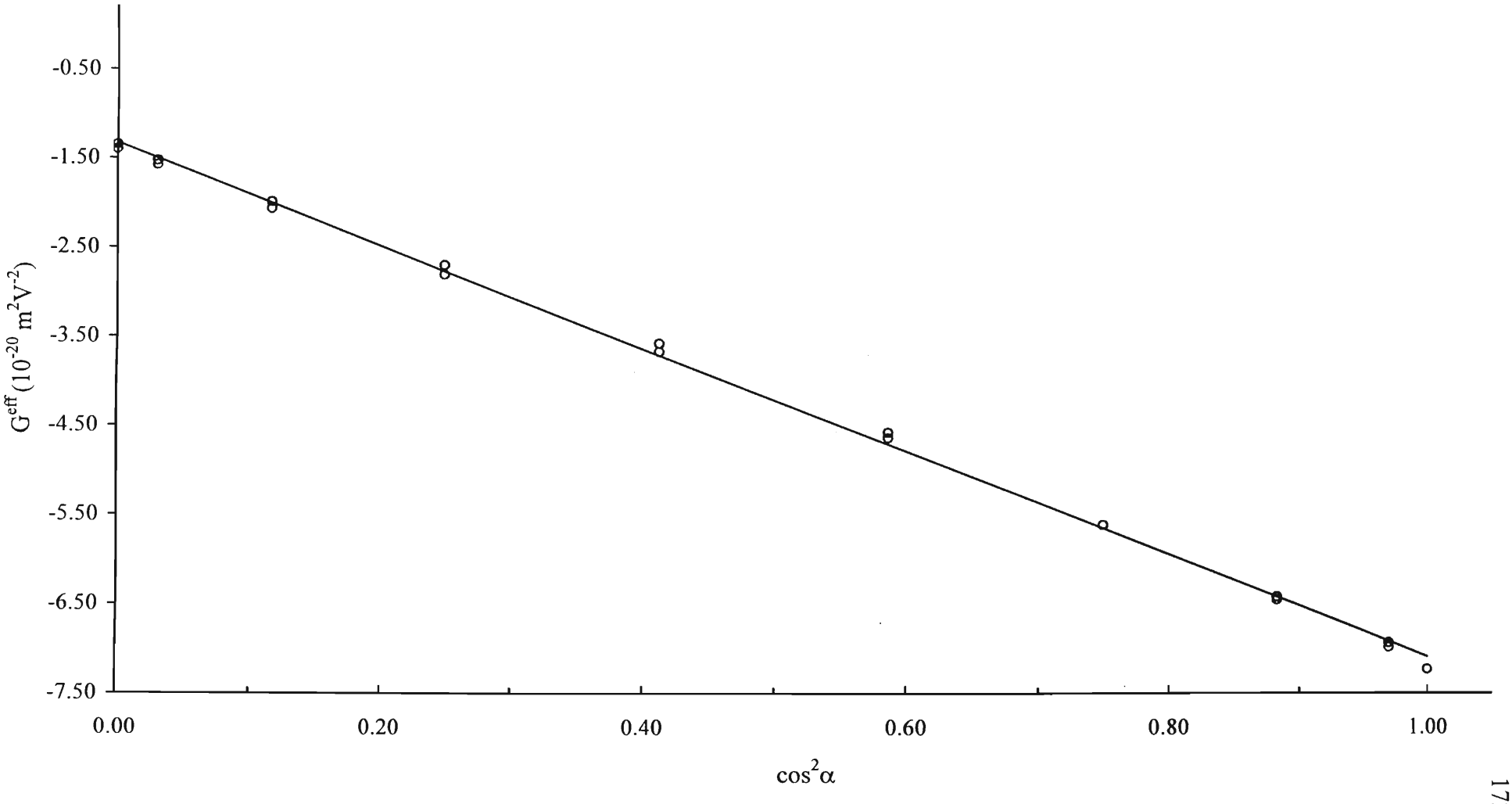

8.4.6 Results for *y*-propagation through the larger ADP crystal in air

For this propagation path similar measurements were made to those for KDP, as described in Subsection 8.4.2. Results for the incident light polarized in turn along the crystallographic *x*- and *z*-axes are tabulated in Tables 8.12 and 8.13, with the final determinations from these values, and including uncertainties in the measured quantities, giving

$$g_{xxxx} - 2(n_o - n_{air})n_o^{-3}\gamma_{xxyy} = -(6.90 \pm 0.44) \times 10^{-20}\,m^2V^{-2}, \tag{8.32}$$

$$g_{zzxx} + n_o^2 r_{xzy}^2 - 2(n_e - n_{air})n_e^{-3}\gamma_{xxyy} = -(0.74 \pm 0.08) \times 10^{-20}\,m^2V^{-2}. \tag{8.33}$$

Table 8.12 Results for *y*-propagation through the larger ADP crystal in air and the incident light polarized at 0° relative to the crystallographic *x*-axis

Number of null determinations	$V^{crystal}$ (V)	E (10^5 Vm^{-1})	V^{null} (V)	$G^{eff} \pm \sigma_m$ (10^{-20} m^2V^{-2})
12	2518	5.026	4.311	-6.905 ± 0.045
15	1943	3.878	2.574	-6.925 ± 0.020
13	2688	5.365	4.881	-6.861 ± 0.036
17	2467	4.924	4.164	-6.948 ± 0.018
16	2347	4.685	3.769	-6.948 ± 0.010
18	2767	5.523	5.154	-6.837 ± 0.031
14	2677	5.343	4.812	-6.819 ± 0.010
19	2379	4.749	3.853	-6.913 ± 0.024
18	2096	4.184	2.979	-6.887 ± 0.040
13	2262	4.515	3.484	-6.915 ± 0.023
			mean	-6.896 ± 0.014

Table 8.13 Results for *y*-propagation through the larger ADP crystal in air and the incident light polarized at |90°| relative to the crystallographic *x*-axis

Number of null determinationss	$V^{crystal}$ (V)	E (10^5 Vm^{-1})	V^{null} (V)	$G^{eff} \pm \sigma_m$ (10^{-20} m^2V^{-2})
15	2944	5.876	0.608	-0.780 ± 0.005
31	2945	5.878	0.614	-0.786 ± 0.008
16	2864	5.717	0.572	-0.775 ± 0.103
7	2971	5.930	0.486	-0.611 ± 0.066
14	3053	6.094	0.617	-0.735 ± 0.022
			mean	-0.738 ± 0.033

8.4.7 Results for *z*-propagation through the smaller ADP crystal in air

The ADP investigations now concentrated on the smaller of the two ADP crystals. The first investigation on this specimen involved propagation along the optic axis with the light polarized in turn parallel to the crystallographic *x*- and *y*-axes. In each instance, V^{null}, $V^{crystal}$, and hence G^{eff} from eqn. (8.11), were determined and tabulated in Tables 8.14 and 8.15. According to these results, and including all uncertainties:

$$g_{xxxx} - 2(n_o - n_{air})n_o^{-3}\gamma_{xxzz} = -(7.26 \pm 0.45) \times 10^{-20}\,m^2V^{-2}, \tag{8.34}$$

$$g_{yyxx} + n_e^2 r_{xzy}^2 - 2(n_o - n_{air})n_o^{-3}\gamma_{xxzz} = -(1.59 \pm 0.11) \times 10^{-20}\,m^2V^{-2}. \tag{8.35}$$

From these expressions, one may calculate that

$$g_{yyxx} - g_{xxxx} + n_e^2 r_{xzy}^2 = (5.67 \pm 0.56) \times 10^{-20}\ m^2V^{-2}. \tag{8.36}$$

Table 8.14 Results for *z*-propagation through the smaller ADP crystal in air and the incident light polarized at 0° relative to the crystallographic *x*-axis

Number of null determinations	$V^{crystal}$ (V)	E (10^5 Vm^{-1})	V^{null} (V)	$G^{eff} \pm \sigma_m$ (10^{-20} m^2V^{-2})
14	1604	2.272	0.645	-7.157 ± 0.081
13	1915	2.712	0.920	-7.167 ± 0.032
14	1728	2.448	0.761	-7.282 ± 0.037
8	2249	3.186	1.289	-7.278 ± 0.041
8	1575	2.231	0.629	-7.237 ± 0.022
11	1263	1.789	0.402	-7.192 ± 0.067
16	2056	2.912	1.066	-7.201 ± 0.028
10	1813	2.568	0.827	-7.186 ± 0.009
15	1778	2.518	0.797	-7.202 ± 0.024
14	1825	2.585	0.836	-7.168 ± 0.016
15	1930	2.734	0.938	-7.192 ± 0.024
14	1779	2.520	0.794	-7.166 ± 0.025
17	1715	2.429	0.746	-7.241 ± 0.022
12	1467	2.078	0.546	-7.246 ± 0.021
9	2935	4.157	2.250	-7.459 ± 0.031
7	2128	3.014	1.193	-7.526 ± 0.015
10	2207	3.126	1.258	-7.375 ± 0.037
12	1951	2.763	0.993	-7.450 ± 0.029
			mean	-7.262 ± 0.026

Table 8.15 Results for z-propagation through the smaller ADP crystal in air and the incident light polarized at |90°| relative to the crystallographic x-axis

Number of null determinations	$V^{crystal}$ (V)	E (10^5 Vm^{-1})	V^{null} (V)	$G^{eff} \pm \sigma_m$ (10^{-20} m^2V^{-2})
10	1865	2.642	0.205	-1.686 ± 0.043
14	2397	3.395	0.312	-1.552 ± 0.024
11	1931	2.735	0.218	-1.673 ± 0.017
13	2466	3.493	0.353	-1.659 ± 0.008
19	2576	3.649	0.385	-1.656 ± 0.012
11	2729	3.865	0.442	-1.694 ± 0.016
15	2339	3.313	0.284	-1.485 ± 0.035
8	2659	3.766	0.395	-1.597 ± 0.012
12	2518	3.567	0.355	-1.598 ± 0.016
8	2573	3.644	0.365	-1.574 ± 0.011
12	2622	3.714	0.368	-1.530 ± 0.021
7	2307	3.268	0.286	-1.535 ± 0.008
9	2927	4.146	0.457	-1.523 ± 0.014
12	2843	4.027	0.422	-1.491 ± 0.011
17	2835	4.016	0.445	-1.582 ± 0.020
9	2736	3.875	0.407	-1.551 ± 0.021
8	2799	3.965	0.454	-1.654 ± 0.014
16	2652	3.756	0.409	-1.660 ± 0.019
			mean	-1.594 ± 0.016

8.4.8 Results for y-propagation through the smaller ADP crystal in air

This investigation was identical to that described in Subsection 8.4.6, but on this occasion the smaller of the ADP crystals was investigated. The light propagation direction was along the crystallographic y-axis and only polarization states parallel to the crystallographic x- and z-axes were used. The results obtained appear in Tables 8.16 and 8.17. From these, and knowledge of the individual uncertainties, were calculated values equivalent to those in eqns. (8.32) and (8.33) for the larger ADP, namely:

$$g_{xxxx} - 2(n_o - n_{air})n_o^{-3}\gamma_{xxyy} = -(6.72 \pm 0.43) \times 10^{-20}\,m^2V^{-2}, \tag{8.37}$$

$$g_{zzxx} + n_o^2 r_{xzy}^2 - 2(n_e - n_{air})n_e^{-3}\gamma_{xxyy} = -(0.75 \pm 0.06) \times 10^{-20}\,m^2V^{-2}. \tag{8.38}$$

Table 8.16 Results for *y*-propagation through the smaller ADP crystal in air and the incident light polarized at 0° relative to the crystallographic *x*-axis

Number of null determinations	$V^{crystal}$ (V)	E (10^5 Vm^{-1})	V^{null} (V)	$G^{eff} \pm \sigma_m$ (10^{-20} m^2V^{-2})
12	1929	2.732	0.831	-6.559 ± 0.028
14	1935	2.741	0.857	-6.717 ± 0.025
20	2021	2.863	0.954	-6.856 ± 0.015
15	2248	3.184	1.170	-6.795 ± 0.018
15	1919	2.718	0.853	-6.798 ± 0.026
11	1472	2.085	0.500	-6.769 ± 0.020
6	2362	3.346	1.222	-6.431 ± 0.010
13	2518	3.567	1.413	-6.544 ± 0.036
9	2056	2.912	0.948	-6.585 ± 0.024
15	2442	3.459	1.376	-6.771 ± 0.004
12	2300	3.258	1.210	-6.715 ± 0.040
11	1965	2.783	0.885	-6.727 ± 0.286
12	2164	3.065	1.058	-6.631 ± 0.021
17	2373	3.361	1.315	-6.852 ± 0.032
19	1550	2.195	0.560	-6.846 ± 0.040
14	2088	2.958	1.029	-6.926 ± 0.035
			mean	-6.720 ± 0.034

Table 8.17 Results for *y*-propagation through the smaller ADP crystal in air and the incident light polarized at |90°| relative to the crystallographic *x*-axis

Number of null determinations	$V^{crystal}$ (V)	E (10^5 Vm^{-1})	V^{null} (V)	$G^{eff} \pm \sigma_m$ (10^{-20} m^2V^{-2})
15	2614	3.703	0.155	−0.729 ± 0.031
15	2679	3.795	0.168	−0.751 ± 0.037
14	2771	3.925	0.196	−0.820 ± 0.014
10	2946	4.173	0.229	−0.847 ± 0.023
9	2452	3.473	0.142	−0.760 ± 0.030
12	2453	3.475	0.142	−0.756 ± 0.017
10	2607	3.693	0.123	−0.582 ± 0.018
13	2543	3.602	0.142	−0.704 ± 0.014
16	2930	4.150	0.198	−0.742 ± 0.015
12	2390	3.385	0.132	−0.740 ± 0.013
13	2810	3.980	0.186	−0.755 ± 0.019
11	2925	4.143	0.201	−0.753 ± 0.035
11	2720	3.853	0.171	−0.744 ± 0.020
8	2681	3.797	0.176	−0.785 ± 0.017
3	2827	4.004	0.191	−0.765 ± 0.016
5	2995	4.242	0.213	−0.763 ± 0.023
16	2906	4.116	0.196	−0.745 ± 0.022
8	2606	3.691	0.149	−0.706 ± 0.013
10	2322	3.289	0.121	−0.721 ± 0.012
			mean	−0.746 ± 0.012

8.4.9 Results for *z*-propagation through the smaller ADP crystal in silicon oil

This subsection and the next describe the only two investigations carried out in this work of ADP in an oil environment. The purpose of these was to allow certain deductions to be made regarding the magnitude of the electrostrictive coefficients that influence the results. Use of the smaller ADP crystal for these readings was on account of the unavailability of the larger specimen at that stage of the experiment. The investigation described here for the smaller ADP in silicon oil is equivalent to that outlined in Subsection 8.4.3, and the results obtained are tabulated in Table 8.18. From these, and including all uncertainties, is obtained:

$$g_{xxxx} - 2(n_o - n_{oil})n_o^{-3}\gamma_{xxzz} = -(7.48 \pm 0.54) \times 10^{-20}\ m^2V^{-2}. \qquad (8.39)$$

Table 8.18 Results for *z*-propagation through the smaller ADP crystal in silicon oil and the incident light polarized at 0° relative to the crystallographic *x*-axis

Number of null determinations	$V^{crystal}$ (V)	E (10^5 Vm^{-1})	V^{null} (V)	$G^{eff} \pm \sigma_m$ (10^{-20} m^2V^{-2})
11	2123	3.007	1.202	-7.614 ± 0.040
9	2402	3.402	1.558	-7.711 ± 0.022
11	2337	3.310	1.484	-7.760 ± 0.017
12	1268	1.796	0.424	-7.531 ± 0.037
9	1450	2.054	0.559	-7.595 ± 0.036
5	2500	3.541	1.656	-7.570 ± 0.010
10	2202	3.119	1.298	-7.645 ± 0.021
7	1294	1.833	0.471	-8.030 ± 0.046
14	1648	2.334	0.738	-7.758 ± 0.018
6	1993	2.823	1.063	-7.644 ± 0.016
12	2083	2.950	1.180	-7.764 ± 0.015
4	2367	3.353	1.524	-7.769 ± 0.085
25	2123	3.007	1.207	-7.650 ± 0.043
11	1946	2.756	1.031	-7.777 ± 0.020
11	2527	3.579	1.704	-7.623 ± 0.021
7	2477	3.508	1.612	-7.506 ± 0.012
6	1683	2.384	0.757	-7.638 ± 0.025
19	2124	3.008	1.078	-6.824 ± 0.036
7	2272	3.218	1.161	-6.424 ± 0.044
8	2363	3.347	1.282	-6.560 ± 0.018
4	1917	2.715	0.865	-6.721 ± 0.114
11	1985	2.812	1.022	-7.410 ± 0.200
			mean	-7.478 ± 0.092

8.4.10 Results for *y*-propagation through the smaller ADP crystal in silicon oil

Again, this is an equivalent investigation to one on KDP, in this instance that mentioned in Subsection 8.4.4. Shown in Table 8.19 are the values of V^{null}, $V^{crystal}$, and G^{eff} for this crystal and propagation path for a linear polarization parallel to the crystallographic *x*-axis. From eqn. (8.9) these results, together with the known uncertainties, yield:

$$g_{xxxx} - 2(n_o - n_{oil})n_o^{-3}\gamma_{xxyy} = -(7.45 \pm 0.52) \times 10^{-20}\ m^2V^{-2}. \qquad (8.40)$$

Table 8.19 Results for *y*-propagation through the smaller ADP crystal in silicon oil and the incident light polarized at 0° relative to the crystallographic *x*-axis

Number of null determinations	$V^{crystal}$ (V)	E (10^5 Vm^{-1})	V^{null} (V)	$G^{eff} \pm \sigma_m$ (10^{-20} m^2V^{-2})
13	2273	3.220	1.344	-7.637 ± 0.018
8	2077	2.942	1.128	-7.678 ± 0.038
17	2337	3.310	1.461	-7.852 ± 0.012
8	2229	3.157	1.318	-7.784 ± 0.014
16	2424	3.433	1.581	-7.900 ± 0.025
9	2333	3.305	1.438	-7.757 ± 0.022
10	1968	2.788	1.020	-7.730 ± 0.017
7	1872	2.652	0.925	-7.747 ± 0.010
7	2133	3.021	1.170	-7.546 ± 0.008
10	2281	3.231	1.299	-7.331 ± 0.022
11	2401	3.401	1.470	-7.488 ± 0.010
14	2054	2.909	1.111	-7.728 ± 0.028
9	2435	3.449	1.523	-7.539 ± 0.014
8	2345	3.322	1.380	-7.367 ± 0.015
9	1947	2.758	0.869	-6.729 ± 0.021
5	1800	2.550	0.757	-6.854 ± 0.011
5	1744	2.470	0.715	-6.902 ± 0.021
8	2422	3.431	1.458	-7.294 ± 0.020
10	2318	3.283	1.348	-7.362 ± 0.009
12	2192	3.105	1.157	-7.067 ± 0.021
21	1925	2.727	0.911	-7.218 ± 0.017
7	1999	2.831	0.999	-7.341 ± 0.019
			mean	-7.448 ± 0.071

8.5 Summary of results

All the results listed in eqns. (8.19) - (8.25) and (8.29) - (8.40) are summarized in Table 8.20. From these, together with the refractive index and linear electro-optic coefficient values for KDP and ADP listed in Table 8.1 and given in Subsection 8.2.1, the individual quadratic electro-optic coefficients g_{xxxx}, g_{yyxx}, and g_{zzxx}, and electrostrictive coefficients γ_{xxzz} and γ_{xxyy}, for both KDP and ADP were evaluated.

Table 8.20 Summary of results (in units of 10^{-20} m^2V^{-2}) contained in Section 8.4

	Quadratic electro-optic - electrostrictive contribution	KDP	ADP (larger)	ADP (smaller)
1	$g_{yyxx} - g_{xxxx} + (n_e r_{xy})^2$	3.22 ± 0.21	5.75 ± 0.40	5.67 ± 0.56
2	$g_{xxxx} - 2(n_o - n_{air})n_o^{-3}\gamma_{xxzz}$	- 3.13 ± 0.20	- 7.07 ± 0.46	- 7.26 ± 0.45
3	$g_{yyxx} + (n_e r_{xy})^2 - 2(n_o - n_{air})n_o^{-3}\gamma_{xxzz}$	0.09 ± 0.02	- 1.32 ± 0.11	- 1.59 ± 0.11
4	$g_{xxxx} - 2(n_o - n_{air})n_o^{-3}\gamma_{xxyy}$	- 3.87 ± 0.23	- 6.90 ± 0.44	- 6.72 ± 0.43
5	$g_{zzxx} + (n_o r_{xy})^2 - 2(n_e - n_{air})n_e^{-3}\gamma_{xxyy}$	- 1.16 ± 0.08	- 0.74 ± 0.08	- 0.75 ± 0.06
6	$g_{xxxx} - 2(n_o - n_{oil})n_o^{-3}\gamma_{xxzz}$	- 3.46 ± 0.22	-	- 7.48 ± 0.54
7	$g_{xxxx} - 2(n_o - n_{oil})n_o^{-3}\gamma_{xxyy}$	- 3.40 ± 0.21	-	- 7.45 ± 0.52

It may be noted, that there is some degeneracy about the results listed in Table 8.20. For instance, in the case of the KDP and smaller ADP results there are five unknowns, g_{xxxx}, g_{yyxx}, g_{zzxx}, γ_{xxyy}, and γ_{xxzz}, and six independent numerical values of the quadratic electro-optic and electrostrictive contributions, those numbered 2 - 7. In calculating the electrostrictive coefficients γ_{xxyy} and γ_{xxzz} of KDP and ADP from these, results for the same experimental propagation and polarization configurations, but different environments, were used, since for these the only difference was due to the extent to which electrostriction contributed to the measured result. Thus for the calculation of γ_{xxyy} results labelled 2 and 6 were used, and for γ_{xxzz} those labelled 4 and 7. Knowing these electrostrictive values, the remaining unknown quadratic electro-optic coefficients g_{xxxx}, g_{yyxx}, and g_{zzxx} were calculated from the results labelled 2 - 5, for both KDP and the smaller ADP, and also for the larger ADP for which the electrostrictive values calculated for the smaller ADP crystal are applicable. There was, however, still some redundancy about this analysis, with two results being found for the coefficient g_{xxxx} for each crystal. This is on account of the same coefficient contributing to the induced change in refractive index for one of the polarization eigenvectors for both *y*- and *z*-propagation. In this case the mean of these values was taken. The sign and magnitude of all the coefficients calculated are tabulated in Table 8.21.

Table 8.21 Calculated results for coefficients (in units of 10^{-20} m^2V^{-2}) of the quadratic electro-optic and electrostrictive effects in KDP and ADP

Coefficient	KDP	ADP (Large)	ADP (medium)	ADP (mean)
g_{xxxx}	- 3.44 ± 0.46	-7.43 ± 1.03	-7.44 ± 1.01	-7.44 ± 1.02
g_{yyxx}	-0.20 ± 0. 40	-1.53 ± 0.93	-1.80 ± 0.93	-1.67 ± 0.93
g_{zzxx}	-0.73 ± 0.41	-1.42 ± 0.89	-1.43 ± 0.89	-1.43 ± 0.89
γ_{xxzz}	-1.02 ± 1.29	-	-0.70 ± 3.13	-0.70 ± 3.13
γ_{xxyy}	1.45 ± 1.35	-	-2.31 ± 3.01	-2.31 ± 3.01

Also, to allow comparison with results of the polarimetric method for each crystal, the following values (in units of 10^{-20} m^2V^{-2}) were calculated:

For KDP:

$$g_{xxxx} - g_{yyxx} = -3.20 \pm 0.21, \tag{8.41}$$

$$n_o^3 g_{xxxx} - n_e^3 g_{zzxx} = -9.48 \pm 2.04. \tag{8.42}$$

For ADP:

$$g_{xxxx} - g_{yyxx} = -5.69 \pm 0.48, \tag{8.43}$$

$$n_o^3 g_{xxxx} - n_e^3 g_{zzxx} = -21.4 \pm 4.6. \tag{8.44}$$

8.6 Discussion

A discussion of the results determined for the various coefficients in this interferometric project, and also those of the polarimetric inquiry presented in Chapters 9 and 10, will be left for Chapter 11. There are, however, some details particular to the interferometric investigation which deserve mention before proceeding to the polarimetric work.

One important difference between this project and the MSc work (Gunning 1995) from which it follows has been the change in the manner in which the piezoceramic plate used as a reference was calibrated. The value of the calibration constant, namely $d = -2.542 \times 10^{-10}$ mV^{-1}, measured in the present work is notably smaller than the result of $d = -3.07 \times 10^{-10}$ mV^{-1} obtained previously, and cannot be dismissed as falling within experimental uncertainty. Because the calibration procedure used in this work, unlike that of the MSc project, involved ac detection techniques and also measured the calibration constant at the frequency of the modulation voltage and over the same range of nulling voltages as used in the experiment, its value is claimed to be

the more reliable. The unsubstantiated assumptions of the previous calibration procedure, discussed in Section 6.5.5, were not involved in the present determination. In fact, the quadratic electro-optic coefficients determined in the initial project for KDP in a silicon oil environment, and which include a small electrostrictive contribution, differ from similar results obtained in this work for the same crystal specimen and silicon oil environment, eqns. (8.24) and (8.25) respectively, by a factor roughly equal to the ratio of the two calibration constants. These are, in units of 10^{-20} m^2V^{-2}:

	This project	MSc project
$g_{xxxx} - 2(n_o - n_{oil})n_o^{-3}\gamma_{xxzz}$	– 3.46	– 4.0
$g_{xxxx} - 2(n_o - n_{oil})n_o^{-3}\gamma_{xyyy}$	– 3.40	– 3.9

The remaining difference in these coefficients, after taking the change in calibration constant into account, may be attributed to the greater stability and sensitivity of the present apparatus. Certainly, the modified apparatus with its active stabilization and feedback is more sensitive in the determination of results. For instance, in the MSc investigation on the same KDP crystal as that in the present work, reliable results for propagation along the optic axis could not be obtained for the incident light linearly polarized at angles greater that |60°| from the crystallographic x-axis, whereas in this work only in the immediate vicinity of |80°| was the effect not measurable. As a consequence of obtaining results over a wider range of angles in this work, the graphical analysis, represented by Graphs 8.2 and 8.3, is more reliable than the corresponding one in the MSc project (Gunning 1995).

Another experimental consideration that required attention concerned the possibility of the two environments in which the crystals were placed at different stages of the experiment displaying a Kerr effect themselves. As the Kerr effect is known to be a property of all media, it is possible that in the experiment the fringing field around the edges of the specimen in the path of the propagating beam induced a birefringence quadratic in the applied field, in either the air or silicon oil. This would in turn influence the determination of the induced optical path-length changes.

The Kerr constant of nitrogen, which would give a measure of the effect to be expected in air, has been reported by Buckingham *et al.* (1970). From this data it may be calculated that for a field of 5×10^5 Vm^{-1}, the Kerr birefringence in nitrogen at atmospheric pressure and room

temperature is of the order of 10^{-14} for a wavelength of 632.8 nm. This compares with a value of about 10^{-8} for KDP-type crystals in similar conditions. Evidently the former effect is negligible in comparison to the latter, and readings taken in the air environment may be safely assumed to be free of induced effects besides those in the crystal.

By contrast, the Kerr constant of the silicon oil used is unknown and various attempts to determine the birefringence induced in it by the fringing field proved unsuccessful. Nevertheless, it was ascertained, by simulating the crystal's electrode surfaces in the oil, that the induced effect was at least two orders of magnitude smaller than that in the crystal. In the end its contribution was also neglected. On account of the slight uncertainty which surrounded the possible Kerr effect in the silicon oil, measurements in this work were, for the most part, conducted in an air environment, except in the cases where results were required in an atmosphere of different refractive index to allow the determination of the electrostrictive contributions.

Chapter 9

THE POLARIMETRIC INVESTIGATION

9.1 Introduction

Undoubtedly the most common technique used to measure coefficients of the electro-optic effect, both linear and quadratic, is the polarimetric method (Narasimhamurty 1981), of which numerous illustrations may be found in the literature (see, for example, Kaminow 1974). One finds examples of its application in determining quadratic electro-optic coefficients in KDP-type crystals listed in Table 5.1, in which both static and modulated perturbing fields were used. Chapters 9 and 10 of this thesis describe a polarimetric investigation carried out in this research. This study, employing dynamic techniques, examined the quadratic electro-optic effect in crystals of KDP, ADP, and DKDP for a field parallel to the crystallographic x-axis and light propagation along the y- and z-axes, with the exception of DKDP which was investigated for z-propagation only. Measured were the quadratic electro-optic coefficients $|g_{xxxx} - g_{yyxx}|$ in all three crystals and $|n_o^3 g_{xxxx} - n_e^3 g_{zzxx}|$ in KDP and ADP, where n_o and n_e are the ordinary and extraordinary refractive indices respectively.

Before a description of this polarimetric investigation is given, it is necessary that it be put into context with the rest of the work completed in this thesis. As mentioned in Section 5.1, the results for the various quadratic electro-optic coefficients presented here were obtained during a visit to the Technical University of Łódź in Łódź, Poland. This experiment was conducted on apparatus which was made available in the research laboratories of that university and which was almost entirely preassembled. All the work was completed over the relatively short period of

three months. In contrast, the interferometric work reported in previous chapters was conducted over a total of three years, and incorporated a thorough background investigation into the design and assembly of the apparatus, besides obtaining the experimental results. Accordingly, to keep it in context with the rest of the research, the polarimetric results are reported in a more concise manner than those of the interferometric work. Notwithstanding this, the polarimetric investigation provides important results for the present experimental study of the quadratic electro-optic effect in KDP-type crystals.

9.2 On the principle of the polarimetric technique

Polarimetric measurement techniques provide a simple and elegant means to study the electro-optic effect. In this approach the coefficients of the electro-optic effect of the crystal under investigation are derived from the induced change in intensity of light passing through the material placed between a polarizer and an analyzer. The principle of this method may be understood as follows: the linearly polarized light emerging from the polarizer propagates through the crystal in the form of two orthogonal polarization eigenvectors which are assumed linear. However, on account of birefringence, natural and field-induced, exhibited by the medium these two polarization eigenvectors will experience unlike refractive indices and hence propagate at different velocities. Thus, after traversing the crystal, a phase difference will exist between these waves, given by

$$\Delta\phi = \frac{2\pi}{\lambda}\left(d_1 - d_2\right) = \frac{2\pi}{\lambda}\left[\left(n_1 - n_2\right)L\right]. \tag{9.1}$$

In this expression d_1 and d_2 are the optical path lengths experienced by each wave respectively, n_1 and n_2 are their refractive indices, λ the wavelength of the light, and L the length of the medium in the direction of light propagation. The analyzer serves to select a particular polarization plane of the two waves emerging from the crystal and to produce an interference pattern between these polarized components on account of the phase difference between them. This process is, in principle, the same as that resulting in the fringe pattern between the two beams, polarized in the same plane, emerging from the interferometer considered in Chapter 5. As in that case, relative changes in the phase difference (or optical path-length difference) between the waves lead to a variation in the intensity of the interference pattern.

Consider the light wave incident on the crystal to be given by

$$\boldsymbol{E} = \boldsymbol{E}^{(o)}\cos\theta,$$

where $\theta = \omega(t - nr/c)$. Then if α is the angle between the polarization plane of this light wave and one of the eigenvectors for a particular light path, the electric field components of the two waves propagating through the crystal are

$$\boldsymbol{E}_1 = \boldsymbol{E}^{(o)}\cos\alpha\cos\theta_1 \quad \text{and} \quad \boldsymbol{E}_2 = \boldsymbol{E}^{(o)}\sin\alpha\cos\theta_2, \tag{9.2}$$

where

$$\theta_i = \omega\left(t - n_i r/c\right), \quad i = 1,\ 2.$$

Furthermore, if the fast axis of the analyzer lies between the polarization eigenvector $\boldsymbol{E}_1$ of the crystal and the incident light polarization plane, at an angle χ to the latter, then the transmitted components of these two waves are, respectively, given by (Born and Wolf 1980)

$$\boldsymbol{E}^{(o)}\cos\alpha\cos(\alpha - \chi)\cos\theta_1 \quad \text{and} \quad \boldsymbol{E}^{(o)}\sin\alpha\sin(\alpha - \chi)\cos\theta_2. \tag{9.3}$$

It is these two electric field components which form the interference pattern depending on the extent of the phase shift between them. Making use of these expressions and eqn. (6.3), which gives the intensity at a point on an interference pattern in terms of the two interfering wave intensities and their relative phase difference, one may write (Born and Wolf 1980)

$$I = I_o\left\{\cos^2\chi - \sin 2\alpha\sin\left[2(\alpha - \chi)\right]\sin^2\left(\frac{\Delta\phi}{2}\right)\right\}. \tag{9.4}$$

In this equation I is the intensity at a point on the interference pattern, and I_o the intensity of the light incident on the crystal.

Since the electro-optic effect manifests itself as a change in refractive index of a medium to which an electric field is applied, an electro-optic material placed between a polarizer and an analyzer will, on the application of a field, introduce a change in intensity of the light transmitted through the optical arrangement. From eqn. (9.4) this intensity variation may be related to the induced phase difference between the orthogonal polarization eigenvectors of the crystal for that light path. Thus measuring this intensity variation allows the electro-optic coefficients responsible for the induced phase shift to be determined. It may be noted, however, that as the interference pattern in this arrangement results from the phase difference between the two orthogonal eigenvectors propagating through the crystal in the presence of the field, it is the difference in electro-optic properties of each eigenvector that is determined from the measured phase change. Thus, if distinct coefficients of the electro-optic effect are responsible for the

behaviour of these eigenvectors in the field, only the difference in these coefficients may be determined by the polarimetric method. By contrast, the interference pattern in the interferometer results from the phase difference between the light wave in one arm of the interferometer and the other. Thus a single eigenvector may be made to propagate through the crystal in the presence of the field. Then one would measure the electro-optic coefficients specific to that eigenvector.

In this work two applications of the polarimetric approach are considered in the investigation of the quadratic electro-optic effect in KDP-type crystals. One involves propagation along the crystallographic *y*-axis for a field in the *x*-direction, and the other propagation along the optic axis in the presence of the same field. These investigations involve similar polarimetric arrangements, and both are describe in the next section.

9.3 The polarimetric investigation of KDP-type crystals

To investigate the quadratic electro-optic effect in KDP-type crystals by the polarimetric approach in this work, the crystal being studied was placed between a polarizer and an analyzer which had their fast axes crossed relative to one another. In addition, the fast axis of the polarizer was oriented so that the light incident on the crystal had its vibration plane at $|45°|$ to the directions of the two orthogonal polarization eigenvectors for the particular propagation path. The theory in Chapter 5 shows that for the two propagation paths of interest in this work, along the crystallographic *y*- and *z*-axes, and for the particular applied field direction the polarization eigenvectors, to a good approximation, lie along the crystallographic axes perpendicular to the propagation direction. Thus, in practice, the polarization plane of the light was oriented at $|45°|$ to the crystallographic *x*-axis for both propagation directions, and the light propagated through the crystal in the form of two equal components polarized along the crystallographic axes perpendicular to the propagation path. Under these circumstances $\alpha = 45°$, $\chi = 90°$, and eqn. (9.4) reduces to

$$I = I_o\left\{\sin^2\left(\frac{\Delta\phi}{2}\right)\right\}. \tag{9.5}$$

At this stage of the analysis the phase difference $\Delta\phi$ between the two orthogonal eigenpolarizations is considered to consist of two parts:

$$\Delta\phi = \Delta\phi_c + \Delta\phi(\omega, 2\omega). \tag{9.6}$$

In this equation $\Delta\phi_c$ is a near-static phase shift, a consequence of the natural birefringence, if any, for the particular propagation path, and $\Delta\phi(\omega,2\omega)$ is a modulated phase variation due to a field

$$E = E^{(\omega)}\cos\omega t \tag{9.7}$$

applied to the crystal, where ω is its frequency. It is important to note that the phase difference $\Delta\phi_c$ may vary slowly with time on account of fluctuating environmental conditions, particularly temperature-induced changes to the ordinary and extraordinary refractive indices of the crystal. The second phase change in eqn. (9.6) is assumed to consist of two modulated terms, one linear in the field and the other quadratic. The former of these is included to allow for the possible occurrence of the linear electro-optic effect, even though the configurations used disallowed it in principle (see below). Thus

$$\Delta\phi(\omega,2\omega) = A\cos^2\omega t + B\cos\omega t, \tag{9.8}$$

where A and B are small perturbations in the field. Typically, B is larger than A for the present electro-optic investigation of KDP for the light-propagation and applied-field configurations used, since the linear contribution to the phase difference, through induced refractive index changes, is larger than the quadratic equivalent, even for very small misalignments of the crystal which lead to propagation paths off the desired axis (see discussion in Section 5.5).

Substituting eqns. (9.6) and (9.8) into eqn. (9.5), one derives the following expression for the emerging light intensity:

$$I \approx \frac{I_o}{2}\left\{1 - \cos\Delta\phi_c + B\cos\omega t\sin\Delta\phi_c + \tfrac{1}{2}\left(1+\cos 2\omega t\right)\left[A\sin\Delta\phi_c + \tfrac{1}{2}B^2\cos\Delta\phi_c\right]\right\}. \tag{9.9}$$

In this two approximations were made: first, only contributions up to second order in the applied field were retained, and, second, for small $\Delta\phi(\omega,2\omega)$

$$\sin\Delta\phi(\omega,2\omega) = \Delta\phi(\omega,2\omega), \quad \cos\Delta\phi(\omega,2\omega) = 1 - \tfrac{1}{2}[\Delta\phi(\omega,2\omega)]^2.$$

The latter approximation was also made below eqn. (6.13), where it was seen to introduce an error of less than 1% for phase changes resulting from path length differences of no more than 13 nm. Hence the intensity of the light emerging from the optical arrangement under consideration consists of three components:

$$I_c = \frac{I_o}{2}\left(1 - \cos\Delta\phi_c + \tfrac{1}{2}A\sin\Delta\phi_c + \tfrac{1}{4}B^2\cos\Delta\phi_c\right) \approx \frac{I_o}{2}\left(1 - \cos\Delta\phi_c\right), \tag{9.10}$$

$$I^{\omega} = \frac{I_o}{2}\left(B\sin\Delta\phi_c\right), \tag{9.11}$$

$$I^{2\omega} = \frac{I_o}{2}\left(\tfrac{1}{2}A\sin\Delta\phi_c + \tfrac{1}{4}B^2\cos\Delta\phi_c\right), \tag{9.12}$$

where I^{ω} and $I^{2\omega}$ are the induced intensity changes at the first and second harmonics respectively of the applied field frequency. As $\Delta\phi_c$ may vary on account of relative temperature-induced changes in the ordinary and extraordinary refractive indices, the static intensity of the interference pattern will fluctuate from a minimum of zero to a maximum of I_o. From eqn. (6.9) this pattern will be at the point most sensitive to small induced phase changes when it is half way between maximum and minimum intensity, i.e. $\frac{1}{2}I_o$. This will be satisfied when

$$\Delta\phi_c = \tfrac{1}{2}(2n+1)\pi, \qquad n = 0,\ 1,\ 2,\ \cdots. \tag{9.13}$$

Equations (9.11) and (9.12) reveal that the amplitudes of the two modulated components of the emerging light intensity have a sinusoidal dependence on $\Delta\phi_c$ and, assuming B^2 to be much smaller than A, will both be a maximum for the same condition for $\Delta\phi_c$ as when the intensity pattern is at its most sensitive point, i.e. when eqn. (9.13) is satisfied. In addition, eqn. (9.12) shows that the modulated intensity variation at the second harmonic, the component of interest in the present quadratic electro-optic effect investigation, in general contains a contribution due to the square of the linear term B. However, this tends to zero for the condition that the intensity pattern is at its most sensitive point, and the term modulated at the second harmonic is at a maximum.

9.3.1 Propagation along the optic axis

Since KDP-type crystals are uniaxial, the only difference in the refractive indices of the polarization eigenvectors for this propagation direction is due to the induced changes brought about by the electro-optic effect. In particular, for the field along the *x*-axis these changes are on account of the quadratic electro-optic effect. Derived in Chapter 5 are the relevant expressions for the induced changes in refractive indices of the polarization eigenvectors for this field and light path. From eqns. (5.37) these are

$$\Delta n_x = -\tfrac{1}{2}n_o^{-3}g_{xxxx}E^2, \tag{9.14}$$

$$\Delta n_y = -\tfrac{1}{2} n_o^{-3}\left[g_{yyxx} + n_e^2 r_{xzy}^2\right]E^2. \tag{9.15}$$

Hence light propagating along the optic axis for a KDP-type crystal between crossed polarizers will emerge with only a very small phase difference between each polarization eigenvector due to the electro-optically induced changes in their respective refractive indices.

There will be no static, or near-static, phase difference $\Delta\phi_c$ since for a uniaxial crystal the field-free refractive indices of these polarization eigenvectors are identical, as are their temperature-induced changes. Under these circumstances the fringe pattern, the intensity of which is given by eqn. (9.5), may be seen to be biased at, or near, minimum intensity, or, more importantly, away from the point of maximum sensitivity to small induced phase variations. To overcome this problem, also included in the polarimetric arrangement for this light path was a $\frac{\lambda}{4}$ - plate situated after the crystal but before the analyzer. This served, in principle, to introduce a constant component to the phase difference between the two orthogonal waves of the light beam propagating through the optical arrangement. When oriented such that its fast axis is at $|45°|$ to the polarization plane of the light incident on the crystal, and hence parallel to one of the polarization eigenvectors, the static phase difference it introduced was, in principle, precisely $|90°|$. Under these circumstances, eqn. (9.13) is satisfied and the possible linear contributions (on account of alignment errors) to the intensity change at the second harmonic (see eqn. (9.11)) due to the square of the linear effect are zero. Thus, eqn. (9.6) may be rewritten as

$$\Delta\phi = \frac{\pi}{2} + \Delta\phi(\omega, 2\omega). \tag{9.16}$$

The latter part of this, in terms only of the induced changes, which are quadratic in the field, in the refractive index of each polarization eigenvector is from eqn. (9.1), (9.7), (9.14), and (9.15):

$$\begin{aligned}\left|\Delta\phi(\omega,2\omega)\right| &= \frac{2\pi}{\lambda}\left(\Delta n(2\omega)\right)L_z \\ &= \frac{2\pi}{\lambda}\left[\tfrac{1}{2} n_o^3\left(g_{xxxx} - g_{yyxx} - n_e^2 r_{xzy}^2\right)L_z\right]\left(E^{(\omega)}\right)^2 \cos^2\omega t.\end{aligned} \tag{9.17}$$

In deriving this expression induced changes in the dimension of the crystal in the direction of light propagation are neglected as small in comparison to the field-free crystal length. Also, the ever-present contributions to the refractive index changes linear in the field are omitted, since their contribution to the intensity modulation at the second harmonic is zero for the static phase difference of interest.

Thus the light intensity emerging from the optical arrangement consists of three parts. One is a constant component of $\frac{1}{2}I_o$ which corresponds to the intensity pattern balanced at the point half way between maximum and minimum intensity and which, from the derivations in Section 6.2, is thus at the point most sensitive to small induced optical path-length or phase changes. The other component of interest, in an experiment that can distinguish light intensities linear and quadratic in the field, is the small change in intensity due to the difference in induced refractive index changes at the second harmonic. From eqns. (9.8), (9.12) and (9.17), this is in terms of the change in intensity of the pattern away from $\frac{1}{2}I_o$ as

$$\left|I^{2\omega}\right| = \frac{I_o \pi n_o^3 L_z}{4\lambda}\left[g_{xxxx} - g_{yyxx} - n_e^2 r_{xzy}^2\right]\left(E^{(\omega)}\right)^2. \qquad (9.18)$$

Experimentally the magnitude of this intensity change, as well as the constant background intensity $\frac{1}{2}I_o$, may be easily determined through the use of a photodetector converting the optical signal into an electronic one. In this case, from such measurements the difference in the unknown quadratic electro-optic coefficients g_{xxxx} and g_{yyxx} is determinable. This is the procedure adopted in this project for the investigation of the quadratic electro-optic effect in crystals of KDP, ADP, and DKDP for propagation along the optic axis in a field parallel to the crystallographic x-axis. The polarimetric arrangement used in this instance is shown in Figure 9.1. Equation (9.18) serves to illustrate the point made in Section 9.2 that since in this case different components of the quadratic electro-optic coefficient are responsible for the electro-optic behaviour of each eigenvector (see eqns. (9.14) and (9.15)) only the difference in these coefficients may be determined by the polarimetric method.

9.3.2 Propagation along the crystallographic *y*-axis

In the second polarimetric investigation light was directed along the crystallographic y-axis of KDP-type crystals to which a field was applied in the x-direction. As for the investigation for z-propagation, the crystal was again sandwiched between a crossed polarizer and an analyzer and the incident light aligned to be linearly polarized at $|45°|$ to the crystallographic x-axis. For these propagation and field directions, the theoretical treatment in Chapter 5 shows that the light will propagate in the form of two orthogonal eigenpolarizations, which to a good approximation oscillate perpendicular to the propagation direction and parallel to the crystallographic x- and z-axes. Their respective refractive indices are, from eqns. (5.30) and (5.31),

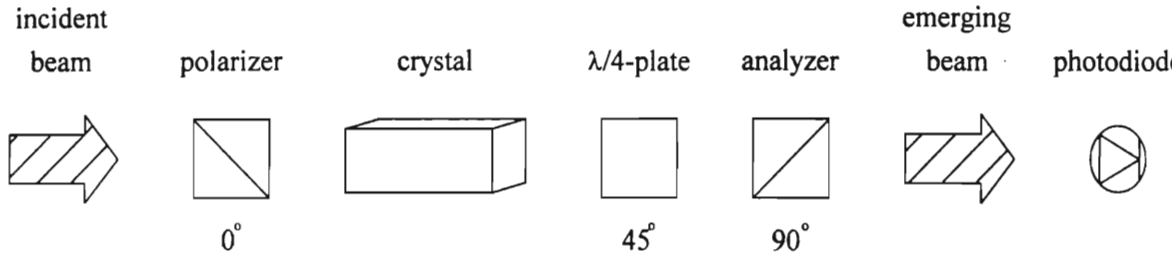

Figure 9.1 Polarimetric arrangement for light propagation along the optic axis

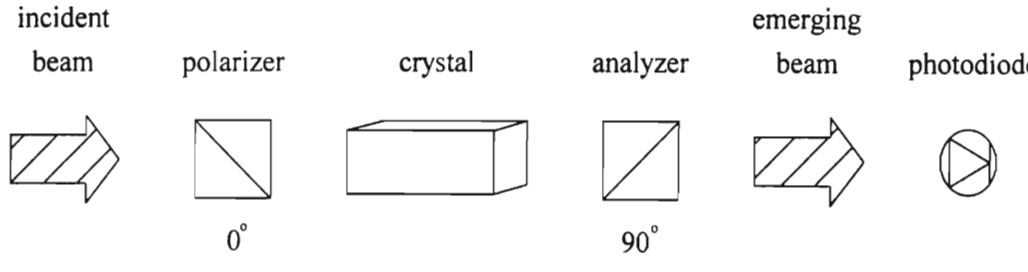

Figure 9.2 Polarimetric arrangement for light propagation along the crystallographic y-axis

$$n_x^2 = n_o^2 - n_o^4 g_{xxxx} E^2, \tag{9.19}$$

$$n_z^2 = n_e^2 - n_e^4 \left[g_{zzxx} + n_o^2 r_{xzy}^2 \right] E^2. \tag{9.20}$$

Since KDP-type crystals are naturally birefringent for this propagation direction, a phase difference will exist between the two waves even in the absence of the applied field. Furthermore, on account of the slight difference in the temperature dependences of the ordinary and extraordinary refractive indices, this natural birefringence, and thus the phase difference arising from it, will vary with temperature. A simple calculation from eqn. (9.1) shows that for the intensity pattern at a point to be shifted a complete fringe for a wavelength of 632.8 nm and a crystal length of 50 mm, the difference in the refractive indices of the two principal eigenvectors need change by only about 1×10^{-5}. As a consequence, biasing the emerging interference pattern to the point corresponding to that most sensitive to small phase, or optical path-length, differences through the use of some constant introduced phase shift, for example with a $\frac{\lambda}{4}$ - plate as in the previous investigation, is not possible. However, this does not rule out the possibility of using this configuration to obtain meaningful results.

In the presence of a modulated applied field the induced change in the difference between the refractive indices of the two polarization eigenvectors, quadratic in the field, is from eqns. (5.36)

$$\Delta n(2\omega) = \tfrac{1}{2} \left[n_o^3 g_{xxxx} - n_e^3 g_{zzxx} - n_e^3 n_o^2 r_{xzy}^2 \right] E^2. \tag{9.21}$$

Consequently, from eqns. (9.1), (9.8), (9.12), and (9.21) the intensity variation at the second harmonic of the applied field frequency may be rewritten in terms of the quadratic electro-optic coefficients g_{xxxx} and g_{zzxx} as

$$\left| I^{2\omega} \right| = \frac{I_o}{2} \left[\frac{\pi L_y}{2\lambda} \left[n_o^3 g_{xxxx} - n_e^3 g_{zzxx} - n_e^3 n_o^2 r_{xzy}^2 \right] \left(E^{(o)} \right)^2 \sin\Delta\phi_c + \tfrac{1}{4} B^2 \cos\Delta\phi_c \right]. \tag{9.22}$$

In this project the crystal to be investigated was placed between a crossed polarizer and an analyzer, and then gradually increasing, or decreasing, the temperature of the laboratory, the dc, first-harmonic, and second-harmonic components of the emerging light intensity were monitored. Given the dc intensity component and the total change in intensity of the optical system (which could be obtained as the polarimeter varied through its complete intensity range) the corresponding near-static phase could be established from eqn. (9.10). This phase, in conjunction with eqn. (9.11) and the measured intensity variation at the first harmonic, allowed the factor B

for the arrangement to be calculated, and hence the B^2 contribution to the intensity variation at the second harmonic to be determined. From these results, from the measured intensity variation at the second harmonic, and eqn. (9.22), a value of $|n_o^3 g_{xxxx} - n_e^3 g_{zzxx}|$ could be found for the crystal. The experimental arrangement used for this investigation is shown in Figure 9.2.

9.4 Components of the polarimeter

The polarimetric arrangement used in this research, including all the optical and electronic components for its operation, is shown schematically in Figure 9.3. An interesting point to note concerning the polarimetric technique is that the two interfering waves travel the same paths from the polarizer to the analyzer, albeit with different polarization states. Consequently, this method of measuring induced path differences is inherently more stable than the interferometric method where the waves propagate along separate paths. The apparatus used in this work, without requiring intricate stabilization, was sensitive to induced phase changes between the two interfering waves equivalent to induced optical path-length variations of the order of 10^{-1} Å.

9.4.1 The optical bench

The optical bench that was used consisted of a single arm approximately 1000 mm in length and rectangular in cross-section measuring about 120 mm × 80 mm. It was to this heavy cast iron structure that the various optical components which formed the polarimeter were securely attached. As in the interferometric work, this was achieved through the use of individual stands which were adjustable in height and also permitted the translation of the component laterally across the arm of the optical bench. Thus each component could be individually positioned and ideally aligned as required. To ensure a degree of isolation from the surroundings, the optical bench was positioned on a heavy cast iron optical table which served to dampen out ambient vibrations, and, furthermore, the apparatus was used in an isolated room free of working machinery.

9.4.2 Source of monochromatic light

In this experiment the source of monochromatic light was a Melles Griot model O5-LHP-171 He-Ne laser which had an intensity of 7 mW and wavelength of 632.8 nm. This linearly polarized beam was found not to diverge and to remain coherent from its source to the light detector, a distance of approximately 700 mm. When the apparatus was assembled, the beam was aligned

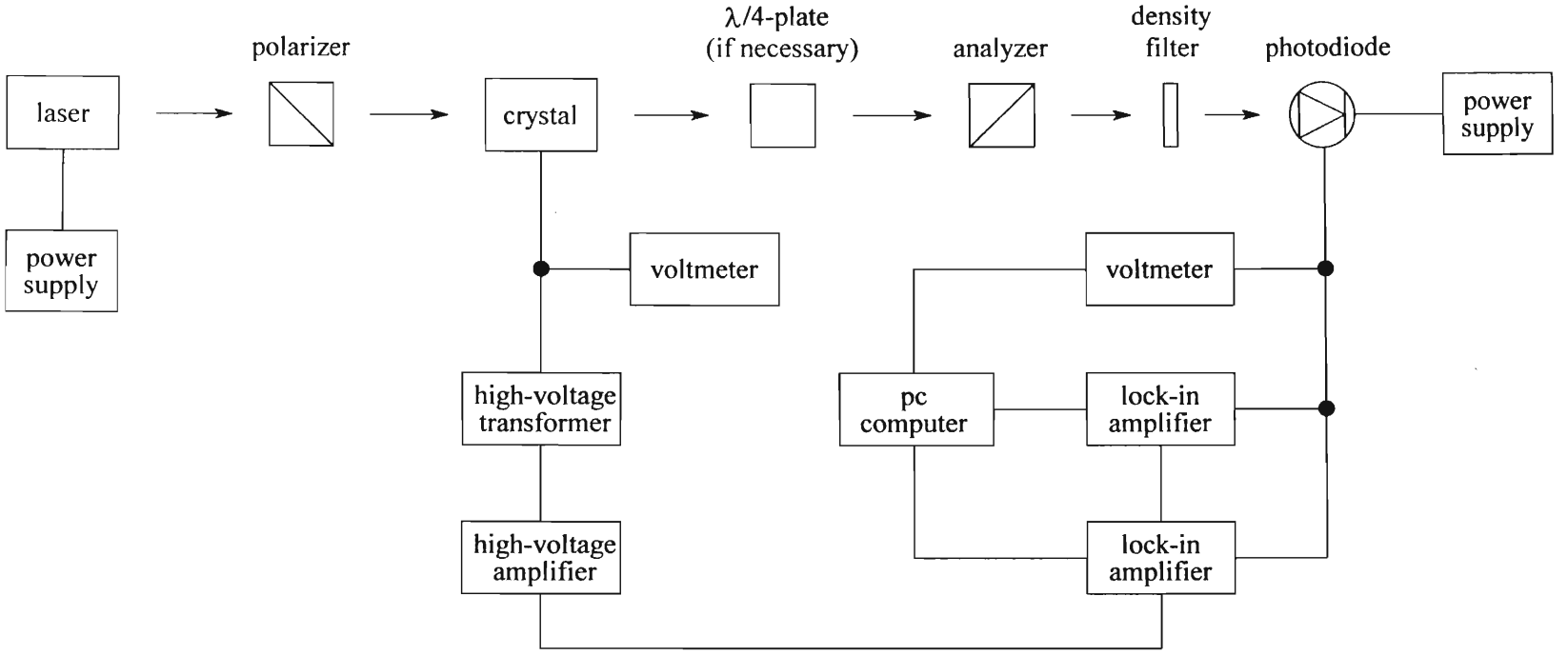

Figure 9.3 Schematic diagram depicting the various optical and electronic components constituting the polarimetric apparatus

by means of the stands which mounted the laser to the optical bench to be both at a set height above, and parallel to, the bench. By rotating the laser about its propagation direction on its stand, one could set the polarization of the incident beam to coincide approximately with the plane of the fast axis of the polarizer. This ensured the greatest possible intensity transmission through the polarizer.

9.4.3 Optical components

The optical arrangement for the polarimetric method was relatively simple, with the two most fundamental components being the polarizer and the analyzer, each in the form of a polarizing sheet sandwiched between strain-free glass plates. These were Dichromic Sheet model 03-FBG-005 polarizers supplied by Melles Griot, and were approximately 40 mm in diameter and 2.5 mm thick. They were mounted individually in divided circles which enabled rotational alignment to within 2′ of arc.

For the experiment with the beam propagating along the optic axis of the crystal, a $\frac{\lambda}{4}$ - plate was also included in the optical arrangement, positioned after the crystal but before the analyzer. That used in this work was a Melles Griot model 02-WRQ-001 quartz plate specified for the He-Ne wavelength and, to introduce a known constant phase shift between the two orthogonal components of the polarimeter's beam, its rotational alignment was facilitated by a divided circle, again of resolution 2′ of arc.

9.4.4 Light detection system

To measure the intensity of the beam emerging from the analyzer a photodiode was used. This was a model B-PYP-30 photodiode made by Tewa, Poland, the intensity response of which was confirmed, as was that in the interferometric arrangement, by Malus' law to be linear for the range of anticipated incident intensities. As a preventative measure to ensure the intensity of the light incident on the photodiode did not exceed its intensity threshold, a light density filter was placed between the analyzer and the photodiode.

The output signal from the photodiode was monitored in three separate ways: the dc component of the static background light intensity was measured by a Meratronik model V541 voltmeter, while the components at the first and second harmonics of the frequency of the modulated

voltage applied to the crystal were measured by separate lock-in amplifiers. A Stanford Research model SR 530 lock-in amplifier was used to detect the component modulated at the first harmonic, while the second harmonic component was observed by an EG&G model 7220 lock-in amplifier. Each signal was carried from the photodiode to the respective meter by coaxial cable, thereby providing sufficient screening against possible spurious signals. These cables were kept well away from the apparatus' power supplies, amplifiers, and high-voltage transformers.

9.5 The crystal specimens

9.5.1 General properties

In this project one KDP, three ADP, and two DKDP crystals were used. The deuteration level of the DKDP crystals was specified as 96% by the supplier (Cobrabid-Optica-Warsaw), and approximate dimensions of the separate specimens were as follows:

Crystal	Approximate dimension (mm)
KDP	50 × 50 × 5
ADP (large)	50 × 50 × 5
ADP (medium)	35 × 35 × 7
ADP (small)	25 × 25 × 4
DKDP (large)	30 × 30 × 5
DKDP (small)	25 × 25 × 4

Each of these crystals was prepared in the same manner, and cut to the same accuracy, as those used in the interferometric investigation. In fact, the KDP and large and medium ADP crystals were the very specimens used in that project. To describe these crystals: they were right-parallelepiped in shape with the plane faces coinciding with the crystallographic *xy*-, *xz*-, and *yz*-planes, as depicted in Figure 7.2. In addition, electrode surfaces were prepared by means of a thin coating of conducting paint on the two plane faces in the *yz*-plane of each specimen. Hence each crystal, to the accuracy with which it was cut relative to the crystallographic axes, allowed the free transmission of light along the crystallographic *y*- and *z*-axes for a field applied in the *x*-direction. For these light-propagation and applied-field geometries, the induced changes to the refractive indices, quadratic in the applied field, of the two polarization eigenvectors which propagate in each case have been derived in Chapter 5, and are also shown in Figure 7.2.

9.5.2 Mounting of the crystals

The crystal under investigation was placed in a circular perspex container approximately 80 mm in diameter and 20 mm in depth. Two strain-free windows mounted on adjacent surfaces of the vertical sides of this container allowed the probing beam to pass freely through it. Fixed centrally to the base of the interior of this container, were three thin, pointed support columns upon which the crystal was positioned. When resting freely on these mounts, the crystallographic *yz*-plane of the specimen (the plane of the electrode surfaces) was approximately in the plane of the optical bench, and the light beam was set to travel through the crystal roughly half way between these surfaces. So mounted, the crystals were considered mechanically free to respond to the applied field.

9.5.3 Orientation of the crystals

To permit the determination of the quadratic electro-optic coefficients $|g_{xxxx} - g_{yyxx}|$ and $|n_o^3 g_{xxxx} - n_e^3 g_{zzxx}|$ specific orientations of the crystal were required relative to the polarization and propagation directions of the light incident on it. Both investigations required the beam to be polarized at $|45°|$ to the crystallographic *x*-axis, and the two propagation paths of interest were those along the crystallographic *y*- and *z*-axes. To this end, the stand mounting the container which housed the crystal in the apparatus was fitted with three independent screw gauges which facilitated limited orientation of the container, and hence the crystal, about three mutually orthogonal axes. Presented below is an outline of the alignment procedure adopted in this polarimetric project. Each of these alignment stages was repeated at intervals throughout the investigation to ensure misalignment had not occurred.

Stage 1: Alignment of the optic axis relative to the light path

This procedure was identical to that described in Stage 1 of Subsection 7.3.3 of the interferometric investigation, and invoked the use of the conoscopic image formed by a uniaxial crystal placed between a crossed polarizer and an analyzer. Since the principle of this alignment has been discussed previously it will not be repeated here. Suffice it to say that when placed in this optical arrangement, the crystal orientation was adjusted with the assistance of the three screw gauges on the stand mounting the crystal's container, so that the conoscopic image formed was precisely symmetric about the beam position in the absence of the crossed analyzer. So oriented, the light wave then propagated along the crystal's optic axis.

Stage 2: Alignment of the crystal relative to the polarization plane of the incident beam

Here the alignment procedure was similar to that outlined in Stage 2 of Subsection 7.3.3, although then it was used without the benefit of the theory since spelt out in the Sections 9.2 and 9.3 of this chapter. The crystal was placed between a crossed polarizer and analyzer, with a $\frac{\lambda}{4}$ - plate also between them to introduce a static phase shift of $|90°|$, and with the field along the x-axis of the crystal and the light path along its optic axis. From eqn. (9.4) it may be shown (Górski *et al.* 1994) that the modulated intensity change at the second harmonic of the applied field frequency for the light emerging from this system will vary from a maximum to a minimum as the angle of the light incident on the crystal is rotated from one crystallographic axis to the other. Furthermore, this intensity relative to the incident light intensity is a maximum for the incident light polarized at $|45°|$ to the crystallographic x- and y-axes and a minimum parallel to them. In principle either the maximum or minimum of this response may be found, but in practice the minimum may be established with greater certainty. Thus in this work, as was done in Stage 2 of Subsection 7.3.3, the emerging light intensity at the second harmonic was monitored by means of the photodiode and lock-in amplifier, relative to the unmodulated background intensity, and the minimum in this response was found. Then by rotating the polarizer's fast axis through $|45°|$ the desired alignment of the incident polarization was achieved. In practice, for the crystal positioned with its crystallographic yz-plane roughly in the plane of the horizontal optical bench, when this alignment was complete the light incident on the crystal was oriented within $1°$ of $45°$ to the laboratory axis perpendicular to the optical bench.

Stage 3: Propagation along the crystallographic y-axis and polarization at $|45°|$ to the x-axis in the xz-plane

In comparison to the previous two alignment procedures and those outlined in Chapter 7 for the corresponding interferometric experiment, this present alignment stage was the least accurate. This consisted of two parts, the first of which was to align the crystal so that the light traversed the y-axis. One possibility considered for this alignment was to rotate the crystal aligned in Stage 1 through roughly $90°$ about the x-axis and then finely adjust its orientation so that light reflected from its front face propagated back along the incident beam. This meant, however, that the alignment was only as accurate as the cutting of the crystal, which is specified to within $3°$ for propagation along the y-axis. The preferred alternative was to use again an interference arrangement. However, for y-propagation through a uniaxial crystal placed between a crossed polarizer and analyzer, the interference pattern so formed was not as definite as that for

z-propagation. Furthermore, on account of relative variations in the ordinary and extraordinary refractive indices, this pattern was seen to change with time. Despite this, it was adopted as the more reliable alignment procedure. By means of the screw gauges on the crystal box assembly, the crystal was oriented between crossed polarizers so that this interference pattern was symmetric about the central beam position in the absence of the crossed analyzer. Throughout this procedure the light beam was kept propagating at a fixed height above the optical bench and travelling parallel to it. So aligned, the light was considered to propagate along the crystallographic y-axis.

Similar alignment problems were encountered when the polarization of the light incident on the crystal was to be set at $|45°|$ to the crystallographic x-axis for this propagation path. Because of phase changes due to temperature-induced fluctuations in the ordinary and extraordinary refractive indices, the steps outlined above for z-propagation were not applicable. But, as mentioned above, light polarized at $|45°|$ to the crystallographic x-axis for z-propagation was seen to be approximately at $|45°|$ to the laboratory axis perpendicular to the optical bench. This suggested that the crystallographic yz-plane, that parallel to the electrode surfaces, was roughly in the plane of the optical bench. It was thus assumed in this part of the project that rotating the crystal through $90°$ about the x-axis, with the beam now traversing the y-axis, did not alter the arrangement, so that the polarization plane, which had been set at $45°$ to the bench perpendicular, was now at $45°$ to the x-axis for y-propagation also. Had more time been available for this experiment, this particular alignment stage could possibly have been improved, perhaps by adopting the procedure used in the interferometric project.

9.5.4 The voltage applied to the crystal

On account of the small magnitude of the effect being investigated, relatively large electric fields had to be applied across the crystals in order to induce a measurable intensity change in the emerging light. As in the interferometric work, these fields were of the order of $10^5 - 10^6$ Vm^{-1}, depending on the specimen, and again were achieved by way of a three-stage process. In this instance, an initial ac signal of amplitude 100 mV rms was derived from the internal generator of the EG&G lock-in amplifier. This signal was then amplified by a Zopan model PO-27 high-voltage amplifier to provide a signal of variable amplitude up to 80 V, which was then further amplified by a two-stage high-voltage transformer. The signal output from this arrangement was of amplitude up to 1.2 kV rms and was then applied directly to the crystal. To measure the crystal

voltages, a second Meratronik model V541 voltmeter was used, wired permanently in parallel to the specimen, and rated to a maximum voltage of 1.2 kV rms. Since the experiment was concerned with the investigation of crystals free to respond to induced strains, the frequency of the applied field was set to be well below that of any mechanical resonance frequency of the crystal under investigation. It was also chosen not to coincide with the 50 Hz line frequency or of its harmonics. A nominal frequency in the range 80 - 399 Hz was used throughout.

Various measures were also taken to ensure the high voltage generated by the transformer did not interfere with the other electronic apparatus. These included the use of coaxial cable to carry the signal from the transformer to the crystal box, and the positioning of the transformer a safe distance away from the other apparatus, particularly the photodiode, lock-in amplifiers, and the cable carrying the measurement signal. To complete the circuit from the high-voltage coaxial cable, where it entered the crystal container, to the electrode surfaces of the crystal, short thin copper wires were used. These served to isolate the crystal from the supply cable, so ensuring no mechanical restriction was placed on its response to the applied field. Relative changes in the position of the high-voltage supply cable and the crystal were found to have no influence on the results.

9.5 Signal measurement and data acquisition

The component in the signal output from the photodiode at the second harmonic of the frequency of the modulated voltage applied to the crystal was measured by the EG&G model 7220 lock-in amplifier. For its reference, this unit used an internal signal from its waveform generator which was the source of the voltage applied to the crystal. All the various functions for its use were operated by selection switches on its front panel. Throughout this work, since the unit was measuring a second harmonic effect, the 2f mode was selected, and a bandpass filter was chosen on the input line tuned automatically to allow the second harmonic component of the input signal through unhindered, while significantly attenuating higher and lower frequency contributions. For this apparatus a time constant of 1 s was selected, and the sensitivity range was generally set to 10 mV rms full scale deflection. During this work one set the apparatus to establish automatically the phase difference between the measurement and reference signal, and then bring the two into phase. Digital displays indicated the phase shift introduced in the input signal to bring it into phase with the reference, and the amplitude of the measurement signal at the second

harmonic.

A second lock-in amplifier, the Stanford Research SR 530, measured the component of the photodiode signal modulated at the first harmonic. This instrument used as its reference the output signal from the internal waveform generator of the EG&G lock-in amplifier. For this signal determination, a band pass filter on the input line was again favoured, tuned this time to permit the free transmission of the signal at the frequency of the first harmonic. Also, a time constant setting of 1 s was used, and the sensitivity range was typically set to 10 mV rms full scale deflection. As in the second harmonic determination, this lock-in amplifier also established automatically the phase difference between the reference and measurement signal, bringing the two into phase, and giving a measure of this phase difference and the amplitude of the measurement signal when the phases were matched.

Meratronik model V541 digital voltmeters provided a measure of the other two voltage signals required for the polarimetric investigation: the dc output voltage from the photodiode, and the alternating voltage applied to the crystal. For each of these the required voltage range and ac/dc settings were selected. Typically, the dc photodiode signal was in the range 0 - 8 V dc, while the crystal voltage reached a maximum of 1.2 kV rms.

For the two separate polarimetric investigations undertaken, namely for *y*- and *z*-propagation, different means were used to record the necessary data. In the case of *z*-propagation through the crystal the polarimetric system was inherently stable due to the absence of natural birefringence and therefore of temperature-induced phase changes. All the necessary voltages in this case were recorded manually. In contrast, for *y*-propagation the polarimetric system was unstable and subject to continuous temperature-induced phase changes. As a result there was a need for fast and reliable recording of the necessary voltages simultaneously at set intervals of time. Thus in this second experiment a pc computer was used to record the data output from the two lock-in amplifiers and the meter monitoring the dc photodiode signal. In this case, the computer addressed each of the relevant components and recorded to a data file the amplitude of the first and second harmonic signals and the dc photodiode voltage. Each set of these readings was repeated in quick succession, and therefore to a good approximation simultaneously, at 5 - 10 s intervals for the duration of the experiment. The modulated crystal voltage, not being subject to change during an experimental run, was still recorded manually but checked over the duration

of the experiment and the mean value used in the calculations.

9.6 Experimental procedure

To start an experimental run, the optical components were carefully aligned perpendicular to the incident light, the crystal was oriented so that the light traversed the desired crystallographic axis (either the y or z), and the polarization of the light incident on the crystal was set, by rotating the polarizer, at $|45°|$ to the crystallographic x-axis for this propagation path. The analyzer and $\frac{\lambda}{4}$ - plate, the latter being used for z-propagation only, were then set with their fast axes at $|90°|$ and $|45°|$ to the light polarization direction respectively. Thereafter the photodiode was positioned so that the light emerging from the analyzer, via the light density filter, was cast on its aperture. A voltage of amplitude up to 1.2 kV rms was applied across the crystal, so inducing a modulated change in intensity of the light emerging from the system, and both lock-in amplifiers were set to read automatically their respective signals at the first and second harmonics.

For each of the separate investigations the necessary data were recorded as described above. Furthermore, since the y-propagation experiment required the emerging light intensity to vary through its intensity curve, the temperature of the laboratory was deliberately changed during the course of an experimental run, either by turning on the central heating of the laboratory which had previously been left to cool significantly, or by turning off the heating of a warm laboratory. In terms of inducing a quicker temperature change the former procedure proved superior. From the data recorded the desired results were then calculated. The procedure for doing this is described in Chapter 10.

Chapter 10

RESULTS OF THE POLARIMETRIC INVESTIGATION

10.1 Introduction

As in Chapter 9, each polarimetric experiment is treated separately in presenting the results. Considered first is that for propagation along the optic axis of a KDP-type crystal, the experimental arrangement for which is shown in Figure 9.1. For the symmetry class $\bar{4}2m$ and the light-propagation and applied-field configuration used, eqn. (9.18) is applicable, namely

$$\left|I^{2\omega}\right| = \frac{I_o \pi n_o^3 L_z}{4\lambda}\left[g_{xxxx} - g_{yyxx} - n_e^2 r_{xzy}^2\right]\left(E^{(o)}\right)^2. \tag{10.1}$$

Furthermore, from eqns. (9.6), (9.10) and (9.16) the unmodulated intensity of the light emerging from the system is, for negligible absorption in the crystal,

$$I_c = \frac{I_o}{2}. \tag{10.2}$$

The amplitude of the photodiode output signal at the second harmonic of the applied field frequency is, from eqns. (10.1) and (10.2),

$$\left|V^{2\omega}\right| = \frac{V^{dc} \pi n_o^3 L_z (V^{crystal})^2}{2\lambda t^2}\left(g_{xxxx} - g_{yyxx} - n_e^2 r_{xzy}^2\right), \tag{10.3}$$

in which it was assumed that the photodiode output voltage is proportional to the light incident on it. In eqn. (10.3) use was made of the relation $E^{(o)} = V^{crystal}/t$ to express the field in the crystal

in terms of the applied voltage and the distance t between its electrode surfaces. Also, V^{dc} is the photodiode dc output voltage which is taken to give a measure of precisely half the intensity of the light incident on the crystal when the system is balanced at the most sensitive portion of the intensity curve. From eqn. (10.3)

$$\left|g_{xxxx} - g_{yyxx} - n_e^2 r_{xzy}^2\right| = \frac{2\lambda t^2 V^{2\omega}}{V^{dc}\pi n_o^3 L_z (V^{crystal})^2}. \qquad (10.4)$$

In order to determine the difference in the quadratic electro-optic coefficients $|g_{xxxx} - g_{yyxx}|$ from eqn. (10.4), values are required of all the other quantities in it, in particular the voltages V^{dc}, $|V^{2\omega}|$, and $V^{crystal}$.

The second polarimetric system, that shown in Figure 9.2, enables the investigation of the quadratic electro-optic effect in KDP-type crystals for propagation along the *y*-axis. However, for this experimental arrangement, a discussion similar to that above to express the difference in the relevant coefficients in terms of the measured observables is complicated by two factors. First, this optical arrangement is subject to a fluctuating difference in phase between the interfering waves due to temperature-induced changes in the ordinary and extraordinary refractive indices. Second, a contribution from the linear electro-optic effect is invariably present, although it can be allowed for, as discussed in Chapter 9. In terms of the analysis in Chapter 5, this contribution probably arises from very slight misalignments of the crystal, field, and light path. Accordingly, it is not always possible to relate it with any certainty to particular electro-optic coefficients and, by virtue of its origin, it can be expected to vary between experimental runs for slightly different crystal alignments. However, given the possible contribution of the square of this linear term to the induced change in intensity at the second harmonic of the light emerging from the optical system, as given in eqn. (9.12), when the interference pattern is not positioned at its most sensitive point, allowance must be made for it in the calculation of results from the induced intensity change at the second harmonic.

For this optical system and crystal type, subject to the particular light-propagation and applied-field configuration, eqn. (9.22) gives the intensity variation, at the second harmonic of the applied field frequency, of the light emerging from the analyzer as

$$\left|I^{2\omega}\right| = \frac{I_o}{2}\left[\frac{\pi L_y}{2\lambda}\left[n_o^3 g_{xxxx} - n_e^3 g_{zzxx} - n_e^3 n_o^2 r_{xzy}^2\right]\left(E^{(o)}\right)^2 \sin\Delta\phi_c + \tfrac{1}{4}B^2\cos\Delta\phi_c\right]. \qquad (10.5)$$

Hence, for a photodiode voltage output linear in the incident light intensity, the intensities in equations (9.10), (9.11), and (10.5) of the light leaving the analyzer give rise to the voltages in the output from the photodiode of:

$$V^{dc} \approx \frac{V_o}{2}\left(1 - \cos\Delta\phi_c\right), \tag{10.6}$$

$$\left|V^{\omega}\right| = \frac{V_o}{2}\left(B\sin\Delta\phi_c\right), \tag{10.7}$$

$$\left|V^{2\omega}\right| = \frac{V_o}{2}\left[\frac{\pi L_y (V^{crystal})^2}{2\lambda t^2}\left(n_o^3 g_{xxxx} - n_e^3 g_{zzxx} - n_e^3 n_o^2 r_{xzy}^2\right)\sin\Delta\phi_c + \tfrac{1}{4}B^2\cos\Delta\phi_c\right]. \tag{10.8}$$

Again, in the derivation of (10.8), the relation $E^{(o)} = V^{crystal}/t$ was used and V_o is assumed, in the absence of absorption, to give a measure of the intensity of the light incident on the crystal and is the peak dc voltage output from the photodiode as the phase $\Delta\phi_c$ changes.

Hence, with the use of eqns. (10.6) - (10.8), knowledge of n_o, n_e, r_{xzy}, L_y, t, and λ, and the analysis of data which represent repeated measurements of V^{dc}, $|V^{\omega}|$, and $|V^{2\omega}|$ for a modulated voltage of fixed amplitude $V^{crystal}$ applied to the crystal when the polarimetric apparatus is left in an environment of gradually changing temperature to fluctuate through its intensity range, the value of $|n_o^3 g_{xxxx} - n_e^3 g_{zzxx}|$ may be calculated.

10.2 The experimental variables

10.2.1 Refractive indices and the linear electro-optic coefficient r_{xzy}

Calculation of the difference in unknown electro-optic coefficients $|g_{xxxx} - g_{yyxx}|$ and $|n_o^3 g_{xxxx} - n_e^3 g_{zzxx}|$ from eqns. (10.4) and (10.6) - (10.8) requires knowledge of the ordinary and extraordinary refractive indices of KDP, ADP, and DKDP for the wavelength and temperature of the experiment, as well as the value of the linear electro-optic coefficient r_{xzy}.

As in the interferometric project, the ordinary and extraordinary refractive indices for the various crystals were calculated from the Sellmeier equations and tabulated Sellmeier coefficients in a paper by Ghosh and Bhar (1982). These results were calculated for a wavelength of 632.8 nm and for an average room temperature of 21 °C. Values for the coefficient r_{xzy} of KDP, ADP, and DKDP were again taken from recommended values by Landolt-Börnstein (1979) for the same

wavelength and temperature. These results are listed in Table 10.1.

Table 10.1 Values used for n_o, n_e, and r_{xy} for KDP, ADP, and DKDP at 632.8 nm and 21 °C

Crystal	n_o	n_e	r_{xy} (10^{-12} mV^{-1})
KDP	1.5075	1.4670	8.7
ADP	1.5222	1.4773	23.4
DKDP	1.5042	1.4653	8.8

10.2.2 Dimensions of the crystals

Measurements of the dimensions of the various KDP, ADP, and DKDP crystals were made by means of a travelling microscope. These results included the distance t between the coated electrode surfaces of each crystal, and the dimensions in the two orthogonal directions L_y and L_z along which the light was set to propagate. All these values are given in Table 10.2. Again, as in the interferometric work, these readings were taken over the entire surface of the respective crystals, and in presenting the results, the mean of a set of measurements for a particular dimension is quoted together with the standard error in that mean σ_m, as defined in eqn. (8.12). This error was the maximum uncertainty in each dimension.

Table 10.2 The dimensions of the crystals

Crystal	t $\pm \sigma_m$ (mm)	$L_y \pm \sigma_m$ (mm)	$L_z \pm \sigma_m$ (mm)
KDP	4.99 ± 0.01	50.05 ± 0.02	49.77 ± 0.02
ADP (large)	5.01 ± 0.02	50.27 ± 0.02	51.22 ± 0.02
ADP (medium)	7.06 ± 0.02	34.58 ± 0.04	35.54 ± 0.02
ADP (small)	4.30 ± 0.05	26.03 ± 0.02	26.12 ± 0.02
DKDP (large)	5.35 ± 0.02	30.22 ± 0.02	29.70 ± 0.03
DKDP (small)	4.22 ± 0.02	25.05 ± 0.03	25.31 ± 0.02

10.2.3 The measured voltages

The voltages that enter eqns. (10.4) and (10.6) - (10.8) required for the determination of the results were the crystal voltage, photodiode dc output voltage, and the modulated components of the photodiode output signal at the first and second harmonics of the applied field frequency. The measurement of each has been described in Section 9.5. Of these, both the crystal voltage

and dc photodiode output were measured by means of Meratronik model V541 voltmeters, the accuracy of which is specified to better than 0.2% in the temperature range 18 - 28°C, and decreasing by 0.1% for each additional 10°C. Since the temperature of the laboratory was observed to drop below 18°C during the course of the research, specifically when varying the temperature of the laboratory for the *y*-propagation investigations, these meters were taken to have an accuracy of 0.3% for this work. The first and second harmonics' voltages in the photodiode output signal were known to within 1% and 0.5%, respectively, in accordance with the Stanford Research and EG&G lock-in amplifiers' manufacturer's ratings.

10.3 Uncertainty in the final results

In each instance of determining a value of the difference in quadratic electro-optic coefficients for a particular voltage applied to the crystal specimen, a number of readings of the voltages V^{dc}, $|V^{\omega}|$ (where applicable), and $|V^{2\omega}|$ was made. These voltage measurements were recorded either for the same static phase conditions for the *z*-propagation investigation, with the only change being the rotation of the $\frac{\lambda}{4}$ - plate in 90° steps through 360° to satisfy each |45°| alignment possibility relative to the incident light polarization, or at regular intervals of time for *y*-propagation as the system varied with the fluctuating phase shift. After each set of readings was complete for a determination of the particular difference in quadratic electro-optic coefficients, the mean of the calculated results was recorded together with the standard error in the mean. At the end of an investigation on a particular crystal, the mean of all the means for each set of determinations was calculated together with the standard error in this mean. This was then taken to be the final result for the particular investigation, with a quoted accuracy which was estimated by taking into account the maximum uncertainties in the quantities entering the relevant equations from which it was calculated, as well as the statistical spread, or standard error, involved in calculating the result from the measured voltages. In this case the maximum relative uncertainty was computed as the square root of the sum of the squares of the relative standard error in its measurement and the relative standard errors in each quantity used in its calculation.

10.4 Results for *z*-propagation through KDP, ADP, and DKDP

This section contains all the results for the *z*-propagation polarimetric investigations on the six separate crystals of KDP, ADP, and DKDP which yield values for the difference in the quadratic electro-optic coefficients $|g_{xxxx} - g_{yyxx}|$. For this configuration measurement of the crystal voltage $V^{crystal}$ and corresponding photodiode dc and second harmonic output voltages V^{dc} and $|V^{2\omega}|$ allowed the calculation of this difference in quadratic electro-optic coefficients through the use of eqn. (10.4). All the results for these voltages for the separate investigations of the various crystal are shown in Tables 10.3 - 10.8. Each set of readings entered in a row of these tables contains the particular voltage applied to the crystal under investigation, the field which it produces in the crystal, and the corresponding means of the photodiode dc and second harmonic output voltages, V^{dc} and $|V^{2\omega}|$, measured for the four possible $|45°|$ orientations of the $\frac{\lambda}{4}$ - plate relative to the polarizer's fast axis. Furthermore, together with the mean of the measured photodiode dc and second harmonic output voltages is quoted the standard error σ_m in the mean as defined by eqn. (8.12). From this data for a particular set of readings, and with the use of eqn. (10.4) and the measured quantities in Tables 10.1 and 10.2, the value of $|g_{xxxx} - g_{yyxx} - (n_e r_{xzy})^2|$ was calculated and entered into the final column of the table. Also given is the standard error of this result, the relative magnitude of which is the square root of the sum of the squares of the relative photodiode dc and second harmonic output voltage standard errors.

Throughout this work for the *z*-propagation investigations, the photodiode output voltage modulated at the first harmonic was monitored, but was seldom observed to exceed 2 mV rms. This indicated, first, that the intensity response linear in the field was sufficiently small to neglect its possible square contribution to the second harmonic's signal of typical magnitude 2 - 3 mV (see Tables 10.3 - 10.8) and, second, that the static phase shift introduced in the optical arrangement was at the desired 90°. When this latter condition was not met, the first harmonic signal was seen to be larger.

Table 10.3 Results for *z*-propagation through the KDP crystal

$V^{crystal}$ (V)	E (10^5 Vm^{-1})	V^{dc} (V)	$V^{2\omega}$ (mV)	$\lvert g_{xxxx} - g_{yyxx} - (n_e r_{xy})^2 \rvert$ (10^{-20} m^2V^{-2})
1078	2.160	2.193 ± 0.018	2.125 ± 0.007	3.470 ± 0.031
1168	2.341	2.546 ± 0.032	2.891 ± 0.037	3.460 ± 0.062
1125	2.255	2.622 ± 0.039	2.787 ± 0.015	3.490 ± 0.055
1004	2.012	2.388 ± 0.029	2.003 ± 0.017	3.460 ± 0.051
1004	2.012	2.108 ± 0.012	1.773 ± 0.016	3.470 ± 0.037
1134	2.273	2.487 ± 0.017	2.702 ± 0.007	3.510 ± 0.026
1177	2.359	2.538 ± 0.031	2.992 ± 0.019	3.540 ± 0.049
1037	2.078	2.032 ± 0.004	1.835 ± 0.004	3.490 ± 0.010
1158	2.321	3.059 ± 0.041	3.201 ± 0.038	3.250 ± 0.058
1115	2.234	3.502 ± 0.058	3.408 ± 0.040	3.260 ± 0.066
1176	2.357	2.606 ± 0.023	2.840 ± 0.015	3.280 ± 0.034
1198	2.401	3.553 ± 0.037	3.966 ± 0.033	3.240 ± 0.043
1182	2.369	3.603 ± 0.030	3.928 ± 0.039	3.250 ± 0.042
				3.398 ± 0.033

Table 10.4 Results for *z*-propagation through the large ADP crystal

$V^{crystal}$ (V)	E (10^5 Vm^{-1})	V^{dc} (V)	$V^{2\omega}$ (mV)	$\lvert g_{xxxx} - g_{yyxx} - (n_e r_{xy})^2 \rvert$ (10^{-20} m^2V^{-2})
1170	2.335	2.019 ± 0.022	4.176 ± 0.031	5.981 ± 0.078
1132	2.259	2.140 ± 0.017	4.241 ± 0.038	6.120 ± 0.072
1106	2.208	2.324 ± 0.022	4.337 ± 0.019	6.037 ± 0.062
1064	2.124	2.360 ± 0.016	4.061 ± 0.022	6.016 ± 0.053
1035	2.066	2.331 ± 0.019	3.782 ± 0.008	5.996 ± 0.049
966.1	1.928	2.264 ± 0.018	3.219 ± 0.012	6.029 ± 0.052
1196	2.387	2.470 ± 0.026	5.395 ± 0.075	6.045 ± 0.105
1099	2.194	2.198 ± 0.023	4.063 ± 0.023	6.058 ± 0.071
1099	2.194	2.084 ± 0.056	3.869 ± 0.040	6.084 ± 0.175
1125	2.246	2.266 ± 0.074	4.345 ± 0.023	5.997 ± 0.198
1079	2.154	2.022 ± 0.063	3.588 ± 0.019	6.033 ± 0.192
1173	2.341	1.619 ± 0.017	3.298 ± 0.033	5.858 ± 0.085
1185	2.365	2.599 ± 0.035	5.387 ± 0.072	5.843 ± 0.111
1008	2.012	2.554 ± 0.020	3.868 ± 0.027	5.899 ± 0.062
1098	2.192	2.603 ± 0.046	4.669 ± 0.048	5.889 ± 0.121
1153	2.301	2.531 ± 0.088	5.190 ± 0.026	6.105 ± 0.215

continued

continued from previous page				
$V^{crystal}$ (V)	E (10^5 Vm^{-1})	V^{dc} (V)	$V^{2\omega}$ (mV)	$\lvert g_{xxxx} - g_{yyxx} - (n_e r_{xzy})^2 \rvert$ (10^{-20} m^2V^{-2})
1153	2.301	2.395 ± 0.014	4.806 ± 0.046	5.975 ± 0.067
1194	2.383	2.709 ± 0.080	5.973 ± 0.070	6.122 ± 0.195
1071	2.138	2.334 ± 0.045	4.000 ± 0.064	5.912 ± 0.149
988.4	1.973	2.718 ± 0.044	4.006 ± 0.027	5.971 ± 0.105
1134	2.263	2.367 ± 0.026	4.750 ± 0.014	6.175 ± 0.071
1194	2.383	2.431 ± 0.011	5.266 ± 0.025	6.015 ± 0.040
1017	2.030	2.589 ± 0.031	4.060 ± 0.058	6.001 ± 0.112
1090	2.176	2.377 ± 0.037	4.303 ± 0.033	6.029 ± 0.105
1090	2.176	1.927 ± 0.034	3.463 ± 0.034	5.987 ± 0.121
1190	2.375	2.519 ± 0.029	5.436 ± 0.043	6.030 ± 0.084
1021	2.038	2.678 ± 0.092	4.456 ± 0.028	6.317 ± 0.219
1143	2.281	2.490 ± 0.028	4.994 ± 0.045	6.076 ± 0.087
1161	2.317	2.807 ± 0.029	5.737 ± 0.052	6.001 ± 0.082
1089	2.174	2.820 ± 0.041	5.045 ± 0.030	5.971 ± 0.093
924.4	1.845	2.791 ± 0.023	3.583 ± 0.027	5.947 ± 0.066
1176	2.347	2.079 ± 0.013	4.326 ± 0.041	5.956 ± 0.068
1176	2.347	2.313 ± 0.070	4.910 ± 0.098	6.074 ± 0.219
1114	2.224	2.698 ± 0.026	5.022 ± 0.013	5.937 ± 0.060
1154	2.303	2.381 ± 0.013	4.857 ± 0.020	5.908 ± 0.099
1003	2.002	2.590 ± 0.033	3.889 ± 0.042	6.128 ± 0.204
1035	2.066	2.512 ± 0.083	4.166 ± 0.023	6.062 ± 0.042
1089	2.174	2.661 ± 0.057	4.909 ± 0.036	6.157 ± 0.140
1032	2.060	2.636 ± 0.043	4.382 ± 0.037	6.177 ± 0.114
1196	2.387	2.360 ± 0.004	5.157 ± 0.009	6.048 ± 0.014
				6.024 ± 0.015

Table 10.5 Results for *z*-propagation through the medium ADP crystal

$V^{crystal}$ (V)	E (10^5 Vm^{-1})	V^{dc} (V)	$V^{2\omega}$ (mV)	$\lvert g_{xxxx} - g_{yyxx} - (n_e r_{xzy})^2 \rvert$ (10^{-20} m^2V^{-2})
1157	1.639	3.357 ± 0.064	2.399 ± 0.010	6.046 ± 0.118
1197	1.695	3.284 ± 0.081	2.514 ± 0.012	6.051 ± 0.153
1017	1.441	3.250 ± 0.075	1.810 ± 0.005	6.100 ± 0.142
1080	1.530	3.302 ± 0.081	2.056 ± 0.026	6.047 ± 0.167
				continued

continued from previous page

$V^{crystal}$ (V)	E (10^5 Vm^{-1})	V^{dc} (V)	$V^{2\omega}$ (mV)	$\lvert g_{xxxx} - g_{yyxx} - (n_e r_{xzy})^2 \rvert$ (10^{-20} m^2V^{-2})
1030	1.459	3.208 ± 0.081	1.824 ± 0.012	6.070 ± 0.158
1087	1.540	3.242 ± 0.076	2.052 ± 0.023	6.068 ± 0.158
1117	1.582	3.216 ± 0.058	2.143 ± 0.031	6.050 ± 0.140
1189	1.684	3.197 ± 0.077	2.421 ± 0.013	6.067 ± 0.150
1190	1.686	3.266 ± 0.067	2.484 ± 0.011	6.083 ± 0.129
1035	1.466	3.157 ± 0.075	1.832 ± 0.011	6.134 ± 0.150
1061	1.503	3.319 ± 0.079	1.990 ± 0.011	6.034 ± 0.148
1116	1.581	3.272 ± 0.081	2.199 ± 0.016	6.112 ± 0.158
1116	1.581	3.207 ± 0.064	2.135 ± 0.006	6.056 ± 0.123
1181	1.673	3.148 ± 0.068	2.362 ± 0.009	6.094 ± 0.134
799.0	1.132	3.201 ± 0.086	1.102 ± 0.004	6.106 ± 0.165
901.4	1.277	3.151 ± 0.053	1.369 ± 0.007	6.057 ± 0.107
1106	1.567	3.171 ± 0.079	2.110 ± 0.010	6.163 ± 0.157
1161	1.644	3.203 ± 0.073	2.341 ± 0.011	6.141 ± 0.144
1199	1.698	3.059 ± 0.074	2.365 ± 0.025	6.091 ± 0.162
1064	1.507	3.078 ± 0.076	1.889 ± 0.023	6.139 ± 0.148
1172	1.660	3.096 ± 0.090	2.294 ± 0.014	6.111 ± 0.149
1125	1.593	3.100 ± 0.089	2.098 ± 0.013	6.057 ± 0.169
1195	1.693	3.030 ± 0.073	2.315 ± 0.010	6.061 ± 0.181
1034	1.465	3.044 ± 0.071	1.766 ± 0.011	6.147 ± 0.161
1034	1.465	2.902 ± 0.068	1.673 ± 0.012	6.107 ± 0.178
1101	1.559	3.204 ± 0.084	2.079 ± 0.010	6.062 ± 0.148
1050	1.487	3.079 ± 0.057	1.869 ± 0.009	6.236 ± 0.119
1120	1.586	3.121 ± 0.074	2.096 ± 0.008	6.064 ± 0.146
1120	1.586	3.202 ± 0.058	2.159 ± 0.007	6.088 ± 0.113
1185	1.678	3.212 ± 0.068	2.432 ± 0.010	6.107 ± 0.132
1052	1.490	3.203 ± 0.073	1.894 ± 0.014	6.053 ± 0.145
1095	1.551	3.205 ± 0.075	2.057 ± 0.007	6.063 ± 0.144
1150	1.629	3.146 ± 0.074	2.228 ± 0.012	6.066 ± 0.147
1191	1.687	2.944 ± 0.069	2.255 ± 0.016	6.116 ± 0.150
1109	1.571	3.251 ± 0.092	2.136 ± 0.023	6.051 ± 0.184
1046	1.482	2.728 ± 0.085	1.593 ± 0.015	6.045 ± 0.198
1047	1.483	3.185 ± 0.095	1.862 ± 0.013	6.041 ± 0.186
998.2	1.414	3.210 ± 0.088	1.702 ± 0.001	6.026 ± 0.165
1112	1.575	3.083 ± 0.085	2.033 ± 0.014	6.041 ± 0.171
1190	1.686	3.328 ± 0.076	2.525 ± 0.009	6.069 ± 0.139

continued

continued from previous page				
$V^{crystal}$ (V)	E (10^5 Vm^{-1})	V^{dc} (V)	$V^{2\omega}$ (mV)	$\lvert g_{xxxx} - g_{yyxx} - (n_e r_{xzy})^2 \rvert$ (10^{-20} m^2V^{-2})
1079	1.528	3.256 ± 0.076	2.033 ± 0.016	6.076 ± 0.149
1143	1.619	3.266 ± 0.070	2.316 ± 0.017	6.148 ± 0.139
1185	1.678	3.280 ± 0.080	2.490 ± 0.006	6.123 ± 0.150
972.9	1.378	3.302 ± 0.056	1.686 ± 0.008	6.109 ± 0.108
973.2	1.378	3.312 ± 0.056	1.669 ± 0.007	6.027 ± 0.104
1061	1.503	3.270 ± 0.046	1.965 ± 0.028	6.047 ± 0.122
1130	1.601	3.199 ± 0.058	2.184 ± 0.010	6.055 ± 0.113
1189	1.684	3.265 ± 0.071	2.486 ± 0.007	6.100 ± 0.134
1189	1.684	3.229 ± 0.079	2.461 ± 0.012	6.108 ± 0.152
1196	1.694	3.310 ± 0.079	2.545 ± 0.021	6.089 ± 0.155
1003	1.421	3.098 ± 0.087	1.757 ± 0.008	6.384 ± 0.181
1119	1.585	3.047 ± 0.099	2.078 ± 0.012	6.169 ± 0.203
1120	1.586	3.301 ± 0.082	2.253 ± 0.014	6.163 ± 0.158
1163	1.647	3.239 ± 0.081	2.365 ± 0.008	6.116 ± 0.155
1103	1.562	3.330 ± 0.081	2.172 ± 0.015	6.074 ± 0.154
1198	1.697	3.277 ± 0.075	2.523 ± 0.023	6.075 ± 0.149
				6.093 ± 0.008

Table 10.6 Results for *z*-propagation through the small ADP crystal

$V^{crystal}$ (V)	E (10^5 Vm^{-1})	V^{dc} (V)	$V^{2\omega}$ (mV)	$\lvert g_{xxxx} - g_{yyxx} - (n_e r_{xzy})^2 \rvert$ (10^{-20} m^2V^{-2})
1196	2.781	3.318 ± 0.093	4.944 ± 0.028	5.956 ± 0.170
1108	2.577	3.346 ± 0.109	4.203 ± 0.034	5.850 ± 0.197
1108	2.577	3.159 ± 0.084	4.077 ± 0.025	6.010 ± 0.163
1151	2.677	3.300 ± 0.100	4.559 ± 0.034	5.963 ± 0.187
1104	2.567	3.203 ± 0.077	4.110 ± 0.028	6.018 ± 0.151
1191	2.770	3.319 ± 0.076	4.897 ± 0.023	5.946 ± 0.139
1037	2.412	3.190 ± 0.089	3.595 ± 0.020	5.991 ± 0.170
1070	2.488	3.268 ± 0.126	3.905 ± 0.024	5.967 ± 0.232
1128	2.623	3.200 ± 0.083	4.274 ± 0.045	6.001 ± 0.169
1167	2.714	3.183 ± 0.079	4.579 ± 0.028	6.039 ± 0.155
1024	2.381	3.180 ± 0.072	3.490 ± 0.026	5.983 ± 0.142
1197	2.784	3.143 ± 0.080	4.731 ± 0.045	6.006 ± 0.163

continued

continued from previous page

$V^{crystal}$ (V)	E (10^5 Vm^{-1})	V^{dc} (V)	$V^{2\omega}$ (mV)	$\lvert g_{xxxx} - g_{yyxx} - (n_e r_{xzy})^2 \rvert$ (10^{-20} m^2V^{-2})
1024	2.381	3.188 ± 0.056	3.514 ± 0.024	6.009 ± 0.112
1172	2.726	3.184 ± 0.047	4.626 ± 0.020	6.048 ± 0.092
1112	2.586	3.403 ± 0.167	4.276 ± 0.008	5.809 ± 0.286
1071	2.491	3.193 ± 0.051	3.859 ± 0.004	6.023 ± 0.097
1187	2.760	3.264 ± 0.047	4.778 ± 0.021	5.940 ± 0.089
1098	2.553	3.197 ± 0.052	4.028 ± 0.028	5.976 ± 0.106
1109	2.579	3.144 ± 0.043	4.040 ± 0.026	5.973 ± 0.091
1142	2.656	3.259 ± 0.034	4.407 ± 0.021	5.928 ± 0.068
1181	2.747	3.101 ± 0.049	4.536 ± 0.029	5.996 ± 0.103
1023	2.379	3.090 ± 0.040	3.377 ± 0.027	5.969 ± 0.090
1068	2.484	3.234 ± 0.041	3.785 ± 0.059	5.866 ± 0.119
1112	2.586	3.127 ± 0.057	4.035 ± 0.031	5.966 ± 0.118
1145	2.663	3.104 ± 0.031	4.284 ± 0.024	6.019 ± 0.069
1194	2.777	3.087 ± 0.020	4.649 ± 0.025	6.039 ± 0.050
1049	2.440	3.090 ± 0.046	3.574 ± 0.029	6.011 ± 0.102
1095	2.547	3.126 ± 0.029	3.940 ± 0.025	6.009 ± 0.069
1153	2.681	3.115 ± 0.015	4.354 ± 0.019	6.011 ± 0.038
1197	2.784	3.152 ± 0.044	4.722 ± 0.057	5.978 ± 0.110
1073	2.495	3.156 ± 0.017	3.813 ± 0.019	6.000 ± 0.044
1036	2.409	3.157 ± 0.050	3.423 ± 0.080	5.775 ± 0.163
1089	2.533	2.960 ± 0.041	3.595 ± 0.028	5.856 ± 0.061
1016	2.363	2.912 ± 0.027	3.114 ± 0.013	5.922 ± 0.086
1070	2.488	2.931 ± 0.019	3.473 ± 0.021	5.917 ± 0.120
1184	2.753	3.014 ± 0.026	4.344 ± 0.026	5.879 ± 0.094
1155	2.686	2.936 ± 0.040	4.033 ± 0.022	5.888 ± 0.061
1101	2.560	3.027 ± 0.060	3.752 ± 0.022	5.846 ± 0.053
1127	2.621	2.952 ± 0.022	3.878 ± 0.012	5.914 ± 0.047
1187	2.760	2.957 ± 0.027	4.320 ± 0.037	5.929 ± 0.074
1156	2.688	3.182 ± 0.068	4.408 ± 0.032	5.926 ± 0.134
1191	2.770	3.250 ± 0.056	4.747 ± 0.044	5.887 ± 0.114
1065	2.477	3.153 ± 0.056	3.707 ± 0.017	5.926 ± 0.109
1123	2.612	3.228 ± 0.061	4.208 ± 0.024	5.909 ± 0.116
1142	2.656	3.227 ± 0.054	4.340 ± 0.032	5.896 ± 0.107
1195	2.779	3.333 ± 0.051	4.916 ± 0.035	5.905 ± 0.099
1102	2.563	3.256 ± 0.042	4.060 ± 0.031	5.870 ± 0.087
1030	2.395	3.362 ± 0.043	3.637 ± 0.022	5.831 ± 0.083
				5.945 ± 0.010

Table 10.7 Results for *z*-propagation through the large DKDP crystal

$V^{crystal}$ (V)	E (10^5 Vm^{-1})	V^{dc} (V)	$V^{2\omega}$ (mV)	$\lvert g_{xxxx} - g_{yyxx} - (n_e r_{xzy})^2 \rvert$ (10^{-20} m^2V^{-2})
1188	2.221	1.543 ± 0.075	0.904 ± 0.011	3.347 ± 0.169
1084	2.026	1.549 ± 0.072	0.756 ± 0.009	3.350 ± 0.160
1007	1.882	2.134 ± 0.083	0.897 ± 0.010	3.344 ± 0.135
974.9	1.822	2.383 ± 0.100	0.934 ± 0.010	3.325 ± 0.145
1141	2.133	2.378 ± 0.101	1.277 ± 0.011	3.327 ± 0.144
1141	2.133	1.563 ± 0.080	0.837 ± 0.012	3.316 ± 0.176
1040	1.944	1.612 ± 0.064	0.726 ± 0.007	3.357 ± 0.137
1108	2.071	2.017 ± 0.065	1.049 ± 0.003	3.416 ± 0.110
1160	2.168	2.064 ± 0.091	1.137 ± 0.017	3.303 ± 0.154
1130	2.112	1.713 ± 0.084	0.900 ± 0.007	3.318 ± 0.164
940.8	1.759	1.759 ± 0.077	0.638 ± 0.007	3.306 ± 0.150
1175	2.196	1.796 ± 0.095	0.998 ± 0.014	3.245 ± 0.178
1190	2.224	1.873 ± 0.082	1.116 ± 0.009	3.392 ± 0.151
1131	2.114	2.660 ± 0.160	1.482 ± 0.012	3.513 ± 0.213
988.9	1.848	2.578 ± 0.099	1.061 ± 0.012	3.394 ± 0.137
1136	2.123	1.634 ± 0.074	0.891 ± 0.007	3.407 ± 0.158
1122	2.097	1.794 ± 0.060	0.962 ± 0.006	3.438 ± 0.118
852.3	1.593	1.616 ± 0.042	0.498 ± 0.006	3.418 ± 0.098
1155	2.159	1.938 ± 0.069	1.100 ± 0.008	3.431 ± 0.125
1129	2.110	1.599 ± 0.069	0.802 ± 0.006	3.176 ± 0.139
1129	2.110	1.490 ± 0.061	0.790 ± 0.010	3.356 ± 0.143
1192	2.228	1.455 ± 0.060	0.862 ± 0.010	3.362 ± 0.144
1142	2.135	2.035 ± 0.106	1.087 ± 0.011	3.303 ± 0.175
1088	2.034	2.767 ± 0.127	1.345 ± 0.011	3.313 ± 0.154
1005	1.879	1.632 ± 0.077	0.687 ± 0.008	3.362 ± 0.164
1175	2.196	1.292 ± 0.060	0.737 ± 0.007	3.332 ± 0.158
1119	2.092	2.240 ± 0.086	1.163 ± 0.008	3.344 ± 0.131
1092	2.041	1.619 ± 0.057	0.807 ± 0.005	3.373 ± 0.120
1014	1.895	1.366 ± 0.052	0.584 ± 0.005	3.353 ± 0.131
1144	2.138	1.813 ± 0.078	0.983 ± 0.004	3.341 ± 0.144
1092	2.041	1.875 ± 0.086	0.927 ± 0.005	3.344 ± 0.155
1030	1.925	2.880 ± 0.121	1.272 ± 0.019	3.358 ± 0.149
1197	2.237	2.039 ± 0.073	1.181 ± 0.004	3.261 ± 0.117
1182	2.209	2.165 ± 0.115	1.252 ± 0.016	3.338 ± 0.182
1023	1.912	1.845 ± 0.082	0.812 ± 0.006	3.393 ± 0.153
1124	2.101	1.850 ± 0.089	0.976 ± 0.007	3.370 ± 0.164
1170	2.187	1.387 ± 0.054	0.795 ± 0.003	3.377 ± 0.133

continued

continued from previous page				
$V^{crystal}$ (V)	E (10^5 Vm^{-1})	V^{dc} (V)	$V^{2\omega}$ (mV)	$\lvert g_{xxxx} - g_{yyxx} - (n_e r_{xy})^2 \rvert$ (10^{-20} m^2V^{-2})
1079	2.017	1.544 ± 0.076	0.748 ± 0.005	3.355 ± 0.166
1198	2.239	1.618 ± 0.076	0.966 ± 0.009	3.357 ± 0.161
1035	1.935	1.729 ± 0.093	0.761 ± 0.005	3.314 ± 0.179
1165	2.178	1.717 ± 0.081	0.972 ± 0.007	3.365 ± 0.160
1100	2.056	1.729 ± 0.084	0.867 ± 0.009	3.342 ± 0.166
1157	2.163	2.223 ± 0.070	1.252 ± 0.009	3.394 ± 0.109
1084	2.026	1.961 ± 0.072	0.963 ± 0.005	3.373 ± 0.126
1009	1.886	2.052 ± 0.086	0.865 ± 0.005	3.340 ± 0.141
1178	2.202	1.847 ± 0.086	1.045 ± 0.010	3.290 ± 0.156
				3.351 ± 0.008

Table 10.8 Results for *z*-propagation through the small DKDP crystal

$V^{crystal}$ (V)	E (10^5 Vm^{-1})	V^{dc} (V)	$V^{2\omega}$ (mV)	$\lvert g_{xxxx} - g_{yyxx} - (n_e r_{xy})^2 \rvert$ (10^{-20} m^2V^{-2})
1188	2.815	2.690 ± 0.092	2.237 ± 0.011	3.470 ± 0.120
1114	2.640	2.706 ± 0.102	1.978 ± 0.010	3.468 ± 0.132
1065	2.524	2.711 ± 0.069	1.835 ± 0.034	3.516 ± 0.111
1162	2.754	2.572 ± 0.096	2.065 ± 0.021	3.502 ± 0.136
1162	2.754	2.642 ± 0.101	2.108 ± 0.014	3.480 ± 0.135
1162	2.754	2.733 ± 0.092	2.101 ± 0.027	3.353 ± 0.120
1188	2.815	3.058 ± 0.064	2.530 ± 0.023	3.452 ± 0.079
1172	2.777	2.689 ± 0.089	2.173 ± 0.018	3.464 ± 0.118
1063	2.519	3.107 ± 0.137	2.075 ± 0.011	3.480 ± 0.155
1064	2.521	3.104 ± 0.130	2.065 ± 0.010	3.461 ± 0.146
1149	2.723	3.089 ± 0.130	2.378 ± 0.020	3.434 ± 0.147
1189	2.818	3.109 ± 0.137	2.585 ± 0.021	3.463 ± 0.155
1082	2.564	3.074 ± 0.101	2.125 ± 0.009	3.477 ± 0.115
1149	2.723	2.878 ± 0.128	2.231 ± 0.028	3.459 ± 0.160
1197	2.836	2.908 ± 0.112	2.468 ± 0.010	3.488 ± 0.135
1100	2.607	2.986 ± 0.113	2.144 ± 0.022	3.495 ± 0.137
1052	2.493	3.026 ± 0.109	1.974 ± 0.008	3.472 ± 0.126
1052	2.493	3.104 ± 0.135	2.006 ± 0.012	3.438 ± 0.151
988.1	2.341	3.084 ± 0.135	1.764 ± 0.015	3.450 ± 0.154

continued

continued from previous page				
$V^{crystal}$ (V)	E (10^5 Vm^{-1})	V^{dc} (V)	$V^{2\omega}$ (mV)	$\lvert g_{xxxx} - g_{yyxx} - (n_e r_{xy})^2 \rvert$ (10^{-20} m^2V^{-2})
1116	2.645	3.067 ± 0.080	2.242 ± 0.014	3.456 ± 0.093
1188	2.815	3.191 ± 0.068	2.625 ± 0.007	3.432 ± 0.074
1020	2.417	3.116 ± 0.124	1.885 ± 0.004	3.424 ± 0.136
1066	2.526	3.185 ± 0.135	2.121 ± 0.011	3.451 ± 0.147
1127	2.671	3.264 ± 0.133	2.451 ± 0.013	3.482 ± 0.143
965.3	2.287	3.306 ± 0.063	1.802 ± 0.020	3.445 ± 0.076
1047	2.481	3.174 ± 0.052	2.064 ± 0.016	3.494 ± 0.064
1164	2.758	3.331 ± 0.075	2.659 ± 0.010	3.469 ± 0.079
1194	2.829	3.174 ± 0.146	2.661 ± 0.043	3.463 ± 0.169
1116	2.645	3.130 ± 0.122	2.312 ± 0.007	3.492 ± 0.137
1157	2.742	3.234 ± 0.138	2.538 ± 0.021	3.452 ± 0.150
1098	2.602	3.263 ± 0.160	2.286 ± 0.031	3.422 ± 0.174
1061	2.514	3.275 ± 0.096	2.138 ± 0.017	3.415 ± 0.103
1004	2.379	3.231 ± 0.040	1.897 ± 0.012	3.429 ± 0.048
1153	2.732	3.572 ± 0.049	2.732 ± 0.013	3.388 ± 0.049
1192	2.825	3.364 ± 0.124	2.750 ± 0.011	3.388 ± 0.126
1018	2.412	3.360 ± 0.163	2.006 ± 0.023	3.392 ± 0.169
				3.453 ± 0.006

Table 10.9 lists the final results for $|g_{xxxx} - g_{yyxx}|$ obtained for the KDP, ADP, and DKDP crystals investigated in this polarimetric work. These results follow from Tables 10.3 - 10.8 and in addition, allowance was made, in the calculation of the maximum error in these values, for the uncertainty in the quantities given in Table 10.2 and from which the coefficients were calculated through the use of eqn. (10.4). Since only the magnitude of the difference in electro-optic coefficients $|g_{xxxx} - g_{yyxx} - (n_e r_{xy})^2|$ is determined by this polarimetric method and because the contribution in the linear electro-optic coefficients r_{xy} represents only about 0.2 % of the measured value, in quoting the result for $|g_{xxxx} - g_{yyxx}|$ in each case the linear electro-optic contribution was, to a very good approximation, neglected. Its magnitude was, however, included in the uncertainty in the result.

Table 10.9 Results for $|g_{xxxx} - g_{yyxx}|$ (in units of 10^{-20} m^2V^{-2}) for *z*-propagation through the various KDP-type crystals investigated in the polarimetric work

Crystal	$\|g_{xxxx} - g_{yyxx}\|$
KDP	3.40 ± 0.11
ADP (large)	6.02 ± 0.18
ADP (medium)	6.09 ± 0.16
ADP (small)	5.95 ± 0.27
DKDP (large)	3.35 ± 0.10
DKDP (small)	3.45 ± 0.11

10.5 Results for *y*-propagation through KDP and ADP

The procedure for obtaining the necessary readings in the *y*-propagation polarimetric study, which are required for calculating a value for $|n_o^3 g_{xxxx} - n_e^3 g_{zzxx}|$, was as follows: at the start of an experimental run a modulated voltage of fixed amplitude was applied to the crystal and then, with the photodiode dc, first harmonic, and second harmonic output voltages being monitored, the system was left running while the laboratory temperature gradually increased or decreased. As the phase difference between the waves forming the interference pattern varied on account of the time-changing temperature, the interference pattern detected by the photodiode fluctuated sinusoidally with phase through its intensity range, and the three components of the photodiode output voltages were recorded, in quick succession, to a data file through the use of the pc computer. Typically, these voltages were recorded at 5 - 10 second intervals. Once the system was observed no longer to vary through its intensity range as the laboratory temperature stabilized, the experimental run was terminated by human intervention.

Due to the large quantity of information recorded in this manner by the computer and written to data files, it is impractical, and really not entirely necessary, to present it all in this thesis. However, to illustrate the range of voltages which formed the basis for the calculation of results in this investigation, recorded data for one particular experimental run involving the large ADP crystal is given in Table F.1 of Appendix F. Furthermore, Graph F.1 in the same appendix shows the variation of these voltages, particularly their relation to one another, as the experiment progressed and the static phase shift varied with temperature. To analyze all the sets of recorded data, such as those appearing in Table F.1, for each of the crystals investigated in this experiment, in order to determine a value for $|n_o^3 g_{xxxx} - n_e^3 g_{zzxx}|$, use was made of the computer

program presented in Appendix G. As explained in Section 10.1, from each simultaneous recording of voltages V^{dc}, $|V^{\omega}|$, and $|V^{2\omega}|$ for a particular voltage applied to the crystal, and by means of eqns. (10.6) - (10.8) and the values in Tables 10.1 and 10.2 for the particular crystal, a value for $|n_o^3 g_{xxxx} - n_e^3 g_{zzxx} - n_e^3 (n_o r_{xzy})^2|$ could be computed for it.

The first step in the analysis of a set of recorded voltage measurements written to a file was to divide the group of results into separate data files consisting only of dc photodiode voltage variations from either just before a maximum to a the following minimum, or alternatively from a minimum to just after the next maximum, and the first and second harmonic voltages corresponding to these. In other words, new sets of data were established which contained static phase difference variations from 0° to 180°, and vice versa. These new data files were then treated separately. Needed for the calculation of $|n_o^3 g_{xxxx} - n_e^3 g_{zzxx}|$ from eqns. (10.6) - (10.8) is the maximum photodiode dc output V_o, which corresponds to the intensity incident on the crystal. When analyzing the sets of results in this experiment, the computer program established this maximum voltage not as the maximum photodiode dc voltage, but rather as its photodiode dc voltage in the vicinity of maximum corresponding to the magnitude of the second harmonic signal being at a minimum. This was necessary since, as may be clearly seen from Graph F.1, the peak dc photodiode signal is subject to noise, while the minimum of the $|V^{2\omega}|$ is clearly defined, and from eqns. (10.6) - (10.8) these conditions coincide for particular static phase differences. The only proviso was that this dc voltage corresponding to the minimum of $|V^{2\omega}|$ should be no less that 80% of the maximum photodiode dc voltage for the analyzed series. From this value of V_o and the relevant equations the phase difference $\Delta\phi_c$ of each set of recorded photodiode voltages in the series could be calculated, together with the value of B and hence $|n_o^3 g_{xxxx} - n_e^3 g_{zzxx} - n_e^3 (n_o r_{xzy})^2|$.

It must be noted, however, that in practice there is a limit to which recorded voltages used in the analysis yield meaningful results. For instance, when the static phase difference $\Delta\phi_c$ between the interfering waves is in the vicinity of 0° or 180°, corresponding to the static interference pattern intensity at a maximum or minimum respectively, the modulated signals at the first and second harmonics tend to zero. This may easily be seen from eqns. (10.6) - (10.8). Conversely, for the condition when $\Delta\phi_c$ approaches 90°, when the interference pattern is at the point most sensitive to induced phase changes, these signals are at a maximum. Sets of results satisfying this phase

condition are thus more reliable. Throughout this work the range over which phases were accepted was set at 80° - 100°. It was typically observed that as the range over which phases were accepted was increased, though the mean result calculated from a series remained consistent, the standard error gradually increased.

Given in Tables 10.10 - 10.13 are the calculated results for $|n_o^3 g_{xxxx} - n_e^3 g_{zzxx} - n_e^3 (n_o r_{xy})^2|$ based on the computational analysis of all the results obtained in the polarimetric research. These tables present the number of readings from the analyzed series which fall into the accepted phase range 80° - 100°, together with the applied crystal voltage, the corresponding electric field strength, and the mean value, with the standard error, for the difference in quadratic electro-optic coefficients calculated for each set of readings. The final row in each table gives the mean of all the means, and the standard error in that mean.

Table 10.10 Results for *y*-propagation through the KDP crystal

Number of readings	$V^{crystal}$ (V)	E (10^5 Vm^{-1})	$\|n_o^3 g_{xxxx} - n_e^3 g_{zzxx} - n_e^3 (n_o r_{xy})^2\|$ (10^{-20} m^2V^{-2})
74	1190	2.385	8.927 ± 0.386
37	1100	2.204	9.610 ± 0.390
52	1101	2.206	9.519 ± 0.217
36	1059	2.122	9.387 ± 0.228
21	1062	2.128	9.539 ± 0.230
34	1125	2.255	9.921 ± 0.653
67	1127	2.259	8.780 ± 0.182
34	1106	2.216	9.057 ± 0.192
43	1106	2.216	9.176 ± 1.114
54	1106	2.216	9.210 ± 0.149
20	1170	2.345	9.633 ± 0.753
28	1171	2.347	9.355 ± 0.123
55	1173	2.351	8.794 ± 1.127
71	1173	2.351	9.463 ± 0.197
			9.312 ± 0.424

Table 10.11 Results for *y*-propagation through the large ADP crystal

Number of readings	$V^{crystal}$ (V)	E (10^5 Vm^{-1})	$\lvert n_o^3 g_{xxxx} - n_e^3 g_{zzxx} - n_e^3 (n_o r_{xzy})^2 \rvert$ (10^{-20} m^2V^{-2})
5	1108	2.212	28.22 ± 2.96
8	1108	2.212	18.10 ± 5.14
6	1108	2.212	16.00 ± 1.52
8	1108	2.212	21.37 ± 1.84
10	1108	2.212	18.89 ± 3.08
8	1108	2.212	17.04 ± 1.86
11	1108	2.212	19.77 ± 5.94
8	1108	2.212	29.52 ± 4.49
14	1108	2.212	18.09 ± 1.98
15	1062	2.120	21.17 ± 0.37
25	1062	2.120	17.66 ± 2.11
10	1062	2.120	22.41 ± 0.54
7	1063	2.122	21.86 ± 0.43
13	1065	2.126	21.35 ± 1.49
12	1065	2.126	19.26 ± 0.77
15	1066	2.128	19.55 ± 0.68
16	1066	2.128	21.36 ± 0.65
17	1066	2.128	19.61 ± 0.72
19	1066	2.128	21.68 ± 0.77
28	1067	2.130	19.76 ± 0.57
27	1067	2.130	17.68 ± 0.78
23	1023	2.042	21.60 ± 0.71
42	1023	2.042	21.38 ± 0.90
24	1023	2.042	21.03 ± 0.32
28	1023	2.042	20.98 ± 0.70
27	1023	2.042	22.10 ± 1.40
28	1023	2.042	21.23 ± 0.76
25	1023	2.042	20.75 ± 1.09
26	1045	2.086	19.58 ± 0.68
36	1045	2.086	19.98 ± 0.42
49	1045	2.086	18.77 ± 0.61
40	1188	2.371	19.18 ± 0.45
8	1063	2.122	22.48 ± 0.81
16	1175	2.345	19.74 ± 0.33
35	1175	2.345	20.76 ± 0.36
17	1175	2.345	21.31 ± 0.34
9	1063	2.122	21.51 ± 0.48

continued

continued from previous page			
Number of readings	$V^{crystal}$ (V)	E (10^5 Vm^{-1})	$\lvert n_o^3 g_{xxxx} - n_e^3 g_{zzxx} - n_e^3 (n_o r_{xzy})^2 \rvert$ (10^{-20} m^2V^{-2})
16	1175	2.345	20.31 ± 0.37
8	1063	2.122	19.65 ± 0.65
13	1175	2.345	20.27 ± 0.97
21	1177	2.349	19.82 ± 0.66
22	1177	2.349	19.93 ± 0.32
22	1177	2.349	20.77 ± 0.17
23	1177	2.349	21.06 ± 0.22
24	1177	2.349	21.03 ± 0.19
27	1177	2.349	20.71 ± 0.33
18	1177	2.349	19.35 ± 0.42
			20.55 ± 1.13

Table 10.12 Results for *y*-propagation through the medium ADP crystal

Number of readings	$V^{crystal}$ (V)	E (10^5 Vm^{-1})	$\lvert n_o^3 g_{xxxx} - n_e^3 g_{zzxx} - n_e^3 (n_o r_{xzy})^2 \rvert$ (10^{-20} m^2V^{-2})
64	1136	1.611	20.35 ± 0.48
17	1137	1.613	19.64 ± 0.39
28	1138	1.614	20.67 ± 0.22
32	1139	1.616	20.79 ± 0.19
54	1139	1.616	20.16 ± 0.14
27	1178	1.671	18.57 ± 0.60
21	1180	1.674	20.75 ± 0.26
22	1182	1.677	21.78 ± 0.26
22	1182	1.677	20.12 ± 0.39
			20.31 ± 0.32

Table 10.13 Results for *y*-propagation through the small ADP crystal

Number of readings	$V^{crystal}$ (V)	E (10^5 Vm^{-1})	$\lvert n_o^3 g_{xxxx} - n_e^3 g_{zzxx} - n_e^3 (n_o r_{xy})^2 \rvert$ (10^{-20} m^2V^{-2})
49	1179	2.742	20.47 ± 0.97
68	1166	2.712	19.13 ± 0.40
63	1166	2.712	20.20 ± 0.64
61	1088	2.530	19.61 ± 0.43
60	1130	2.628	19.60 ± 0.62
18	1129	2.626	18.97 ± 0.30
40	1130	2.628	19.72 ± 0.50
75	1130	2.628	18.59 ± 0.35
25	1023	2.379	24.03 ± 1.28
18	1022	2.377	20.12 ± 0.82
42	1022	2.377	23.28 ± 1.05
23	1023	2.379	20.52 ± 0.65
48	1024	2.381	21.73 ± 1.22
55	1148	2.670	19.53 ± 0.75
			20.39 ± 0.71

Table 10.14 brings together the final results for $\lvert n_o^3 g_{xxxx} - n_e^3 g_{zzxx} \rvert$ for the KDP and ADP crystals investigated in this work. The uncertainty shown against each result includes the standard error in the corresponding value in Tables 10.10 – 10.13, as well as the maximum errors in the quantities entering the expression from which the result was calculated. Also, as in the case for *z*-propagation, the contribution of the linear electro-optic coefficient r_{xy} was neglected, but its magnitude included in the uncertainty.

Table 10.14 Results for $\lvert n_o^3 g_{xxxx} - n_e^3 g_{zzxx} \rvert$ (in units of 10^{-20} m^2V^{-2}) for *y*-propagation through the KDP and ADP crystals investigated in the polarimetric work

Crystal	$\lvert n_o^3 g_{xxxx} - n_e^3 g_{zzxx} \rvert$
KDP	9.31 ± 0.64
ADP (large)	20.6 ± 1.7
ADP (medium)	20.3 ± 0.8
ADP (small)	20.4 ± 1.6

10.6 Summary of the polarimetric results

From Tables 10.9 and 10.14 the following mean values for the difference in quadratic electro-optic coefficients are obtained for the KDP, ADP, and DKDP crystals investigated in this work:

KDP: $$|g_{xxxx} - g_{yyxx}| = 3.40 \pm 0.11 \text{ m}^2\text{V}^{-2}, \quad (10.9)$$

KDP: $$|n_o^3 g_{xxxx} - n_e^3 g_{yyxx}| = 9.31 \pm 0.64 \text{ m}^2\text{V}^{-2}, \quad (10.10)$$

ADP: $$|g_{xxxx} - g_{yyxx}| = 6.02 \pm 0.20 \text{ m}^2\text{V}^{-2}, \quad (10.11)$$

ADP: $$|n_o^3 g_{xxxx} - n_e^3 g_{yyxx}| = 20.41 \pm 1.4 \text{ m}^2\text{V}^{-2}, \quad (10.12)$$

DKDP: $$|g_{xxxx} - g_{yyxx}| = 3.40 \pm 0.11 \text{ m}^2\text{V}^{-2}. \quad (10.13)$$

Chapter 11

DISCUSSION OF EXPERIMENTAL RESULTS

11.1 Comparison with previous results

Tabulated in Table 11.1 is a summary of all the results for the individual coefficients, and differences in coefficients, of the quadratic electro-optic and electrostrictive effects measured for KDP, ADP, and DKDP by the interferometric and polarimetric experiments in this research. One notes that where comparison can be drawn between the same results determined by the two different approaches ($|g_{xxxx} - g_{yyxx}|$ and $|n_o^3 g_{xxxx} - n_e^3 g_{zzxx}|$ for both KDP and ADP), these are in satisfactory agreement with one another taking experimental uncertainty into consideration.

Results contained in Table 11.1 may also be compared with other published values contained in Tables 5.1 and 5.2. The first important point to note concerning the values measured in this work is their order of magnitude of 10^{-20} m^2V^{-2}. This is consistent with results listed in Table 5.1 measured by dynamic methods and in itself may be seen to provide further evidence that the results determined by static means, of the order of magnitude 10^{-18} - 10^{-19} m^2V^{-2} and which are quoted extensively in the literature, are over estimated, as has been noted previously (Górski and Kucharczyk 1987b; Kucharczyk 1992; Górski *et al.* 1994). Considering specifically the published results determined by dynamic means, one notes that the KDP results in this work for the individual electro-optic coefficients g_{xxxx}, g_{yyxx}, and g_{zzxx} are slightly lower in magnitude than those determined previously in an identical experiment of which this interferometric work may

Table 11.1 Summary of results (in units of 10^{-20} m^2V^{-2}) for coefficients of the quadratic electro-optic and electrostrictive effects of KDP, ADP, and DKDP obtained in this research at room temperature and a wavelength of 632.8 nm

Crystal	Coefficient	Value	Method
KDP	$\lvert g_{xxxx} - g_{yyxx} \rvert$	3.40 ± 0.11	Polarimetric
	$g_{xxxx} - g_{yyxx}$	− 3.20 ± 0.21	Interferometric
	$\lvert n_o^3 g_{xxxx} - n_e^3 g_{zzxx} \rvert$	9.31 ± 0.64	Polarimetric
	$n_o^3 g_{xxxx} - n_e^3 g_{zzxx}$	− 9.48 ± 2.04	Interferometric
	g_{xxxx}	− 3.44 ± 0.46	Interferometric
	g_{yyxx}	− 0.20 ± 0.40	Interferometric
	g_{zzxx}	− 0.73 ± 0.41	Interferometric
	γ_{xxzz}	− 1.02 ± 1.29	Interferometric
	γ_{xxyy}	1.45 ± 1.35	Interferometric
ADP	$\lvert g_{xxxx} - g_{yyxx} \rvert$	6.02 ± 0.20	Polarimetric
	$g_{xxxx} - g_{yyxx}$	− 5.69 ± 0.48	Interferometric
	$\lvert n_o^3 g_{xxxx} - n_e^3 g_{zzxx} \rvert$	20.4 ± 1.4	Polarimetric
	$n_o^3 g_{xxxx} - n_e^3 g_{zzxx}$	− 21.4 ± 4.6	Interferometric
	g_{xxxx}	− 7.44 ± 1.02	Interferometric
	g_{yyxx}	− 1.67 ± 0.93	Interferometric
	g_{zzxx}	− 1.43 ± 0.89	Interferometric
	γ_{xxzz}	− 0.70 ± 3.13	Interferometric
	γ_{xxyy}	− 2.31 ± 3.01	Interferometric
DKDP	$\lvert g_{xxxx} - g_{yyxx} \rvert$	3.40 ± 0.11	Polarimetric

be seen as a continuation (Kucharczyk *et al.* 1995, Gunning 1995). Likewise, values for the difference in coefficients g_{xxxx} - g_{yyxx} and $n_o^3 g_{xxxx}$ - $n_e^3 g_{zzxx}$ calculated from the measured results in both instances are also lower in the present work. This difference was discussed in Chapter 8 and attributed to, first, the inaccurate calibration of the reference plate undertaken in the earlier interferometric work, and, second, the improved sensitivity of the present apparatus. There exist no known published values of the individual quadratic electro-optic coefficients for ADP with which to compare the present results

The values of $|g_{xxxx} - g_{yyxx}|$ and $g_{xxxx} - g_{yyxx}$ determined for KDP and DKDP by the polarimetric and interferometric approaches, respectively, are in agreement with the value of $< 10 \times 10^{-20}$ m^2V^{-2} determined by Jamroz and Karniewicz (1979) for both crystals by a dynamic polarimetric approach. The same difference in coefficients for both KDP and ADP determined by the two

techniques in this research are slightly larger in both instances than the values of $(2.5 \pm 0.5) \times 10^{-20} m^2V^{-2}$ and $(4.7 \pm 1.0) \times 10^{-20} m^2V^{-2}$ measured for these crystals, respectively, in the polarimetric investigation of Górski and Kucharczyk (1987b). This difference is most likely due to the inaccurate calibration of a selective amplifier used by these researchers in their experiment (Gunning *et al.* 1999), and the results determined in this work are thus considered more reliable.

It is also interesting to note that the coefficients $|g_{xxxx} - g_{yyxx}|$ and $g_{xxxx} - g_{yyxx}$ determined by polarimetric and interferometric means respectively for KDP are comparable, within experimental error, to the same difference in coefficients determined for DKDP by the polarimetric method. Likewise, the KDP results for $|n_o^3 g_{xxxx} - n_e^3 g_{zzxx}|$ and $n_o^3 g_{xxxx} - n_e^3 g_{zzxx}$ are similar to the value of $|n_o^3 g_{xxxx} - n_e^3 g_{zzxx}| = (10.4 \pm 0.6) \times 10^{-20}\ m^2V^{-2}$ determined by Ledzion *et al.* (1999), again by the polarimetric approach. However, this is contrary to what may be expected by Miller's rule. Assuming the intrinsic quadratic electro-optic coefficients M_{ijkl} (related to g_{ijkl} by eqn. (11.2) below) in KDP and DKDP are the same, as is actually the case for the intrinsic linear electro-optic coefficient m_{ijk}, then from Miller's rule relating the electro-optic behaviour of a crystal to the magnitude of the low-frequency dielectric constants, one expects from $\varepsilon_{xx} = 43.2$ and $\varepsilon_{xx} \approx 60$ for KDP and DKDP, respectively, (Landolt-Börnstein 1979, 1984) that $|g_{xxxx} - g_{yyxx}|$ in DKDP should be almost twice that in KDP. The results of this work contradict this expectation. However, they are consistent with findings for the linear electro-optic coefficient r_{yzx}, also measured for a field in the *x*-direction, which is similarly observed to remain constant between the two crystals (Landolt-Börnstein 1979, 1984). Thus, from the results for $|g_{xxxx} - g_{yyxx}|$ and $g_{xxxx} - g_{yyxx}$, it has been suggested by Gunning *et al.* (1998a) that for a low-frequency perturbing field along the crystallographic *x*-axis, the deuteration effect on the intrinsic electro-optic coefficients is not negligible and Miller's rule is not followed.

Turning now to the electrostrictive results for KDP and ADP, one notes that the results listed in Table 5.2 determined with the use of a static electric field are at least an order of magnitude greater than those measured in the present research. Of the values not derived by static means, all of which are of order of magnitude $10^{-20}\ m^2V^{-2}$ with the exception of that reported for $|\gamma_{xxzz}|$ by Zaitseva and Fotchenkov (1967) which is of the order of $10^{-19}\ m^2V^{-2}$, the value of γ_{xxzz} for KDP determined in this work compares favourably with that of $\gamma_{xxzz} = 0.8 \times 10^{-20}\ m^2V^{-2}$ measured by Troussant *et al.* (1988). It is, however, opposite in sign. There exist no known published values

of γ_{xxyy} for either crystal.

11.2 On the nature of the quadratic electro-optic effect in KDP, ADP, and DKDP

From results for the quadratic electro-optic coefficients listed in Table 11.1 and from eqns. (5.3) and (5.48) it is possible to draw certain conclusions regarding the relative magnitude of the various contributions to the measured electro-optic effect which are identified in eqn. (5.48). These are the ionic, or lattice, part of the quadratic electro-optic coefficient, the corresponding electronic part, the elasto-optic–electrostrictive contribution, and also a term related to the electrostatic attraction of the crystal's electrode plates. Such a comparison of terms has been made previously, for instance: from *z*-propagation results for KDP and ADP (Górski and Kucharczyk 1987b), from the interferometric values obtained for KDP by Kucharczyk *et al.* (1995), and also in the paper by Gunning *et al.* (1999) from the *y*-propagation results for the differences $|g_{xxxx} - g_{yyxx}|$ and $|n_o^3 g_{xxxx} - n_e^3 g_{zzxx}|$ for KDP and ADP, using the values presented in this thesis. In each instance it was estimated from the experimental results that the ionic contribution to the quadratic electro-optic coefficient is at least an order of magnitude greater than the remaining contributions to the measured effect, including the electronic term.

A similar conclusion is reached in respect of all the quadratic electro-optic coefficients, and their differences, measured in this research: the ionic contribution can be shown to be by far the largest. From eqn. (5.3) and experimental results for $\chi^{(o)}_{ijkl}$ (measured, for example, by wave mixing experiments (Levenson and Bloembergen 1974; Eichler *et al.* 1977)), the electronic quadratic electro-optic term is estimated to be the order of magnitude 10^{-23} m^2V^{-2}. Likewise, from electrostrictive data (~10^{-20} m^2V^{-2}, measured by dynamic means) and elasto-optic values (Landolt-Börnstein 1979; 1984) the elasto-optic–electrostrictive contribution to the measured quadratic electro-optic effect, which from eqn. (5.48) enters this as a product, is less than 10^{-21} m^2V^{-2}. Finally, from piezo-optic results and the equation

$$\sigma_{xx} = -\tfrac{1}{2}\varepsilon_o\varepsilon_x(0)E^2,$$

for the mechanical stress σ_{xx} for a field along the crystallographic *x*-axis (as it was for the crystals in this experiment), the term due to the attraction of the electrodes in each case is about 10^{-22} m^2V^{-2}. Thus, for the electro-optic coefficients measured of order of magnitude 10^{-20} m^2V^{-2}, the

ionic contribution may be seen to be dominant, in agreement with previous findings (Górski and Kucharczyk 1987b, Kucharczyk *et al.* 1995).

This may be interpreted as implying that in these KDP-type crystals the electro-optic effect's dominant contribution stems from the applied electric field's interaction directly with the crystal lattice, and the modification of the electronic susceptibility which results. Furthermore, an estimation of the magnitude of the ionic contribution to the quadratic electro-optic effect (Kucharczyk *et al.* 1995) predicts that the coefficient g_{xxxx} is largest in magnitude. This is in agreement with the independent quadratic electro-optic results measured interferometrically for both KDP and ADP in this work.

11.3 Spontaneous anti-polarization in ADP

Finally, it is possible to use the quadratic electro-optic coefficients for ADP to derive results for the spontaneous anti-polarization P in antiferroelectric ADP, as was done by Gunning *et al.* (1998b). This anti-polarization is defined by

$$\Delta n_s = \tfrac{1}{2} n_o^3 \left(M_{xxxx} - M_{yyxx} \right) P^2 , \tag{11.1}$$

where Δn_s is the spontaneous birefringence induced by the anti-polarization in the antiferroelectric phase of ADP, n_o the ordinary refractive index measured in the paraelectric phase, and M_{ijkl} the intrinsic quadratic electro-optic coefficient. (This equation follows from eqns. (5.37), but neglects the linear electro-optic effect and is in terms of induced polarization and the corresponding intrinsic coefficient M_{ijkl}.) The coefficient M_{ijkl} may be related to the g_{ijkl} by (Kaminow 1974)

$$g_{ijkl} = \varepsilon_o^2 \left(\varepsilon_{kk} - 1 \right) \left(\varepsilon_{ll} - 1 \right) M_{ijkl} , \tag{11.2}$$

where ε_o is the permitivitty of free space, ε_{kk} the principal component of the low-frequency dielectric constant, and summation over the indices is not implied. These intrinsic coefficients for ferroelectric crystals are known to obey Miller's rule in the sense that they show only a weak dependence on temperature, being roughly equal in the paraelectric and ferroelectric phases of the crystal. If one assumes the same holds true for antiferroelectric ADP, namely that the difference $M_{xxxx} - M_{yyxx}$ in the paraelectric intrinsic coefficients is temperature-independent and is the same in the antiferroelectric phase, then from eqns. (11.1) and (11.2) and values of $\varepsilon_{xx} = \varepsilon_{yy} \sim 60$ (Landolt-Börnstein 1979, 1984) and a reported value for the spontaneous birefringence

in ADP of 1×10^{-3} at 535 nm, it may be shown that the anti-polarization is of the order of 5×10^{-6} Ccm^{-2} (Gunning *et al.* 1998b). This is comparable to the spontaneous polarization in ferroelectric KDP-type crystals, for instance 5.0×10^{-6} Ccm^{-2} in KDP.

Appendix A

QUANTUM-MECHANICAL EXPRESSIONS FOR VARIOUS POLARIZABILITY TENSORS

Quantum-mechanical expressions for some of the macroscopic polarizability tensors introduced and used in the various chapters of this thesis have been derived previously by means of first-order perturbation theory and are given in the literature. These results, in the absence of absorption which is assumed for simplicity, for a macroscopic volume element ΔV in the quantum state n described by the eigenket $|n\rangle$, are (Graham and Raab 1990)

$$\alpha_{\alpha\beta} = 2\hbar^{-1}\Delta V\sum_{j\neq n} Z_{jn}\omega_{jn} Re\left[\langle n|P_\alpha|j\rangle\langle j|P_\beta|n\rangle\right], \tag{A.1}$$

$$a_{\alpha\beta\gamma} = 2\hbar^{-1}\Delta V\sum_{j\neq n} Z_{jn}\omega_{jn} Re\left[\langle n|P_\alpha|j\rangle\langle j|Q_{\beta\gamma}|n\rangle\right], \tag{A.2}$$

$$a_{\alpha\beta\gamma} = 2\hbar^{-1}\Delta V\sum_{j\neq n} Z_{jn}\omega_{jn} Re\left[\langle n|Q_{\alpha\beta}|j\rangle\langle j|P_\gamma|n\rangle\right] = a_{\gamma\alpha\beta}, \tag{A.3}$$

$$G'_{\alpha\beta} = -2\hbar^{-1}\Delta V\sum_{j\neq n} Z_{jn}\omega_{jn} Im\left[\langle n|P_\alpha|j\rangle\langle j|M_\beta|n\rangle\right], \tag{A.4}$$

$$G'_{\alpha\beta} = -2\hbar^{-1}\Delta V\sum_{j\neq n} Z_{jn}\omega_{jn} Im\left[\langle n|M_\alpha|j\rangle\langle j|P_\beta|n\rangle\right] = -G'_{\beta\alpha}. \tag{A.5}$$

In the above expressions

$$\omega_{jn} = \hbar^{-1}(E_j - E_n),$$

E_i is the energy of state i, $\hbar = h/(2\pi)$, where h is Planck's constant, and

$$Z_{jn} = (\omega_{jn}^2 - \omega^2)^{-1}.$$

For each of these macroscopic tensors a molecular equivalent exists, the expressions of which are given in papers by Buckingham and Longuet-Higgins (1968) and de Figueiredo and Raab (1981).

Of the remaining polarizability tensors for which quantum-mechanical expressions are required in Part 1 of this thesis, namely, $\beta_{\alpha\beta\gamma}$, $b_{\alpha\beta\gamma\delta}$, and $J'_{\alpha\beta\gamma}$, expressions for only the molecular polarizabilities have been derived (Buckingham and Longuet-Higgins 1968; Imrie and Raab 1991). However, from these the equivalent macroscopic tensors may be derived by analogy, and these are

$$\begin{aligned}\beta_{\alpha\beta\gamma} = 2\hbar^{-2}\Delta V Re\Bigg[& \sum_j Z_{jn}^2\left(\omega_{jn}^2 + \omega^2\right)\Big(\langle j|P_\gamma|j\rangle - \langle n|P_\gamma|n\rangle\Big)\langle n|P_\alpha|j\rangle\langle j|P_\beta|n\rangle \\ & + \sum_{j,\,k\neq n} Z_{jn}\,\omega_{kn}^{-1}\,\omega_{jn}\Big(\langle n|P_\gamma|k\rangle\langle k|P_\alpha|j\rangle\langle j|P_\beta|n\rangle + \langle n|P_\alpha|j\rangle\langle j|P_\beta|k\rangle\langle k|P_\gamma|n\rangle\Big) \\ & + \sum_{j,\,k\neq j} Z_{jn}\,\omega_{kj}^{-1}\,\omega_{jn}\Big(\langle n|P_\alpha|k\rangle\langle k|P_\gamma|j\rangle\langle j|P_\beta|n\rangle + \langle n|P_\alpha|j\rangle\langle j|P_\gamma|k\rangle\langle k|P_\beta|n\rangle\Big)\Bigg],\end{aligned} \tag{A.6}$$

$$\begin{aligned}b_{\alpha\beta\gamma\delta} = 2\hbar^{-2}\Delta V Re\Bigg[& \sum_j Z_{jn}^2\left(\omega_{jn}^2 + \omega^2\right)\Big(\langle j|P_\delta|j\rangle - \langle n|P_\delta|n\rangle\Big)\langle n|P_\alpha|j\rangle\langle j|Q_{\beta\gamma}|n\rangle \\ & + \sum_{j,\,k\neq n} Z_{jn}\,\omega_{kn}^{-1}\,\omega_{jn}\Big(\langle n|P_\delta|k\rangle\langle k|P_\alpha|j\rangle\langle j|Q_{\beta\gamma}|n\rangle + \langle n|P_\alpha|j\rangle\langle j|Q_{\beta\gamma}|k\rangle\langle k|P_\delta|n\rangle\Big) \\ & + \sum_{j,\,k\neq j} Z_{jn}\,\omega_{kj}^{-1}\,\omega_{jn}\Big(\langle n|P_\alpha|k\rangle\langle k|P_\delta|j\rangle\langle j|Q_{\beta\gamma}|n\rangle + \langle n|P_\alpha|j\rangle\langle j|P_\delta|k\rangle\langle k|Q_{\beta\gamma}|n\rangle\Big)\Bigg],\end{aligned} \tag{A.7}$$

$$\begin{aligned}d_{\alpha\beta\gamma\delta} = 2\hbar^{-2}\Delta V Re\Bigg[& \sum_j Z_{jn}^2\left(\omega_{jn}^2 + \omega^2\right)\Big(\langle j|P_\delta|j\rangle - \langle n|P_\delta|n\rangle\Big)\langle n|Q_{\alpha\beta}|j\rangle\langle j|P_\gamma|n\rangle \\ & + \sum_{j,\,k\neq n} Z_{jn}\,\omega_{kn}^{-1}\,\omega_{jn}\Big(\langle n|P_\delta|k\rangle\langle k|Q_{\alpha\beta}|j\rangle\langle j|P_\gamma|n\rangle + \langle n|Q_{\alpha\beta}|j\rangle\langle j|P_\gamma|k\rangle\langle k|P_\delta|n\rangle\Big) \\ & + \sum_{j,\,k\neq j} Z_{jn}\,\omega_{kj}^{-1}\,\omega_{jn}\Big(\langle n|Q_{\alpha\beta}|k\rangle\langle k|P_\delta|j\rangle\langle j|P_\gamma|n\rangle + \langle n|Q_{\alpha\beta}|j\rangle\langle j|P_\delta|k\rangle\langle k|P_\gamma|n\rangle\Big)\Bigg] \\ = b_{\gamma\alpha\beta\delta}\,,\end{aligned} \tag{A.8}$$

$$
\begin{aligned}
J'_{\alpha\beta\gamma} = 2\hbar^{-2}\Delta V Im\Bigg[& \sum_j 2Z_{jn}^2 \omega\, \omega_{jn}\Big(\langle j|P_\gamma|j\rangle - \langle n|P_\gamma|n\rangle\Big)\langle n|P_\alpha|j\rangle\langle j|M_\beta|n\rangle \\
& + \sum_{j,\,k\neq n} Z_{jn}\,\omega_{kn}^{-1}\omega\Big(\langle n|P_\gamma|k\rangle\langle k|P_\alpha|j\rangle\langle j|M_\beta|n\rangle + \langle n|P_\alpha|j\rangle\langle j|M_\beta|k\rangle\langle k|P_\gamma|n\rangle\Big) \\
& + \sum_{j,\,k\neq j} Z_{jn}\,\omega_{kj}^{-1}\omega\Big(\langle n|P_\alpha|k\rangle\langle k|P_\gamma|j\rangle\langle j|M_\beta|n\rangle + \langle n|P_\alpha|j\rangle\langle j|P_\gamma|k\rangle\langle k|M_\beta|n\rangle\Big)\Bigg],
\end{aligned}
\tag{A.9}
$$

$$
\begin{aligned}
J'_{\alpha\beta\gamma} = 2\hbar^{-2}\Delta V Im\Bigg[& \sum_j 2Z_{jn}^2 \omega\, \omega_{jn}\Big(\langle j|P_\gamma|j\rangle - \langle n|P_\gamma|n\rangle\Big)\langle n|M_\alpha|j\rangle\langle j|P_\beta|n\rangle \\
& + \sum_{j,\,k\neq n} Z_{jn}\,\omega_{kn}^{-1}\omega\Big(\langle n|P_\gamma|k\rangle\langle k|M_\alpha|j\rangle\langle j|P_\beta|n\rangle + \langle n|M_\alpha|j\rangle\langle j|P_\beta|k\rangle\langle k|P_\gamma|n\rangle\Big) \\
& + \sum_{j,\,k\neq j} Z_{jn}\,\omega_{kj}^{-1}\omega\Big(\langle n|M_\alpha|k\rangle\langle k|P_\gamma|j\rangle\langle j|P_\beta|n\rangle + \langle n|M_\alpha|j\rangle\langle j|P_\gamma|k\rangle\langle k|P_\beta|n\rangle\Big)\Bigg] \\
= & -J'_{\beta\alpha\gamma}.
\end{aligned}
\tag{A.10}
$$

Appendix B

PROOF THAT n^2 IS REAL AND POSITIVE

Thanks must be given to Dr. C. Zaverdinos of the University of Natal Pietermaritzburg Mathematics Department for providing the following proof, for a nonabsorbing medium described in the electric-dipole order, that the solutions n^2 of eqn. (1.17) are real and positive for any propagation direction σ. To this end eqn. (1.17) is written as

$$an^4 - bn^2 + c = 0, \tag{B.1}$$

where

$$a = \varepsilon_x\sigma_x^2 + \varepsilon_y\sigma_y^2 + \varepsilon_z\sigma_z^2, \tag{B.2}$$

$$b = \varepsilon_x\varepsilon_y(\sigma_x^2 + \sigma_y^2) + \varepsilon_y\varepsilon_z(\sigma_y^2 + \sigma_z^2) + \varepsilon_z\varepsilon_x(\sigma_z^2 + \sigma_x^2), \tag{B.3}$$

$$c = \varepsilon_x\varepsilon_y\varepsilon_z. \tag{B.4}$$

It follows from the quantum-mechanical expression for $\alpha_{\alpha\beta} = \varepsilon_o\chi_{\alpha\beta}$ for a crystal in its ground state (see Appendix A) that the χ_{ii}, i = x, y, z, are real and positive for frequencies well below those of any electronic absorption line. As these conditions usually apply to transparent crystals, ε_x, ε_y, ε_z in eqns. (1.18) are taken to be real and positive. So also, then, are a, b, c, in eqns. (B.2) - (B.4). For n^2 to be real and positive as well we require from eqn. (B.1) that

$$b^2 - 4ac \geq 0. \tag{B.5}$$

Expressing the left-hand side of relation (B.5) in terms of ε_x (this choice is arbitrary), then one may write

$$b^2 - 4ac = \alpha\varepsilon_x^2 + \beta\varepsilon_x + \gamma\,, \tag{B.6}$$

where from eqns. (B.2) - (B.4)

$$\alpha = [\varepsilon_y(1-\sigma_z^2) - \varepsilon_z(1-\sigma_y^2)]^2 + 4\varepsilon_y\varepsilon_z\sigma_y^2\sigma_z^2 > 0, \tag{B.7}$$

$$\beta = 2\varepsilon_y\varepsilon_z\{(\sigma_y^2+\sigma_z^2)[\varepsilon_y(1-\sigma_z^2)+\varepsilon_z(1-\sigma_y^2)] - 2(\varepsilon_y\sigma_y^2+\varepsilon_z\sigma_z^2)\}, \tag{B.8}$$

$$\gamma = [\varepsilon_y\varepsilon_z(\sigma_y^2+\sigma_z^2)]^2 \geq 0. \tag{B.9}$$

In eqns. (B.6) - (B.9) use is made of

$$\sigma^2 = \sigma_x^2 + \sigma_y^2 + \sigma_z^2 = 1. \tag{B.10}$$

Then from eqn. (B.6)

$$\varepsilon_x = \frac{-\beta \pm \{\beta^2 - 4\alpha[\gamma - (b^2 - 4ac)]\}^{\frac{1}{2}}}{2\alpha}. \tag{B.11}$$

Since ε_x is real,

$$\beta^2 - 4\alpha[\gamma - (b^2 - 4ac)] \geq 0$$

or

$$b^2 - 4ac \geq \frac{4\alpha\gamma - \beta^2}{4\alpha}. \tag{B.12}$$

From relations (B.7) and (B.12) it follows that relation (B.5) is satisfied, provided that

$$4\alpha\gamma - \beta^2 \geq 0. \tag{B.13}$$

It can be shown from eqns. (B.7) - (B.9) that

$$4\alpha\gamma - \beta^2 = 16\varepsilon_y^2\varepsilon_z^2(\varepsilon_y - \varepsilon_z)^2\sigma_x^2\sigma_y^2\sigma_z^2. \tag{B.14}$$

Then from eqn. (B.14) it may be seen that eqn. (B.13) holds and so therefore does eqn. (B.5). Consequently, the solutions n^2 of eqn. (B.1) are real and positive for any propagation direction in the medium for which ε_x, ε_y, ε_z are real and positive.

Appendix C

SOME RESULTS CONCERNING ORTHOGONALITY

It is shown in this appendix that for a general propagation direction σ in a biaxial crystal the two eigenpolarizations $\boldsymbol{E}_1^{(o)}$ and $\boldsymbol{E}_2^{(o)}$ that exist are not orthogonal to each other or to σ. To show this, a result quoted by Yariv and Yeh (1984) is used, which in the notation of this thesis is

$$\boldsymbol{E}^{(o)} = \left(\frac{n\sigma_x}{n^2 - \varepsilon_x}, \frac{n\sigma_y}{n^2 - \varepsilon_y}, \frac{n\sigma_z}{n^2 - \varepsilon_z} \right). \tag{C.1}$$

From this is can be shown, after considerable manipulation, that the angle α between and $\boldsymbol{E}_1^{(o)}$ and $\boldsymbol{E}_2^{(o)}$ is given by

$$\begin{aligned} \tan\alpha &= \frac{|\boldsymbol{E}_1^{(o)} \times \boldsymbol{E}_2^{(o)}|}{\boldsymbol{E}_1^{(o)} \cdot \boldsymbol{E}_2^{(o)}} \\ &= \frac{[(b^2 - 4ac)(\varepsilon_x^2\sigma_x^2 + \varepsilon_y^2\sigma_y^2 + \varepsilon_z^2\sigma_z^2)]^{\frac{1}{2}}}{(\varepsilon_x - \varepsilon_y)(\varepsilon_y - \varepsilon_z)(\varepsilon_z - \varepsilon_x)\sigma_x\sigma_y\sigma_z}, \end{aligned} \tag{C.2}$$

where the expressions for a, b, c appear in eqns. (B.2) - (B.4). It is evident from eqn. (C.2) that $\alpha \neq 90^\circ$ when all components of σ exist, so that eqn. (1.41) applies, and also when no two ε_i are equal, as in a biaxial crystal.

To give a sense of the value of α, the following numbers for ε_i (Gray 1972) and σ_i are substituted into eqn. (C.2):

$$\varepsilon_x = 5.6169, \qquad \varepsilon_y = 6.2500, \quad \varepsilon_z = 7.0255, \tag{C.3}$$

$$\sigma_x^2 = 3/12, \qquad \sigma_y^2 = 4/12, \qquad \sigma_z^2 = 5/12, \tag{C.4}$$

to obtain

$$\alpha = 89.778^\circ .$$

There is no simple expression for the angle between σ and $\boldsymbol{E}^{(o)}$ that is equivalent to eqn. (C.2). However, it is obvious from eqn. (C.1) that $\sigma \cdot \boldsymbol{E}^{(o)} \neq 0$ for an arbitrary propagation direction in a biaxial crystal. Thus neither eigenvector is orthogonal to σ in general. To calculate the angle ϕ between σ and each eigenvector for the values in eqns. (C.3) and (C.4), the refractive indices and corresponding normalized eigenvectors must first be determined from eqns. (B.1) and (C.1), respectively. These are

$$\begin{aligned} n_1 &= 2.4109083, \\ \boldsymbol{E}_1^{(o)} &= (0.87371359, \ -0.45098329, \ -0.18231472), \\ n_2 &= 2.5715952, \\ \boldsymbol{E}_1^{(o)} &= (0.21871419, \ 0.69288996, \ -0.68707175). \end{aligned}$$

Then from $\cos\phi = \sigma \cdot \boldsymbol{E}^{(o)}$ one finds

$$\phi_1 = 86.629^\circ, \qquad \phi_2 = 86.222^\circ .$$

Appendix D

DIAGRAM OF THE FEEDBACK CONTROL CIRCUIT USED TO ACTIVELY STABILIZE THE INTERFEROMETER

This appendix gives a diagram of the feedback circuit designed and assembled by the University of Natal Electronics Centre for the purpose of providing active stabilization of the interferometer against low-frequency noise influences. The principal of operation of this control circuit, which involved manipulating the voltage applied to a piezotransducer element to control the mirror position in the one arm, has been described in detail in Subsection 7.5.3. Special care was taken with the power supply to this circuit to ensure the dc voltage did not contain any signal at the 50 Hz line frequency.

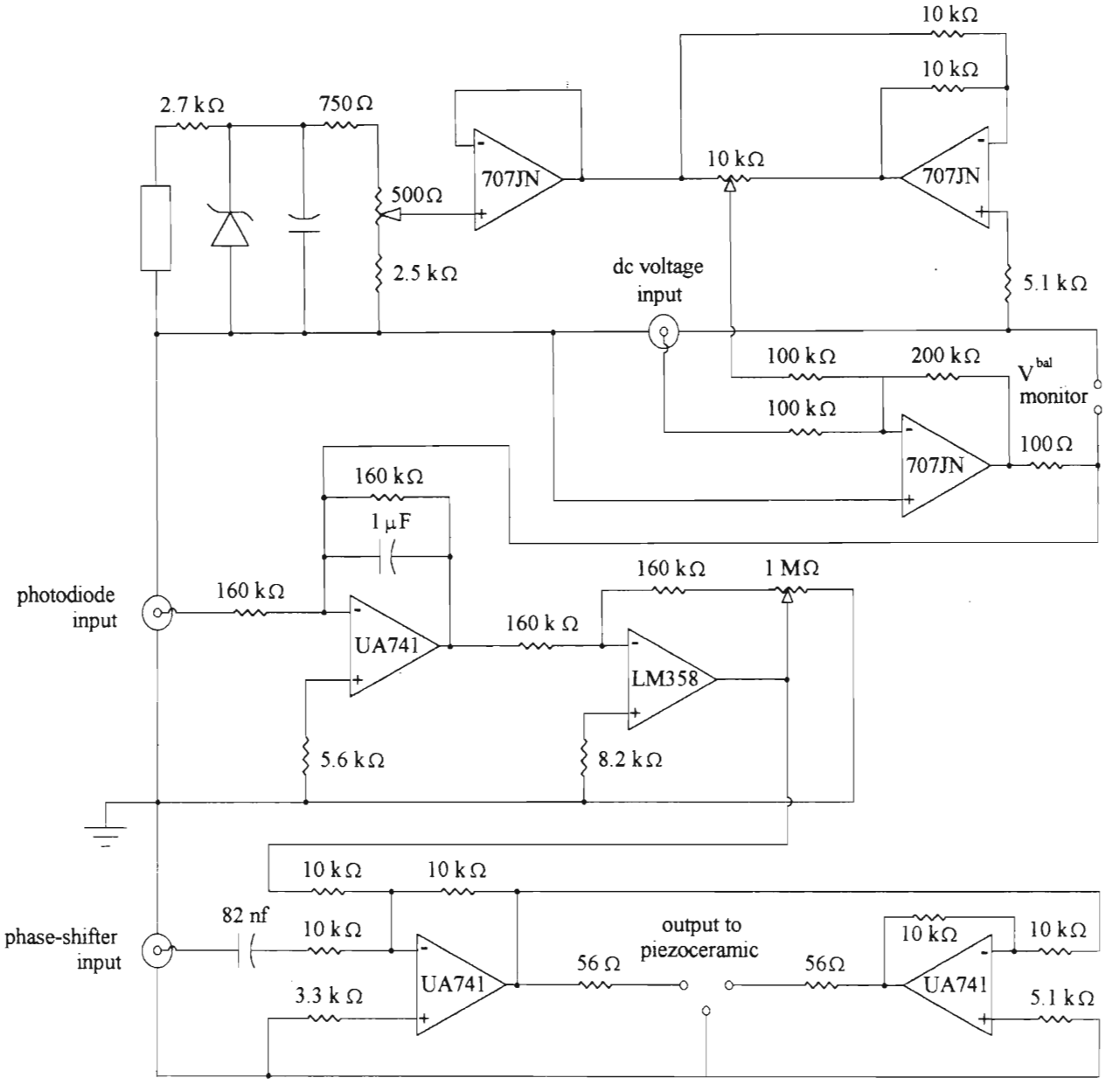

Figure D.1 Diagram of the interferometer feedback circuit

Appendix E

HP 86B PROGRAM FOR THE ACCUMULATION OF RESULTS AND CONTROL OF THE INTERFEROMETRIC EXPERIMENT

The following is the code, written in *Basic,* of the Hewlett-Packard 86B control program for the determination of the compensation voltages and control of the experiment in the interferometric investigation. This program is based to an extent on those written by Pierrus (1989) and Imrie (1993) in their respective experiments using the same Hewlett-Packard equipment and also involving null methods. Variables contained in the program are those for the 50 mm × 50 mm × 5 mm KDP crystal for light propagation along the optic axis; these were changed as required.

```
10   REM  **********************************
20   REM  *** HP 86B PROGRAM FOR THE ACCUMULATION OF DATA IN THE ***
30   REM  *** VIBRATING MIRROR MICHELSON INTERFEROMETER BY THE  ***
40   REM  *** NULL METHOD. THIS PROGRAM WAS WRITTEN BY MARK     ***
50   REM  *** GUNNING, FEBRUARY 1997                            ***
60   REM  **********************************
70   REM
80   REM
90   REM *** VARIABLES FOR THE CALCULATION OF THE RESULTS ***
```

```
100  L = 0.04977 ! LENGTH OF THE CRYSTAL IN THE DIRECTION OF LIGHT
     PROPAGATION IN m
110  T = 0.00499 ! THICKNESS OF THE CRYSTAL IN m
120  N = 1.5075 ! REFRACTIVE INDEX OF THE CRYSTAL FOR THE POLARIZATION
     STATE OF THE LIGHT
130  D = -2.542e-10 ! CALIBRATION CONSTANT OF THE PIEZOCERAMIC IN mV-1
140  REM
150  REM * * * INITIAL EXPERIMENTAL PARAMETERS * * *
160  IMAGE = 7/80A
170  PRINTER IS 701
180  DIM N(12) @ DIM X(12) @ DIM Y(12) @ DIM X2(12) @ DIM Y2(12) @ DIM XY(12)
190  X = 0
200  OUTPUT 614; "A00.0D00";CHR$ (3) ! SETTING DC VOLTAGE TO FEEDBACK CIRCUIT
     TO ZERO
210  OUTPUT 609; "CLS0" ! CLOSING THE RELAY TO HIGH-VOLTAGE AMPLIFIER
220  REM
230  REM * * * INPUT DATA * * *
240  CLEAR
250  DISP
260  DISP "Enter the incident light polarization angle: " @ INPUT ANGLE$
270  DISP "Enter the incident light propagation direction: " @ INPUT PROP$
280  DISP "Enter the crystal type: " @ INPUT CRYSTAL$
290  DISP "Enter present date: " @ INPUT D$
300  DISP "Enter the lock-in amplifier time constant setting: " @ PSDTC
310  DISP "Enter any comments for this run: " @ INPUT COMMENTS$
320  REM
330  REM * * * PRINTING INITIAL DATA * * *
340  PRINT
350  PRINT "              DATE: ";D$; "              CRYSTAL: ";CRYSTAL$
360  PRINT "    POLARIZATION: ";ANGLE$; " degrees          DIRECTION: ";PROP$
370  PRINT "   TIME CONSTANT: "; PSDTC; " s"
380  PRINT "        COMMENTS: ";COMMENT$
390  REM
400  REM * * * STARTING EXPERIMENT * * *
410  PRINT
420  PRINT "  CRYSTAL        NULL          r          k          E-O"
430  PRINT "  VOLTAGE        VOLTAGE                              COEFFICIENT"
440  CLEAR
450  BEEP 50, 150
460  Q, W, B = 0
```

```
470  ENTER 625; CVA @ CV1 = INT(CVA*10000000)/10000 ! INITIAL CRYSTAL VOLTAGE
     READING FOR USE AS A REFERENCE
480  DISP USING 180; "                    * * * STARTING EXPERIMENT * * *"
490  DISP
500  DISP
510  DISP
520  DISP
530  DISP "          The crystal voltage is:  ;"CV1;" V"
540  DISP "          Enter the approximate piezoceramic null voltage: " @ INPUT VBAL
550  CLEAR
560  DISP USING 180; "  * * * INITIATE FEEDBACK CIRCUIT, AND PRESS 'CONT' TO
     CONTINUE * * *"
570  PAUSE
580  BEEP 50,150
590  OUTPUT 609; "DCV6"
600  ENTER 609; FEEDV1 ! DC PHOTODIODE OUTPUT VOLTAGE CORRESPONDING TO
     THE INTERFEROMETER BALANCED AT ITS MOST SENSITIVE POINT
610  CLEAR
620  DISP USING 180; "* * * * * * * * * * * * * * * * * * * * * * * * * * * * * *
     * * * * * * * * "
630  DISP "* * * * * * * * * * * * * *     EXPERIMENT RUNNING     * * * * * *
     * * * "
640  DISP "* * * * * * * * * * * * * * * * * * * * * * * * * * * * * * * * * * *
     * * * "
650  REM
660  REM * * * SUBROUTINE TO TAKE LOCK-IN AMPLIFIER READINGS * * *
670  IF VBAL < 5.25 THEN R = VBAL ELSE R = 10 - VBAL
680  FOR I = 1 TO 6
690  N(I) = INT (((I-1)/12*2*R + (VBAL-R))*100/10)/10000+.0001
700  NEXT I
710  FOR I = 7 TO 12
720  N(I) = INT (((I-1)/12*2*R + (VBAL-R))*100/10)/10000+.0001
730  NEXT I
740  K = 0
750  OUTPUT 609; N(1)
760  GOSUB MEASURE
770  GOSUB BALANCE
780  OUTPUT 609; N(12)
790  GOSUB MEASURE
800  GOSUB BALANCE
```

```
810  OUTPUT 609; N(2)
820  GOSUB MEASURE
830  GOSUB BALANCE
840  OUTPUT 609; N(11)
850  GOSUB MEASURE
860  GOSUB BALANCE
870  OUTPUT 609; N(3)
880  GOSUB MEASURE
890  GOSUB BALANCE
900  OUTPUT 609; N(10)
910  GOSUB MEASURE
920  GOSUB BALANCE
930  OUTPUT 609; N(4)
940  GOSUB MEASURE
950  GOSUB BALANCE
960  OUTPUT 609; N(9)
970  GOSUB MEASURE
980  GOSUB BALANCE
990  OUTPUT 609; N(5)
1000 GOSUB MEASURE
1010 GOSUB BALANCE
1020 OUTPUT 609; N(8)
1030 GOSUB MEASURE
1040 GOSUB BALANCE
1050 OUTPUT 609; N(6)
1060 GOSUB MEASURE
1070 GOSUB BALANCE
1080 OUTPUT 609; N(7)
1090 GOSUB MEASURE
1100 GOSUB BALANCE
1110 BEEP 200, 100 @ BEEP 30, 200
1120 ENTER 625;CV @ CV2 = INT (CV*10000000)/10000 ! CRYSTAL VOLTAGE FOR THE
     PARTICULAR EXPERIMENTAL RUN
1130 GOSUB REGRESSION
1140 GOSUB RESULTS
1150 BEEP 200, 20 @ BEEP 100, 20
1160 GOSUB REBALANCE
1170 GOTO 610
1180 OUTPUT 609; "OPN0" ! OPENING THE RELAY TO THE HIGH-VOLTAGE AMPLIFIER
1190 END
```

```
1200 REM
1210 REM * * * TAKING MEASUREMENTS * * *
1220 MEASURE:
1230 K = K+1
1240 WAIT 11000*PSDTC
1250 TOTV, TVCER = 0
1260 FOR I = 1 TO 25
1270 OUTPUT 609; "DCV3"
1280 ENTER 609; V ! MEASURING THE LOCK-IN AMPLIFIER DC OUTPUT CHANNEL
     SIGNAL
1290 ENTER 623; VCER ! MEASURING THE PIEZOCERAMIC VOLTAGE
1300 TOTV = TOTV+V
1310 TVCER = TVCER+TVCER
1320 NEXT I
1330 X(K) = TOTV/25 ! AVERAGE LOCK-IN AMPLIFIER DC OUTPUT
1340 Y(K) = TVCER/25 ! AVERAGE PIEZOCERAMIC VOLTAGE
1350 ENTER 625; CVB ! CHECKING THE CRYSTAL VOLTAGE
1360 IF ABS (CVA-CVB) > 0.01 THEN GOTO 1180
1370 RETURN
1380 REM
1390 REM * * *REGRESSION ANALYSIS * * *
1400 REGRESSION:
1410 X, Y, XY, X2, XY = 0
1420 FOR I = 1 TO 12
1430 X = X+X(I)
1440 Y = Y+Y(I)
1450 X2 = X2+X(I)^2
1460 Y2 = Y2+Y(I)^2
1470 NEXT I
1480 M = (10*XY-X*Y)/(12*X2-X^2) ! SLOPE OF PLOT
1490 C = (Y*X2-X*XY)/(12*X2-X^2) ! INTERCEPT OF PLOT
1500 R = (10*XY-X*Y)^2/((12*X2-X^2)*(12*Y2-Y^2)) ! CORRELATION COEFFICIENT OF
     PLOT
1510 CV = INT(CV2*100)/100
1520 V_NULL = INT(C*100000)/100000
1530 K = INT(V_NULL/(CV/1000)^2*1000000)/1000000
1540 G_EFF = INT(2*2^0.5*D*V_NULL*T^2/(N^3*L*CV^2)*1.0E26)/1000000
1550 R = INT(R*100000)/100000
1560 RETURN
1570 REM
```

```
1580 REM * * *BALANCE * * *
1590 BALANCE:
1600 OUTPUT 609; "DCV6"
1610 ENTER 609; FEEDV2 ! CHECK OF THE DC PHOTODIODE OUTPUT VOLTAGE
1620 DIFF = FEEDV-FEEDV2
1630 IF DIFF > 0.05 THEN GOSUB SHIFTUP
1640 IF DIFF < -0.05 THEN GOSUB SHIFTDOWN
1650 IF DIFF > -0.05 AND DIFF < 0.05 THEN GOTO 1670
1660 GOTO 1590
1670 RETURN
1680 SHIFTUP:
1690 Q = Q+1
1700 W = ABS(Q)
1710 IF W = 90 THEN DISP "OUT OF BALANCE RANGE: TERMINATING RUN" @ WAIT
     3000 @ GOT0 1180
1720 IF Q <= 0 THEN GOSUB 1820
1730 IF Q > 0 THEN GOSUB 1850
1740 RETURN
1750 SHIFTDOWN:
1760 Q = Q-1
1770 W = ABS(Q)
1780 IF W = 90 THEN DISP "OUT OF BALANCE RANGE: TERMINATING RUN" @ WAIT
     3000 @ GOT0 1180
1790 IF Q <= 0 THEN GOSUB 1820
1800 IF Q > 0 THEN GOSUB 1850
1810 RETURN
1820 IF W < 10 THEN OUTPUT 614; "A00.0D-0";W;CHR$ (3)
1830 IF W > 9 THEN OUTPUT 614; "A00.0D-";W;CHR$ (3)
1840 RETURN
1850 IF W < 10 THEN OUTPUT 614; "A00.0D0";W;CHR$ (3)
1860 IF W > 9 THEN OUTPUT 614; "A00.0D";W;CHR$ (3)
1870 RETURN
1880 REM
1890 REM * * *REBALANCE * * *
1900 REBALANCE:
1910 OUTPUT 609; "DCV5"
1920 ENTER 609; REBV
1930 IF REBV > 2 THEN GOTO 1970
1940 IF REBV < -2 THEN GOTO 1990
1950 GOSUB BALANCE
```

```
1960 RETURN
1970 GOSUB SHIFTUP
1980 GOTO 1890
1990 GOSUB SHIFTDOWN
2000 GOTO 1890
2010 REM
2020 REM * * *PRINTING RESULTS * * *
2030 RESULTS:
2040 PRINT "      ";CV;"      ";V_NULL;"      ";R;"      ";K;"      ";G_EFF
2050 RETURN
```

Appendix F

ILLUSTRATED DATA FOR THE *Y*-PROPAGATION POLARIMETRIC INVESTIGATION

This appendix gives an illustration of the voltages recorded and written to a data file by the pc computer while investigating the KDP and ADP crystals in the *y*-propagation polarimetric investigation. These voltages, recorded in quick succession at set intervals of time, consisted of the photodiode dc, first harmonic, and second harmonic output voltages. Such data files, after being divided into manageable portions, were then analyzed by the computer program in Appendix G, so yielding results for the difference in quadratic electro-optic coefficients $|n_o^3 g_{xxxx} - n_e^3 g_{zzxx} - n_e^3 (n_o r_{xy})^2|$.

Presented in Table F.1 are the photodiode dc, first harmonic, and second harmonic output voltage measurements, V^{dc}, $|V^{\omega}|$, and $|V^{2\omega}|$ respectively, written to a data file for a single investigation on the large ADP crystal to which a voltage of 1023 V rms was applied. From these results Graph F.1 is plotted, showing the variation of each voltage with reading number to give an indication of their change with time, and hence phase, as the temperature of the laboratory increased or decreased steadily, and also their relation to one another.

Table F.1 An illustration of a set of voltage measurements written to a data file for the *y*-propagation polarimetric investigation on the large ADP crystal

Reading number	$\lvert V^{2\omega}\rvert$ (mV)	$\lvert V^{\omega}\rvert$ (mV)	V^{dc} (V)
1	0.33	2.25	3.31
2	0.41	1.53	3.32
3	0.39	0.68	3.28
4	0.50	0.65	3.24
5	0.57	1.23	3.27
6	0.79	1.93	3.31
7	0.44	3.45	3.34
8	0.51	4.41	3.35
9	0.46	5.21	3.30
10	0.91	4.72	3.30
11	0.62	5.93	3.22
12	0.95	6.23	3.19
13	0.97	7.76	3.13
14	1.06	8.72	3.18
15	1.15	9.81	3.18
16	1.20	11.02	3.17
17	1.29	11.87	3.19
18	1.33	12.40	3.12
19	1.41	13.05	3.12
20	1.26	14.81	3.11
21	1.32	14.27	3.15
22	1.58	15.58	3.09
23	2.10	15.62	3.02
24	1.64	17.46	2.97
25	1.70	18.07	2.94
26	1.79	18.83	2.94
27	1.82	19.23	2.88
28	1.76	19.61	2.88
29	1.88	20.03	2.86
30	1.76	19.67	2.80
31	1.86	21.10	2.77
32	2.03	22.97	2.78
33	2.10	23.76	2.74
34	2.17	24.36	2.67
35	2.16	24.98	2.65
36	2.14	25.11	2.65

continued

continued from previous page

Reading number	$\|V^{2\omega}\|$ (mV)	$\|V^{\omega}\|$ (mV)	V^{dc} (V)
37	2.11	24.90	2.61
38	2.11	25.05	2.54
39	2.11	26.56	2.47
40	2.17	27.15	2.45
41	2.33	28.33	2.40
42	2.34	28.33	2.32
43	2.39	28.50	2.28
44	2.39	29.15	2.25
45	2.39	29.30	2.18
46	2.43	29.85	2.17
47	2.47	30.12	2.14
48	2.47	30.93	2.10
49	2.51	31.12	2.09
50	2.48	31.20	2.06
51	2.52	31.58	2.00
52	2.58	32.37	1.96
53	2.55	31.38	1.88
54	2.49	31.58	1.80
55	2.49	31.73	1.74
56	2.51	32.16	1.73
57	2.55	32.66	1.74
58	2.56	32.60	1.67
59	2.52	32.70	1.59
60	2.38	33.25	1.55
61	2.53	32.68	1.51
62	2.45	31.78	1.44
63	2.48	31.47	1.40
64	2.47	31.45	1.35
65	2.40	31.55	1.31
66	2.41	31.85	1.28
67	2.43	31.70	1.24
68	2.35	31.38	1.20
69	2.31	31.78	1.15
71	2.20	33.45	1.05
72	2.25	33.56	1.01
73	2.24	32.57	0.97

continued

continued from previous page

Reading number	$\lvert V^{2\omega}\rvert$ (mV)	$\lvert V^{\omega}\rvert$ (mV)	V^{dc} (V)
74	2.05	30.60	0.93
75	2.18	30.18	0.91
76	2.17	28.38	0.79
77	2.01	27.62	0.75
78	1.93	26.81	0.71
79	1.86	26.26	0.67
80	1.84	26.28	0.67
81	1.84	25.52	0.60
82	1.86	25.60	0.57
83	1.69	24.32	0.52
84	1.61	23.66	0.49
85	1.60	23.33	0.47
86	1.59	22.86	0.44
87	1.53	22.21	0.41
88	1.44	21.33	0.37
89	1.42	21.25	0.40
90	1.31	20.33	0.32
91	1.27	19.48	0.30
92	1.23	18.98	0.28
93	1.20	18.52	0.28
94	1.14	18.06	0.26
95	1.12	17.40	0.23
96	1.00	16.92	0.22
97	0.93	15.23	0.17
98	0.85	14.12	0.15
99	0.79	13.37	0.14
100	0.72	12.53	0.12
101	0.71	12.21	0.11
102	0.63	11.25	0.10
103	0.55	10.38	0.08
104	0.48	9.41	0.07
105	0.41	8.38	0.06
106	0.35	7.48	0.04
107	0.29	6.72	0.04
108	0.21	5.88	0.03
109	0.16	5.08	0.02
110	0.09	4.15	0.01

continued

continued from previous page

Reading number	$\|V^{2\omega}\|$ (mV)	$\|V^{\omega}\|$ (mV)	V^{dc} (V)
111	0.01	3.30	0.01
112	0.05	2.38	0.01
113	0.12	1.57	0.01
114	0.16	0.78	0.01
115	0.23	0.10	0.00
116	0.28	0.78	0.01
117	0.34	1.81	0.01
118	0.43	2.95	0.01
119	0.51	3.86	0.02
120	0.58	4.71	0.02
121	0.64	5.57	0.03
122	0.71	6.37	0.04
123	0.78	7.16	0.04
124	0.84	8.00	0.05
125	0.88	8.66	0.06
126	0.92	9.31	0.08
127	0.99	10.26	0.10
128	1.06	11.25	0.11
129	1.12	12.15	0.12
130	1.19	13.07	0.14
131	1.24	13.85	0.16
132	1.29	14.56	0.17
133	1.35	15.22	0.19
134	1.40	15.98	0.21
135	1.45	16.66	0.23
136	1.50	17.37	0.25
137	1.53	18.06	0.28
138	1.60	18.86	0.30
139	1.64	19.42	0.32
140	1.64	19.65	0.34
141	1.68	20.22	0.36
142	1.73	20.78	0.39
143	1.75	21.35	0.42
144	1.81	22.06	0.44
145	1.86	22.75	0.47
146	1.87	23.53	0.49
147	2.01	24.60	0.55

continued

continued from previous page

Reading number	$\lvert V^{2\omega}\rvert$ (mV)	$\lvert V^{\omega}\rvert$ (mV)	V^{dc} (V)
148	2.04	25.43	0.58
149	2.06	25.91	0.61
150	2.09	26.31	0.64
151	2.14	27.02	0.68
152	2.18	27.66	0.72
153	2.21	28.23	0.76
154	2.22	28.40	0.78
155	2.21	28.58	0.80
156	2.25	28.90	0.84
157	2.28	29.36	0.88
158	2.29	29.86	0.92
159	2.37	30.56	0.97
160	2.29	30.16	1.00
161	2.49	30.90	1.02
162	2.46	31.30	1.07
163	2.48	31.93	1.11
164	2.42	32.26	1.16
165	2.41	32.40	1.18
166	2.39	32.13	1.19
167	2.39	32.05	1.23
168	2.40	32.33	1.26
169	2.41	32.47	1.31
170	2.43	32.53	1.35
171	2.46	32.86	1.40
172	2.49	33.12	1.44
173	2.48	33.20	1.48
174	2.41	32.91	1.51
175	2.40	32.97	1.53
176	2.39	32.96	1.57
177	2.42	33.88	1.62
178	2.41	34.48	1.65
179	2.45	33.90	1.70
180	2.45	33.52	1.73
181	2.41	33.53	1.78
182	2.40	33.31	1.82
183	2.47	34.30	1.88
184	2.48	34.50	1.93

continued

continued from previous page

Reading number	$\|V^{2\omega}\|$ (mV)	$\|V^{\omega}\|$ (mV)	V^{dc} (V)
185	2.41	34.06	1.97
186	2.42	33.77	2.01
187	2.39	33.63	2.04
188	2.36	33.32	2.07
189	2.32	32.93	2.11
190	2.41	33.20	2.17
191	2.31	33.21	2.20
192	2.16	31.86	2.21
193	2.03	31.37	2.23
194	2.17	30.96	2.25
195	2.28	31.92	2.33
196	2.10	31.31	2.35
197	2.07	30.81	2.37
198	2.06	30.56	2.41
199	2.04	30.58	2.45
200	1.99	29.93	2.47
201	1.99	29.36	2.52
202	1.89	28.97	2.54
203	1.87	28.08	2.57
204	1.82	27.81	2.60
205	1.74	27.21	2.63
206	1.71	26.72	2.65
207	1.68	26.15	2.70
208	1.58	25.42	2.72
209	1.56	24.76	2.70
210	1.50	23.88	2.70
211	1.49	23.10	2.74
212	1.70	22.50	2.82
213	1.45	22.51	2.82
214	1.46	21.90	2.87
215	1.31	21.96	2.90
216	1.11	21.97	2.92
217	0.84	21.90	2.95
218	1.11	20.50	2.93
219	1.04	19.42	2.96
220	0.98	18.92	2.98
221	1.00	18.15	2.94

continued

continued from previous page

Reading number	$\|V^{2\omega}\|$ (mV)	$\|V^{\omega}\|$ (mV)	V^{dc} (V)
222	0.90	16.77	2.91
223	0.88	15.68	2.90
224	0.86	14.30	2.93
225	1.01	13.10	2.95
226	0.77	12.72	2.98
227	0.71	12.20	3.02
228	0.73	11.47	3.01
229	0.95	10.30	3.17
230	0.54	11.12	3.17
231	0.35	11.61	3.09
232	0.31	10.52	3.15
233	0.30	9.31	3.13
234	0.43	10.03	3.07
235	0.29	9.32	3.07
236	0.24	8.55	3.07
237	0.24	8.13	3.03
238	0.22	6.87	3.03
239	0.25	6.47	3.07
240	0.31	5.37	3.07
241	0.10	2.35	3.07
242	0.21	2.02	3.21
243	0.24	1.37	3.19
244	0.44	2.18	3.13
245	0.42	0.33	2.96
246	0.39	0.51	3.05
247	0.42	1.11	3.03
248	0.49	1.20	3.05
249	0.59	1.75	3.09
250	0.63	2.43	3.12
251	0.82	3.23	3.09
252	1.11	2.30	3.10
253	1.04	3.97	3.07
254	1.06	4.75	3.11
255	0.97	6.08	3.10
256	1.04	6.98	3.16
257	1.18	7.80	3.02

continued

continued from previous page

Reading number	$\|V^{2\omega}\|$ (mV)	$\|V^{\omega}\|$ (mV)	V^{dc} (V)
258	1.19	8.51	2.99
259	1.19	9.08	2.90
260	1.04	9.68	2.90
261	1.45	9.32	2.92
262	1.22	11.01	2.95
263	1.41	9.38	2.92
264	1.21	12.41	2.97
265	0.97	14.86	2.99
266	1.45	15.13	2.97
267	1.24	15.52	2.94
268	1.52	16.00	2.89
269	1.65	16.53	2.86
270	1.66	16.86	2.82
271	1.69	17.53	2.80
272	1.79	17.70	2.76
273	1.64	18.53	2.73
274	1.70	20.17	2.74
275	1.77	20.67	2.72
276	1.80	20.80	2.68
277	1.89	21.08	2.64
278	1.98	21.32	2.64
279	1.84	22.21	2.61
280	2.11	22.88	2.63
281	2.09	23.63	2.60
282	2.11	23.80	2.49
283	2.08	23.61	2.44
284	2.02	24.36	2.43
285	2.14	24.80	2.38
286	2.14	24.88	2.29
287	2.12	24.23	2.22
288	2.11	24.23	2.19
289	2.18	24.87	2.17
290	2.18	25.61	2.18
291	2.21	26.02	2.15
292	2.27	25.68	2.11
293	2.24	26.43	2.09
294	2.30	26.02	2.00

continued

continued from previous page

Reading number	$\|V^{2\omega}\|$ (mV)	$\|V^{\omega}\|$ (mV)	V^{dc} (V)
295	2.17	26.77	1.98
296	2.17	28.50	2.11
297	2.25	30.41	2.10
298	2.48	30.31	2.01
299	2.45	30.18	2.01
300	2.70	31.47	1.91
301	2.66	31.66	1.94
302	2.42	30.96	1.88
303	2.15	32.63	1.75
304	2.24	31.87	1.77
305	2.26	30.92	1.74
306	2.83	31.87	1.67
307	2.71	30.62	1.57
308	2.40	29.42	1.53
309	2.37	29.88	1.51
310	2.37	30.45	1.48
311	2.35	30.80	1.44
312	2.35	30.82	1.40
313	2.35	31.02	1.38
314	2.36	31.17	1.37
315	2.37	31.30	1.33
316	2.35	31.31	1.30
317	2.33	31.22	1.27
318	2.33	30.68	1.22
319	2.28	30.20	1.18
320	2.24	29.85	1.16
321	2.29	30.70	1.17
322	2.27	30.91	1.13
323	2.26	30.98	1.11
324	2.27	31.06	1.07
325	2.26	30.78	1.04
326	2.19	29.95	0.96
327	2.15	29.21	0.91
328	2.11	28.83	0.87
329	2.06	28.41	0.84
330	2.03	27.92	0.80
331	1.99	27.32	0.77

continued

continued from previous page

Reading number	$\|V^{2\omega}\|$ (mV)	$\|V^{\omega}\|$ (mV)	V^{dc} (V)
332	1.95	26.91	0.74
333	1.91	26.55	0.71
334	1.88	26.68	0.68
335	1.86	26.38	0.65
336	1.79	25.82	0.62
337	1.79	26.11	0.61
338	1.77	25.37	0.57
339	1.73	24.58	0.54
340	1.69	23.93	0.50
341	1.62	23.25	0.47
342	1.55	22.72	0.45
343	1.51	22.10	0.42
344	1.47	21.58	0.41
345	1.42	21.05	0.38
346	1.38	20.53	0.35
347	1.33	20.08	0.33
348	1.29	19.57	0.31
349	1.25	19.05	0.29
350	1.19	18.56	0.27
351	1.15	18.00	0.25
352	1.11	17.37	0.23
353	1.07	16.50	0.21
354	1.00	15.67	0.19
355	0.93	14.87	0.18
356	0.87	14.18	0.16
357	0.81	13.55	0.15
358	0.77	13.08	0.13
359	0.71	12.53	0.11
360	0.63	11.48	0.10
361	0.57	10.65	0.08
362	0.53	9.97	0.07
363	0.46	9.23	0.06
364	0.40	8.47	0.05
365	0.34	7.70	0.04
366	0.29	6.91	0.04
367	0.24	6.16	0.03
368	0.16	5.40	0.02

continued

continued from previous page

Reading number	$\lvert V^{2\omega}\rvert$ (mV)	$\lvert V^{\omega}\rvert$ (mV)	V^{dc} (V)
369	0.12	4.67	0.02
370	0.09	4.11	0.02
371	0.03	3.51	0.02
372	0.03	2.71	0.01
373	0.08	2.11	0.01
374	0.14	1.31	0.01
375	0.20	0.41	0.01
376	0.24	0.62	0.01
377	0.34	1.48	0.01
378	0.42	2.32	0.01
379	0.47	3.05	0.01
380	0.52	3.75	0.02
381	0.57	4.47	0.02
382	0.62	5.17	0.03
383	0.68	5.96	0.04
384	0.72	6.57	0.04
385	0.80	7.48	0.06
386	0.85	8.25	0.06
387	0.90	8.92	0.07
388	0.94	9.60	0.08
389	0.99	10.17	0.09
390	1.05	11.01	0.11
391	1.13	11.92	0.13
392	1.17	12.72	0.14
393	1.24	13.61	0.16
394	1.30	14.42	0.18
395	1.35	15.08	0.19
396	1.40	15.85	0.21
397	1.45	16.63	0.23
398	1.53	17.52	0.26
399	1.60	18.50	0.28
400	1.68	19.30	0.31
401	1.69	19.90	0.33
402	1.74	20.70	0.36
403	1.78	21.35	0.38
404	1.82	21.98	0.41
405	1.86	22.37	0.43

continued

continued from previous page

Reading number	$\lvert V^{2\omega}\rvert$ (mV)	$\lvert V^{\omega}\rvert$ (mV)	V^{dc} (V)
406	1.89	22.92	0.46
407	1.93	23.60	0.48
408	1.96	24.08	0.52
409	2.00	24.61	0.54
410	2.05	25.30	0.58
411	2.09	25.82	0.60
412	2.16	26.22	0.64
413	2.18	26.88	0.67
414	2.21	27.46	0.71
415	2.23	28.00	0.74
416	2.25	28.26	0.77
417	2.26	28.50	0.79
418	2.27	28.88	0.82
419	2.31	29.42	0.86
420	2.35	29.95	0.89
421	2.31	29.38	0.90
422	2.32	28.97	0.92
423	2.31	29.43	0.97
424	2.30	30.12	1.01
425	2.14	29.93	1.04
426	2.29	30.58	1.08
427	2.27	29.95	1.10
428	2.34	30.26	1.12
429	2.30	30.00	1.17
430	2.37	30.86	1.22
431	2.43	31.75	1.29
432	2.46	32.78	1.34
433	2.42	32.85	1.38
434	2.46	33.06	1.43
435	2.43	33.58	1.47
436	2.46	33.98	1.51
437	2.37	33.45	1.52
438	2.42	34.32	1.57
439	2.41	32.57	1.63
440	2.45	32.76	1.68
441	2.47	32.97	1.70
442	2.47	33.02	1.71

continued

continued from previous page			
Reading number	$\lvert V^{2\omega}\rvert$ (mV)	$\lvert V^{\omega}\rvert$ (mV)	V^{dc} (V)
443	2.39	32.65	1.73
444	2.38	32.73	1.76
445	2.33	32.53	1.83
446	2.44	32.57	1.86
447	2.37	32.18	1.87
448	2.35	31.63	1.89
449	2.23	30.86	1.93
450	2.19	31.30	1.98
451	2.14	31.47	2.04
452	2.09	31.87	2.10
453	2.15	31.72	2.17
454	2.14	31.06	2.22
455	2.13	30.65	2.23
456	2.04	29.46	2.19
457	2.04	28.62	2.21
458	2.03	28.63	2.30
459	2.01	28.76	2.35
460	1.99	28.68	2.40
461	1.97	28.60	2.47
462	1.89	28.26	2.47
463	1.80	27.25	2.47
464	1.67	26.22	2.47
465	1.69	25.87	2.49
466	1.62	25.55	2.52
467	1.52	24.88	2.56
468	1.60	24.31	2.59
469	1.64	23.63	2.65
470	1.65	22.95	2.74
471	1.53	23.35	2.76
472	1.43	23.47	2.79
473	1.36	22.96	2.78
474	1.35	21.36	2.76
475	1.30	20.01	2.79
476	1.21	19.51	2.80
477	1.14	18.95	2.80
478	1.02	18.47	2.86
479	0.96	18.05	2.95
			continued

continued from previous page

Reading number	$\lvert V^{2\omega}\rvert$ (mV)	$\lvert V^{\omega}\rvert$ (mV)	V^{dc} (V)
480	0.94	17.47	2.96
481	0.94	16.93	2.98
482	0.82	16.46	2.98
483	0.74	15.95	3.01
484	0.71	15.02	3.00
485	0.87	13.82	3.04
486	0.74	12.30	3.09
487	0.64	11.71	3.10
488	0.61	10.81	3.12
489	0.50	10.30	3.13
490	0.41	10.27	3.14
491	0.34	9.63	3.13
492	0.27	8.62	3.08
493	0.21	8.26	3.05
494	0.14	7.85	3.08
495	0.08	7.00	3.08
496	0.02	6.21	3.07
497	0.19	7.75	3.01
498	0.21	6.06	3.07
499	0.21	6.25	3.04
500	0.26	6.52	3.03
501	0.39	4.08	3.02
502	0.22	0.95	3.07
503	0.29	0.41	3.07
504	0.46	0.28	3.09
505	0.41	0.83	3.03
506	0.42	3.08	3.05
507	0.55	3.38	3.07
508	0.63	3.88	3.06
509	0.69	4.75	3.03
510	0.82	4.56	3.06
511	1.14	3.92	3.04
512	1.14	4.25	2.98
513	1.22	4.47	2.93
514	0.96	7.33	2.89
515	1.13	7.37	2.87
516	1.00	9.08	2.89

continued

continued from previous page

Reading number	$\lvert V^{2\omega}\rvert$ (mV)	$\lvert V^{\omega}\rvert$ (mV)	V^{dc} (V)
517	1.04	9.92	2.83
518	1.18	10.33	2.81
519	1.22	11.00	2.84
520	1.23	11.96	2.82
521	1.26	12.83	2.87
522	1.40	14.88	2.87
523	1.42	15.21	2.85
524	1.44	15.60	2.8
525	1.50	16.37	2.79
526	1.59	17.26	2.75
527	2.13	16.53	2.81
529	1.77	19.43	2.72
530	1.77	20.45	2.70
531	1.77	20.76	2.67
532	1.79	20.97	2.64
533	1.89	21.47	2.61
534	1.91	22.08	2.56
535	1.92	22.18	2.55
536	1.92	23.25	2.51
537	1.90	24.07	2.50
538	2.01	24.78	2.47
539	2.18	25.00	2.46
540	2.19	25.67	2.44
541	2.11	25.47	2.39
542	2.18	26.28	2.37
543	2.14	26.78	2.34
544	2.36	27.80	2.32
545	2.30	28.52	2.29
546	2.32	28.63	2.25
547	2.32	28.62	2.20
548	2.36	28.68	2.14
549	2.37	28.82	2.11
550	2.32	29.56	2.06
551	2.40	29.87	2.03
552	2.41	30.33	1.98
553	2.39	30.85	1.94
554	2.46	31.08	1.89

continued

continued from previous page

Reading number	$\lvert V^{2\omega} \rvert$ (mV)	$\lvert V^{\omega} \rvert$ (mV)	V^{dc} (V)
555	2.52	31.40	1.87
556	2.48	31.78	1.83
557	2.53	31.57	1.75
558	2.55	31.70	1.73
559	2.62	31.76	1.71
560	2.47	30.85	1.66
561	2.38	30.45	1.64
562	2.42	30.63	1.59
563	2.37	29.95	1.52
564	2.27	29.21	1.45
565	2.22	28.82	1.40
566	2.21	28.53	1.33
567	2.26	29.81	1.27
568	2.21	29.51	1.21
569	2.17	28.90	1.18
570	2.15	28.51	1.14
571	2.11	28.30	1.10
572	2.10	28.07	1.06
573	2.02	27.83	1.06
574	1.94	27.62	1.01
575	1.86	27.77	1.02
576	2.00	27.50	0.99
577	2.12	28.13	0.95
578	2.35	29.21	0.96
579	2.47	28.83	0.91
580	2.26	29.20	0.92
581	2.07	28.30	0.82
582	2.04	27.60	0.79
583	1.96	27.53	0.76
584	1.94	27.28	0.72
585	1.90	26.82	0.69
586	1.89	26.20	0.65
587	1.76	25.63	0.62
588	1.74	24.97	0.57
589	1.71	24.32	0.57
590	1.67	23.62	0.52
591	1.69	23.67	0.52

continued

continued from previous page			
Reading number	$\|V^{2\omega}\|$ (mV)	$\|V^{\omega}\|$ (mV)	V^{dc} (V)
592	1.64	23.28	0.49
593	1.58	22.76	0.46
594	1.56	22.08	0.41
595	1.43	21.25	0.40
596	1.41	20.58	0.37
597	1.35	19.96	0.34
598	1.28	19.11	0.30
599	1.18	18.27	0.27
600	1.14	17.56	0.25
601	1.08	16.78	0.22
602	1.01	15.63	0.20
603	0.93	14.90	0.18
604	0.88	14.21	0.17
605	0.87	13.88	0.15
606	0.81	13.27	0.13
607	0.78	12.51	0.13
608	0.69	11.83	0.10
609	0.68	11.48	0.10
610	0.57	10.33	0.09
611	0.27	9.41	0.08
612	0.44	8.75	0.06
613	0.39	8.08	0.05
614	0.32	7.36	0.04
615	0.26	6.53	0.03
616	0.20	5.76	0.02
617	0.18	4.95	0.02
618	0.08	4.15	0.01
620	0.04	2.47	0.00
621	0.11	1.67	0.00
622	0.19	1.05	0.00
623	0.23	0.15	0.01
624	0.24	0.18	0.01
625	0.30	0.92	0.01

Graph F.1 Plot of V^{dc}, $|V^{\omega}|$, $|V^{2\omega}|$ versus reading number for the results that appear in Table F.1

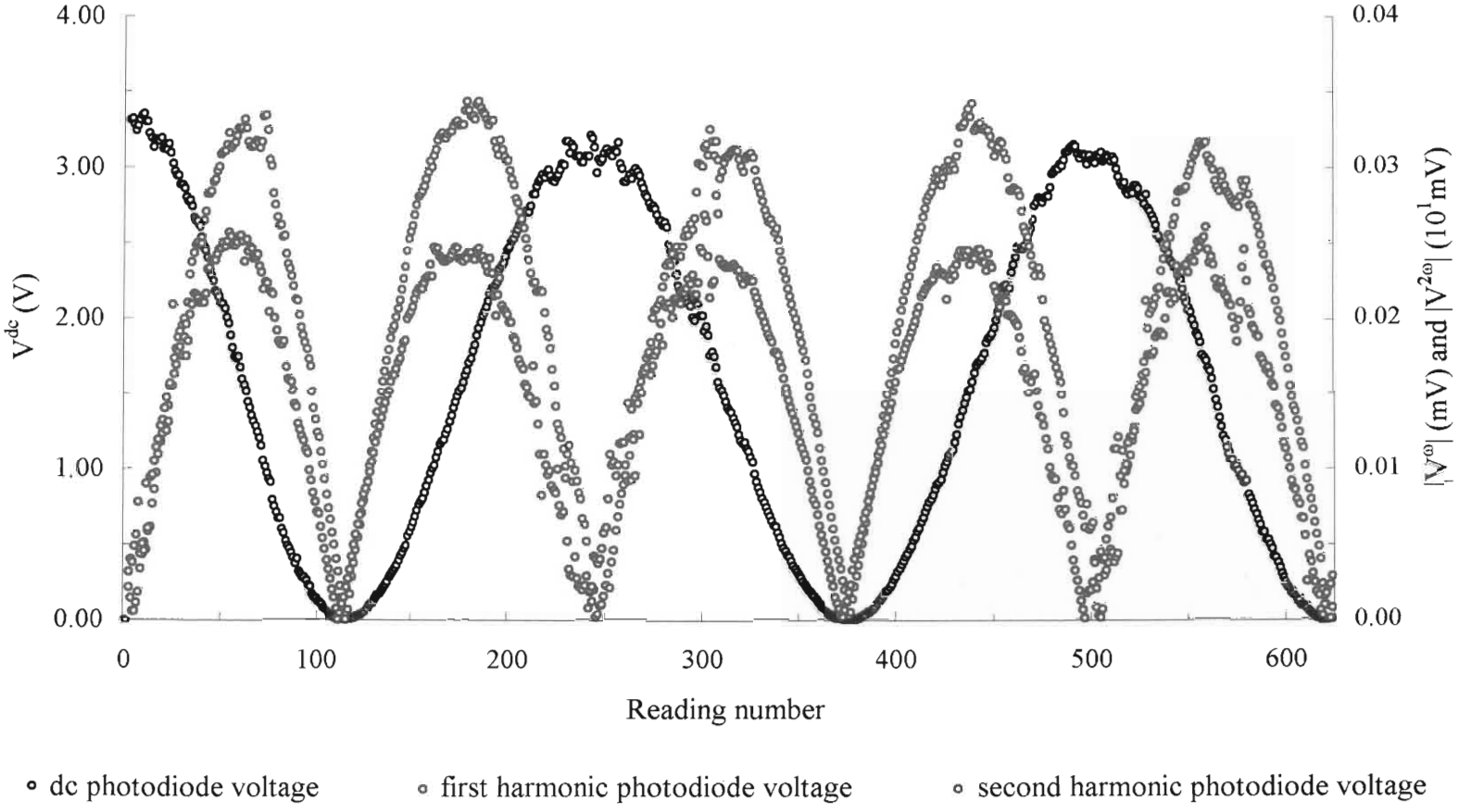

Appendix G

PROGRAM FOR THE ANALYSIS OF RESULTS FOR *Y*-PROPAGATION IN THE POLARIMETRIC ARRANGEMENT

This appendix presents the code of the program used to analyze the results written to the data files in the polarimetric investigation for *y*-propagation through KDP-type crystals. This program, written in *Pascal*, is based almost entirely on one written initially by Prof. W. Kucharczyk at the Technical University of Łódź in Łódź, Poland for the analysis of this data. The values of some variables in this program were changed as required. For instance, the applied crystal voltage for a particular run must be specified, as well as the dimensions of the crystal under investigation. It is also necessary, where appropriate, to enter the file name of the data file to be analyzed. As the program is presented, the variables are for the analysis of a particular data file for an investigation of the medium ADP crystal in the presence of a voltage of 1180 V rms.

Program *y*-propagation analysis;

{This program serves to analyze sets of recorded photodiode dc, first harmonic, and second harmonic photodiode output voltages to compute from these the difference in electro-optic coefficients $|n_o^3 g_{xxxx} - n_e^3 g_{zzxx} - n_e^3 (n_o r_{xzy})^2|$ for the crystal under investigation}

```
uses crt, dos, printer;
var
ucmax, u1min, v, fp, l, t, lambda, cond2, ucmaxu1, numb, cx, sx, tx,
gg, gval, gerr, sumg: real;
uc, u1, u2, f, a, b, g: array [1..1500] of real;
i, k, n, nc, li: integer;

procedure experiment;
{Initial variables for the analysis; these may be changed as required}
begin
   v:= 1180;        {Applied crystal voltage in V}
   l:= 34.58e-3;    {Length of crystal in the direction of light propagation in m}
   t:= 7.06e-3;     {Thickness of crystal in m}
   lambda:= 632.8e-9;      {Wavelength of light wave in m}
   fp:= 80;         {Accepted phase limit from 90° in degrees}
   cond2:= 0.8;     {Accepted position of the maximum dc voltage corresponding to minimum |V2ω|
                    relative to the actual dc peak}
end;

procedure read;
{Procedure to read the recorded voltages from the data file}
var
data:text;
begin
   assign (data,'c:\myfiles\y-prop\adp\medium\adpm8a.dat');     {Directory and file name of data file
                                                               to be analyzed}
   reset (data);
   while not eof(data) do
   begin
      inc(i);
      readln (data,u2[i],u1[i],uc[i],numb);
```

```
    end;
    close (data);
end;

procedure write_results;
{Procedure to write the computed results to a data file}
var
wyn : text;
begin
    assign (wyn,'c:\myfiles\y-prop\programs\output\adpmnew.dat');   {Directory and file name to
                                                                    which results are written}
    append (wyn);
    writeln (wyn,'adpm8c  ',v:3:0,' ',gval,'  ',,gerr,'  ',li);
    close (wyn);
end;

begin
    writeln ('  ');
    i:= 0;
    read;
    experiment;
    nc:= i;
    ucmax:=1.0e-20;
    u1min:=1.0e10;
    ucmaxu1:=1.0e-20;
    for k:=1 to nc do
    begin
    if abs(uc[k]) > ucmax then ucmax:=abs(uc[k]);
end;

{Establishing the maximum photodiode dc voltage corresponding to minimum |V^2ω|}
for k:=1 to nc do
begin
    if (abs(uc[k])/ucmax > cond2) and (abs(u1[k]) <  u1min)
    and (abs(uc[k]) >= ucmaxu1) then u1min := abs(u1[k]);
end;
```

```
for k:=1 to nc do
begin
    if (abs(u1[k])=u1min) and (abs(uc[k])/ucmax > cond2) then
    ucmaxu1 :=abs(uc[k]);
end;
for k := 1 to nc do
{Computing results for all voltage sets recorded to the data file}
begin
    if (abs(Uc[k]) < ucmaxu1) then
    begin
        cx :=0; sx :=0; tx :=0;
        cx := 1 - 2*abs(uc[k])/ucmaxu1;
        sx := sqrt(1 - cx*cx);
        if cx =0 then cx := 1e-10;
        tx := sx/cx;
        f[k] := 360/(2*pi)*arctan(tx);
        if sx =0 then sx :=1e-10;
        b[k] := 2*sqrt(2)*u1[k]/(ucmaxu1*sx);
        a[k] := (-2*sqrt(2)*u2[k]/ucmaxu1 - b[k]*b[k]*cx/4)/(0.5*sx);
        g[k] := a[k]*lambda*t*t/(2*pi*l*v*v);
    end;
    if (abs(Uc[k])>= ucmaxu1) then
    begin
        g[k]:=0; f[k]:=0;
    end;
end;
gg:=0; li:=0; sumg:=0; gerr:=0; gval:=0;
for k:=1 to nc do
{Accepting results that fall in preset phase range}
begin
    if (a[k] <> 0) and (b[k] <> 0) and (abs(f[k])>fp) then
    begin
        gg:=gg + g[k];
        li:=li + 1;
    end;
end;
```

```
gval:=gg/li;
for k:=1 to nc do
{Calculation of standard error}
begin
    if (a[k] <> 0) and (b[k] <> 0) and (abs(f[k])>fp) then
    begin
        sumg:= (sumg + ((g[k]*1e20 -gval*1e20)*(g[k]*1e20-gval*1e20)));
    end;
end;
gerr := sqrt((sumg)/(li{*(li-1)}))/1e20;
{Printing output to screen}
writeln ('geff = ',gval);
writeln ('standard error = ',gerr);
writeln ('no. of readings = ',li);
writeln ('  ');
end.
```

REFERENCES

Agranovich, V.M. and Ginzberg, V.L. 1984 *Crystal Optics with Spatial Dispersion, and Excitons*, 2nd ed. Springer-Verlag, Berlin.

Allensworth, D.L. 1980 *Rev. Sci. Instrum.* **51**, 1330.

Anastassakis, E. 1972 *Appl. Phys. Lett.* **5**, 212.

Argyres, P.N. 1955 *Phys. Rev.* **97**, 334.

Barford, N.C. 1967 *Experimental Measurements: Precision, Error and Truth*, Addison-Wesley, London.

Barron, L.D. 1982 *Molecular Light Scattering and Optical Activity*, Cambridge U. Press, Cambridge.

Barron, L.D. and Buckingham, A.D. 1971 *Molec. Phys.* **20**, 1111.

Barron, L.D. and Gray, C.G. 1973 *J. Phys.* A **6**, 59.

Bierlein, J.D. and Arweiler, C.B. 1986 *Appl. Phys. Lett.* **49**, 917.

Billings, B.H. 1949 *J. Opt. Soc. Am.* **39**, 797.

Binder, K. and Reger, J.D. 1992 *Adv. Phys.* **41**, 547.

Birss, R.R. 1966 *Symmetry and Magnetism*, 2nd ed. North-Holland, Amsterdam.

Blatt, J.M. and Weisskopf, V.F. 1952 *Theoretical Nuclear Physics*, Wiley, New York.

Bohatý, L. and Haussühl, S. 1977 *Acta. Crysta.* A **33**, 114.

Born, M. and Wolf, E. 1980 *Principles of Optics*, 6th ed. Pergamon Press, New York.

Brandão Farla, J.A. 1993a *Microwave Opt. Technol. Lett.* **6**, 657.

Brandão Farla, J.A. 1993b *Microwave Opt. Technol. Lett.* **6**, 815.

Buckingham, A.D. 1959 *Quart. Rev.* **13**, 183.

Buckingham, A.D. 1967 in *Intermolecular Forces*, Hirschfelder, J.0. ed. *Adv. Chem. Phys.* **12**, 107.

Buckingham, A.D. and Dunn, M.B. 1971 *J. Chem. Soc.* A, 1988.

Buckingham, A.D. and Longuet-Higgins, H.C. 1968 *Molec. Phys.* **14**, 63.

Buckingham, A.D. and Raab, R.E. 1975 *Proc. R. Soc. Lond.* A **345**, 365.

Buckingham, A.D. and Stiles, P.J. 1972 *Molec. Phys.* **24**, 99.

Buckingham, A.D., Bogaard, M.D., Dunmur, D.A., Hobbs, C.P., and Orr, B.J. 1970 *Trans.*

Farad. Soc. **66**, 1548.

Buckingham, A.D., Graham, C., and Raab, R.E. 1971 *Chem. Phys. Lett* **8**, 622.

Buckingham, A.D. and Pople, J.A. 1955 *Proc. Phys. Soc. Lond. Sect.* A **68**, 905.

Carpenter, R.O'B. 1950 *J. Opt. Soc. Am.* **40**, 225.

Churcher, C.D. and Stedman, G.E. 1982 *J. Phys. C* **15**, 5507.

Condon, E.U. and Seitz, F. 1932 *J. Opt. Soc. Am.* **22**, 393.

de Figueiredo, I.M.B. and Raab, R.E. 1981 *Proc. R. Soc. Lond.* A **375**, 425.

Doswell, G. and Kunov, H. 1990 *Rev. Sci. Instrum.* **61**, 1986.

Eichler, H.J., Fery, H., Knof, J., and Eichler, J. 1977 *Z. Physik B* **28**, 297.

Fotchenkov, A.A. 1957 *Sov. Phys. Crystallogr.* **2**, 643.

Fowler, P.W. and Steiner, E. 1990 *Molec. Phys.* **70**, 377.

Fritsch, K. and Adamovsky, G. 1981 *Rev. Sci. Instrum.* **52**, 996.

Fujii, Y. and Sakudo, T. 1970 *J. Appl. Phys.* **41**, 4118.

Gibbs, J.W. 1882 *Am. J. Sci.* **23**, 460.

Górski, P. 1987 PhD Thesis, Technical University of Łódź; Górski, P. and Kucharczyk, W. unpublished.

Górski, P. and Kucharczyk, W. 1987a *Phys. Stat. Sol. (a)* **100,** K73.

Górski, P. and Kucharczyk, W. 1987b *Phys. Stat. Sol. (a)* **103,** K65.

Górski, P. and Kucharczyk, W. 1990 *Phys. Stat. Sol (a)* **121**, K243.

Górski, P., Mik, D., Kucharczyk, W., and Raab, R.E. 1994 *Physica B* **193**, 17.

Gosh, G.C. and Bhar, G.C. 1982 *IEEE J. Quantum Electron* **QE-18**, 143.

Graham, C. and Raab, R.E. 1994 *J. Opt. Soc. Am.* A **11**, 2137.

Graham, E.B. and Raab, R.E. 1983 *Proc. R. Soc. Lond.* A **390**, 73.

Graham, E.B. and Raab, R.E. 1990 *Proc. R. Soc. Lond.* A **430**, 593.

Graham, E.B. and Raab, R.E. 1991a *J. Appl. Phys.* **69**, 2549.

Graham, E.B. and Raab, R.E. 1991b *Phil. Mag.* B **64**, 267.

Graham, E.B. and Raab, R.E. 1992 *Phil. Mag.* B **66**, 269.

Graham, E.B. and Raab, R.E. 1994 *Ferroelectrics* **162**, 161.

Graham, E.B., Pierrus, J., and Raab, R.E. 1992 *J. Phys.* B **25**, 4673.

Gray, D.E. 1972 *American Institute of Physics Handbook*, 3rd ed. McGraw-Hill, New York.

Grib, B. N., Kondilenko, I. I., and Korotkov, P. A. 1975 *Zh. Prikl. Spectrosk.* **23**, 804; 1975 *J. Appl. Spectrosc.* (English Transl.) **23**, 1449.

Gunning, M.J. 1995 MSc Thesis, University of Natal Pietermaritzburg.

Gunning, M.J. and Raab, R.E. 1997a *Molec. Phys.* **91**, 589.

Gunning, M.J. and Raab, R.E. 1997b *J. Opt. Soc. Am.* B **14**, 1692.

Gunning, M.J. and Raab, R.E. 1998a *J. Opt. Soc. Am.* A **15**, 2199.

Gunning, M.J. and Raab, R.E. 1998b *Appl. Opt.* **37**, 1.

Gunning, M.J., Bondarczuk, K., Górski, P., and Kucharczyk, W. 1998a *Phys. Stat. Sol. (a)* **168**, 305.

Gunning, M.J., Raab, R.E., Górski, P., and Kucharczyk, W. 1998b *Ferroelectric Lett.* **24**, 63.

Gunning, M.J., Ledzion, R., Górski, P., and Kucharczyk, W. 1999 *Proceedings SPIE* in press.

Haesen, W.M. and Kwaaitaal, Th. 1976 *Rev. Sci. Instrum.* **47**, 434.

Hanna, D.C., Yuratich, M.A., and Cutter, D. 1979 *Nonlinear Optics of Free Atoms and Molecules*, Springer-Verlag, Berlin.

Hariharen, P. 1992 *Basics of Interferometry* Academic Press, New York.

Haussühl, S. and Walda, G. 1971 *Phys. Stat. Sol. (a)* **5**, K163.

Holloway, A.J. and Emmony, D.C. 1988 *J. Phys. E: Sci. Instrum.* **21**, 384.

Hornreich, R.M. and Shtrikman, S. 1968 *Phys. Rev.* **171**, 1065.

Hruška, K. 1965 *Kristallografiya* **10**, 351; 1965 *Sov. Phys. Crystallogr.* (English Transl.) **10**, 351.

Imrie, D.A. and Raab, R.E. 1991 *Molec. Phys.* **74**, 833.

Jackson, D.A., Priest, R., Dandridge, A., and Tveten, A.B. 1980 *Appl. Opt.* **19**, 2926.

Jackson, J.D. 1975 *Classical Electrodynamics*, Wiley, New York.

Jacquerod, A. (1942) quoted (1968) in *Helv. Phys. Acta.* **14**, 136.

Jamroz, W. and Karniewicz, J. 1979 *Opt. Quantum Electronics* **11**, 23.

Jamroz, W., Karniewicz, J., and Stachowiak, J. 1979 *Kvant. Elekt.* **6**, 605.

Jenkins, F.A and White, H.E. 1976 *Fundamentals of Optics*, McGraw-Hill, New York.

Jones, R.C. 1948 *J. Opt. Soc. Am.* **38**, 671.

Kaminov, I.P. 1974 *An Introduction to Electrooptic Devices*, Academic Press, New York.

Kaminow, I.P. and Johnston, W.D. 1967 *Phys. Rev.* **160,** 519.

Kaminow, I.P. and Johnston, W.D. 1969 *Phys. Rev.* **188,** 1209.

Kauzmann, W. 1957 *Quantum Chemistry*, Academic Press, New York.

Kaye, G.W.C. and Laby, T.H. 1986 *Tables of Physical and Chemical Constants*, 15ed. Longman, New York.

Kerr, J. 1875 *Phil. Mag.* **40**, 337.

Kerr, J. 1880 *Phil. Mag.* **9**, 157.

Klein, M.V. 1970 *Optics*, Wiley, New York.

Kobayashi, J., Tamada, M., Hosogaya, N., and Someya, T. 1998 *Ferroelectric Lett.* **8**, 145.

Kucharczyk, W. 1992 *Physica B* **176**, 189.

Kucharczyk, W. and Górski, P. 1983 *Phys. Stat. Sol. (a)* **75**, K87.

Kucharczyk, W., Gunning, M.J., Raab, R.E., and Graham, C. 1995 *Physica B* **212**, 5.

Kundt, A. 1883 *Ann. Phys. Chem.* **18**, 228.

Kwaaitaal, Th. 1974 *Rev. Sci. Instrum.* **45**, 39.

Kwaaitaal, Th., Luymes, B.J., and van der Pijll, G.A. 1980 *J. Phys. D: Appl. Phys.* **13**, 1005.

Landau, L.D. and Lifshitz, E.M. 1979 *The Classical Theory of Fields*, Pergamon Press, Oxford.

Landolt-Börnstein 1979 *Numerical Data and Functional Relationships in Science and Technology*, New Series, Group III, Vol. 11, Springer-Verlag, Berlin.

Landolt-Börnstein 1984 *Numerical Data and Functional Relationships in Science and Technology,* New Series, Group III, Vol. 18, Springer-Verlag, Berlin.

Ledzion, R., Bondarczuk, P., Górski, P., and Kucharczyk, W. 1999 *Cryst. Res. Technolog.* in press.

Levenson, M.D. and Bloembergen, N. 1974 *Phys. Rev.* B **10**, 4447.

Logan, D.E. 1982 *Molec. Phys.* **46**, 271.

Lomova, L.G., and Sonin, A.S. 1968 *Fiz. Tverd. Tela* **10**, 1565; 1968 *Sov. Phys. - Solid State* (English Transl.) **10**, 1241.

Lorentz, H.A. 1878 *Verh. K. Akad. Wet* **18**, 1 (1878); also in Lorentz, H.A *Collected Papers* Zeeman, P. and Fokker, A.D. eds. 1936 Nijhoff, The Hague.

Lorentz, H.A. 1922 *Proc. K. Ned. Acad. Wet.* **24**, 333; also in Lorentz, H.A *Collected Papers* Zeeman, P. and Fokker, A.D. eds. 1936 Nijhoff, The Hague.

Luymes, B.J. 1983 *Rev. Sci. Instrum.* **54**, 90.

Madhu Mohan, M.L.N., and Haranadh, C. 1995 *Bull. Mater. Sci.* **18**, 599.

Maldonado, T.A. and Gaylord, T.K. 1988 *Appl. Opt.* **27**, 5051.

Maldonado, T.A. and Gaylord, T.K. 1989 *Appl. Opt.* **28**, 2075.

Massey, G.A., Loehr, T.M., Willis, L.J., and Johnson, J.C. 1980 *Appl. Opt.* **19**, 4136.

Meintjes, E.M. and Raab, R.E. 1999 *J. Opt. A: Pure Appl. Opt.* in press.

Nakano, H. and Kimura, H. 1969 *J. Phys. Soc. Jpn.* **27**, 519.

Namba, S. 1961 *J. Opt. Soc. Am.* **51**, 76.

Narasimhamurty, T.S. 1981 *Photoeleastic and Electro-optic Properties of Crystals*, Plenum Press, New York.

Nelson, D.F. 1975 *J. Opt. Soc Am.* **65**, 1144.

Nye, J.F. 1985 *Physical Properties of Crystals*, Claredon Press, Oxford.

O'Dell, T.H. and White, E.A.D. 1970 *Philos. Mag.* **22**, 649.

Olsson, A., Tang, C.L., and Green, E.L. 1980 *Appl. Opt.* **29**, 1897.

Onuki, K., Uchida, N., and Saku, T. 1972 *J. Opt. Soc. Am.* **62**, 1030.

Pan, W.Y. and Cross, L.E. 1989 *Rev. Sci. Instrum.* **60**, 2701.

Pan, W.Y. and Jang, S.J. 1990 *Rev. Sci. Instrum.* **61**, 2109.

Pastrnak, J. and Cross, L.E. 1971 *Phys. Stat. Sol. (b)* **44**, 313.

Pastrnak, J. and Vedam, K. 1971 *Phys. Rev.* B **3**, 2567.

Peck, E.D. and Obetz, S. W. 1953 *J. Opt. Soc. Am* **43**, 505.

Pekar, S.I. 1983 *Crystal Optics and Additional Light Waves*, Benjamin/Cummins, Menlo Park.

Perfilova, V.E. 1967 *Kristallografiya* **12**, 715; 1968 *Sov. Phys. Crystallogr.* (English Transl.) **12**, 4.

Perfilova, V.E. and Sonin, A.S. 1965 *Kristallografiya* **10**, 427; 1965 *Sov. Phys. Crystallogr.* (English Transl.) **10**, 349.

Perfilova, V.E. and Sonin, A.S. 1967 *Isv. Akad. Nauk SSSR, Ser. Fiz.* **31**, 1336; 1967 *Bull. Acad. Sci. USSR Phys. Ser.* (English Transl.) **31**, 1154.

Perfilova, V.E., Sonin, A.S., and Lomova, L.G. 1965 *Kristallografiya* **10**, 701; 1966 *Sov. Phys. Crystallogr.* (English Transl.) **10**, 588.

Pockels, F. 1906 *Lehrbruck der Kristralloptik*, Liepzig, Teubner.

Raab, R.E. 1975 *Molec. Phys.* **29**,1323.

Raab, R.E. and Cloete, J.H. 1994 *J. Electromagn. Waves Appl.* **8**, 1073.

Ramachandran, G.N. and Ramaseshan, S. 1961 in *Handbuch der Physik* Flugge, S. ed. Springer-Verlag, Berlin.

Robinson, F.N.H.1973 *Macroscopic Electromagnetism*, Pergamon Press, Oxford.

Röntgen, W.C. 1880 *Phil. Mag.* **10**, 77.

Röntgen, W.C. 1883 *Phil. Mag.* **18**, 213.

Rosenfeld, L. 1951 *Theory of Electrons*, North-Holland, Amsterdam.

Salvestrini, J.P., Fontana, M.D., Aillerie, M., and Czapla, Z. 1994 *Appl. Phys. Lett.* **64**, 1920.

Schneider, J. and Robertson, S. 1979 *Rev. Sci. Instrum.* **50**, 856.

Shajenko, P. and Green, E.L. 1980 *Appl. Opt.* **19**, 1985.

Shurcliff, W.A. 1962 *Polarised Light* Harvard University, Cambridge, Mass.

Sizgoric, S. and Gundjian, A.A. 1969 *Proc. IEEE* **57**, 1313.

Stephens, P.J. 1970 *J. Chem. Phys.* **52**, 3489.

Sysoev, A.M. 1992 *Fiz. Tverd. Tela* **34**, 2874; 1992 *Sov. Phys. - Solid State* (English Transl.) **34**, 1538.

Takizawa, K. and Okada, M. 1982 *J. Opt. Soc. Am. B* **72**, 809.

Takizawa, K. and Okada, M. 1985 *J. Opt. Soc. Am. B* **2**, 289.

Tan, C.Z. and Arndt, J. 1996 *Physica B* **225**, 202.

Troussant, F., Bastie, P., and Vallade, M. 1988 *Ferroelectrics* **88**, 45.

van Sterkenburg, S.W.P., Kwaaitaal, Th., and van der Eijnden, W.M.M.M. 1990 *Rev. Sci. Instrum.* **61**, 2318.

van Vleck, J.H. 1932 *The Theory of Electric and Magnetic Susceptibilities*, Claredon Press, Oxford.

Vilkomerson, D. 1976 *Appl. Phys. Lett.* **29**, 183.

Vlasov, V.L. and Medvedev, A.N. 1972 Prib. Techn. Eksp. 1, 179.

Wang, B.L. and Liu, X.Q. 1992 *Rev. Sci. Instrum.* **63**, 5340.

White, R.G. and Emmony, D.C. 1985 *J. Phys. E: Sci. Instrum.* **18**, 658.

Yariv, A and Yeh, P. 1984 *Optical Waves in Crystals*, Wiley, New York.

Yariv, A. 1975 *Quantum Electronics*, 3rd ed. Wiley, New York.

Yasuda, A., Kanai, Y., Kusunoki, J., Kawahata, K., and Takeda, S. 1980 *Rev. Sci. Instrum.* **51**, 1652.

Zaitseva, M. P. and Fotchenkov, A.A. 1967 *Kristallografiya* **12**, 45.

Zhang, Q.M., Jang, S.J., and Cross, L.E. 1989 *J. Appl. Phys.* **65**, 2907.

Zhang, Q.M., Pan, W.Y., and Cross, L.E. 1988 *J. Appl. Phys.* **63**, 2492.

Zheludev, I.S. and Fotchenkov, A.A. 1958 *Sov. Phys. Crystallogr.* **31**, 312.

Zheludev, I.S. 1965 *Sov. Phys. Crystallogr.* **9**, 418.

Zhongyan, M., Kwaaitaal, Th., and van den Eijnden, W.M.M.M. 1988 *J. Phys. D: Appl. Phys.* **21**, 175.

Zook, J.D., Chen, D., and Otto, G.N. 1967 *Appl. Phys. Lett.* **11**, 159.

Zwikker, B. and Scherrer, P. 1944 *Helv. Phys. Acta.* **17**, 346.